The cardiac hERG channel: a multiple approach for a better understanding of the Long QT Syndrome

Sintra Grilo, Liliana

UNIVERSITÉ DE GENÈVE

Section des Sciences Pharmaceutiques

FACULTÉ DES SCIENCES
Professeur P.-A. Carrupt
Professeur H. Abriel

The Cardiac hERG Channel: A Multiple Approach For A Better Understanding Of The Long QT Syndrome

THÈSE

présentée à la Faculté des Sciences de l'Université de Genève
pour obtenir le grade de Docteur ès Sciences, mention sciences pharmaceutiques

par

Liliana Sintra Grilo

de

Lausanne (VD)

Thèse n° 4224

Atelier ReproMail - Genève

Août 2010

UNIVERSITÉ
DE GENÈVE

FACULTÉ DES SCIENCES

Doctorat ès sciences
Mention sciences pharmaceutiques

Thèse de *Madame Liliana SINTRA GRILO*

intitulée :

" The Cardiac hERG Channel : A Multiple Approach for a Better Understanding of the Long QT Syndrome "

La Faculté des sciences, sur le préavis de Messieurs P.-A. CARRUPT, professeur ordinaire et directeur de thèse (Section des sciences pharmaceutiques, Pharmacochimie), H. ABRIEL, professeur et codirecteur de thèse (Université de Berne, Faculté de médecine, Département de recherche clinique, Berne, Suisse), A. DAINA, docteur (Section des sciences pharmaceutiques, Pharmacochimie), de Madame E. SCHENKER, docteure (Institut de Recherches Servier, Suresnes, France), de Messieurs S. KELLENBERGER, docteur (Université de Lausanne, Département de pharmacologie et de toxicologie, Lausanne, Suisse) et O. MICHIELIN, professeur assistant (University of Lausanne, Swiss Institute of Bioinformatics, Lausanne, Switzerland), autorise l'impression de la présente thèse, sans exprimer d'opinion sur les propositions qui y sont énoncées.

Genève, le 22 juin 2010

Thèse - 4224 -

Le Doyen, Jean-Marc TRISCONE

N.B.- La thèse doit porter la déclaration précédente et remplir les conditions énumérées dans les "Informations relatives aux thèses de doctorat à l'Université de Genève".

“Ce n'est pas dans la science qu'est le bonheur,

mais dans l'acquisition de la science.”

Edgar Allan Poe
Le Pouvoir des mots

Remerciements

Je tiens à adresser ma plus sincère reconnaissance au Professeur Pierre-Alain Carrupt pour m'avoir accordé sa confiance et permis d'effectuer ce travail de thèse, partagé entre son groupe de Pharmacochimie et d'autres horizons. Merci pour son soutien, pour les ressources exceptionnelles mises à disposition et pour la liberté d'action qui m'a été accordée durant ces années de thèse.

Je tiens également à remercier tout particulièrement le Professeur Hugues Abriel pour m'avoir accueilli au sein de son groupe et m'avoir permis de profiter d'un environnement de travail très motivant. Merci également pour tous les apports scientifiques de premier plan concernant les canaux ioniques et la recherche scientifique en général, ainsi que pour son énergie inépuisable.

J'aimerais aussi remercier le Docteur Antoine Daïna qui a su me guider dans le monde (pas si) virtuel de la modélisation moléculaire. Merci pour sa disponibilité et sa motivation de tous les instants, et bien évidemment pour sa bonne humeur contagieuse!

J'aimerais également remercier tous mes collègues de Pharmacochimie, en particulier Elisabeth Favre pour sa « *joie de vivre »* et sa camaraderie lors des TPs, Delphine Cressend, Amandine Guillot, Bénédicte Gross-Vallotton, les Docteurs Yveline Henchoz, Saviana Di Giovanni, Bruno Bard et Sophie Martel pour les moments de bonne humeur partagés au cours de mes séjours annuels et visites inopinées.

Un grand merci à tous mes collègues côtoyés au Département de Pharmacologie et Toxicologie de même qu'au Département de Recherche Clinique. Je tiens à témoigner ma profonde reconnaissance aux membres du « *groupe HA* », d'avant et après le déménagement, avec qui j'ai partagé l'essentiel de mes journées de thèse, mais soirées aussi. Un merci particulier aux ''patcheurs'' – à mon *parrain* le Docteur Jean-Sébastien Rougier pour l'enseignement de son art, à ma *moitié* de tous les voyages, le Docteur Séverine Petitprez, et à Cédric Laedermann – avec lesquels de nombreuses discussions, d'ordre scientifique ou pas, ont agréablement comblé le

manque de conversation de mes petites cellules. Un grand merci également aux ‘‘biochimistes’’ pour le partage de leurs connaissances et leur bonne humeur, que j’adresse spécialement au Docteur Bruno Gavillet et à notre *Smooth* du laboratoire, alias Anne-Flore Zmoos, pour sa gentillesse à toute épreuve et son professionnalisme. Merci à Maria Essers pour son dévouement et son implication à simplifier notre installation dans le nouveau laboratoire d’outre-Sarine. Merci à tous mes collègues qui ont rendu ce séjour parmi eux si agréable.

J’aimerais exprimer également mes remerciements aux ‘‘*touristes HA*’’ que la science ou l’amitié amenait plus souvent à se retrouver. J’adresse un merci particulier aux Docteurs Christine Gonzales, Armelle Takeda et Stéphany Gardier, à Sarah★Pedretti, Luca Cariolato et Liliane Abuin pour leur contribution au bon déroulement de cette thèse, par leurs conseils avisés et leur expérience, scientifiques mais avant tout humains.

Je remercie TOUS ceux qui m’ont accompagné durant ces années de thèse sur les différents sites, sans oublier celles qui ont toujours su m’aider efficacement et agréablement dans les différentes démarches administratives, c’est-à-dire Sylvia Passaquay-Rion, Isabelle Rivier-Flühmann, Chantal Demont, Sabrina Kittel et Verena Frazao.

Merci aux membres du jury de thèse, le Docteur Antoine Daïna, le Docteur Esther Schenker, le Docteur Stephan Kellenberger et le Docteur Olivier Michielin, pour leur lecture attentive, leur regard critique et leurs précieuses recommandations.

Ma profonde gratitude va naturellement à ma famille et à mes amis – en particulier à mes parents et à ma sœur Daniela – pour leur présence, leurs encouragements et leur soutien irremplaçable au cours de ces années (qui ont dû leur paraître plus longues qu’à moi). Et finalement, j’adresse des remerciements particuliers à Christophe, pour la sérénité qu’il a su m’apporter dans les moments plus difficiles, pour son amour et sa présence à mes côtés pour écarter les doutes, soigner les blessures et partager les joies.

Merci !

Table of content

– Part II –

– Part III –

– Part IV –

– Part V –

Avant-propos

La présente thèse a été effectuée conjointement au sein de la Section des Sciences Pharmaceutiques (Université de Genève, Université de Lausanne) et du groupe Canaux Ioniques (Université de Lausanne, Université de Berne), sous la direction du Professeur Pierre-Alain Carrupt du Professeur Hugues Abriel. Le travail de thèse présenté dans ce manuscrit se divise en plusieurs parties distinctes qui disposent d'une introduction théorique spécifique et des articles scientifiques, publiés ou en préparation, réalisés dans les différents domaines de recherche ayant pour sujet principal le canal potassique hERG.

Résumé de la thèse

Le canal hERG ou *human ether à-gogo related gene* est responsable de la *composante rapide du courant potassique rectifiant retardé* (I_{Kr}) qui détermine en partie la durée du potentiel d'action dans une cellule cardiaque. Il est désormais établi que ce canal potassique dépendant du voltage est formé par l'assemblage de quatre sous-unités α codées par le gène *KCNH2*.

En réduisant les courants de repolarisation, de nombreuses mutations de type "perte de fonction" dans le gène *KCNH2* peuvent allonger l'intervalle QT sur l'électrocardiogramme; ces maladies génétiques sont appelées *syndrome du QT long* (SQTL) de type *congénital*. Un intervalle QT prolongé est un facteur de risque d'arythmies potentiellement mortelles désignées sous le nom de *Torsades de Pointes*. Une autre forme de SQTL liée au canal hERG est source de préoccupation dans le domaine pharmaceutique. En effet, de nombreux médicaments ont la capacité indésirable de bloquer le canal hERG ; il en résulte une forme de SQTL *induite par le médicament*. Puisque les structures et classes thérapeutiques des médicaments impliqués sont variées, la susceptibilité de tout nouveau médicament envers le canal hERG doit être évaluée. Ceci peut conduire à une perte économique considérable si la molécule s'avère bloquer le canal potassique après des années de développement. Il existe également une forme *acquise* de SQTL qui ne s'explique pas par des mutations dans les gènes liés au SQTL ni par un blocage du canal hERG. Le SQTL acquis est également reconnu pour augmenter le risque d'arythmies ventriculaires dangereuses, bien que les mécanismes sous-jacents soient moins bien connus.

Depuis la découverte du canal hERG dans le milieu des années 90 et de son rôle central dans le SQTL, de nombreux travaux ont été entrepris afin d'élucider ses mystères. Le présent travail de thèse a cherché à mettre en lumière différents aspects de ce fascinant canal potassique.

La première étude présentée dans ce manuscrit traite de la régulation du canal hERG. Dans un système de surexpression, il a été montré que le canal potassique hERG interagit avec l'ubiquitine-ligase Nedd4-2 *via* un motif particulier (le motif PY)

présent sur sa partie carboxy-terminale. Cette interaction induit l'ubiquitylation de la protéine hERG par l'enzyme. Cette modification déclenche la régulation négative du canal présent à la membrane plasmatique et la diminution du courant mesuré. L'amélioration des connaissances sur la physiologie normale du canal hERG est un premier pas vers la compréhension de modifications physiopathologiques qui sous-tendraient le SQTL acquis.

Le deuxième aspect traité et présenté dans ce manuscrit concerne la forme *congénitale* du SQTL. Deux mutations dans le gène *KCNH2*, non décrites auparavant, ont été caractérisées fonctionnellement et présentées dans des rapports de cas distincts. Les deux sujets sont des femmes, portant toutes deux une mutation dans la partie amino-terminale de la protéine hERG, plus précisément dans une région hautement structurée, le domaine PAS. Les mutations ont été reproduites dans des systèmes de surexpression à l'état hétérozygote et ont montré une réduction d'environ 50% et 75% du courant. Cette diminution est vraisemblablement due à un défaut dans le routage des canaux mutants nouvellement synthétisés. Dans les deux cas, la perte de fonction du canal hERG peut expliquer le phénotype SQTL du patient.

La dernière section de ce mémoire aborde, par deux travaux différents, la question de la stéréosélectivité dans le blocage du canal hERG. La composante stéréosélective a été négligée en ce qui concerne l'allongement de l'intervalle QT induit par des médicament. Néanmoins, dans la première étude, l'énantiomère (S) de la méthadone a démontré être un inhibiteur plus puissant que la forme (R), cette dernière étant l'énantiomère actif pour les cibles pharmacologiques. Une reévaluation de la prescription du médicament sous sa forme racémique en faveur de la seule (R)-méthadone est également proposée. En effet, près de 6% de la population de type caucasienne et africaine serait à risque plus élevé de prolongation de l'intervalle QT dû à une métabolisation lente de la méthadone touchant préférentiellement la forme (S). La deuxième étude a tiré parti de la technique de mutagenèse et de simulations d'ancrage pour évaluer les fondements moléculaires qui régissent le bloc stéréosélectif du canal hERG par la bupivacaïne. En outre, l'ancrage d'énantiomères dans un modèle d'homologie s'est révélé être un moyen élégant de tester la stratégie développée.

Abstract of the thesis

The potassium hERG channel or *human ether à-gogo related gene* channel is responsible for the *rapid component of the delayed rectifier potassium current* (I_{Kr}), which is an important determinant of the action potential duration in the heart. It is now established that this functional voltage-gated potassium channel is formed by assembly of four α-subunits encoded by the *KCNH2* gene.

By reducing repolarizing currents, many loss-of-function mutations in *KCNH2* gene can prolong the QT interval on the ECG; such genetic disorders are referred to as *congenital Long QT Syndrome* (LQTS). Lengthening of the QT interval is a well-known risk factor for potentially lethal arrhythmias named *Torsades de Pointes*. Another hERG-related form of LQTS has been identified and causes important concern in the pharmaceutical area. Indeed, a variety of medications have the undesired ability of blocking the hERG channel and resulting in a *drug-induced* form of LQTS. Since structures and therapeutic classes are diverse, hERG liability has to be assessed for all new drugs, sometimes leading to considerable economic loss if, after years of development, the drug reveals to block the potassium channel. An *acquired* form of LQTS, which is not explained by variants in LQTS-genes or due to hERG-blocker drugs, is also recognized as increasing the risks of malignant arrhythmias, although its underlying mechanisms are less well understood.

Since discovery of the hERG channel in the mid 1990's and its central role in LQTS, a lot of work has been undertaken in the attempt of unveiling its mysteries. The present thesis work focused on bringing some light on different aspects of this fascinating hERG channel.

The first study presented in this manuscript deals with regulation of the hERG channel. In an overexpressing system, the potassium channel has been shown to interact with the ubiquitin-ligase Nedd4-2 *via* a particular motif at its carboxy-terminus, the PY motif. This protein-protein interaction promotes ubiquitylation of the hERG protein that leads to down-regulation of the channel at the plasma membrane accompanied by decrease of current. Understanding normal physiology

of the hERG channel is a first step towards comprehension of pathophysiological modifications underlying the *acquired* LQTS.

The second aspect of the hERG channel investigated and presented in the manuscript regards the *congential* form of LQTS. Two yet-undescribed *KCNH2* mutations were functionally characterized and presented in separate case reports. Both probands are females carrying mutations in the amino-terminus of the channel, more precisely in the highly structured PAS domain. The mutations were reproduced at the heterozygous state in overexpression systems and yielded about 50 to 75% decrease of current, resulting from a defect in trafficking of the synthesized mutant channel. In both cases, the reduced function of hERG may explain the LQTS phenotype of the patient.

The last section of this manuscript discusses the stereoselectivity of hERG block by drugs in two different works. The stereoselective property of channel blockade has been neglected as regards *drug-induced* prolongation of the QT interval. However, in the first study, (S)-methadone demonstrated to be a more potent blocker than the (R)-form, this latter being the active enantiomer for the intended pharmacological targets. Moreover, reevaluation of the racemic prescription in favor of the single (R)-methadone is suggested, since in addition about 6% of Caucasian and African population may be at higher risks for QT interval prolongation due to a slow metabolism affecting preferentially the (S)-form. The second study took advantage of mutagenesis analysis and docking simulations to assess the molecular determinants that govern the stereoselective block of hERG by bupivacaine. Moreover, docking of enantiomers in a homology model proved to be an elegant way to challenge the computational strategy developed.

List of abbreviations

ALLN : *N*-Acytyl-*L*-Leucyl-*L*-Leucyl-*L*-Norleucinal (proteasome inhibitor)
AP : Action potential
APD : Action potential duration
AV node : Atrio-ventricular node
C2 domain : Calcium/lipid binding domain
cAMP : cyclic Adenosine Monophosphate
Ca_v channels : Voltage-gated calcium channels
CHO cells : Chinese Hamster Ovary cells
cNBD : cyclic Nucleotide Binding Domain (in hERG C-terminus)
CPVT : Catecholaminergic Polymorphic Ventricular Tachycardia
DAAM : Dextro-α-Acetylmethadol
DAD : Delayed After Depolarization
DAG : Diacyglycerol
DM : Diabetes Mellitus
DUB : Deubiquitylating enzyme
E1 : Ubiquitin-activating enzyme
E2 : Ubiquitin-conjugating enzyme or ubiquitin-carrier enzyme
E3 : Ubiquitin protein ligase
EAD : Early After Depolarization
ECG : Electrocardiogram
EM : Extensive Metabolizer
ENaC : Epithelial sodium Channel
ER : Endoplasmic Reticulum
ERP : Effective Refractory Periode
HECT domain : Homologous to E6-associated protein C-terminus domain
HEK293 : Human Embryonic Kidney 293 cells
hERG : human Ether-à-gogo Related Gene
IC_{50} : Half-maximal Inhibitory Concentration
ICD : Implantable Cardioverter-Defribrillator
IP3 : 1,4,5-Inositol-Triphosphate
JLNS : Jervell-Lange-Nielsen Syndome
$[K^+]_{e/i}$: external/internal K^+ concentration
KO mouse : Knock-Out mouse
K_v channels : Voltage-gated potassium channels
LAAM : Levo-α-Acetylmethadol
LQT2 : Long QT Syndrome type 2
LQTS : Long QT Syndrome

List of abbreviations (continued)

MD : Molecular Dynamics
MiRP1 : Mink-Related Peptide 1 (*KCNE2*)
MMT : Methadone Maintenance Treatment
Na_v channels : Voltage-gated sodium channels
Nedd4 : Neural precursor cell-expressed Developmentally Downregulated gene 4
NMD : Nonsense-Mediated mRNA Decay
PAS domain : Per-Arnt-Sim domain (in hERG N-terminus)
PD : Pharmacodynamics
PK : Pharmacokinetics
PKA : Protein Kinase A (cAMP-dependent Protein Kinase)
PKC : Protein Kinase C
ROS : Reactive Oxygen Species
RT : Room Temperature
RWS: Romano-Ward Syndrome
SA node : Sino-atrial node
SM : Slow Metabolizer
SQTS : Short QT Syndrome
TdP : Torsades de Pointes
TTCM : Takotsubo Cardiomyopathy
UBD : Ubiquitin binding domain
WT : Wild-Type
WW : Double tryptophan (W) residues

Current and respective ion channel (official* and alternative nomenclatures)

I_{Na}	$Na_v1.5$	SCN5A
I_{to}	$K_v4.3$	KCND3
I_{Kur}	$K_v1.5$	KCNA5 or HK2
$I_{Ca,L}$	$Ca_v1.2$	CACN2 (Type L)
I_{Kr}	$K_v11.1$	hERG1 (hERG)
I_{Ks}	$K_v7.1$ (+ MinK)	KvLQT1 or KCNQ1 (+ KCNE1 or IsK)
I_{K1}	Kir2.1-Kir2.3	IRK1-IRK3
$I_{K,Ach}$	Kir3.1-Kir3.4	GIRK1-GIRK4
$I_{K,ATP}$	Kir6.2	KATP (+ SUR2)

*official name according to the IUPHAR database.

Part I
Background

I. Background

I.A. The heart

The heart has always been a mysterious organ for the human being. It has long been, and is even nowadays, considered as *the* emotional organ. Indeed, we all have experienced that intense emotions influence the heart beating rate. The Greek-Roman physician Galen (2nd century AD) was one of the first to describe the heart anatomy and to make the postulate that arteries carry "vital blood" and not air as it was previously thought (Furley & Wilkie 1984). However, Galen failed to recognize the heart's true role as a circulatory pump. It was William Harvey, physician of the 17th century, that finally related the anatomy of the heart to its blood-pumping function (Bylebyl 1979). Although great scientists, over two thousand years time, have made significant breakthroughs in our understanding of the heart and circulation system, a lot of unknown remains for modern time scientists to investigate.

The current knowledge of cardiac anatomy and function, which is a necessary prerequisite for the reading of this thesis, is summarized in the following sections.

I.A.1. Heart and circulatory system

The heart is situated obliquely in the middle, slightly to the left, *mediastinum* (the central compartment of the *thoracic cavity*), between the lungs, behind the sternum and above the diaphragm. To protect the heart and anchor it to the diaphragm, a double-walled sac, named pericardium, surrounds the organ. However, major vessels connect the heart to the entire body, which can be separated into those arriving (vena cava and pulmonary veins) and those leaving the heart (aorta and the pulmonary trunk or arteries, **Figure 1**). The heart is a hollow organ constituted of four chambers: two atria and two ventricles. A septum separates the left and the right side of the heart into two distinct pumps. In each side, specialized valves are present at the junctions of atrium and ventricle (tricuspid and mitral valves), as well as ventricle and artery (pulmonary and aortic valves, for left and right side,

respectively, **Figure 1**). The role of this double pump is to ensure the correct circulation of oxygenated blood and nutriments to the different organs of the body, including the heart itself. Oxygenated blood from the lungs, coming through the pulmonary veins into the left atrium, is pumped to the left ventricle. By contracting, the left ventricle drives the oxygen-rich blood into the aorta and back-flow of blood is prevented by the presence of the mitral valve and papillary muscles (**Figure 1**). Simultaneously, the right side of heart contracts. Deoxygenated blood from the organs arrives in the right atrium through both superior and inferior vena cava. Contraction of the atrium expels the blood into the right ventricle. Then the ventricle pumps out the blood to the lungs via the pulmonary trunk to terminate the cycle. Here again, valves and papillary muscles ensure the correct route of blood. As mentioned above, the heart too has to be provided with oxygen-rich blood; another circulatory system, the coronary circulation, allows for efficient irrigation of the pumping organ (Marieb 1998).

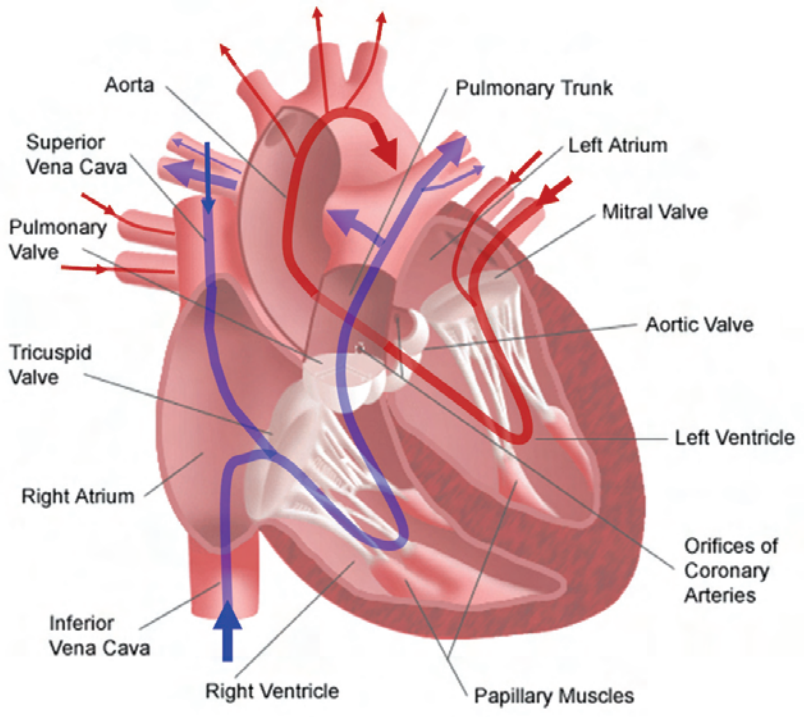

Figure 1 : **Detailed structure of the inner heart and blood circulation**.
Red arrows standing for oxygenated blood and blue for non-oxygenated blood. Modified from (Internet source 1).

I.A.2. The myocardium

As mentioned before, the heart's function is essentially to contract in order to ensure blood circulation. Contraction can only be achieved by a muscular tissue, the cardiac muscle, which is an involuntary striated muscle tissue found only within this organ. The name myocardium, literally the *muscle of the heart* (*myos kardia* in Greek), is internally covered by the endocardium and externally by the epicardium (**Figure 2**). These layers constitute the wall of the heart that isolates the heart chambers.

The *epicardium* is also known as the visceral pericardium and is involved in the pericardium *double-sac* structure that anchors the heart and protects it from friction during beating (**Figure 2**). This layer encloses the coronary blood vessels and nerves which supply the heart.

The *endocardium* is the innermost layer of tissue that lines the chambers of the heart and the valves (**Figure 2**). It is an endothelium based on a thin loose connective tissue, and it connects with the endothelium of the vessels. By creating a flat coating, it decreases friction of blood against the cardiac walls.

The *myocardium* is the middle layer of the wall and the most important constituent of the heart (**Figure 2**). It might further be divided into subendocardial, mid-myocardial and subepicardial regions. This myocardium is made of diverse types of cells, but primarily contractile cells provided with actin and myosin *myofilaments*: cardiomyocytes and M cells (in the mid-myocardium). The cardiac muscle fibers are short, thick and often branched cells, containing one or at most two nuclei. Long finger-like extensions of the plasma membrane, the *transverse* (*T*) *tubules*, penetrate deeply into the cell. T tubules are broader and less abundant (few or no T tubules in atrial cells) than in skeletal fibers, but play similarly a critical role in excitation-contraction coupling. The cardiac myocyte is the most physically energetic cell in the body, contracting constantly, without tiring, 3 billion times or more in an average human lifespan (Severs 2000). Intracellular spaces are filled with

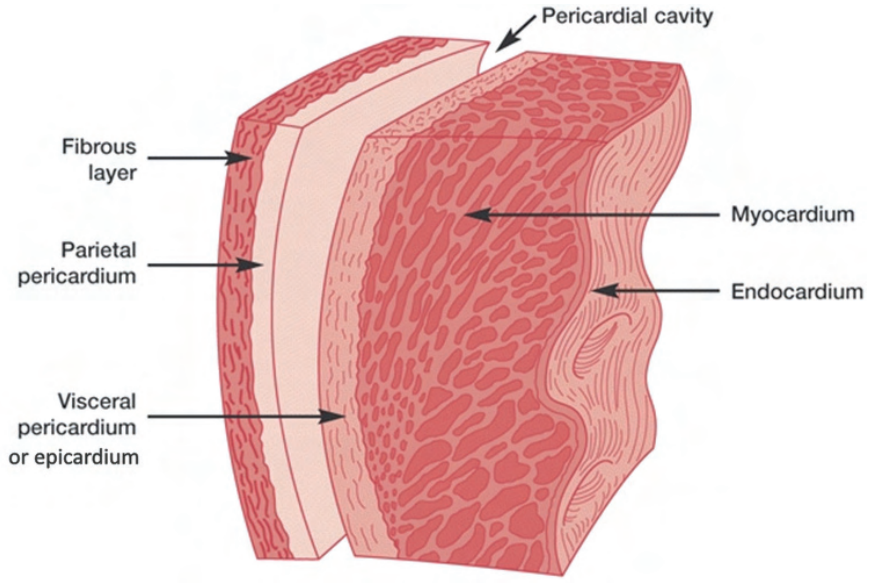

Figure 2 : Section depicting pericardium and layers of the heart wall.

The pericardium is composed by the fibrous pericardium, the parietal pericardium and the parietal cavity. The three layers of the heart wall are, from outside to inside, the epicardium or visceral pericardium, the myocardium and the endocardium. Figure modified from (Internet source 2).

endomysium, a loose connective tissue. The cardiomyocytes are associated with the *fibrous skeleton* in circular or spiral bundles that will produce a torsion movement that helps to efficiently squeeze the blood out from the heart (Marieb 1998). In contrast with skeletal muscle cells that are structurally and functionally independent, cardiomyocytes are connected through an undulating membrane structure separating adjacent cells, the *intercalated discs*. These specialized areas of the membrane contain different junctional complexes (desmosomes, adherens junctions, gap junctions) that allow force transmission during muscle contraction and enable the myocardium to function as a syncytium, with mechanical and electrical coupling of all fibers (Gutstein *et al.* 2003). They support the rapid spread of the electric impulse and the synchronized contraction of the myocardium. Coordination of contraction is achieved by a specialized conducting system that will be discussed hereafter.

I.A.3. Electrical properties of the heart

I.A.3.a. Electrical conduction system of the heart

Although the heart rhythm is largely controlled by the autonomic nervous system, a heart devoid of all nervous connections keeps beating in a regular rhythm. The independent and coordinated activity of the heart is due to the already mentioned coupling of the cardiomyocytes and to the *electrical conduction system* of the heart, also known as *nodal system* (Marieb 1998). The role of these specialized cells is to produce impulses and propagate them through the heart to obtain a synchronized contraction of the whole muscle, by coordinating its beating activity with that of its 3 billion neighbors (Severs 2000). Cells of the conducting system – derived from myocytes but with relatively low percentage of myofilaments (Opthof 1988) – join to form distinctly defined tissues: the nodes and conducting pathways (**Figure 3**). These cells have increased permeability to sodium. The slow entry of sodium produces the *pacemaker potential*, which will gradually change polarity of the membrane until a threshold and thus automatically generates an excitation wave (Solc 2007; Marieb

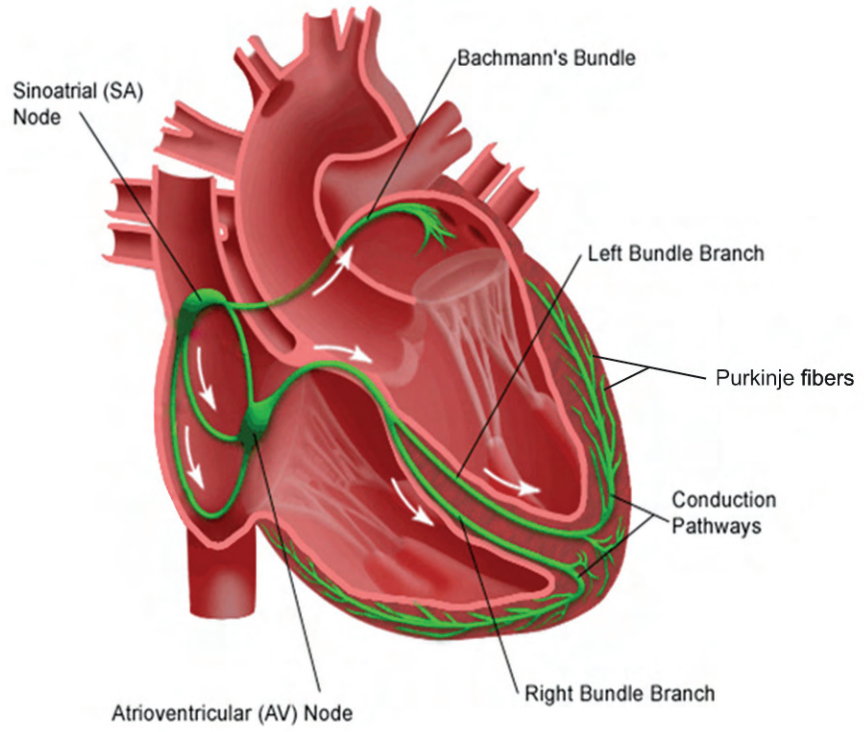

Figure 3 : Excitatory elements and conduction system of the heart (green).
Arrows indicate the direction of the impulse. Modified from (Internet source 3).

1998). It is noteworthy to mention that each portion of the conduction system exhibits the property of automaticity, with its own frequency. If a rhythmogenic center fails, the next (slower) might pace the heart.

Propagation of the excitation follows the electrical conducting pathways (**Figure 3**), with the starting point found in a cluster of cells located in the right atria and known as the *sino-atrial* (*SA*) *node*. Because it spontaneously depolarizes ~75 times per minute, the sinus rhythm determines the heart rate and is thus considered as the "pacemaker" of the heart. The excitation wave, or *action potential*, rapidly spreads through the gap junctions to the atria and propagates to the other important excitatory element, the *atrio-ventricular* (*AV*) *node*. At the AV node, just above the tricuspid valve, the influx is delayed by 100 ms to allow termination of atrial contraction before the ventricles start their own (Marieb 1998). It is noteworthy that the AV node is the only electrical connection between the atria and the ventricles (Meijler & Janse 1988). From this node, the excitation spreads along the *His bundle* and cross the ventricular septum through the right and left bundle branches. Then, *Purkinje fibers* finally carry the contraction impulse from both bundle branches to the myocardium of the ventricles (**Figure 3**). Purkinje fibers are larger than cardiac muscle fibers, thus the impulse conduction along these fibers is extremely rapid. The impulse spreads without delay throughout the ventricular myocardium, followed almost immediately by contraction of the ventricles (Marieb 1998).

I.A.3.b. Cardiac action potential and ECG

Action potential and ion channels

A cardiomyocyte, as any cell of the body, is surrounded by a phospholipid bilayer: the plasma membrane. Electric impulses propagate easily in an electrolyte solution by means of ion movements, but not in lipidic medium, which is an electric insulator. Ionic transfer through gap junctions is a current that rapidly decreases as a function of distance and could not ensure proper excitation and therefore contraction of the whole heart. Propagation of the impulse coming from the conducting system is

relayed from cell to cell in the myocardium, because cardiomyocytes are excitable cells. Their plasma membrane encompasses specialized pore-forming proteins, named *voltage-gated ion channels* because their permeabilities to ions are sensitive to the voltage (or potential) across the membrane. It is the sequential action of ion channels, involving influx and efflux of multiple ions, that produces the *action potential* (AP) of the cell. The difference in ion concentration between the inside and the outside of the cardiomyocyte creates electrical gradients and generates the membrane potential. The resting potential of myocardial cells is around -85 mV (*i.e.* the inside of the cell being negative), but under a propagating impulse from an adjacent cell the potential across the membrane becomes less negative; this phenomenon is known as *depolarization*. Depolarization is sensed by the voltage-gated sodium channels ($Na_v1.5$) that trigger a rapid sodium (Na^+) influx into the cardiomyocyte (**Figure**). The inward sodium current (I_{Na}) is typically responsible for the AP *phase 0*. $Na_v1.5$ channels will then rapidly enter into a non-conducting state (inactivated state). Thereafter follows *phase 1* with partial repolarization due to the efflux of potassium (K^+) ions through outward K^+ channels mediating I_{to}, for transient outward current (**Figure**). In the meantime, calcium (Ca^{2+}) channels, mainly L-type, are activated. Importantly, the change in intracellular calcium resulting from these currents ($I_{Ca,L}$) is essential for activating the contraction machinery of cardiomyocytes through a process called excitation-contraction coupling. The cardiac AP is characterized by a plateau (*phase 2*). The plateau phase reflects the balance between inward currents (mostly $I_{Ca,L}$) and outward currents, mainly *via* delayed rectifier K^+ channels (KCNQ1 associated with KCNE1, and hERG) as presented in **Figure** . Other currents, the sodium/calcium exchanger current ($I_{Na,Ca}$) and the sodium/potassium pump current ($I_{Na,K}$) also play minor roles during *phase 2*. The net repolarization of the membrane during the following *phase 3* is due to increased currents of the delayed rectifier K^+ channels (responsible for I_{Kr} and I_{Ks}) along with inactivation of the Ca^{2+} channels (**Figure**). Finally the inward potassium current, I_{K1}, ends the repolarization phase and sets the resting membrane potential (*phase 4*).

Importantly, after an action potential initiates, the cardiac cell is unable to start another AP until mid-phase 3, mainly due to the inactivation process of depolarizing

channels that need time to recover. This period of time is referred to as the *refractory period*, divided into a first *effective refractory period* (ERP, during which even strong stimuli are blocked) and *relative refractory period* (might allow depolarization by a strong stimulus). ERP acts as a protective mechanism, keeps the heart rate in check to prevent arrhythmias due to early after depolarizations (EADs) or delayed after depolarizations (DADs), and coordinates muscle contraction. In addition, it is a crucial condition to conduct the electrical signal in one unique direction.

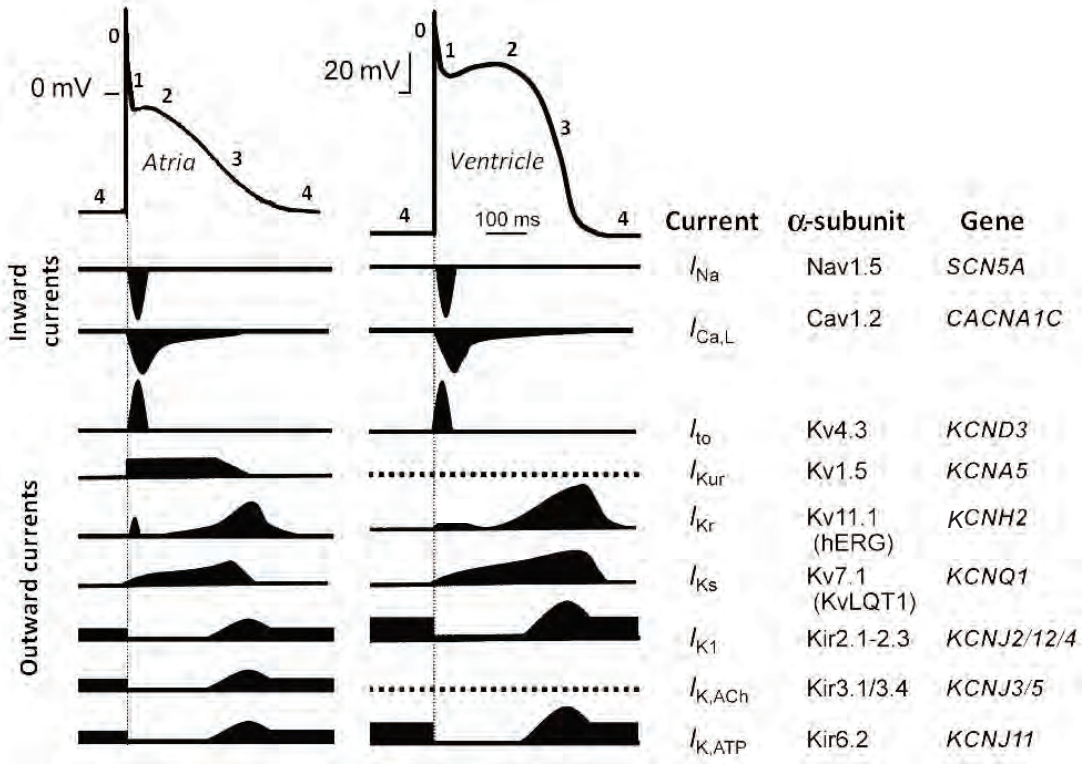

Figure 4 : Inward, depolarizing and outward, repolarizing currents that underlie atrial and ventricular action potential.

Phase 0, rapid depolarization; *phase 1*, rapid early repolarization phase; *phase 2*, plateau phase; *phase 3*, late repolarization phase; *phase 4*, resting membrane potential. Modified from (Ravens & Cerbai 2008).

Despite general similarity in the mechanisms of AP generation, action potentials exhibit distinct shapes in atrial and ventricular myocardium (**Figure**). Major differences are that the plateau phase occurs at more negative potentials in atrial cells and overall duration of the AP is shorter when compared with ventricular cells. Note, for instance, that I_{Kur} is only present in atria (Ravens & Cerbai 2008). These

differences are due to the heterogeneous distribution of ion channels and other proteins that constitute cardiac ion currents (Roden *et al.* 2002).

Cardiac ECG

Electric currents are easily transmitted in the body liquids, and electric potential differences generated in the heart can be measured by an electrocardiographic device at the surface of the body. The Dutch physiologist Willem Einthoven is known as the creator of the *electrocardiograph*, which was at the time (1902) known as

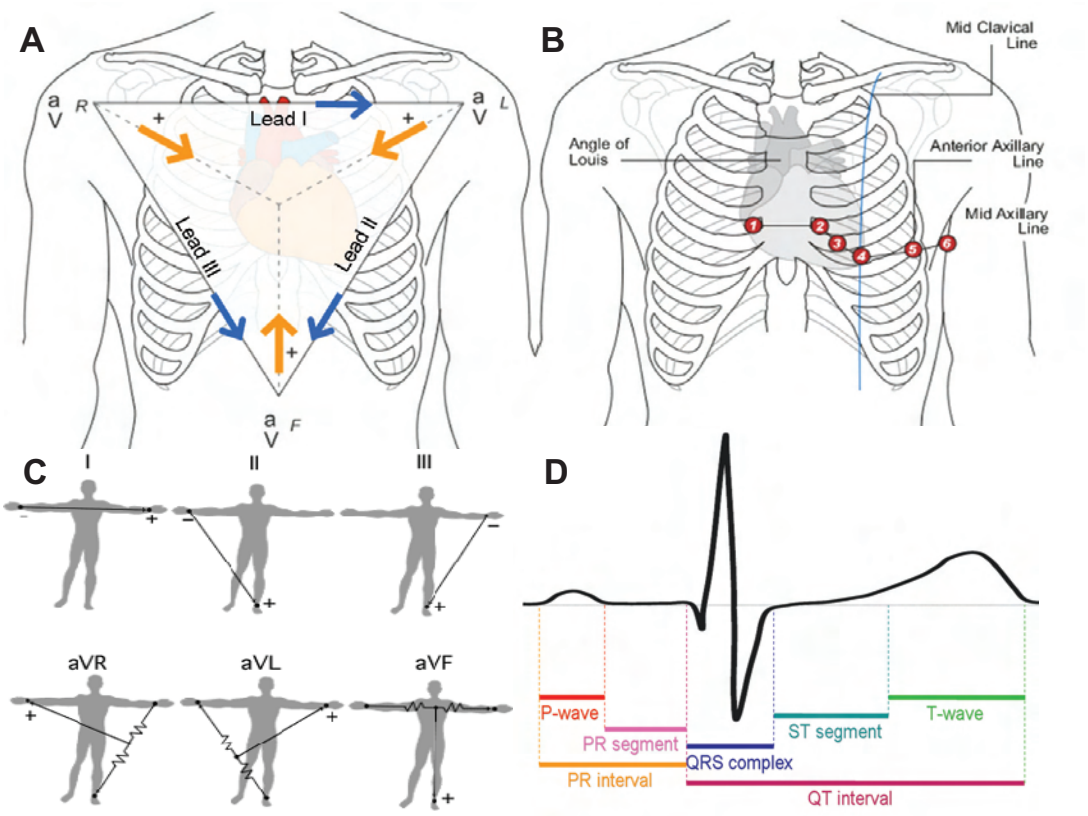

Figure 4 : Electrocardiographic leads and electrodes location, and ECG signal with characteristic features.

(A) Einthoven's triangle with bipolar (blue arrows: I, II, III) and unipolar (orange arrows: aVR, aVL, aVF) limb leads. Adapted from (Internet source 4).

(B) Precordial chest leads (V1-V6) used to record the heart's electrical activity in the horizontal plane (orange square). Adapted from (Internet source 4).

(C) The standard and augmented leads reflect the limb electrodes (left arm, right arm, left foot) used to record the heart's electrical axis in the frontal plane. Image from (Internet source 5).

(D) Representative ECG recording with typical waves and segment measurements.

string galvanometer, and is today one of the most frequently used cardiac diagnostic devices (Rivera-Ruiz *et al.* 2008). Einthoven was awarded a Nobel Prize in 1924 for his contributions to the field of electrocardiography, and his name remained in the triangle's name (**Figure 4A**) that explains the relationship between the *standard leads*.

In modern electrocardiographs, 12 leads are typically used to record the signal, which is called *electrocardiogram* or ECG. A lead can be seen as the voltage between two electrodes (positive and negative). The principle behind the way the electrical impulse is recorded in an ECG is simple, although interpretation of the results by untrained people is not always the case. When the overall electrical current of the heart goes towards a particular lead, it registers a positive deflection. Conversely, when current goes away from the lead, it produces a negative deflection, and finally, current perpendicular to the vector of the lead is recorded as an isoelectric line. By placing one electrode on each arm (right, R, and left, L) and on the lower limb (left foot, F), the *limb leads* can be obtained (**Figure 4C**). They are further separated into bipolar limb leads (I, II, III) and augmented unipolar limb leads (aVR, aVL, aVF); their vectors are presented respectively in blue and in orange arrows in **Figure 4A**. Whereas limb leads allow to view the electrical activity of the heart from the *frontal plane* (see Einthoven's triangle), electrodes placed directly on the surface of the chest (over different regions of the heart) record projections of the time-dependent changes in voltages of the heart on the *horizontal plane*. Six electrodes can be used and placed as presented in **Figure 4B** to provide unipolar precordial leads named V1 to V6, which follow the same rules of interpretation as for the limb leads.

Consequently, a typical ECG signal that reflects complete cardiac contraction presents five deflections (**Figure 4D**). The first deflection is the P wave, which represents the wave of depolarization that spreads from the SA node throughout the atria (nearly simultaneous depolarization of both atria). Deflections Q, R and S are considered altogether and referred to as the QRS complex, which reflects the ventricular depolarization. Atrial repolarization occurs during ventricular depolarization. However, because the signal of atrial repolarization is relatively small in amplitude (*i.e.* low voltage), it is masked by the large QRS complex signal. Finally,

the T wave is the result of the ventricular repolarization. Sometimes a small U wave may be seen following the T wave. The origin of this wave is still not clear and controversial, although three hypothesis are frequently quoted: i) the repolarization of the Purkinje fibers, ii) the prolonged repolarization of the M cells in the mid-myocardium or iii) after-potentials, possibly caused by mechanical forces in the ventricular wall (Ritsema van Eck *et al.* 2005). U waves appear often, but not always, in normal ECGs. Nevertheless, inverted or prominent U waves indicate underlying pathology or conditions affecting repolarization (Girish *et al.* 2005; Chikamori *et al.* 1996; Antzelevitch *et al.* 1995; Kirchhof *et al.* 2009; Perez Riera *et al.* 2008).

Assessment of the morphology and duration of the different waves serves as an important diagnosis tool. Similarly, different portions of the ECG recording have been defined (**Figure 4D**) and their duration provides useful information about the heart's activity (Marieb 1998):

- PR interval: time from the onset of the P wave to the beginning of the QRS complex. It reflects the period between the onset of atrial depolarization and the onset of ventricular depolarization.

- PR segment: isoelectric tracing that follows the P wave and ends with the beginning of the Q wave. It represents the delay of the electrical impulse at the AV node.

- QT interval: time between deflection of the Q wave and end of the T wave. It corresponds to both ventricular depolarization and repolarization, and its value roughly estimates the duration of an average ventricular AP. Importantly, at high heart rates, ventricular action potentials shorten in duration, which decreases the QT interval. In order to assess the QT interval independently of heart rate, the QT interval is expressed as a *corrected QT* interval (QTc), using *e.g*. the *Bazett's formula* that divides the QT interval by the square root of the RR interval.

- ST-segment: isoelectric tracing between end of the QRS and T-wave deflection. Its duration roughly corresponds to the plateau phase of the ventricular AP.

- RR interval: time between consecutive R waves of the ECG recording. It represents the duration of a ventricular cardiac cycle and is an indicator of ventricular rate.

I.B. Cardiac channelopathies

As mentioned earlier, every electrical activity of the heart, hence every heartbeat, is dependent on the finely orchestered activity of diverse ion channels. Disorders involving ion channels – or *channelopathies* – form a key group of heart diseases (Marban 2002), and resting or under-exercise ECGs are pivotal for their diagnosis (Schimpf *et al.* 2009). In 1957, Jervell and Lange-Nielson reported on four boys of a family who suffered congenital deafness in association with prolongation of the QT interval and syncope (Jervell & Lange-Nielsen 1957). Both parents were asymptomatic, had a normal ECG and no hearing problems. The Jervell-Lange-Nielsen syndrome (JLNS) was rapidly defined as an autosomal recessive disorder. Soon after, Romano and Ward described independent reports of prolonged QT interval associated with sudden cardiac death (SCD), though in absence of deafness (Romano *et al.* 1963; Ward 1964). This Romano-Ward syndrome (RWS) is now known to be inherited (autosomal dominant), more common than JLNS, and the severity of the disease varies considerably (Perrin *et al.* 2008; Medeiros-Domingo *et al.* 2007). Even though the genetic basis of the prolongation of the QT interval was evident, it was only in 1995-96 that the connection was achieved with the three main genes causing the so-called congenital *Long QT Syndrome* (LQTS) (Wang *et al.* 1995; Wang *et al.* 1996; Curran *et al.* 1995). The genes *KVLQT1*, *KCNH2* and *SCN5A* encode respectively the ion channels KCNQ1, hERG and $Na_v1.5$, and are now known to account for at least two-thirds of LQTS (Ackerman 2004). As often, the function of proteins is unraveled by their dysfunction (Jentsch *et al.* 2004), and since the mid

Table 1 : Additional heritable arrhythmic syndromes linked with the three principal ion channels accounting for LQTS. Adapted from (Ackerman 2004).

Gene	Ion channel	Loss-of-function	Gain-of-function
KVLQT1	KCNQ1	• Long QT syndrome (LQTS)	• Familial atrial fibrillation • Short QT syndrome (SQTS)
KCNH2	hERG1	• Long QT syndrome (LQTS)	• Short QT syndrome (SQTS)
SCN5A	$Na_V1.5$	• Brugada syndrome (BrS1) • Idiopathic ventricular fibrillation • Progressive cardiac conduction disease • Congenital sick sinus syndrome	• Long QT syndrome (LQTS)

1990's, the burst in translational research – *e.g*. high-throughput DNA sequencing, genetic linkage analyses, gene cloning, electrophysiological characterization, mathematical and molecular modelings – broadened the knowledge on cardiac channelopathies. The list of potentially heritable primary electrical diseases is not anymore restricted to LQTS, and loss- or gain-of-function mutations of a same gene can lead to different symptomatic abnormalities of the cardiac rhythm (**Table 1**). Moreover, channelopathies are nowadays not restricted to the plasma membrane ion channels (α-subunits) but also to accessory (β-)subunits or interacting proteins (Ackerman 2004). Intracellular ion channels can also be affected, such as the *ryanodine receptor-calcium release channel* (*RYR2* gene) present at the cardiac muscle sarcoplasmic reticulum, which is important for the mediation of the excitation-contraction coupling. Mutations of the RyR2 protein can lead to increased intracellular Ca^{2+} levels, increasing thereby dispersion of repolarization through the ventricular wall (transmural dispersion) responsible for arrhythmias observed in the *Catecholaminergic Polymorphic Ventricular Tachycardia* or CPVT. Individuals with CPVT characteristically present with exercise-induced syncope and/or sudden cardiac death. Unfortunately, patients show a normal resting ECG, which makes the diagnosis of difficult (Schimpf *et al.* 2009).

I.B.1. LQTS

I.B.1.a. Congenital LQTS

The long QT syndrome is the first cardiac channelopathy genetically described and is maybe the most studied, with abnormal prolongation of the QT interval as its main hallmark. The incidence of congenital LQTS is estimated at 1/3000-5000 individuals (Medeiros-Domingo *et al.* 2007). As explained earlier, prolongation of the interval ranging from the beginning of the QRS complex and end of the T wave represents the total time for ventricular depolarization and repolarization. If ventricular depolarization is affected and/or repolarizing currents are decreased (**Figure 5A**), ECG recordings will present longer QT interval values. Ventricular repolarization of the female heart is characterized by a longer heart rate-corrected QT interval. For this reason, definition of a prolonged QTc interval is gender-specific. For women, QTc

intervals are considered normal when ≤450 ms, borderline when presenting with 451 to 470 ms, and prolonged if >470 ms; for men, the cut-off is 20-ms lower, *i.e.* QTc intervals are normal when ≤430 ms, borderline between 431 and 450 ms, and prolonged when duration is >450 ms (Committee for Proprietary Medicinal Products 1997). Abnormally long QT intervals present a higher risk of generating a malignant type of ventricular tachycardia commonly called *Torsades de Pointes* or TdP (Dessertenne 1966). This was symbolically termed "twistings of the points" (about the isoelectric axis, see **Figure 5B**) because it reminded the original author of the *torsades de pointes* movement in ballet. Despite the nice image it refers to, TdP causes syncope that can either solve spontaneously, lead to seizures or, in the worst case, lead to sudden cardiac death (Ackerman 2004). Mechanisms underlying arrhythmogenesis in LQTS are complex. However, it is widely accepted that prolongation of repolarization may lead to activation of an inward depolarization

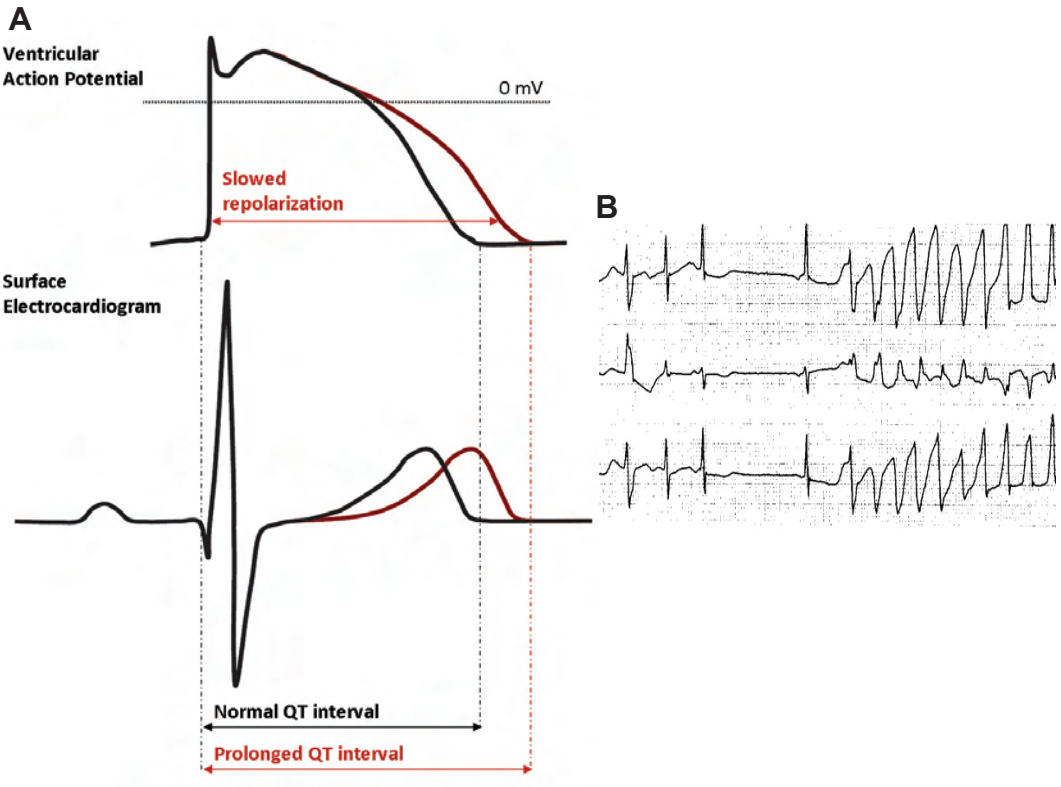

Figure 5 : Ventricular action potentials and related ECG signals. Prolonged QT interval is a risk factor for *Torsades de Pointes*.

(A) Prolongation of ventricular action potential duration (red) is reflected in prolongation of QT interval on the ECG recording (red trace).

(B) ECG recording presenting onset of TdP in a patient with long QT syndrome. Modified from (Internet source 6).

current ($I_{Ca,L}$ and I_{Na}) that generates EADs (due to the relative shortening of ERP), which in turn promotes triggered activity at the end of the repolarization. When accompanied with marked dispersion of repolarization, this may induce reentry phenomena and provoke TdP, sustained by further reentry or spiral wave activity (Camm *et al.* 2004).

For many years, it was taken for granted that each patient affected by LQTS had a prolonged QT interval (Priori *et al.* 1999). However, some patients do not present clinical symptoms and up to 36% of patients with a genetic subtype of LQTS (affecting *KVLQT1*) present with normal QTc intervals (Priori *et al.* 2003). The congenital long QT syndrome (*c*LQTS) is far from being a homogeneous disease, notably because of the variable penetrance of the disease, *i.e.* patients who have the mutation and manifest the phenotype (Priori *et al.* 1999), and the genetic heterogeneity. Indeed, several hundreds of mutations distributed in 12 genes have been described in this condition: *KVLQT1, KCNH2, SCN5A, KCNE1, KCNE2, ANKB, KCNJ2, CACNA1, CAV3, SCN4B,* and more recently *AKAP9* (Chen *et al.* 2007) and *SNTA1* (Ueda *et al.* 2008). The genes involved in *c*LQTS are conventionally named LQT1-12 as detailed in **Table 2**. It is not surprising to see that the main genes related to congenital LQTS are encoding ion channels and associated subunits. Genetic

Table 2 : First ten described genes involved in the long QT syndrome. Adapted from (Medeiros-Domingo *et al.* 2007).
Two additional forms of LQTS (with frequencies <1%) should be added to this table: LQT11 - AKAP9 gene (locus 7q21-q22) encoding the AKAP9/Yotiao protein, and LQT12 - *SNTA1* gene (locus 20q11.2) encoding the α-1-syntrophin protein.

Type	Locus	Gene	Protein	Current	Effect	Frequency, %
Romano-Ward (autosomal dominant)						
LQT 1	11p15.5	*KCNQ1/KVLQT1*	Principal, I_{Ks} α-subunit	K	↓	30-35
LQT 2	7q35-36	*KCNH2/HERG*	Principal, I_{Kr} α-subunit	K	↓	25-30
LQT 3	3p21-p24	*SCN5A*	Principal, I_{Na} α-subunit	INa	↑	5-10
LQT 4	4q25-q27	*ANKB*	Accessory, ankyrin-β	Na/Ca	↑	<1
LQT 5	21q22.1	*KCNE1/minK*	Accessory, I_{Ks} β-subunit	K	↓	<1
LQT 6	21q22.1	*KCNE2/MiRP1*	Accessory, I_{Kr} β-subunit	K	↓	<1
LQT 7[a]	17q23	*KCNJ8*	Principal, K_{ir}2.1 α-subunit	K	↓	<1
LQT 8[b]	12p13.3	*CACNA1*	Principal, C_{av}1.2 α-subunit	Ca type L	↑	<1
LQT 9	3p25	*CAV3*	Accessory, caveolin 3	Na	↑	<1
LQT 10	11q23	*SCN4B*	Accessory, I_{Na} β4-subunit	Na	↑	<1
Jervell-Lange-Nielsen (autosomal recessive)						
JLN1	11p15.5	KCNQ1/KVLQT1	Principal, I_{Ks} α-subunit	K	↓	>90.5
JLN	21q22.1	KCNE1/minK	Accessory, I_{Ks} β-subunit	K	↓	<0.5

[a]Andersen-Tawil Syndrome
[b]Timothy syndrome

testing in LQTS can detect an underlying mutation (genetic diagnosis) in ~70% of patients (Schimpf *et al.* 2009). However, negative genetic screening cannot rule out the disease.

Interestingly, for the most common and better-known forms of Romano-Ward syndrome (LQT1-3, **Table 2**), specific characteristics can be mentioned at the ECG level, as well as potential triggers for TdP and response to treatment (Schimpf *et al.* 2009; Medeiros-Domingo *et al.* 2007; Khan 2002a; Schwartz *et al.* 1995).

Patients with LQT1 often present with broad-base T wave of very prolonged duration. Physical activity was identified as the trigger in >70% of arrhythmic events in patients with an LQT1. More precisely, swimming is a typical predisposing factor for cardiac events. As regards long term treatment, β-blockers (*e.g. atenolol*), which reduce the adrenergic stimulation, are particularly effective in patients with I_{Ks} channel mutations.

Individuals diagnosed with LQT2 commonly present a biphasic (with notching) and low-amplitude T wave on the ECG recordings. They characteristically have syncope or sudden death following sudden auditory stimuli (~50%) or with strong emotion, and less frequently during sleep (~20%) or exercise (~30%). Women with LQT2 in the postpartum period are a particularly susceptible subset of patients. As regards preventive treatment, β-blocker medication seems also effective to reduce TdP events, though less than for LQT1. Oral potassium supplementation was shown to correct the abnormalities of repolarization duration and shorten the QTc interval in the *c*LQTS type 2 (Etheridge *et al.* 2003).

In contrast, the ECGs in LQT3 patients usually show a delayed, pointed T wave and allow clear observation of the ST segment prolongation. Patients with LQT3 have a higher incidence of sudden death during rest (sleep) or bradycardia. These patients usually have fewer symptoms than those with LQT1 or LQT2, but the events are characteristically more lethal. The understanding of the molecular basis of the LQT3 allowed new therapeutic treatments. Sodium channel blockers of the anaesthetics class such as *mexiletine* and *flecainide* – drugs that significantly shorten the QTc interval – were reported to be beneficial to this subtype of *c*LQTS (Schwartz *et al.*

1995; Benhorin *et al.* 2000). Because they are more prone to SCD at low heart rates, LQT3 patients may be more likely to benefit from implantation of pacemakers pacing at relatively high rates.

Regarding the long-term preventive therapy, which aims at shortening the QTc interval and preventing *Torsades de Pointes*, many other drugs have been used sporadically, and among them Ca^{2+} channel blockers (*verapamil*), K^+ channel activators for *c*LQTS subtype 1 and 2 (*nicorandil*, *pinacidil*, *chromakalim*) and other Na^+ channel blockers for LQT3 (*pentisomide*, *lidocaine*, *phenytoin*), but their use needs further investigation (Khan & Gowda 2004). Implantable cardioverter-defribrillators (ICDs) are an invasive solution for high-risk LQTS patients with documented malignant arrhythmias, recurrent syncope, or an aborted cardiac arrest. However, an ICD does not prevent *Torsades de Pointes*: it precludes sudden cardiac death when TdP are prolonged or degenerate into ventricular fibrillation (very rapid, uncoordinated and ineffective contractions). Thus, combination of first-line treatment β-blockers and ICD should be continued to prevent occurrence of TdP. Moreover, unnecessary shocks from the device may produce emotional distress and cause adrenergic stimulation, sufficient to precipitate TdP. This is another reason that motivates β-blocker co-treatment. For patients who experienced frequent shocks from their ICD, or for whom first-line therapies failed (high doses of β–blockers, pacemakers and ICDs), the left cervicothoracic sympathectomy is a highly effective method for adrenergic therapy (Khan 2002a). It consists in the removal of part of the stellate ganglia and T2-T4 left thoracic ganglia of the sympathetic chain. Beneficial effects were confirmed for LQT1, but are likely to be smaller for LQT2 and LQT3 patients (Medeiros-Domingo *et al.* 2007).

Moreover, it is important to recommend exercise restriction, for both symptomatic and asymptomatic patients, as it might trigger TdP. More importantly, aggravating factors, such as modified health conditions or consumption of several drugs that prolong the QT interval, have to be strictly controlled if not avoided. By themselves, theses factors are known to cause the *acquired* (*a*LQTS) or, when involving drugs, the *drug-induced* (*di*LQTS) form of long QT syndrome.

I.B.1.b. Acquired LQTS

Studies on channelopathies have yielded important insights into the pathophysiology of some far more common diseases (Marban 2002), such as *congestive heart failure* that afflicts hundreds of millions of people worldwide. We now know that heart failure represents a common *acquired* form of the long QT syndrome. Myocytes from failing hearts show prolongation of action potentials, and their repolarization *in vivo* is abnormally labile (Marban 2002). Other cardiovascular diseases, such as coronary artery disease, left ventricular hypertrophy or cardiomyopathy, produce remodeling of cardiac ion channel expression resulting in electrical imbalance of AP-generating currents, thus leading to *a*LQTS (Swynghedauw & Chevalier 1995; Tsuji *et al.* 2002).

Electrolyte disturbances have been linked with the acquired LQTS. Low extracellular potassium is known to prolong the AP duration (APD) – an effect not predictable from simple electrochemical considerations (Roden 2006). Apart from hypokalaemia, other electrolytic imbalances have also been reported, such as hypomagnesaemia or hypocalcaemia (Khan 2002b).

Many other conditions – connected directly or not with the cardiovascular system (Khan 2002b) – have been related to the acquired form of the syndrome and increased risks for arrhythmic events, although in the absence of mutations in the known LQTS-genes or drugs prolonging the QT interval. These health conditions are

Table 3 : Selected causes of acquired LQTS, modified from (Camm *et al.* 2004).

Heart disease	**Renal disease**
Coronary artery disease	**Endocrine disorder**
Heart failure	Hypothyroidism
Ventricular tachyarrhythmias	Hyperparathyroidism
Dilated cardiomyopathy	Pheochromocytoma
Left Ventricular hypertrophy	Hyperaldosteronism
Hypertension	**Intracranial pathology**
Bradycardia (SA nodal dysfunction, AV block)	Subarachnoid hemorrhage
Myocarditis	Head injury
Metabolic abnormalities	Encephalitis
Hypokalaemia	**Diabetes mellitus**
Hypocalcaemia	**Anorexia nervosa/starvation**
Hypomagnesaemia	**Bulimia**
Liver disease	**Obesity**
Cirrhosis	**Liquid protein diet**
Hepatic failure	**Human Immunodeficiency Virus (HIV) infection**

namely hypothyroidism, stroke or CNS lesions, malnutrition, human immuno-deficiency virus infections, hypothyroidism or myocardial ischemia (**Table 3**).

I.B.1.c. Drug-induced LQTS

From what has been explained, drugs that cause an electrolyte imbalance, *e.g.* potassium-wasting diuretics, could be considered as a factor for both *drug-induced* and *acquired* LQTS. In fact, drugs prolonging the LQTS have long been included as an additional risk factor for the acquired form. Moreover, drug interaction with any ion channel that contributes to cardiac repolarization could in theory produce LQTS. However, clinically relevant prolongation of QT interval is invariably the result of drug blockade of a unique target: the *hERG channel* (Perrin *et al.* 2008). Nowadays, drug-induced LQTS is regarded as a separate form of this arryhthmogenic disorder almost restricted to *blockers* of the hERG channel.

The first described case of *di*LQTS is probably attributable to *quinidine* (antiarrhythmic agent class Ia, intended to act on Na^+ channels) in the 1920's, *i.e.* much before description of the disease and the understanding of the molecular bases involved. Indeed, syncope on initiation of quinidine therapy was recognized shortly after the introduction of the drug (reviewed in Roden 2006). Later in the development of antiarrhythmic therapy, molecules have been designed to specifically block K^+ currents (class III): *dofetilide* and *ibutilide* (for structure, refer to Appendix I). Unfortunately, such drugs predictably evoke prolongation of the QTc interval, which is sufficient to cause potentially lethal ventricular arrhythmias in 5-7% of recipients (Marban 2002). Theses drugs, along with other molecules of the methaneulfonanilide group, were reported to block the hERG channel (Spector *et al.* 1996a; Yang *et al.* 1997). In fact, many structurally unrelated drugs (see Appendices I and II), designed to act as non-cardiac targets, unintentionally block the repolarizing current I_{Kr}. In the past 15 years, the most common cause of withdrawal or restriction of use of drugs already marketed has been the prolongation of the QT interval associated with *polymorphic ventricular tachycardia* or TdP. The rare incidence of these arrhythmias explains why they were not readily observed during clinical trials or post-marketing surveillance. Many drugs have therefore been removed from the

market after years of use or had their availability severely restricted because of this rare form of potentially fatal toxicity. These compounds (see Appendices I and II for structures) can be antimuscarinic drugs like *terodiline* (withdrawal in 1991) or antianginal agents like *mibefradil* (1998); drugs used to treat allergy symptoms like the anti-histaminic *terfenadine* and *astemizole* (withdrawal in 1998 and 1999, respectively); antibiotics like *grepafloxacin* (1999); gastrointestinal prokinetic *cisapride* (2000) and analgesic *levo-α-acetylmethadol* (2003) were concerned; some neuroleptic drugs are no more commercialized, like *sertindole* (since 1998) or *thioridazine* (2005). This is not an exhaustive list of hERG channel blockers. Many drugs known to prolong the ventricular repolarization are still on the market (see *www.QTdrugs.org*), because their benefits are considered higher than the cardiac risk. As regards newly developed drugs, regulatory authorities demand systematic assessment of the TdP risk (for preclinical tests, see Appendix III) to avoid other disastrous consequences for both pharmaceutical companies and public health.

It is noteworthy that prolongation of the QT interval is not always linked with occurrence of *Torsades de Pointes*. As mentioned previously, patients with prolonged QTc interval can live without symptoms; only 12% of asymptomatic patients will develop arrhythmias and may experience SCD (Medeiros-Domingo *et al.* 2007). A decade ago, Roden proposed the principle of *repolarization reserve*, *i.e.* that a normal heart includes multiple, redundant mechanisms to accomplish normal repolarization. Hence, lesion of one of these mechanisms may not be sufficient to elicit an absolute LQTS phenotype (Roden 1998). For example, a subject with subclinical congenital LQTS can become manifest only on exposure to an I_{Kr} blocker. Similarly, a female patient presenting with anorexia or under strict diet – factors reducing the repolarization reserve – might experience TdP under *fluconazole* (an antifungal treatment that blocks the hERG channel). Interestingly, the concept of repolarization reserve has the advantage of drawing connections between all forms of LQTS – *congenital*, *acquired* and *drug-induced* – and allowing a better understanding of the risks for asymptomatic *c*LQTS-diagnosed patients.

I.B.2. SQTS

In 2000, the link between a persistently shortened QT interval and arrhythmia was first described in a sporadic case suffering from SCD and paroxysmal atrial fibrillation (Gussak *et al.* 2000). Since then, the arrhythmic potential of shortened QT interval was confirmed, and *Short QT Syndrome* (SQTS) is now considered a new cardiac channelopathy. The risk of arrhythmic events is high in patients with SQTS and cardiac arrest is the most frequent clinical presentation. Atrial fibrillation was also documented in about 30% of patients (Schimpf *et al.* 2009). Electrocardiographic hallmarks of SQTS are constantly short QTc intervals, short or even absent ST segment, and often tall, narrow and symmetrical T waves in chest leads (Schimpf *et al.* 2009). In contrast to prolonged QTc values, there is no clear consensus for the lower limit of the QTc interval, and therefore no threshold value is available to differentiate between pathological and healthy individuals (Schimpf *et al.* 2009).

Regarding the genetic base of the SQTS, the disease reveals to be also genetically heterogeneous with, until now, five genes affected. Underlying gain-of-function mutations in repolarizing K^+ channels are responsible for SQT1 (*KCNH2* gene), SQT2 (*KVLQT1* gene) and SQT3 (*KCNJ28* gene, for I_{K1} current); loss-of-function mutations in α1-subunit (*CACNA1c* gene) and β-subunits (*CACNB2b* gene) of cardiac L-type calcium channels, give rise to SQT4 and SQT5, respectively (Patel & Antzelevitch 2008). Note that, likewise to *c*LQTS, KCNQ1 and hERG channel-encoding genes are one of the molecular bases of the arryhthmogenic disorder.

In the first two chapters, the essentials regarding cardiac function and ion channel disorders were presented. Description of the cardiac activity and AP fundamentals highlighted that the outward I_{Kr} current, mediated by hERG channels, is one of the most important determinants for termination of the plateau phase. Either gain-of-function or loss-of-function mutations in the *KCNH2* gene (encoding hERG) demonstrated to be responsible for congenital cardiac disorders (LQTS, SQTS) that can lead to potentially lethal ventricular tachyarrhythmias. Moreover, the drug-

induced form of LQTS seems to be almost uniquely linked to the block of the hERG channel. The following chapter will get to the heart of the matter and introduce in more details the main protagonist of this thesis work. Some important advances in the knowledge of this puzzling, though fascinating, potassium channel will be summarized.

I.C. The hERG potassium channel

I.C.1. Discovery of hERG *and the* EAG *channel family*

Discovery of the hERG channel started with the identification of the mutated gene (the *ether-à-gogo* locus - *EAG*) responsible for leg-shaking behavior of *Drosophila melanogaster* during ether anesthesia. The striking hyper-excitability of *eag* mutants demonstrated the importance of these channels in maintaining normal neuronal excitability in the fly. Using homology screening, related cDNA sequences were obtained from different species, namely human and mice (Warmke & Ganetzky 1994). They were later divided into three different subfamilies of the *EAG* gene family: i) *eag,* ii) *eag*-like K^+ channel (*elk*) and iii) *eag*-related gene (*erg*) (Trudeau *et al.* 1995). The hERG channel, or the human *ether-à-gogo* related gene channel, belongs to the last subfamily.

In the human, the *eag*-related gene or *erg* subfamily comprises three members, named hERG1, hERG2 and hERG3 that are encoded by three different genes (*KCNH2*, *KCNH6* and *KCNH7*, respectively). According to another nomenclature system, these proteins can be referred to as $K_v11.1$, $K_v11.2$ and $K_v11.3$ (for K_v family 11, members 1, 2 and 3, respectively). The strong conservation of sequences from *Drosophila* to mammals suggests preservation of neuronal functions as well. Indeed in humans, hERG channels are expressed in neurons (Emmi *et al.* 2000), but also in a range of other tissues including neuroendocrine glands (Rosati *et al.* 2000), various cancer cells lines (among others gastric, breast, lung, colon, lymphocytes) (Chen *et al.* 2005; Bianchi *et al.* 1998) and smooth muscle cell (Shoeb *et al.* 2003). However, hERG1 channels have been better characterized in the heart, where their expression is higher in ventricles than atria (Pond *et al.* 2000).

Finally, the subfamily member hERG1 has three[1] splice variants identified so far (refer to **Figure 7**, page 28): hERG1a (longest transcript), hERG1b (isoform with a shorter N-terminus) and hERG-$_{USO}$ (shorter isoform with a different C-terminus) (Bauer & Schwarz 2001). In the heart the hERG1a isoform, the originally described cDNA, is commonly regarded as the primary subunit that forms the channel mediating I_{Kr}. In the context of the present work, we will further use hERG (or hERG1 in particular publications) to refer to the cardiac hERG1a isoform.

I.C.2. Structure and function

Sequence alignments of *Drosophila*, mouse and human EAG channels with sequence databases have shown that they are structurally related to voltage-gated K^+ channels (K_v channels) and cyclic nucleotide-gated cation channels (Warmke & Ganetzky 1994). Electrophysiological recordings from Trudeau *et al.* (1995) revealed that the *KCNH2* gene encoded a K^+ channel with inwardly rectifying properties, despite the extensive homology (49% of amino acid identity) with the outwardly rectifying members of the EAG family. This appeared unusual, because inward rectifiers, like the cardiac Kir2.1 (I_{K1}), were known to be constituted of two transmembrane domains and, in contrast, hydropathy profiles for hERG channel predicted six putative transmembrane domains. Combinations of methods as different as the patch-clamp technique, biochemical assays, mutagenesis analyses and atomic resolution of ion channels allowed for a better assessment of the contribution of structural elements in hERG K^+ channels to their functions of eliciting the I_{Kr} current.

I.C.2.a. Predicted topology of hERG

As other K^+ channels, hERG channels are suggested to be tetramers formed by the assembly of four α-subunits, each consisting of six putative transmembrane domains (named S1 to S6) with the S1 to S4 domains serving as the voltage sensor (**Figure 6A**). As for other EAG channels, the S5 , pore- and S6 helices are the pore-forming

[1] A fourth splice variant, hERG1b-$_{USO}$, has recently been identified in cancer cells (Guasti *et al.* 2008).

domains and contain in the upstream of S6 a characteristic motif (GxG, G for glycine and x for any amino acid) known as the signature sequence of the *Selectivity Filter* (SF) for K^+ ions. hERG possesses a unique turret loop or S5-P linker that, as suggested by the name, connects the S5 with the pore-helix. Finally, both carboxyl- (C-) and amino- (N-)termini are intracellular, similarly to all K_v channels.

Importantly, Warmke and Ganetzky (1994) rapidly identified a *cyclic Nucleotide Binding Domain* (cNBD) in the C-terminus of the hERG protein (**Figure 6A**, **Figure 7B**). When Keating's group linked *KCNH2* mutations to the LQTS, they reported a family

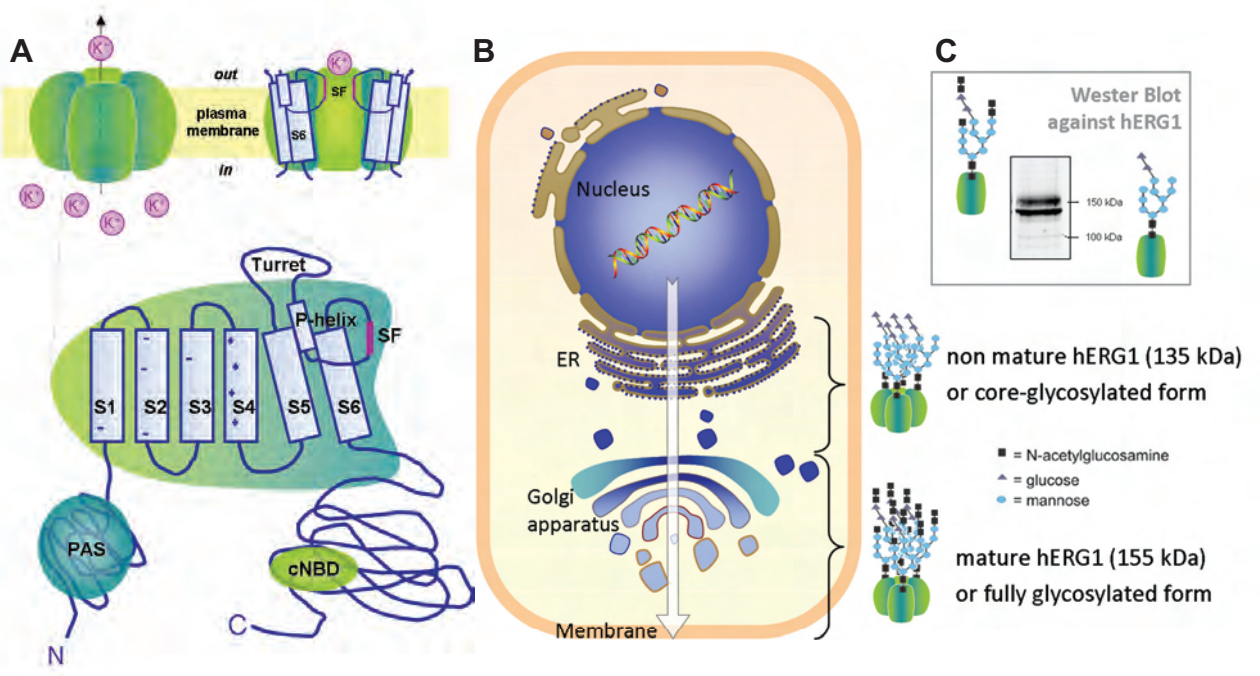

Figure 6 : Series of cartoons depicting putative hERG channel structure and maturation process.

(A) Schematized hERG tetramer (left) and pore-forming region (right) of the channel at the plasma membrane. Magnification of one α-subunit (down) with six transmembrane domains (S1-S6), S5-P linker or turret loop, pore-helix (P-helix) and selectivity filter (SF). Both N- and C-termini are intracellular with respectively identified *Per-Arnt-Sim* (PAS) domain and *cyclic Nucelotide Binding Domain* (cNBD). **(B)** Post-translational processing of hERG channels through *Endoplasmic Reticulum* (ER) and *Golgi apparatus*, with localization of non-mature or core-glycosylated and mature or fully glycosylated forms.

(C) Western blotting against a C-terminal epitope of hERG allows for identification of mature (155 kDa) and non-mature (135 kDa) α-subunits of hERG channel.

with splice-error mutation affecting the cNBD (Curran *et al.* 1995). Though importance of this domain was exemplified in 1995, its role is not yet well understood. Logically, and as proposed by the discoverers of *EAG* channel (Warmke & Ganetzky 1994), cNBD might be a modulation site involving direct binding of cAMP to the channel. This hypothesis was tested a few years later (Cui *et al.* 2000) and the study brought conclusions that cAMP regulated the hERG K^+ channel by dual and opposed pathways: i) activation of cAMP-dependent *protein kinase A* (PKA) causes phosphorylation of hERG accompanied by reduction in current amplitude, and ii) in parallel, cAMP direct binding to the hERG protein causes opposing effects (leftward shift in voltage-dependence of activation). Summation of cAMP-mediated effects leads to a net diminution of the current. However, when adding MinK or MiRP1 (MinK Related Peptide 1), which are two accessory proteins of K^+ channels, stimulatory effects of cAMP are favored (Cui *et al.* 2000). Regarding the cNBD function, a recent study analyzing lysine mutations at surface residues of the cNBD showed that the presence of a band of hydrophobic residues is crucial for inactivation and also deactivation kinetics (Al-Owais *et al.* 2009). The mechanism is not yet understood and could act through interaction of hydrophobic regions within the channel or involvement of conformational movement of the protein.

On the contrary to what was described for other six transmembrane/one pore K_v channels, in which a cytoplasmic N-terminal T1-domain was involved in assembly, a domain required for the tetramerization of α-subunits appears to be encompassed in the C-terminus of hERG (Ludwig *et al.* 1997; Jenke *et al.* 2003; Kupershmidt *et al.* 1998). Ludwig *et al.* (1997), using various truncated protein constructs, defined a minimal *C-terminal assembly domain* for homophilic rat *eag* subunit interaction and suggest the same for hERG. Moreover, a later study on the *EAG* superfamily showed that mutations in this region dramatically impair channel functional expression and proposed this domain to have a *coiled coil structure* (Jenke *et al.* 2003). Coiled coils are protein-protein interaction domains with a helical arrangement and sequences that drive formation of multimers in an aqueous environment. Interestingly, the 3'-splice variant hERG-$_{USO}$ is devoid of part of the C-terminus (**Figure 7B**). Alone, hERG-$_{USO}$ is not able to generate current in heterologous expression systems, but co-

expression with variant 1a of hERG leads to modified currents. This suggests that, though lacking the coiled coil domain, hERG-$_{USO}$ subunits may be assembled in a heteromultimer (Kupershmidt *et al.* 1998). Moreover, an endoplasmic reticulum (ER) retention signal – the RxR consensus sequence (R for arginine) in **Figure 7B** – was also identified at the C-terminal end of hERG (Kupershmidt *et al.* 2002; Jenke *et al.* 2003). This motif appears to play an important role in the correct maturation of the channel proteins. When mutated (to LxL, L for leucine) or masked by correct folding or tetramerization of the protein, the protein escapes the ER; if the RxR motif is exposed, the protein will be trapped in the ER resulting in reduced cell surface trafficking (Kupershmidt *et al.* 2002).

The other important intracellular stretch of the hERG α-subunit is at the N-terminus (~400 *versus* ~500 amino acids for C-terminus). Interestingly, the variant hERG1b is lacking a long sequence in the amino-end, including the so-called proximal domain and the Per-Arnt-Sim (PAS) domain (**Figure 7A**). Both terminal domains revealed to be important for gating of hERG channel and will therefore be discussed later. Similarly, transmembrane domains and connecting loops have shown

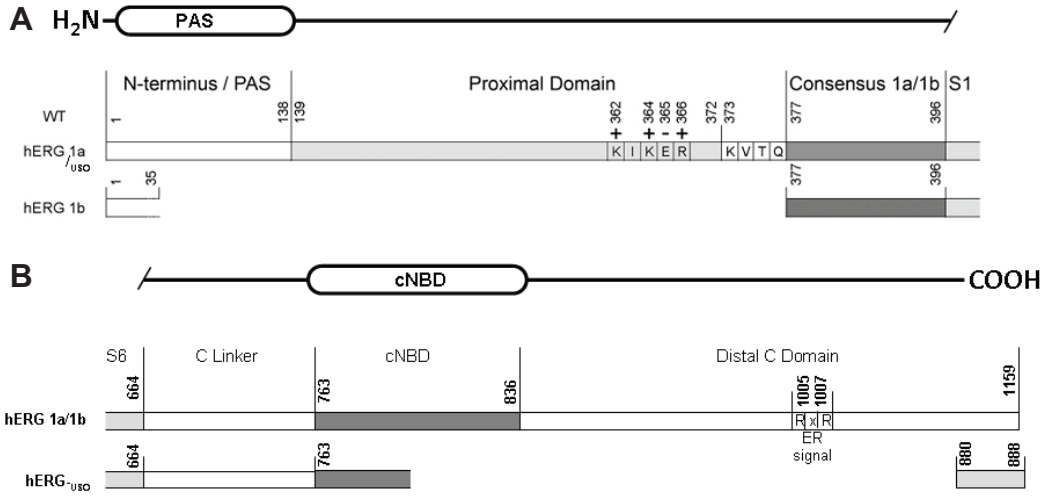

Figure 7: Schematic intracellular N- and C-terminal cDNA of hERG splice variants.
(A) Details of the N-terminus sequences (bars are not to scale) of the three isoforms of hERG with identified domains. Cluster of charged residues marked with (+) and (-) signs. Modified from (Saenen *et al.* 2006).
(B) Details of the C-terminus sequences (bars are not to scale) of the three isoforms of hERG with identified domains. Adapted from (Kupershmidt *et al.* 1998; Perrin *et al.* 2008).

involvement in the hERG gating; their structure-function relationship will be described hereafter.

One of the last important features identified by Warmke and Ganetzky (1994) when they analyzed the sequence alignment of the hERG transcript was a consensus site for N-glycosylation at position 598 (downstream of the S5 transmembrane domain). Indeed, the hERG1a sequence is a 1159 amino acid-long protein that would be expected in a Western blot at ~126 kDa (ExPASy calculation tool, *www.expasy.ch/tools/pi_tool.html*), but practically two clearly separate bands are observed at about 135 and 155 kDa (refer to **Figure 6C**, page 26). The group of Zhou and January related these bands with two different N-glycosylation patterns: the core- and the fully glycosylation of hERG subunits (Zhou *et al.* 1998b; Gong *et al.* 2002). As hERG is a membrane-associated protein, it will follow the secretory pathway, which consists in, in order, the endoplasmic reticulum, pre-Golgi intermediates, the Golgi apparatus, and different types of post-Golgi carriers and vesicles (**Figure 6B**). The secretory system accomplishes a multitude of interrelated functions: trafficking of *de novo* synthesized membrane proteins, quality control of glycoprotein folding and assembly, sorting of glycoproteins to their final cellular destinations (in this case, the plasma membrane), and posttranslational N-glycosylation (Roth 2002). The biosynthesis of asparagine-linked oligosaccharides proceeds in distinct but complex steps that are initiated in the ER; it is now admitted that the 135-kDa hERG protein results from these first post-translational modifications. Through the different cisternae of the Golgi apparatus, hERG-oligosaccharides undergo subsequent elongation, trimming and branching of sugar moieties. From the Golgi to the final destination, the hERG protein will present a weight of 155 kDa (**Figure 6B** and **7C**). As the fully glycosylated form is mainly found at the membrane, it is often called mature form (*versus* precursor or non-mature form for the 135-kDa band). The role of the hERG glycosylation was thought to be essential for proper trafficking to the cell surface (Petrecca *et al.* 1999). Conversely, Gong *et al*. (2002) demonstrated that unglycosylated α-subunits were still detected at the cell surface and could elicit a functional current (though smaller). Nevertheless, hERG channel stability at the membrane was decreased when unglycosylated. More generally, mutations in the *KCNH2* gene that result in poor or

non-detection of the mature band are associated with trafficking defects rather than essential glycosylation defects.

I.C.2.b. Gating of hERG

When considering the profile of I_{Kr} (in full name: the *rapid component of the delayed rectifier potassium current*) during the time-course of one AP, it is noteworthy to see that only little current passes during the plateau phase and that it becomes much larger during the repolarization phase (refer to **Figure** , page 10). The crucial function of hERG currents in normal repolarization and suppression of propagation of premature beats (Lu *et al.* 2001) is due to the gating of hERG channels and their peculiar kinetics. hERG channels, just like K_v channels, can exist in at least three distinct conformational states (**Figure 8**): closed (C; thus non-conducting), open (O; the only conducting state) and inactivated (I; another non-conducting state). During depolarization of the membrane, the channel undergoes sequential change of conformation (C ⇨ O ⇨ I), and repolarization reverses the transitions between these channels states (**Figure 8**). Transitions between C and O are due to constriction and widening of an "activation gate" in the intracellular half of the S6 helices. Transition from O to I is known as a *C-type inactivation* resulting, in hERG channels, from constriction of the conduction pathway at the level of the selectivity filter ("inactivation gate") (**Figure 8**).

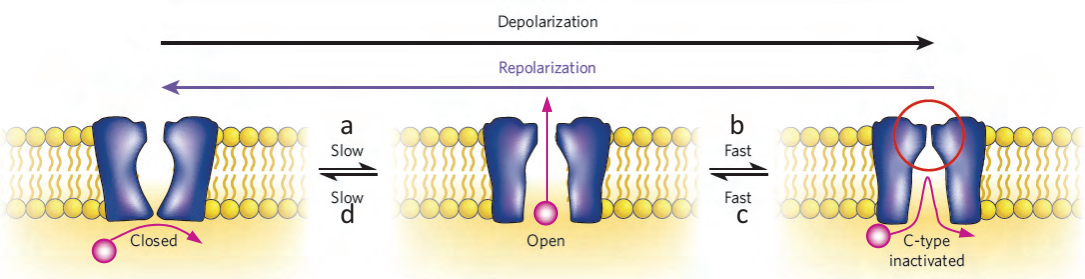

Figure 8 : Voltage-dependent conformation of a single hERG channel.

A single hERG channel is closed, open or inactivated, depending on transmembrane voltage. The open state is the only conformation allowing the passage of K^+ ion (pink sphere). C-type inactivation is thought to be caused by constriction of the selectivity filter (red circle). Transition **a** is called *activation*, **b** *inactivation*, **c** *recovery from inactivation*, and **d** *deactivation*. Modified from (Sanguinetti & Tristani-Firouzi 2006).

Despite the significant sequence homology with other K_v channels, hERG channels have very distinct kinetics. They are characterized by slow activation (time constant (τ) for activation of hundreds of milliseconds to seconds, whereas few milliseconds for other K_v), but very rapid and voltage-dependent inactivation (τ of inactivation of 1-10 milliseconds, whereas it is tens of milliseconds up to seconds for other K_v channels and independent of voltage) (Perrin *et al.* 2008). Therefore, when the membrane potential becomes more positive (depolarization), the opening of hERG channels is followed by rapid transition to the inactivation state, leading to small passage of K^+ ions. Reduced outward currents contribute to the maintenance of the AP plateau (*phase 2*) allowing sufficient time for Ca^{2+} entry, and render the cell refractory to premature excitation (such as EADs). As the membrane repolarizes (*phase 3*), hERG channels recover from inactivation much faster than they deactivate: channels are kept longer in the open state thereby passing more current, which will contribute to the termination of AP. The current finally decreases as a resultant combination of decreased driving force (membrane voltage closer to reversal potential of K^+) and deactivation (Perrin *et al.* 2008). Because hERG gating kinetics are essential for normal and abnormal cardiac function, numerous studies (including characterization with the patch-clamp technique of LQT2-linked or non-naturally occurring mutations) aimed at understanding the voltage-dependent molecular rearrangements/interactions of the different parts of the channel.

Activation

In K_v channels, transition between C and O is thought to be due to the splay-out of the intracellular part of the S6 helices. This is illustrated in crystal structures of various channels obtained these last years (open: KvAP, MthK; closed: KcsA, KirBac1.1). According to Doyle's analysis, the S6 helices are tilted with respect to the membrane and are slightly kinked (Doyle *et al.* 1998). When the channel is closed, S6 helices form a bundle crossing, so that the opening is too narrow to permit passage of K^+ ions (Doyle *et al.* 1998). When depolarization occurs, the lower part of these helices splay outwards, so that the subunits open like the petals of a flower facing the outside of the cell (**Figure 9**). The "open petals" house the structure formed by

the pore region (a cavity) restraint at the extracellular surface by the SF. In most K_v channels, a Pro-x-Pro motif that generates a dynamic molecular hinge is highly conserved in the sixth transmembrane helix (Sansom & Weinstein 2000). However, this kink motif is absent in hERG channel. Glycine residues found in the corresponding region (Gly648, Gly657) of hERG S6 helix were proposed to form the gating hinge. Nevertheless, a recent work presented contradicting results and argued that S6 glycines are not essential for the opening of hERG (Hardman *et al.* 2007). Understanding the molecular basis of splaying of S6 would need more studies.

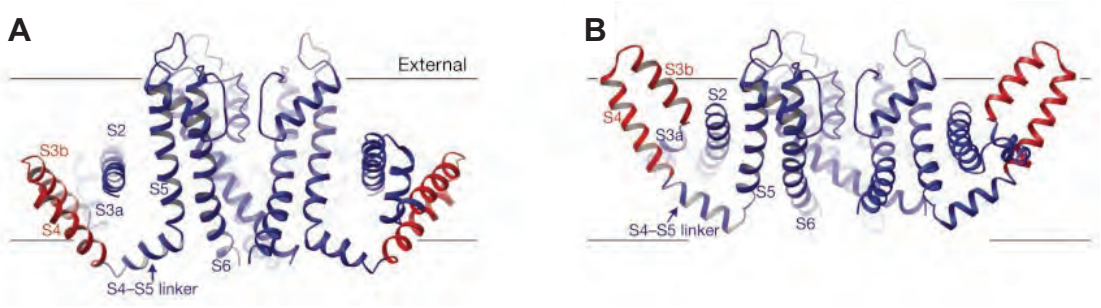

Figure 9 : Paddle model for voltage-sensor coupling to opening of the activation gate.

(A) Model of closed K_v channel structure (based on crystallized bacterial KvAP channel) with paddle (in red) adjusting the S5 and S6 helices to closed positions.

(B) The opened structure is due to the "paddles" (in red), presented at the external surface of the membrane, adjusting the S5 and S6 helices *via* the S4-S5 linker to open positions. Figures from (Jiang *et al.* 2003)

As opening of K_v channels is sensitive to variations in the membrane potential, they need a *voltage sensing domain*. The transmembrane S4, because of the presence of highly conserved basic residues, constitutes the primary voltage sensor (Piper *et al.* 2005). However, it seems that the voltage sensor of hERG is not exclusively composed of S4, and that transmembrane helices S2, S3 and possibly S1 also contribute to voltage sensing (Vandenberg *et al.* 2004; Subbiah *et al.* 2005). Indeed, hERG contains additional negative charges in S2 and S3 compared with most other K_v channels, and the clustering of negative and positive charges might be an important contributor to the slow activation (Vandenberg *et al.* 2004). To open the channel, the voltage sensing domain has to be linked to the activation gate in the

intracellular region of S6. Different models have been proposed for K_v channels, but we will discuss only the more probable (based on the current knowledge) for hERG channel: the *paddle model* (**Figure 9**). The voltage sensor will act as a "paddle", present on each subunit at the outer perimeter of the channel. Under depolarization, basic charges allow for S4 movement across the membrane near the interface (through the electric field). By this means, the paddles, which are coupled to the pore forming domain (mainly S5 and S6) through the S4-S5 linker, allow opening of the activation gate (Jiang *et al.* 2003; Long *et al.* 2005). This does not, however, explain why activation is particularly slow in hERG channels. This could be due either to slow movement of the voltage sensor or to slow coupling of the paddle movement to opening of the activation gate (Vandenberg *et al.* 2004). The slow movement hypothesis seemed to be the most likely according to the results of Piper *et al.* (2003) or Smith and Yellen (2002), but recent work suggests the second mechanism (Es-Salah-Lamoureux *et al.* 2010).

Interestingly, Snyders' group identified a charge cluster in the intracellular N-proximal domain (the KIKER sequence, refer to **Figure 7A**, page 28) that modulates the activation gating properties (Saenen *et al.* 2006). Indeed, when positive residues are mutated to glutamate (negatively charged), a hyperpolarizing shift is observed in the voltage-dependence of activation, thus indicating that the closed state is destabilized and that the effect is largely due to electrostatic interactions (Saenen *et al.* 2006).

Inactivation and recovery from inactivation

The inactivation process may occur by two mechanisms, either *ball-and-chain* (N-type) or *collapse of the pore* (C-type) inactivation. Current knowledge, based mainly on mutational studies, suggests that inactivation of hERG channel is analogous to the C-type inactivation of K_v1 (*Shaker* family) channels, though with (orders of magnitude) faster kinetics. Indeed, inactivation of hERG is sensitive to extracellular *tetraethylammonium* (TEA), whereas not when it is applied intracellularly: external TEA would act by physically preventing the "collapse" of the SF (Fraser-Reid *et al.* 1991). Moreover, a number of mutations in the S5-P linker and

pore-helix have been identified to abolish or substantially decrease inactivation, namely Ser620Thr and Ser631Ala (Pardo-Lopez *et al.* 2002), thus confirming that this region is critical for inactivation. The reason for the rapid process is not yet understood. As reviewed by Vandenberg and colleagues (2003), the nature of the aromatic residues in the signature sequence of the SF might be a reason. In most K^+ channels, the carbonyl atoms of the Gly-Tyr-Gly sequence form the selectivity filter for K^+ ions, and the hydroxyl of the tyrosines (directed away from the ion conduction pathway) would stabilize the SF with hydrogen bonding with residues of the transmembrane helix (Doyle *et al.* 1998). In hERG, however, the sequence is Gly-Phe-Gly. Still according to Vandenberg *et al.* (2003), disruption of the stabilizing hydrogen bonds would result in a "weaker spring" holding the SF in the correct conformation leading to a faster inactivation. This hypothesis needs yet to be proved.

The other important feature of inactivation of hERG is that its kinetics is voltage-dependent, and thus implies a voltage sensor. Experiments realized by Smith and Yellen (2002) with fluorescent groups attached to the S4 showed that structural rearrangements near the S4 occur during inactivation. Mutations in the S5-P linker and near the SF have also been shown to affect voltage dependence of inactivation (reviewed in Vandenberg *et al.* 2004). Nowadays, the molecular determinants of voltage-dependent inactivation are not clearly understood. Nevertheless, the inward rectification mechanism of the hERG channel was rapidly elucidated by analyzing kinetics of inactivation (Trudeau *et al.* 1995; Smith *et al.* 1996). Indeed, the inward rectification properties of hERG currents were apparently not consistent with the architecture of an inward rectifier channel (Kir family), because hERG presented six transmembrane domains and not two. hERG channels act like inward rectifiers because of their extremely fast and voltage-dependent inactivation. Inactivation rates are increased at more depolarized potentials. Therefore, at higher membrane potentials, inactivation of channels proceeds at a much faster rate than activation, such that no outward current is observed upon depolarization at these voltages (Spector *et al.* 1996b). Spector and colleagues (1996b) discovered the capital role of fast inactivation of hERG and the resulting effect of rectification during the plateau phase of ventricular action potentials.

Deactivation

The major structural components that contribute to slow deactivation of hERG channel are the *PAS domain* present at the N-terminus and the S4-S5 linker, although contributions of other regions have been reported (negative charges of S2 and S3, and cNBD). Deletion of the hERG N-terminus has been shown to profoundly affect the rate of deactivation (Schonherr & Heinemann 1996; Wang *et al.* 1998). Although this region is not highly conserved, it seemed sufficiently unique to Warmke and Ganetzky (1994) to be considered as a defining feature of the *EAG* K^+ channel family. The *eag domain*, as it was called, was crystallized by MacKinnon's group in 1998. They identified a three-dimensional structure similar to those of PAS domains (PAS is the acronym for the gene products of *Per*, *Arnt* and *Sim*), which are usually found in proteins involved in the circadian rhythm (Morais Cabral *et al.* 1998). Similarly to truncation of the N-terminus, mutations in this PAS domain speeded up the deactivation kinetics (Morais Cabral *et al.* 1998), but application of an endogenous peptide corresponding to the N-terminal region or part of it is able to restore the slow deactivation (Gustina & Trudeau 2009; Wang *et al.* 2000). Interestingly, MacKinnon and colleagues also revealed the presence of a large hydrophobic patch that could form a putative interface with the body of the channel to which it is thought to bind (Morais Cabral *et al.* 1998). Indeed, mutation of a glycine in position 546 in the S4-S5 linker into a chemically modified cysteine (thus disrupting potential interactions) resulted in faster deactivation kinetics similar to truncation of the N-terminus (Wang *et al.* 1998). Altogether, these data are consistent with a model where the N-terminus binds to sites in the S4-S5 linker that are exposed following channel opening (refer to *paddle model*) and subsequently slow closure of the channels (Vandenberg *et al.* 2004; Gustina & Trudeau 2009). Regarding the cNBD contribution, similarly to the work carried on the PAS domain, Al-Owais *et al.* (2009) defined a patch of hydrophobic residues, which resulted, when mutated to lysines, in accelerated kinetics of deactivation (see I.C.2.a).

I.C.3. Regulation of hERG channel

As manifested by the outcome of hERG channel dysfunctions in LQT2, a fine control of cardiac channels and currents is essential to ensure the correct pumping function of the heart. Magnitude of hERG current (*I*) in a cardiomyocyte can be determined by three parameters: i) the total number of channels at the plasma membrane (*N*), ii) the probability that any given channel is open (*Po*) and iii) the unitary conductance of a single channel (*g*); and they are presented in Equation 1:

$$I = N \cdot Po \cdot g \qquad \text{(Equation 1)}$$

With the use of this equation, it is possible to explain all forms of LQTS. As regards the *congenital* form, all three parameters can be reduced, simultaneously or not, by a loss-of-function mutation. Indeed, a mutated hERG channel can present impaired or defective synthesis (affecting *N*); be not properly targeted to the membrane (affecting *N*); present defective gating (affecting *Po*) or decreased conductance (affecting *g*). This will be discussed in more details in Part III (see III.A.4). Considering the *drug-induced* form of LQTS, interaction of a drug with (in most cases) the hERG channel cavity may decrease the current by reducing *N*, but usually reduces *g* and/or *Po*. In the case of *acquired* LQTS, the presented parameters might be affected upon unbalanced regulation of hERG, as it might occur in pathophysiological conditions. Therefore, downregulation of the synthesis or, conversely, increased degradation rate of membrane channels would naturally affect *N*. On the other hand, abnormal modulation of the channel function is believed to change mainly *Po.* Fundamentals of the acquired LQTS, specially those linked to the hERG channel, are still poorly understood. Nevertheless, studies about cardiac channel regulation could bring useful information for patient management and risk assessment. For instance, hypokalaemia and female gender have long been identified as risk factors for LQTS and potentially fatal arrhythmias. Only recently have evidences of regulation of hERG channels by K^+ ions and estrogens allowed for comprehension of the mechanism. The purpose of this section is to bring a few insights on hERG regulation studies and not to provide an exhaustive list. Moreover, for clarity purposes, we proposed a two-group classification, though some factors may belong to both.

I.C.3.a. Regulation of cell surface density of hERG channels (N)

MicroRNA

MicroRNAs (miRNAs) are small endogenous non-coding RNAs that anneal to inexactly complementary sequences of target mRNAs. The major characteristic of miRNA actions is to specify translational repression without affecting the levels of the targeted mRNA. In a study by Xiao *et al*. (2007), hERG post-transcriptional repression by both *miR-1* and *miR-133* – miRNAs specifically expressed in adult cardiac and skeletal muscle tissues – were tested in healthy and diabetic hearts. In fact, the same group previously showed that hearts of a *Diabetes Mellitus* (DM) rabbit model presented hERG levels reduced by ~60% compared to healthy controls, whereas mRNA levels remained unaltered (Zhang *et al.* 2006). In rabbit and human DM hearts, *miR-1* and *miR-133* were increased by 2.2- and 3-fold, respectively. In isolated rabbit cardiomyocytes, hERG currents and total protein levels were dose-dependently decreased with *miR-133*, but not *miR-1* transfection (Xiao *et al.* 2007). Importantly, these results showed that *miR-133* represses hERG protein and therefore I_{Kr} in hearts. Increased *miR-133* levels in DM hearts likely contribute to slowing repolarization and thus prolongation of QT interval in diabetic patients. As a reminder, *Diabetes Mellitus* is a known risk factor for *a*LQTS and associated TdP.

Caveolae and lipid raft association

Caveolae are specialized membrane microdomains (popularly known as *lipid raft domains*) enriched with cholesterol and sphingolipids, which are present in multiple cell types including cardiomyocytes. A number of different cardiac ion channels have been localized in caveolae including $Ca_v1.2$, $Na_v1.5$ and $K_v1.5$ (reviewed in Balijepalli & Kamp 2008). Caveolar localization of ion channels may contribute to their regulation: i) by the unique lipid environment that can directly impact on biophysical properties, ii) by bringing together macromolecular complexes that regulate the channel function, or iii) by regulating availability and trafficking of ion channels (Balijepalli & Kamp 2008). Caveolin proteins are the essential feature defining caveolae, and among the three known isoforms, cavelolin-3 is the one specifically expressed in the cardiac and skeletal muscle. Recent studies (Robenek *et al.* 2008)

have also identified caveolin-1 in human cardiomyocyte surface, though other groups could not detect expression of this isoform in this tissue (Balijepalli & Kamp 2008). In 2008, the group of Lin *et al*. published about hERG interaction and regulation by caveolin-1 in transfected HEK293 cells. According to their results, hERG interacts with caveolin-1, which is consolidated by the finding of two consensus caveolin-binding motifs in the intracellular termini of the channel. Overexpression of caveolin-1 produced decreased hERG currents and modified biophysical properties of the channel (Lin *et al.* 2008). This effect was counteracted by siRNA targeted against caveloin-1 or use of *methyl-β-cyclodextrin*, which disrupts caveolae by reducing membrane cholesterol (Lin *et al.* 2008). Nevertheless, hERG expression levels in HEK293 cells or cardiomyocytes were not performed to exclude an effect on cell surface density. Moreover, it is known that *ceramide*, the main structural component of sphingolipids, can act as a second messenger to stimulate multiple signalling cascades (Balijepalli & Kamp 2008). The group of Chapman *et al*. (2005)[2] showed that hERG membrane expression and currents were rapidly downregulated under ceramide treatment. Indeed, deactivation kinetics were hastened in ceramide-treated HEK293 cells but, above all, plasma membrane hERG K^+ channels appeared internalized and targeted to lysosomal degradation (Chapman *et al.* 2005). Recently, Ganapathi *et al*. (2010) concluded that ceramide-induced gating changes observed resulted from translocation of hERG channels into lipid rafts. Again, *in vivo* experiments are lacking to confirm such results.

Intra- and extracellular K^+ concentration

Patients presenting with hypokalaemia have long been recognized to be at higher risk for *a*LQTS and TdP. Indeed, cardiac APs *in vitro* are shorter at higher external K^+ ion concentration while longer when its concentration is low (reviewed in Guo *et al*. 2009). Reducing the external K^+ concentration (or $[K^+]_e$) would be expected to increase the driving force and, in opposition to what is seen under hypokalaemic conditions, increase the outward current through hERG. Therefore, many groups investigated the effect of variations of external K^+ and other ion concentration in

[2] Note that the results of Chapman et al. (2005) will be further discussed in section II.B.

hERG channels. Reducing $[K^+]_e$ was shown to enhance channel inactivation and thus further suppress current during the action potential (Yang *et al.* 1997). Importantly, owing to its specialized selectivity filter, the hERG channel shows a sequence for selective permeation of ions of $K^+ \approx Rb^+ > Cs^+$, whereas permeability for the smallest metal ions Na^+ and Li^+ is very low (Doyle *et al.* 1998). Nevertheless, extracellular Na^+ ions were shown to flow through hERG channels in absence of K^+ and to block hERG current (I_{hERG}) at higher Na^+ concentrations. Extracellular K^+ was demonstrated to compete with Na^+ for binding to the hERG external pore mouth (Numaguchi *et al.* 2000; Gang & Zhang 2006). Numaguchi *et al*. (2000) declared that, in presence of extracellular Na^+, small changes in $[K^+]_e$ over the physiological range (3-6 mM) produced a >2-fold change in amplitude of the I_{hERG} due to ion competitive effects, thus giving an explanation to the impact of hypokalaemia on I_{Kr}. It is worth mentioning that all these demonstrations were assessing acute effects of $[K^+]_e$. Recently, two different groups evaluated the chronic effects of low intracellular ($[K^+]_i$) and low extracellular potassium effects on hERG channel, and ended with quite similar conclusions.

Initially, the group of Ficker sought to assess the reason why cardiac glycosides potently inhibited hERG channel trafficking (Wang *et al.* 2009). Using a series of pharmacological inhibitors and techniques, they unveiled the importance of $[K^+]_i$ in the trafficking of hERG channels. Indeed, depletion of *intracellular* K^+ concomitant with increase of Na^+ by overnight treatment with cardiac glycosides – *e.g*. *digoxin*, a potent inhibitor of the Na^+/K^+ pump – reduced the fully-glycosylated form of hERG and its current due to impaired export from the ER. Interestingly, reduced temperatures in presence of digoxin could rescue the transport to the membrane, but not the hERG current (Wang *et al.* 2009). The authors proposed that K^+ ions are important for the right conformation of the conductive filter sequence during protein folding, and thus misfolding of this important feature leads to ER retention and degradation. hERG channels that reached the cell surface when incubated at low temperature retained the non-conductive conformation, which explained the discrepancy observed between rescue of mature protein and current levels (Wang *et al.* 2009).

Conversely, the group of Zhang explored the effects of chronic low *extracellular* K^+ concentration. According to their publications, $[K^+]_e$ is a prerequisite for the function and membrane stability of hERG channels (Guo *et al.* 2009; Massaeli *et al.* 2010). Indeed, overnight treatment of hERG-expressing cells with medium devoid of K^+ lead to important decrease of hERG protein and current. This effect was shown to be K^+ dose-dependent as well as time-dependent (Guo *et al.* 2009). Guo and colleagues demonstrated that the observed decrease of hERG surface density could be explained by an increased internalization and the targeting of endosomes to the lysosomal and, potentially too, the proteasomal pathway (Guo *et al.* 2009). Further investigations demonstrated that time-dependent decrease of current (in 0 mM $[K^+]_e$) was faster than cell surface protein decrease. To explain this phenomenon, the group of Zhang proposed that, in absence of extracellular K^+, the external pore mouth changes rapidly conformation and enters a non-conducting state. Results obtained with hERG pore mutants and hERG permeant cations (Rb^+ and Cs^+) in place of K^+ strongly support this hypothesis. In a yet unclear mechanism, the conformational change would trigger intracellular ubiquitylation and internalization (Massaeli *et al.* 2010)[3]. Nevertheless, these recent works provided a relevant mechanism for how chronic hypokalaemia exacerbates long QT syndrome and TdP.

I.C.3.b. Regulation of function (g, Po)

Heteromeric assembly of α-subunits

Since Sanguinetti *et al*. (1995) brought convincing evidences that *KCNH2* encodes the cardiac I_{Kr} potassium channel, hERG1a homotetramers have been commonly considered as the molecular structure of the *rapid component of the delayed rectifier potassium current*. Indeed, the C-terminus splice-variant, hERG-$_{USO}$, yields no current in cell lines when expressed alone. The idea of homotetramers was however challenged, since co-expression of both hERG1a and hERG-$_{USO}$ isoforms lead to I_{hERG}, although with faster activation kinetics and reduced amplitude (Kupershmidt *et al.* 1998). Moreover, the same investigators found that hERG-$_{USO}$ mRNA is ~2-fold more

[3] Note that the results of Guo *et al*. (2009) and Massaeli *et al*. (2010) will be further discussed in section II.B.

abundant than that for hERG1a in the human heart. Although the relatively high abundance of hERG-$_{USO}$ transcripts is intriguing, the physiological function and expression of its protein in the human heart remains to be elucidated. Intriguingly, Kupershmidt *et al*. (1998) found no obvious changes in current amplitude or gating with a 1:1 ratio of each isoform. Therefore, the authors carried out the experiments with 10-fold excess of hERG-$_{USO}$ compared with hERG1a, which is more than the difference observed at the mRNA levels (2-fold) and casts doubt on the physiological relevance of their results.

The third splice alternative, hERG1b, possesses a different N-terminus. Recently, Larsen *et al*. (2008) characterized the current after co-expression of hERG1a and hERG1b (hERG1a/b) in the *Xenopus* oocyte system, in comparison with hERG1a or 1b homomeric currents. The most pronounced difference between hERG1a and hERG1b is that the deactivation rate is markedly increased for hERG1b channels, as expected by the lack of PAS domain. In a 1:1 ratio hERG1a/b, deactivation time constants are intermediate (Larsen *et al.* 2008). Similarly to the previous study of Kupershmidt *et al*. (1998), mRNA levels of the different splice variants were assessed in human hearts. Transcripts of hERG1b were in average between 10 and 20% of total hERG1a/1b mRNA, and Larsen *et al*. (2008) proved that such amount of hERG1b was sufficient to significantly alter the deactivation rate in heterologous expression system. Nevertheless, their suggestion that deactivation kinetics of I_{Kr} in human cardiomyocytes is strongly governed by the relative expression of hERG1a and 1b needs further *in vivo* evidences.

Putative β-subunits of hERG

As previously mentioned, I_{Kr} and I_{Ks} provide the major repolarizing force to end the cardiac AP in human ventricular cardiomyocytes. It is now widely accepted that I_{Ks} is mediated by a tetramer of KCNQ1 α-subunits and two MinK β-subunits. Indeed, MinK provides to KCNQ1 currents the gating and pharmacological characteristics of cardiac I_{Ks} (reviewed in Anantharam & Abbott 2005). With regard to I_{Kr}, homomeric hERG channels pass an inwardly rectifying K^+ current (I_{hERG}) that largely resembles native I_{Kr}, presenting only subtle differences in unitary conductance and gating

kinetics (Sanguinetti *et al.* 1995). Nevertheless, there is supportive evidence for assembly of hERG α-subunits with ancillary β-subunits. Because MinK suppression in neonatal mouse cardiomyocytes reduced I_{Kr} and was co-immunoprecipitated with the K^+ ion channel in equine cardiac tissue, this protein encoded by the *KCNE1* gene was rapidly proposed as the hERG β-subunit (Anantharam & Abbott 2005). Interestingly, MinK increased hERG current, but it did not alter its unitary conductance (McDonald *et al.* 1997). Thus, its association with hERG is not sufficient to explain I_{hERG}-I_{Kr} differences. To our knowledge, MinK-hERG interaction in human heart has not yet brought evidence for co-assembly. Then the *MinK-Related Peptide 1* or MiRP1 (*KCNE2* gene) was reported as the essential β-subunit of hERG, but understanding the role of MiRP1 has been complicated. Initially, human MiRP1 and hERG were found to co-assemble, which resulted in reduced I_{hERG} by ~40% (due to decrease of unitary conductance) and in activation and deactivation changes (Abbott *et al.* 1999). Then, inconsistent effects of MiRP1 on hERG were reported in several subsequent studies (reviewed in Anantharam & Abbott 2005). In addition, ventricular expression of MiRP1 appears to be low, specially compared to MinK (Bendahhou *et al.* 2005). Nevertheless, for both MinK and MiRP1, mutations have been reported to cause *c*LQTS (LQT5 and LQT6, respectively) and polymorphisms to reduce I_{hERG} or influence drug-block affinity for hERG (reviewed in Anantharam & Abbott 2005), which in both cases speaks for an interaction.

Interestingly, evidence of functional interaction of I_{Kr} and I_{Ks} has been noticed *in vivo*. When I_{Kr} is reduced, the AP is prolonged causing I_{Ks} activation, which in turn prevents excess repolarization delay. Ehrlich and colleagues (2004) further investigated the interaction between hERG and KCNQ1. Coexpression of both α-subunits in a mammalian expression system (CHO cells) significantly accelerated the hERG current deactivation, thus making I_{hERG} more I_{Kr}-like (Ehrlich *et al.* 2004). Moreover, hERG current amplitude doubled in parallel to the protein immunostaining at the membrane, whereas no significant changes were observed in current density or kinetics of KCNQ1/MinK. In addition, Ehrlich *et al*. (2004) could co-immunoprecipitate hERG and KCNQ1 and pull-down KCNQ1 with the C-terminus of hERG protein in CHO cells. Co-immunostaining of both subunits in canine

cardiomyocyte membranes further reinforces the suggestion of interaction of α-subunits (Ehrlich *et al.* 2004). Unfortunately, it remains to be determined the mechanism for increased plasma membrane density and deactivation rates, and especially if hERG-KCNQ1 form heterotetramers or if the KCNQ1 α-subunit plays the role of an ancillary (β) subunit of hERG.

Reactive Oxygen Species

In the heart, *Reactive Oxygen Species* (ROS) participate in the tissue damage observed under ischemia-reperfusion conditions. One of the first studies on the topic demonstrated that only outward currents carried by hERG channels were selectively modulated by changes in ROS production, and that the ROS-induced increase of current was highly specific, since the bovine EAG channels were not affected (Taglialatela *et al.* 1997). Using another free-radical generator (H_2O_2, hydrogen peroxide at physiologically relevant doses), Berube and colleagues (2001) observed increased hERG currents due to accelerated activation and deactivation kinetics. According to their conclusions, faster hERG kinetics could be involved in reperfusion-induced arrhythmias by specifically reducing K^+ conductance in the early diastole, increasing thereby the risks of premature beats (Berube *et al.* 2001). However, a more recent study yielded contradicting results. As oxidative sensitivity of ion channels is often conferred by amino acids containing sulfur, Su and colleagues (2007) used *chloramine-T* as a methionine-preferring oxidant to assess functional effects on hERG currents. Application of chloramine-T drastically decreased current amplitude, which was in part reversible by the action of a reductase enzyme (Su *et al.* 2007). These results are in line with an impaired function of hERG by exposure to ROS-generators, such as tumor necrosis factor-α and hyperglycemia (Su *et al.* 2007). Though contradictory, these data evoke impairment of hERG conductance, which may explain why cardiac reperfusion injury is often complicated by arrhythmias. The reason of such a discrepancy may be that different reactive species are used or generated under various experimental settings. Nevertheless, it seems capital to better assess the physiological role of ROS in hERG function.

External pH

Acidosis is also encountered in myocardial ischemia, in which reduction of extracellular pH develops quickly. General agreement appears among authors on the effect of pH on I_{hERG} or I_{Kr} amplitude and deactivation kinetics. To our knowledge, all studies reported reduced current amplitudes and a marked enhancement of deactivation rates upon acidification (reviewed in Vereecke & Carmeliet 2000; Berube *et al.* 1999; Terai *et al.* 2000). However, no agreement is found among the same authors for the voltage-dependence of activation, with either hyperpolarizing or depolarizing shifts, or no effect upon change of external pH. Remarkably, no effect of external H^+ has been reported on voltage-sensitivity or kinetics of hERG inactivation. This is surprising, since the hERG C-type inactivation resembles inactivation of K_v1 (*Shaker* family) channels, which are affected by both external concentrations of K^+ as well as H^+ (Terai *et al.* 2000). Various mechanisms have been proposed for external acidosis effects, even though authors have diverging opinions. Among them, changes in H^+ concentration was proposed to i) alter negative surface potentials, ii) titrate charged residues that contribute to the channel structure, iii) repel cationic charges like K^+ that affect amplitude of I_{hERG} and/or iv) block the channel on the same site as divalent cations (Ca^{2+}, Mg^{2+}) (Berube *et al.* 1999; Vereecke & Carmeliet 2000; Terai *et al.* 2000). Nevertheless, acidosis may have clinical implications on the occurrence of arrhythmias in ischemia-reperfusion events. Indeed, acceleration of deactivation could reduce the current at the end of the AP and during the first part of diastole, which precludes the normal preventive effect of slow deactivation against premature beats (Berube *et al.* 1999).

Adrenergic stimulation – PKA and PKC pathways

The clinical observation that patients with LQTS typically develop arrhythmias during physical or emotional stress suggests a link between adrenergic stimulation and hERG channel function. Benefits of β-blocker treatment in LQT2 also support the idea of a negative impact of adrenergic stimulation. As stimulation of cardiac *β1-adrenergic receptors* is the main mechanism that increases heart rate and contractility, considerable attention has been given to the cAMP-PKA pathway.

Agonist binding to β1-adrenergic receptors causes a rise in the intracellular concentration of cAMP through the adenylate cyclase activation, and downstream effectors of this second messenger include the cAMP-dependent *protein kinase A* (PKA). Effects of cAMP increase and PKA-dependent phosphorylation of hERG[4] led to contradictory results in the literature. One of the first studies concluded that *isoproterenol*, a non-selective β-agonist, did not increase I_{Kr} in guinea pig cardiomyocytes (Sanguinetti *et al.* 1991). In contrast, Heath and Terrar (2000) found that activation of PKA caused an increase in I_{Kr} tail currents of guinea pig ventricular myocytes, and that the *protein kinase C* (PKC) was also involved in this upregulation. Others, employing the same cellular model, observed an I_{Kr} inhibition by β1-adrenergic receptor activation *via* cAMP/PKA-dependent pathways (Karle *et al.* 2002). As mentioned previously, the group of Cui *et al*. (2002) showed that cAMP could regulate gating of hERG channels by dual pathways, with stimulating effects of direct cAMP binding (hyperpolarizing shift in activation curve) and inhibitory effects of PKA-phosphorylation of hERG (accelerated deactivation kinetics and decreased current at all voltages). Moreover, this group demonstrated that participation of putative β-subunits of hERG could further modulate this effect (Cui *et al.* 2000). In other words, the cellular model and experimental conditions used are crucial and may produce opposing results.

Interestingly, most investigations focused on short-term or acute β1-adrenergic effects. However, it is known that sustained sympathetic stimulation, which may occur in chronic heart diseases, results in a process known as *electrical remodeling*. Cardiac electrical remodeling can affect ion channel function and expression, which may change AP morphology, synchronization and impulse propagation. The group of Chen *et al*. (2009) recently demonstrated that chronic treatment with membrane-permeant cAMP increases specifically hERG K^+ channel abundance (both non-mature and mature forms) as well as current density. The authors proved the involvement of PKA-phosphorylation of the channel and speculated that phosphorylation of hERG promotes a more productive folding of the channel (Chen *et al.* 2009). In a failing

[4] Note that phosphorylation of the hERG channel will be further discussed in section II.C.

heart, these changes may initially compensate for decreased cardiac function, but eventually become counterproductive. Moreover, prolonged stimulation of β1-adrenergic receptors with catecholamines leads to a phenomenon called *desensitization*, which reduces the number of receptors and thus their ability to promote cAMP accumulation.

Since β1-adrenergic receptors are the most expressed in the heart muscle, this justified the important focus on their pathway for hERG regulation. *α1-adrenergic receptors* are also present in the heart, though at a relatively small amount. These receptors are coupled to a positive inotropic response in atria and possibly in ventricular myocardium, and their percentage relatively to β1-receptors was shown to be increased in failing hearts (Bristow *et al.* 1988). α1-adrenergic response is mediated through generation of 1,4,5-inositol-triphosphate (IP3) and diacyglycerol (DAG). IP3 leads to intracellular Ca^{2+} mobilization and DAG is the physiological activator of *protein kinase C*. Heath and Terrar (2000) reported an increase of I_{Kr} mediated by activation of PKC, due to a decrease of rectification and C-type inactivation of hERG channels. Later, the group of Thomas *et al*. (2003) used a toolkit of kinases inhibitors and observed an opposite effect of PKC. Upon activation of PKC, the activation curve of hERG currents was strongly shifted towards more positive potentials (approx. +30 mV), which speaks for a significant decrease of current upon α1-adrenergic stimulation. Moreover, this effect appeared to be indirect, as phosphorylation of hERG channels by PKC was not necessary (Thomas *et al.* 2003).

Adrenergic regulation of hERG channels has been intensively studied over the past decade. However, complexity of the pathway and uncertainties about involvement of accessory subunits of hERG, as well as variety of cardiac cell models, do not enable at present a clear understanding of the physiological and, with greater reason, pathophysiological situations.

Estrogens

The fact that the QTc interval is longer in females than in males has already been mentioned by Bazett about one hundred years ago (Bazett 1918). Later, different studies showed that, in human and other animal species, females demonstrate a slower ventricular repolarization than males. In addition, propensity towards drug-induced TdP in both premenopausal and postmenopausal women supported the hypothesis of a pivotal role of sex hormones (Abi-Gerges *et al.* 2004). Genomic effects of sex hormones have been shown to underlie transcriptional modifications of some cardiac ion channels, such as $Ca_v1.2$, KCNE1 and $K_v1.5$, thereby explaining modifications of QTc interval in females hearts (Drici *et al.* 1996; Pham & Rosen 2002). However, Drici and co-workers (1996) did not notice changes in mRNA levels of hERG in ovariectomized rabbit hearts upon hormonal supplementation. Kurokawa *et al.* (2008) postulated that 17β-estradiol (E2) may acutely modulate the I_{hERG} *via* a non-genomic pathway[5]. In their comprehensive study, the authors first showed a bi-directional effect of E2 on the QT interval from Langendorff-perfused guinea pig hearts. Using high physiological concentrations of E2 (1 nM) QTc intervals were significantly prolonged, whereas at higher and non-physiological concentrations (100 nM) it was shortened. The 1-nM effect was due to I_{Kr} inhibition, since patch-clamp recordings of cardiomyocytes showed that E2 reduced I_{Kr}, but did not affect I_{Ks} or $I_{Ca,L}$. Higher E2 concentrations affected all tested currents, thus resulting in APD shortening. Since an estrogen-receptor inhibitor did not antagonize the E2 effect, a direct, receptor-independent, inhibition of the cardiac I_{Kr} current by female hormone E2 was proposed. Biophysical assessments of hERG currents in transfected HEK293 cells revealed that maximum current was not decreased upon E2 perfusion, but voltage-dependence of activation was shifted towards depolarized potentials (Kurokawa *et al.* 2008). Altogether, these results suggest that estrogen hormone acts as a gating modifier, which provided new insights into the possible causes making women more prone to particularly develop *di*LQTS.

[5] Note that we wrote a *Perspectives* article (see Appendix IV) for the publication of Kurokawa *et al.* (2008).

Drugs as blockers and activators of hERG

Many drugs with varying structures and therapeutic targets have been found to unintentionally block the hERG channel (refer to I.B.1.c). As previously mentioned, hERG channel *blockers* slow repolarization and prolong the QTc interval, which underlies the mechanism for the *drug-induced* LQTS. Based on the opposite rationale, drugs designed to intentionally activate hERG currents could prevent LQT2 if I_{Kr} current is not completely lost by the mutation[6]. Indeed, in the recent years, drug development allowed to foresee a new class of compounds with anti-arrhythmic properties: the *hERG channel agonists* or *activators*. The main purpose of these molecules is to increase hERG currents, though significant changes are seen in their molecular mode of action when described in heterologous expression systems. Contrary to hERG blockers, the list of known hERG activators is currently limited and their properties can be summarized in **Table 4**. Interestingly, most compounds have been developed by pharmaceutical companies (NeuroSearch: *NS1643*, *NS3623*; Sanofi-Aventis: *RPR260243* ; and Pfizer: *PD-118057* and *PD-307243*), whereas one molecule, *mallotoxin*, is a naturally occurring substance extracted from a tree named *Mallotus phillippinensis* (Grunnet *et al.* 2008; Zeng *et al.* 2006).

Table 4 : Summarized properties of hERG channel activators. Modified from (Grunnet *et al.* 2008).

Compound	Activation of cloned channels	Cardiomyocytes	Isolated muscle or wedge	Langendorff	*In vivo*
NS1643	Right-ward shifts inactivation curve	Shortens action potential duration and prevents triggered activity		Shortens QT interval but induced VF in 4/ 6 hearts	Reverse acquired long QT and TdP in rabbits
NS3623	Delays inactivation and right-ward shifts inactivation curve	Shortens action potential duration	Shortens action potential duration in papillary muscle	Prevents triggered activity	Reverse acquired long QT
RPR260243	Delays deactivation	Minor shorting of action potentials at high (30 μM) concentration. Shortening at lower concentrations after pre-treatment with hERG inhibitor	NA	NA	NA
PD-118057	No kinetic changes	Shortens action potential duration	Shortens action potential and decrease dispersion in rabbit. Increase dispersion in canine	NA	NA
PD-307243	Delays deactivation and inactivation	NA	NA	NA	NA
Mallotoxin	Delays deactivation increased activation	NA	NA	Shortens QT interval but induced VF in 7/ 7 hearts	NA

NA: non-available, VF: ventricular fibrillation, and TdP: Torsade de Pointes

[6] Note that hERG channel *activators* will be discussed again in section III.D.

The *NS3623* is maybe the best publicly described hERG activator. Application of this compound results in a rightward shift (+20 mV) in the steady-state inactivation curve. This explains how these compounds can activate hERG, since, at any given physiological membrane potential, channels will be less inactivated and thereby able to conduct more current (reviewed in Grunnet *et al*. 2008). Importantly, playing with hERG agonists might be risky, since gain-of-function mutations in *KCNH2* are related to SQTS and arrhythmic events. The short QT mutant hERG-N588K does in principle act in similar manner to *NS3623*, *i.e*. a depolarizing shift of inactivation. Nevertheless, the drug-induced shift is modest in comparison with the dramatic change of the mutant (in average more than +100 mV), therefore making arrhythmia as a consequence of QT shortening unlikely. Moreover, this compound has been shown to effectively reverse an acquired long QT interval in *ex vivo* and *in vivo* models (guinea pigs or rabbits) and to prevent triggering activity elicited by EADs, indicating a likely anti-arrhythmic property (reviewed in Grunnet *et al*. 2008). Recently, another potential undesired effect of hERG agonists came out. As mentioned, the use of hERG activators such as *NS3623* increases K^+ conductance in *phase 3* of the AP, which is desired to promote faster repolarization, but it also increases open probability in *phase 4*. Increased K^+ conductance in early *phase 4* is expected to affect membrane excitability and slow cardiac impulse propagation (mainly at fast heart rates); this is generally considered to be pro-arrhythmic. In a recent study (Larsen *et al.* 2010), cardiac conduction velocity was assessed in *NS3623*-treated guinea pigs. No major differences were seen at slower pacing rates, but impairment of cardiac impulse propagation was unmasked by faster pacing and when I_{Na} was decreased (Larsen *et al.* 2010). These findings suggest a role of I_{Kr} in modulating cardiac conduction and may have implications for the use and development of hERG agonists as anti-arrhythmic drugs.

I.D. Aims of the thesis

The remaining manuscript is divided into three distinct sections, which introduce the different aspects of hERG channel studied during this thesis work. Since it includes a specific introduction to the subject, each section can be read separately. Publications in support of this thesis are presented and discussed in the respective parts.

In ***Regulation of cardiac hERG channels by Nedd4-2 ubiquitin ligase*** **(Part II)**, we aimed at identifying molecular determinants of regulation of hERG channel cell surface density. We hypothesized that ubiquitin-ligases of the Nedd4 family, especially Nedd4-2, play a role in hERG channel abundance at the plasma membrane. Our findings are exposed in *Publication 1*.

In ***Characterization of congenital LQTS mutations*** **(Part III)**, we described in heterologous expression systems the electrophysiological and biochemical characteristics of two recently discovered *KCNH2* mutations. We hypothesized that the reduced function of the mutant hERG channels identified could be responsible for the phenotype of the probands. *Publication 2* and *Publication 3* present the case reports and experimental results obtained.

In ***Stereoselective block and drug-induced LQTS*** **(Part IV)**, we aimed at assessing the importance of stereoselectivity in the block of the hERG channel. In *Publication 4*, we hypothesized that methadone enantiomers may block differently the hERG channel resulting, in association with a stereoselective *slow metabolizer* phenotype, in increased risk of cardiac arrhythmias. In *Publication 5*, we aimed at explaining bupivacaine stereoselectivity towards the hERG channel using a dual approach based on mutagenesis studies and docking simulations.

Part II:
hERG channel regulation

II. hERG channel regulation by the ubiquitin ligase Nedd4-2

II.A. Introduction

Post-translational modifications of proteins are fundamental regulatory mechanisms controlling intracellular and extracellular events. Phosphorylation, discovered in the mid 1950's, is one of the best known protein modifications involving attachment of phosphate groups. Specific enzymes, known as *kinases* and *phosphatases*, take part in this reversible process. Ubiquitylation (or ubiquitination) is another post-translational modification discovered about 30 years ago (Hershko *et al.* 1980). Similarly to phosphorylation, it consists in adding covalently a molecule – the *ubiquitin* peptide – to lysine side chains, which is also a reversible process. However, the ubiquitin system is vastly more complex compared with phosphorylation, mainly due to the fact that ubiquitin can form polymers, or chains, with various linkages.

II.A.1. Ubiquitin and ubiquitylation forms

Ubiquitin is a small 76 amino acid-long polypeptide (~8.5 kDa) and, as its name lets suggest, it is expressed in all animal and plant cells. Remarkably, this globular protein (**Figure 10A**) is highly conserved throughout eukaryotes, with only three amino acid changes from yeast to human. Its covalent conjugation to proteins has initially been found to regulate the half-life of proteins, given that the ubiquitylated proteins would undergo a fast degradation (Hershko *et al.* 1983). Conjugation of ubiquitin to the substrate occurs essentially to a lysine (K) residue and thus different forms of ubiquitylation are found in living cells. The substrate can be mono-ubiquitylated (when only one peptide is added) or multi-mono-ubiquitylated (if several different K on the protein have been modified with one ubiquitin). Because ubiquitin comprises seven accessible lysine residues (K6, K11, K27, K29, K33, K48 and K63, **Figure 10A**), chains of ubiquitin can be formed, linked through isopeptide bonds between the C-terminus of one ubiquitin and a lysine residue of the second peptide, and so on. Polyubiquitylation can, consequently, take different forms and be either

homotypic (same type of linkage) or heterotypic (mixed or branched of linkages) as presented in **Figure 10**.

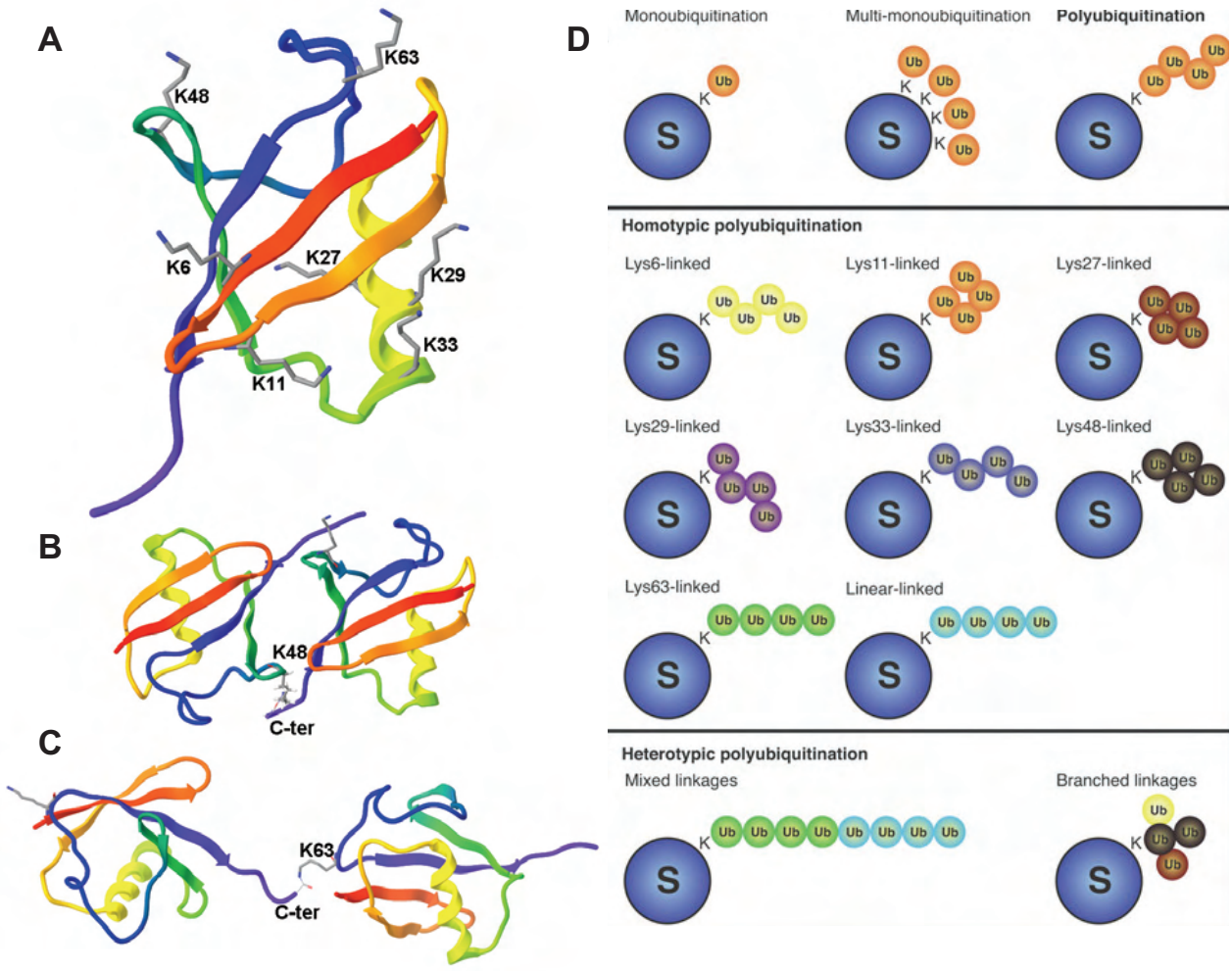

Figure 10 : Crystal structures of free ubiquitin or dimers as well as a simplified representation of different forms of ubiquitylation.

(A) Crystal structure of a free ubiquitin (pdb entry: 1ubq).

(B) Crystal structure of a K48-linked di-ubiquitin (pdb entry: 2bgf) presenting compact conformation.

(C) Crystal structure of a K63-linked di-ubiquitin (pdb entry: 2jf5) with extended conformation.

(D) The three general layouts of ubiquitin modification are presented (mono-, multi-mono- and polyubiquitylation) in the upper panel. Homotypic and heterotypic polyubiquitylations are presented respectively in middle and low panels. Modified from (Komander 2009).

In opposition to what was believed when discovered, ubiquitylation is not only a molecular "death-tag", but it is integrated in myriad processes such as cell progression, organelle biosynthesis, cellular differentiation, quality control in the ER, protein transport, inflammation, antigen processing, DNA repair or stress responses (reviewed in Komander 2009; Weissman 2001). The diversity of the processes under control of ubiquitin modifications is in part due to the ubiquitylation forms. Indeed, mono- and multi-mono-ubiquitylation of cell surface receptors trigger their internalization and subsequent degradation in lysosomes, or recycling to the cell surface. Polyubiquitylation with K63-linkage appears to have a non-degradative role in endocytosis, in the DNA-damage response and cell signaling. Moreover, proteomic analysis revealed that all chain types except K63-linked polymers accumulated in the yeast when the 26S proteasome was inhibited (Komander 2009). The proteasome is a large multimeric protein complex (~30 subunits), whose main function is to degrade unneeded or damaged proteins. Its catalytic complex (20S core) is capped at each end by the regulatory complex (19S cap), which fulfills several roles and among them recognition of ubiquitin chains (by the identified S5a component). Even though most ubiquitin chain types appear to target the modified protein to the proteasome, the K48-linked polymer seems to be the canonical form of ubiquitylation for the degradation pathway. Moreover, tetramers of ubiquitin linked in position 48 have been recognized as the minimal motif for the proteasome recognition (Komander 2009; Weissman 2001). Substrates modified with ubiquitin chains linked by K11 seem generally targeted to the *Endoplasmic Reticulum-Associated Degradation* pathway or ERAD (Komander 2009). Regarding distinct processes initiated by the other types of ubiquitylation, a lot of work is in progress and, thanks to techniques including mass spectrometry, chain-specific antibodies or conditional transgenic mouse models, an improved understanding is expected in the near future.

Recent evidence indicates that biochemical mechanisms of ubiquitylation events involve the recognition of a specific ubiquitylated target by a downstream *ubiquitin-binding protein*. Ubiquitin-binding proteins bear *ubiquitin binding domains* (UBDs) that can interact directly with monoubiquitin and/or polyubiquitin chains. UBDs are structurally diverse and are found in proteins with different biological

functions, such enzymes that catalyze ubiquitylation or deubiquitylation, or in ubiquitin receptors that recognize and interpret signals from ubiquitin conjugated substrate proteins (Hicke *et al.* 2005). As presented in **Figure 10B** and **C**, conjugation of ubiquitins through different lysine residues leads to different conformations of the oligomer obtained. Indeed, K48-linkage yields a more compact chain, due to higher interaction between ubiquitin molecules, whereas K63-linkage gives rise to a linear conformation. In this latter case, hydrophobic patches (Ile44 patches) are exposed and might allow different types of interactions with UBDs (Komander 2009).

II.A.2. Deubiquitylation

Similarly to phosphorylation, ubiquitin modification of a protein is reversible, and the removal of ubiquitin moieties is tightly regulated. Introducing the deubiquitylation process before ubiquitylation might seem counterintuitive, as de-ubiquitylation suggests subtraction of the modifier peptide. In reality, cellular free ubiquitins can be produced from *de novo* synthesized linear chains of ubiquitin processed by specialized *deubiquitylating enzymes* or DUBs. Linear chains, resulting from head-to-tail (and not K-linked) assembly of ubiquitins and ubiquitin fused to the N-terminus of two ribosomal proteins, are encoded by four human genes (*UBC*, *UBB, UBA52* and *UBA80*, **Figure 11a**). Generation of free ubiquitin is one of the three major functions of DUBs, including recycling of the small peptide, which contributes to ubiquitin homeostasis (**Figure 11a-f**). DUBs of the second group remove ubiquitin chains from modified proteins, leading to reversal of ubiquitin signaling or to protein stabilization by rescue from proteasomal or lysosomal degradation (**Figure 11b-c**). The third category involves DUBs that can be used to “edit” ubiquitylation forms by trimming of ubiquitin chains (**Figure 11f**) (Komander *et al.* 2009). There are nearly 100 DUBs in mammals; this diversity implies that considerable substrate specificity exists (Wilkinson 2009). Moreover, many DUBs have one or more UBDs. Though the roles of these domains in deubiquitylation reactions have not been defined yet, ubiquitin binding domains of DUBs are thought to be involved in substrate recognition by binding to specific ubiquitylation forms (Hicke *et al.* 2005). Association of DUBs with *ubiquitin ligases* (see II.A.3), scaffold proteins and/or substrate adaptors

might occur and such associations might function as regulators of enzyme activity, though this hypothesis awaits further studies (Hicke *et al.* 2005; Wilkinson 2009).

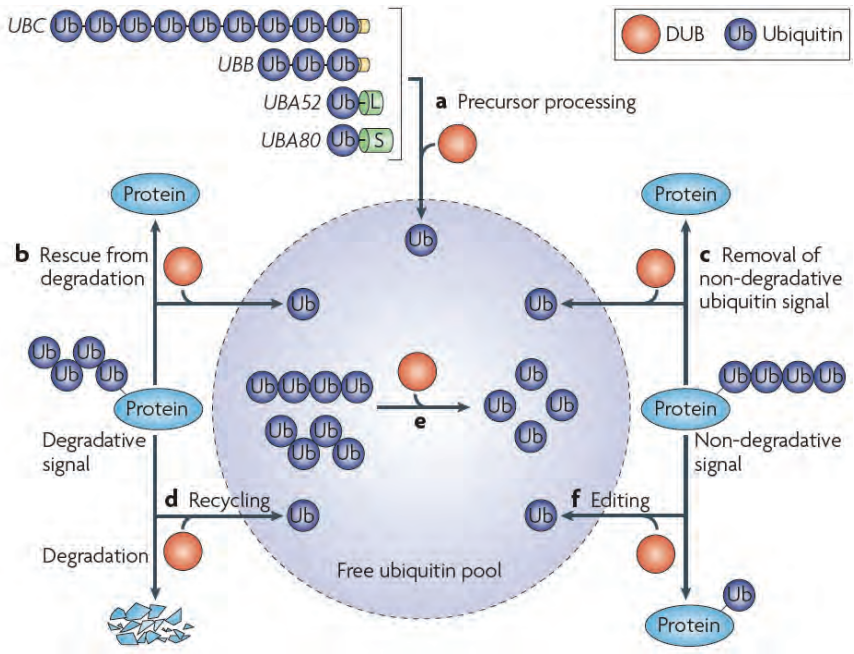

Figure 11 : General roles of deubiquitylating enzymes (DUBs).

a) *De novo* ubiquitin is synthesized as fusion proteins with either multiple copies or one ubiquitin fused to the N-terminus of two ribosomal proteins (L and S). Deubiquitylation **b)** can rescue proteins from degradation, **c)** can remove a non-degradative ubiquitin signal, **d)** can maintain ubiquitin homeostasis and prevent its degradation, **e)** can ensures disassembly of *en bloc* ubiquitin chains to fill the free ubiquitin pool, and **f)** might function to edit ubiquitin chains and thereby help to exchange one type of ubiquitin signal for another. Adapted from (Komander *et al.* 2009)

II.A.3. Ubiquitylation

Covalent attachment of ubiquitin moieties to proteins is a multistep process and involves the successive action of three types of enzymes (**Figure 12**). First, an *ubiquitin-activating enzyme* (also known as E1) forms a thioester bond with an internal cysteine and the C-terminus of ubiquitin in an ATP-dependent process. Then, an *ubiquitin-conjugating* or *ubiquitin-carrier enzyme* (E2) accepts ubiquitin from the E1 by a *trans*-thiolation reaction, involving the same C-terminus of ubiquitin. Finally, an *ubiquitin (protein) ligase* (E3) catalyzes the transfer of the ubiquitin moiety from

the E2 enzyme to the ε-amino group of a lysine residue on the substrate protein. Importantly, two major families of E3 families, namely RING (*Really Interesting New Gene*) that act as adaptors and bind to both the charged E2 and the substrate, and HECT (*Homologous to the E6-associated protein C-terminus*) domain. HECT-domain E3s form thioester intermediates with ubiquitin before final ubiquitylation of the substrate. Members of the RING E3 class are now believed to mediate the direct transfer of ubiquitin from E2 to the targeted protein (reviewed in Weissman 2001). Until now, how E3s ligases facilitate isopeptide bond formation between ubiquitin and substrate, and also how they add ubiquitin to a growing end of a polyubiquitin chain is poorly understood. An accessory factor (E4) that facilitates the formation of chains has been identified for one E3 in yeast. However, E4s are not generally required for the formation of multi-ubiquitin chains (Weissman 2001).

Importantly, the human genome encodes only two E1 enzymes, tens of E2 enzymes but at least 600 to putatively 1000 different E3 ligases (Komander 2009). At

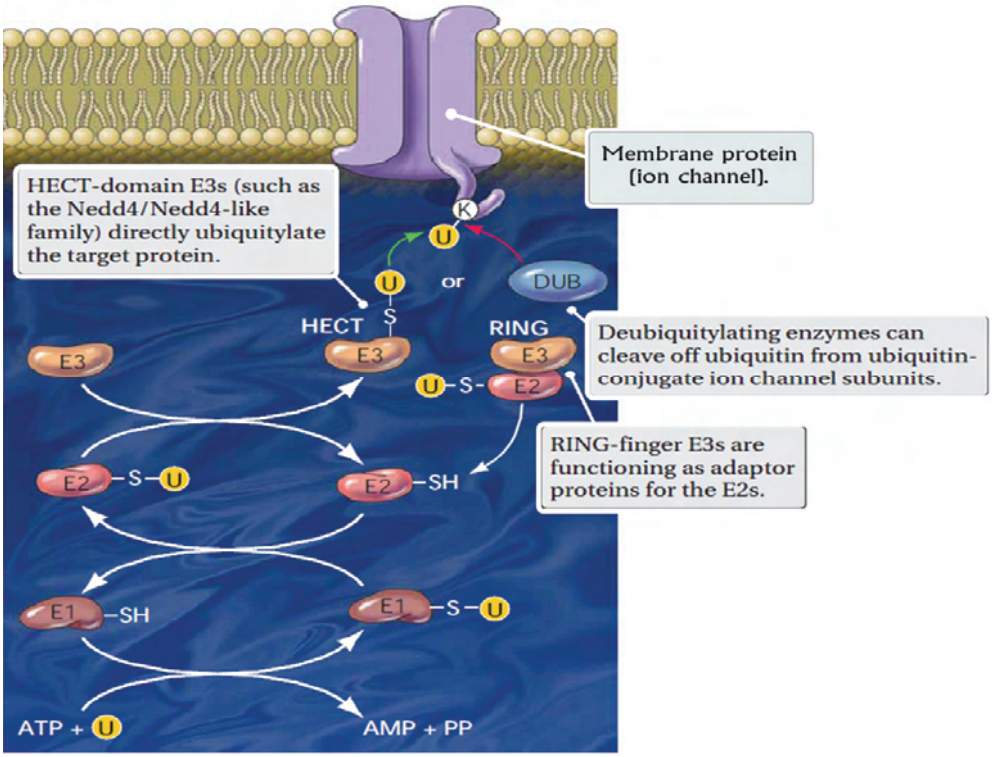

Figure 12 : Ubiquitin conjugation pathway.

Enzymes E1, E2 and E3 successively carry the ubiquitin (U) to the final protein. E3 enzymes are responsible for specific recognition of target proteins (here, an ion channel at the plasma membrane). Modified from (Abriel & Staub 2005)

each step, the number of proteins that can potentially be involved increases, as does the specificity of binding to the next component. It is finally the E3 that determines the substrate recognition. Therefore, regulation of E3s by post-translational modifications, subcellular localization and/or interacting proteins that may act as adaptors or accessory subunits, might have an important role in the diversity of ubiquitin-dependent protein fates (Weissman 2001; Shearwin-Whyatt *et al.* 2006).

II.A.4. Regulation of ion channels by the Nedd4 family ligases

The textbook case of ion channel ubiquitin-dependent regulation is the *epithelial sodium channel* or ENaC. This sodium channel is expressed in the apical membrane of epithelia found in the lung and colon, and in the distal part of the nephron, where it is involved in sodium homeostasis and blood pressure control by the kidney. ENaC is a protein complex composed of three subunits (α, β and γ), each subunit containing at the C-terminus a proline-rich sequence, the so-called *PY motif* (L/PPxY; L for lysine, P for proline and Y for tyrosine). When the PY motif is altered or deleted, it causes an inherited form of salt-sensitive hypertension named *Liddle's syndrome* (Abriel *et al.* 1999). Indeed, Liddle's mutations reproduced in the *Xenopus* oocyte expression system led to increased channel activity due to augmented plasma membrane expression (Schild *et al.* 1996). At the same time, Staub and colleagues demonstrated that specific domains, named *WW domains*, of the E3 ligase rNedd4-1 (r for rat) were interacting with PY motifs in β and γ subunits of ENaC (Staub *et al.* 1996). Finally, Abriel *et al.* (1999) showed that cell surface expression of ENaC appeared negatively regulated upon co-expression of the ubiquitin ligase xNedd4-1 (x for *Xenopus*), whereas a catalytically defective xNedd4-1 produced a marked increase of ENaC current and expression. Finally in 2001, the main pieces for understanding the molecular mechanisms of Liddle's syndrome were in place (Kamynina *et al.* 2001b): ENaC interacts *via* its PY motifs with the hNedd4-2 (h for human), which ubiquitylates ENaC channels and leads to their internalization; Liddle's mutations in the PY motif of ENaC result in an impaired interaction with hNedd4-2 and less-efficient internalization, therefore increasing the ENaC activity at the apical surface of epithelial kidney cells.

The ubiquitin protein ligase Nedd4-1 is the likely ancestral member of the *Nedd4 family*, also referred to as *Nedd4/Nedd4-like family*. The prototypic member was discovered as a developmentally regulated gene in the central nervous system of mouse, hence its name Nedd4-1 (or simply Nedd4) for the product of the *Neural precursor cell-expressed Developmentally Downregulated gene 4* (Yang & Kumar 2010). The Nedd4 family is one of the major families of HECT-domain E3s, and contains nine members in humans including Nedd4-1 (**Figure 13**). Nedd4 family enzymes have a distinct modular domain architecture, each member consisting of two to four WW domains, an N-terminal *C2 domain* and the catalytic HECT domain at the C-terminus (**Figure 13**). Nedd4-1 and Nedd4-2 (also named NEDD4L) are most closely related to each other.

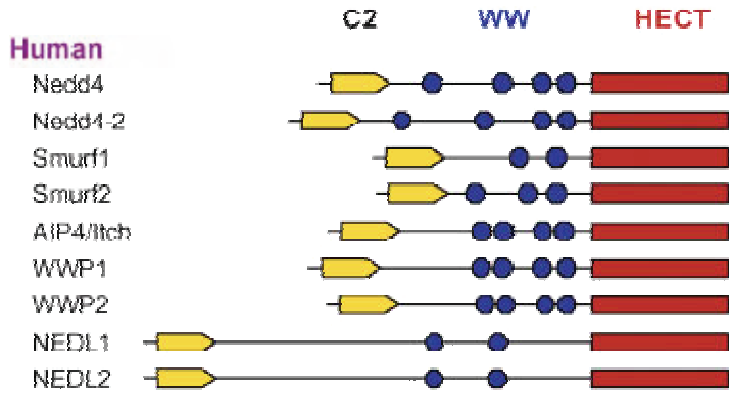

Figure 13 : Nedd4 family belonging to the HECT ubiquitin protein ligases (E3).
The approximate domain architectures of the nine members of the human Nedd4 family are shown with C2 domain (in yellow), WW domains (in blue) and catalytic HECT domain (in red). Adapted from (Shearwin-Whyatt *et al.* 2006).

The putative role of the C2 domain of Nedd4-1 was described by the group of Rotin as a Ca^{2+}/lipid binding domain, which function would be to associate Nedd4-1 with phospholipids and membranes upon increase of cytosolic calcium (Plant *et al.* 1997). According to this study, the presence of a functional C2 domain in Nedd4 E3s may help in determining the array of substrates targeted for ubiquitylation by guiding the subcellular distribution of these E3s in a calcium-dependent fashion.

In addition, the Nedd4 family ligases contain two to four WW domains, which are small globular modules (~30 amino acids) important for protein-protein interactions.

The name refers to the two conserved tryptophan (W) residues that play an important role in the compaction of the antiparallel β-sheet structure as well as in the function of the domain (Ilsley *et al.* 2002). The WW domains of the Nedd4 family interact with proline-rich motifs – most commonly the PY motif sequence – and phosphoserine or phosphothreonine followed by a proline residue (Shearwin-Whyatt *et al.* 2006).

Finally, the HECT domain – characteristic of this subtype of E3s – is a highly conserved sequence, ~350 amino acid-long, located at the C-terminus. It is the catalytic region of HECT-type E3s, defined by the presence of a conserved cysteine residue, whose side chain forms a thioester bond with ubiquitin before transfer of the ubiquitin moiety to the target protein. Moreover, HECT domains of Nedd4-1 and Nedd4-2 contain a PY motif located adjacent to the conserved catalytic cysteine. It has it has been recently shown that Nedd4-2 regulates its own stability through self-ubiquitylation, which is inhibited by interaction between Nedd4-WW domains and the PY motif in its own HECT domain (Bruce *et al.* 2008).

Similarly to ENaC, other ion channels demonstrated to be regulated by Nedd4 family members. Indeed, most Na_v1 channels isoforms – neuronal ($Na_v1.1$-$Na_v1.3$ and $Na_v1.6$-$Na_v1.8$) and cardiac ($Na_v1.5$) – bear a consensus PY motif and showed to bind to the two WW domains of Nedd4-1 and Nedd4-2 closest to the HECT domain (Fotia *et al.* 2004). Moreover, $Na_v1.2$, $Na_v1.5$ and $Na_v1.7$ were ubiquitylated and presented reduced current in presence of Nedd4-2 (Fotia *et al.* 2004; van Bemmelen *et al.* 2004). The proposed mechanism appears to be similar to the one previously mentioned for ENaC subunits, *i.e.* of an ubiquitin-dependent downregulation, even if it concerns two unrelated classes of sodium channels. In the abovementioned cases, it is worth mentioning that experiments performed in heterologous expression systems led to a weaker or absence of response upon Nedd4-1 co-expression, despite interaction of WW domains with PY motifs demonstrated by pull-down assays (Fotia *et al.* 2004; Rougier *et al.* 2005; Kamynina *et al.* 2001a; Staub *et al.* 1996). In a study by Jespersen *et al*. (2007), the cardiac channel complex KCNQ1/KCNE1 – underlying the *slow component of the delayed rectifier potassium*

current, I_{Ks} – was shown to be downregulated by ubiquitylating enzymes of the Nedd4 family. Although Nedd4-1 and WWP2 also interacted *in vitro* and decreased significantly KCNQ1/KCNE1 current in transfected mammalian cells, Nedd4-2 produced the highest effect. Moreover, quantification of mRNA of the nine members of the Nedd4 family – mRNA isolated from human heart, brain and kidney – showed that Nedd4-2 had the highest mRNA expression level in heart and kidney, while Nedd4-1 showed low abundance in all three organs (Jespersen *et al.* 2007). The probable physiological role of Nedd4-2 in I_{Ks} regulation was further reinforced by *ex vivo* experiments on isolated guinea pig cardiomyocytes (Jespersen *et al.* 2007).

The list of membrane proteins known to be ubiquitylated, such as ion channels, transporters and receptors, has been increasing over the last decade (reviewed in Abriel & Staub 2005; Shearwin-Whyatt *et al.* 2006; Yang & Kumar 2010). Remarkably, Nedd4-2, rather than Nedd4-1, demonstrated to regulate several ion channels, including the chloride channels ClC-5 involved in constitutive albumin endocytosis in renal proximal tubule cells (Hryciw *et al.* 2004), the potassium channels $K_v1.3$ (KCNA3) that are essential for immune response (Henke *et al.* 2004) or $K_v1.5$ (KCNA5) expressed in the atria (I_{Kur}) and pancreatic β-cells (Boehmer *et al.* 2008), KCNQ2/3 and KCNQ3/5 heteromeric channels that stabilize membrane potential in neurons (Ekberg *et al.* 2007), and recently chloride channels of the human *Tweety* family (mainly TTYH2, and TTYH3), whose expression in renal cell carcinoma and colon cancer was reported upregulated (He *et al.* 2008). Although these membrane proteins were ubiquitylated upon Nedd4-2 co-expression, not all contain WW-binding motifs (KCNQ3 and $K_v1.3$ are lacking a PY motif). Thus, it was suggested that Nedd4-2 may, in these cases, become effective through participation of an adaptor protein that includes a PY motif, or by regulating another E3 ubiquitin ligase (Shearwin-Whyatt *et al.* 2006; Ekberg *et al.* 2007; Henke *et al.* 2004).

As a conclusion, even if the two members are the most similar among the human Nedd4 family (67% amino acid identity), Nedd4-1 and Nedd4-2 seem to have different global substrate recognition. Recent work by Persaud and colleagues, using proteome arrays for identification of human Nedd4-1 and Nedd4-2 partners, brought

compelling evidence of substrate specificity (Persaud *et al.* 2009). Among the top hits, 25 partners were shared between Nedd4-1 and Nedd4-2, 19 substrates were unique to Nedd4-1 and 13 to Nedd4-2. Although numerous *serine/threonine kinases* were found as common substrates, a significant number of *tyrosine kinases* (Tyr kinases) were substrates of Nedd4-1 only. Conversely, numerous ion channel subunits – most of them bearing a PY motif – were identified as Nedd4-2 *in vitro* substrates, namely voltage-gated channels (KCNB1, KCNAB1, KCNAB3), the voltage-gated anion channel VDAC2, the calcium channel CACNB1 and the chloride channel CLIC2 (Persaud *et al.* 2009). Unfortunately, already documented ion channels regulated by Nedd4-2 were not present on the proteome array. Nevertheless, from the apparent non-overlapping phenotypes of the *NEDD4-1* and *NEDD4-2* gene knock-out (KO) mice, it seems even more clear that the main substrates of these E3s are distinct, despite their close similarity (Yang & Kumar 2010). The predominant phenotype of mice lacking Nedd4-1 is growth retardation associated with perinatal lethality (Cao *et al.* 2008). On the basis of the *NEDD4-1* KO mice phenotype and the known role of Tyr kinases in the regulation of cell proliferation, it was expected that some Tyr kinases were identified *in vitro* as substrates of Nedd4-1 (Persaud *et al.* 2009). As regards mice deficient in Nedd4-2, the phenotype is mild upon normal-salt diet, whereas chronic high-salt diet causes hypertension and cardiac hypertrophy. Moreover, the *NEDD4-2* KO mice have higher expression of all three subunits of ENaC in kidney, which is consistent with impaired downregulation of cell surface ion channels by Nedd4-2 (Shi *et al.* 2008).

II.B. Publication 1 (under review at the *J. of Biological Chemistry*)

Nedd4-2 dependent ubiquitylation and regulation of the cardiac potassium channel hERG1

In the latest years, the voltage-gated cardiac potassium channel hERG has been reported ubiquitylated in different conditions. To our knowledge, the first report of its ubiquitylation dates back to 2003, when Ficker and colleagues investigated the role of cytosolic chaperones, such as *Heat shock proteins* Hsp70 and Hsp90, in the maturation of the cardiac hERG channels. It appeared that specific inhibition of Hsp90 by *geldamycin* prevented hERG maturation (*i.e.* further glycosylation of the 135-kDa precursor into the 155-kDa mature form) and increased channel ubiquitylation (Ficker *et al.* 2003). They also observed that trafficking-deficient mutants, namely hERG-R752W, demonstrated prolonged association with the chaperones. Similarly, the group of Gong *et al.* (2005) analyzed another LQT2 mutation leading to defects in trafficking of the K^+ channel. In the presence of proteasome inhibitors (*ALLN* and *lactacystin*), both hERG WT and Y622H channels presented increased levels of the immature form without apparent increase of the mature channel, whereas no change was observed with a lysosome inhibitor (*leupeptin*). Moreover, proteasome inhibitor ALLN significantly increased the ubiquitylation of WT and mutant hERG, and presence of ubiquitin-labelled channels was demonstrated in both membrane and cytosolic fractions (Gong *et al.* 2005). According to this study, misfolded hERG proteins appear to be retained in the ER and eventually degraded by the ERAD process. Hence, hERG mutant channels that fail the quality control are seemingly ubiquitylated, dislocated from the ER to the cytosol where they are targeted for degradation by the proteasome (Gong *et al.* 2005). Both studies of Ficker *et al.* (2003) and Gong *et al.* (2005) are consistent with an ER folding-control of hERG proteins associated with degradation *via* the ubiquitin-proteasome pathway.

Intriguingly, hERG channels demonstrated to be regulated at the cell surface level by a ceramide-dependent ubiquitylation (Chapman *et al.* 2005). In presence of this

sphingolipid particularly important in lipid raft domains, hERG membrane expression and currents were rapidly downregulated (maximal effect after 1 h). Ubiquitylation response under ceramide treatment, concomitant with colocalization of hERG and lysosomal protein Lamp1, spoke for an ubiquitin-mediated lysosomal degradation. Nevertheless, this study also brought evidence of proteasome involvement in hERG regulation, since the proteasome inhibitor *MG132* importantly increased the hERG K^+ channel ubiquitylation (Chapman *et al.* 2005). How ceramide is capable of triggering ubiquitylation remains to be studied.

Recently, the group of Zhang and colleagues provided important insights into regulation of cell surface density of hERG channels. They showed that extracellular concentration of K^+ ion controls hERG channel stability at the plasma membrane. Notably, response to low $[K^+]_e$ was analyzed with dynamic colocalization of hERG with different markers of the lysosome pathway as well as ubiquitin. The results obtained gave strength to the hypothesis that chronic low $[K^+]_e$ leads to specific (no influence on the related EAG channel) hERG ubiquitylation, which accelerates the K^+ channel internalization and degradation (Guo *et al.* 2009; Massaeli *et al.* 2010). In Guo *et al*. (2009), proteasome inhibitor *lactacystin* impeded low K^+-induced internalization, which indicated probable involvement of the proteasomal pathway.

These recent studies on cell surface regulation suggest that hERG channel density is commonly controlled by ubiquitylation-dependent processes. Regulation of protein levels at the plasma membrane by the Nedd4 family members – especially Nedd4-2 – has been reported for different cardiac ion channels, namely $Na_v1.5$, KCNQ1 and $K_v1.5$ (see II.A.4). Similarly to most substrates of the Nedd4-family ubiquitin ligases, the hERG channel bears a typical PY motif at its C-terminal end. In addition, the tyrosine of the canonical sequence is followed by a hydrophobic residue (Φ) three positions downstream, hence forming an *extended PY motif* (L/PPxYxxΦ) providing potential additional binding to WW domains (Kanelis *et al.* 2001; Rougier *et al.* 2005). Taken together, the *human ether-à-gogo related gene* channel emerges as a good candidate for Nedd4-2 regulation of cardiac cell surface density and therefore I_{hERG}/I_{Kr}. This hypothesis was addressed in the following study.

Contribution to the study:

In this study I generated the plasmid encoding mutant hERG1-ΔPY, carried out all electrophysiological experiments in HEK293 cells and some preliminary assays of biochemistry (immunoprecipitation, pull-down with GST-S5A, cell surface biotinylation). I was in charge of the cell culture, preparation and transfection for most experiments. I also contributed to the writing of the manuscript in collaboration with M. Albesa.

Nedd4-2 dependent ubiquitylation and regulation of the cardiac potassium channel hERG1*

Maxime Albesa[1‡], Liliana Sintra Grilo[1, 2‡], Bruno Gavillet[3], and Hugues Abriel[1]

[1] Department of Clinical Research, University of Bern, Switzerland [2] Pharmacochemistry, School of Pharmaceutical Sciences, University of Geneva, University of Lausanne, Switzerland [3] Department of Pharmacology, University of Lausanne, Switzerland

[‡]These authors contributed equally to this study

Running title: Ubiquitylation of hERG1 by Nedd4-2

Address correspondence to: Dr. Hugues Abriel, MD PhD, University of Bern, Department of Clinical Research, Murtenstrasse, 35, 3010 Bern, Switzerland, Phone: +41-31-6320928, Fax: +41-31-6320946, e-mail: Hugues.Abriel@dkf.unibe.ch

The voltage-gated cardiac potassium channel hERG1 (human ether-à-gogo-related gene 1) plays a key role in the repolarization phase of the cardiac action potential (AP). Mutations in its gene, *KCNH2,* can lead to defects in the biosynthesis and maturation of the channel, resulting in congenital long QT syndrome (LQTS). To identify the molecular mechanisms regulating the density of hERG1 channels at the plasma membrane, we investigated channel ubiquitylation by ubiquitin ligase Nedd4-2, a post-translational regulatory mechanism previously linked with other ion channels. We found that whole-cell hERG1 currents recorded in HEK293 cells were decreased upon Nedd4-2 co-expression. The amount of hERG1 channels in total HEK293 lysates and at the cell surface, as assessed by Western blot and biotinylation assays, respectively, were concomitantly decreased. Results showed that Nedd4-2 and hERG1 interact via a PY motif located in the C-terminus of hERG1. Deletion of this motif affects Nedd4-2-dependent regulation. Finally, we determined that Nedd4-2 mediates ubiquitylation of hERG1 by adding mixed ubiquitin K63-Kx-linked chains (K for lysine, x for undetermined position) to the channel. These results suggest that ubiquitylation of the hERG1 protein by Nedd4-2, and its subsequent down-regulation, could represent an important mechanism for modulation of the duration of the human cardiac action potential.

The voltage-gated cardiac potassium channel hERG1 (human ether-à-gogo-related gene 1) plays a key role in the repolarization phase of the cardiac action potential (AP) (1). Mutations in its gene, *KCNH2,* can cause both congenital long QT syndrome (LQTS) (2) and short QT syndrome (3). Many different mechanisms are involved in the mutation-induced alterations of hERG1 function, with defects in trafficking playing a prominent role (4). The investigation into the molecular determinants of channel density at the cell surface is very important since the hERG1 current determines the AP duration, directly affecting cardiac function.

Ubiquitylation of ion channels has recently been shown to be involved in many different regulatory mechanisms (5). Ubiquitylation, a post-translational modification, involves the covalent attachment of a molecule, or a chain of ubiquitin molecules, to lysine residues of target proteins via a ubiquitin-protein ligase. The ubiquitin peptide consists of 76 amino acids, including seven lysines to which other ubiquitin moieties can bind, allowing for the distinction of seven different types of ubiquitin linkages (6). The physiological role of each ubiquitin chain remains poorly understood. It has been proposed that the ubiquitin chains linked with lysine in position 48 (K48) or 63 (K63) may regulate degradation and trafficking of membrane proteins, respectively (7-8). Target specificity is controlled by the ubiquitin ligases, E3s enzymes of the ubiquitylation cascade responsible for target recognition (9).

The epithelial sodium channel (ENaC) was the first ion channel shown to be regulated by ubiquitylation (10). Two cardiac ion channels, $Na_V1.5$ and KCNQ1, have recently been shown to be down-regulated by Nedd4-2, a ubiquitin-protein ligase of the Nedd4/Nedd4-like family (11-13). The mechanisms implicated in the down-regulation of both $Na_V1.5$ and KCNQ1 are similar

to those described for ENaC, *i.e.* the ubiquitylation of channels leads to enhanced internalization (14). Ubiquitin ligases of the Nedd4 family are characterized by several WW binding domains (15), a catalytic HECT domain (16), and an amino-terminal calcium-dependent lipid-binding domain (C2 domain) (17). The down-regulation of ion channels is mediated by the interaction between the PY motif in the cytoplasmic carboxy-terminus of the channel and one of the WW interacting motifs of the ubiquitin ligase Nedd4-2. Jespersen *et al*. demonstrated that among the nine members of Nedd4/Nedd4-like family, Nedd4-2 is the one most commonly expressed in the human heart (12), providing more evidence for its role in cardiac function through the proposed regulation of ion channels at the cell membrane (18). In the present study, using the HEK293 cell expression system, we demonstrate that hERG1 bears a classical PY motif that mediates the interaction of the channel with the ubiquitin ligase Nedd4-2, resulting in channel ubiquitylation. hERG1 modulation by Nedd4-2 leads to the specific reduction of functional channel levels at the cell surface and the subsequent decrease of hERG1-mediated currents.

Experimental Procedures

Cell culture – Human Embryonic Kidney (HEK293) cells were cultured with DMEM medium supplemented with Glutamine 4 mM, FBS 10 % and gentamycine 20 µg/ml. All cell medium components except Glutamine (Sigma Aldrich, Buchs, Switzerland) were purchased from Life Technologies Inc. (Basel, Switzerland). HEK293 cells were maintained at 37°C in a 5%/95% CO_2/O_2 incubator. Empty vector, pcDNA3.1-(+)Zeo-hERG1 wild type (WT) or PY-motif mutants (ΔPY and YA), pcDNA3.2(-)hNedd4-2 WT, -C801S or –S-tag, as well as different ubiquitin-HA-tag constructs (gift of Dr. Philip Shaw, University Hospital of Lausanne, Switzerland) were used to transfect HEK293 cells using either calcium phosphate for patch clamp experiments or JetPEI reagent from Polyplus-Transfection (llkirch, France), according to the manufacturer's instructions. cDNAs ratio for transfection of hERG1: Nedd4-2 was 1:6.

Electrophysiological procedures – HEK293 cells were used for electrophysiological measurements 48 hours after transient transfection. cDNA coding for the reported gene CD8 was used to identify transfected cells decorated with anti-CD8 beads (Invitrogen, Basel, Switzerland). Patch-clamp recordings in whole-cell configuration were carried out using an internal solution containing (mmol/L) KCl 145; EGTA 10; MgCl2 1; HEPES 5; and Mg_2^+-ATP 5, pH 7.3 with KOH; and external solution NaCl 140; KCl 5; $CaCl_2$ 2; $MgCl_2$ 1; HEPES 20; and glucose 5, pH 7.4 with NaOH. Pipette resistance was in the range of 2.0–3.5 MΩ. Measurements were carried out using an Axopatch 200B amplifier (Axon Instruments, Union City, CA), and were performed at room temperature (25 ± 1°C). To study current amplitude, voltage was stepped from a holding potential (HP) of -80 mV to +40 mV, 300 ms, followed by repolarization to -120 mV, 600 ms. Steady-state inactivation was obtained using a double-pulse protocol modified from Vandenberg *et al.* (19); a first depolarizing pulse at +40 mV, 1000 ms, followed by a step pulse ranging from -150 to +40 mV, 1000 ms, by 10-mV increments and then to -120 mV, 400 ms and finally back to HP. Fast inactivation and deactivation kinetics were assessed using the same protocol. Time constant (Tau) of fast inactivation was extracted from fitting onset of current during the step pulse with a mono-exponential according to: $f(t) = (A_1 \cdot e^{-t/Tau}) + C$. Fitting the deactivation part of the tail current between -110 and -60 mV, well described at these potentials by a mono-exponential, enabled extraction of a time constant of deactivation. An activation curve was achieved by subjecting cells to depolarizing steps in the range of -80 to +40 mV, 1000 ms, before measuring tail currents at -120 mV, 500 ms. Boltzmann sigmoidal function was used to analyze both activation and steady-state inactivation curves in current (I/Imax) versus membrane potential (V_m) plots and is expressed according to the formula: $I/Imax = 1/(1+\exp((V_{0.5}-V_m)/k))$ to determine the voltage of half maximal activation or inactivation ($V_{0.5}$) and the slope factor (k). Activation and slow inactivation kinetics were assessed with the activation curve protocol, where onset of the current between -30 and +30 mV and subsequent decrease of the current in pulses between +20 and +60 mV were independently fitted with a mono-exponential to extract time

constants of activation and slow inactivation, respectively.

Cell surface biotinylation assay – HEK293 cells were transiently transfected with hERG1 WT or PY-mutant cDNAs 48 hours prior to treatment with EZ-Link™ Sulfo-NHS-SS-Biotin (Pierce, Rockford, IL) at 0.35 mg/ml in cold PBS for 30 min at 4°C. Following cell surface biotinylation, HEK293 cells were washed three times with cold Glycine solution 200 mM in PBS, plus once in cold PBS to inactivate and remove excess biotin. The cells were lysed for 45 min in lysis buffer containing (mmol/L) HEPES 50 pH 7.4; NaCl 125; $MgCl_2$ 1,5; EGTA 1 pH 8; and 8.7 % glycerol; 1% Triton X-100; 24 mg N-ethylmaleimide and 1 tablet of Complete® protease inhibitors cocktail (Roche Diagnosis, Mannheim, Germany). Cell lysates were spun at 16000 x g for 15 min, and the supernatants were incubated for 2 h at 4°C with Steptavidin Sepharose™ beads (GE Healthcare, Uppsala, Sweden). Beads were subsequently spun and washed 5 times with lysis buffer supplemented with 1% of PMSF 100 mM in isopropanol. Pelleted beads were then resuspended in 2.5 x SDS-PAGE loading buffer, denatured 30 min at 37 °C, and analyzed in 7% polyacrylamide gel electrophoresis.

Immunoprecipitation – The cells were lysed 48h after transfection in lysis buffer as described above. Triton-X100 soluble fractions from HEK293 cells were incubated for 2 hours by rotation at 4°C with anti-hERG1 antibody (APC062, Alomone) preincubated at room temperature for 30 minutes with Dynabeads® Protein A (Invitrogen), according to the provider's protocol. After washing of the beads 3 times with lysis buffer, immunoprecipitated-fractions were analyzed by Western blot.

Pull down assays- S5A cDNA was cloned into pGEX-4T1 (Amersham Bioscience, Uppsala, Sweden). Expression of GST-fusion proteins in *E. coli* cells was induced with 0.2 mmol/L IPTG for 4 h at 29°C. Cells were harvested by centrifugation and resuspended in lysis buffer. Soluble fractions from a 15 min-centrifugation at 13,000 *g* (4°C) were rotated for 1 h in the presence of Glutathione-Sepharose beads (GE Healthcare) at 4°C. Beads containing bound fusion proteins were recovered after washing and used in pull-down experiments. 1 mg of total protein was added to 50 µg of beads and incubated for 2 h at 4°C with rotation. After washing of the beads, precipitated proteins were analyzed by Western blot.

Western blot – Antibodies against the carboxy-terminus of hERG1 and against actin were purchased from Alomone (APC-062, Jerusalem, Israel) and Sigma Chemical (A2066, Sigma Aldrich, Buchs, Switzerland), respectively. Antibodies against Nedd4-2 (gift of Dr. O. Staub, University of Lausanne, Switzerland) were produced as previously described (20) and Nedd4-2-S-tag proteins were revealed with S-protein horseradish peroxidase conjugate from Novagen (69047-3). Antibodies against HA-tag (H3663, Sigma Chemical) were used to detect the overexpression of ubiquitin peptides.

Data analysis and statistics – Electrophysiological data were analyzed using pClamp software, version 10 (Axon Instruments, Union City, CA). Western blots were scanned and quantified with Odyssey infrared imaging system and software, version 2.1 (LI-COR, Lincoln, NE), respectively. The statistical significance of the differences between the means was determined, as specified, by either a two-tailed Student t-test or by a one-way ANOVA, using GraphPad Prism software, version 5 (GraphPad Softwares, La Jolla, CA). $P<0.05$ was considered statistically significant. Data are presented as means ± standard error of the means (SEM).

RESULTS

hERG1 current is down-regulated by Nedd4-2. hERG1 possesses an extended PY motif (P/LPxYxxΦ) in its carboxy-terminal tail, which is conserved across species (Figure 1). The PY motif is known to interact with WW binding domains of the Nedd4/Nedd4-like family ubiquitin ligases (5). Due to the presence of this characteristic PY motif, we investigated whether the potassium current mediated by hERG1 (I_{hERG1}) is regulated by the ubiquitin ligase Nedd4-2, as been observed for two other cardiac ion channels, $Na_V1.5$ and KCNQ1 (11-12). The functional effects of the ubiquitin ligase Nedd4-2 on I_{hERG1} were assessed using whole-cell patch clamp experiments. As shown in Figure 2, transient overexpression of

hERG1 and Nedd4-2 in HEK293 cells leads to a robust reduction of I_{hERG1} (-74 ± 4%) compared to hERG1 alone. We investigated whether a mutation in the PY motif of hERG1 could abolish the Nedd4-2 effect on I_{hERG1}. Rougier *et al.* previously demonstrated the primordial role of the tyrosine residue of the PY motif of $Na_V1.5$ channels in the Nedd4-2-dependent down-regulation (21). The tyrosine residue of the PY motif of hERG1 was mutated into alanine, referred to as hERG1-YA (Figure 1). The effect of Nedd4-2 was only partially abolished (Figure 2), since the hERG1-YA current was decreased by 36 ± 9% upon Nedd4-2 co-transfection. To determine if other amino acids containing the hERG1 PY motif might also be of importance, the three amino acids forming the canonical PY motif of hERG1, PPxY, were mutated into alanine, thus completely removing this interaction motif (Figure 1). The currents elicited by the PY motif-free channel (hERG1-ΔPY) were no longer down-regulated by Nedd4-2 ($I_{hERG1\text{-}\Delta PY+Nedd4\text{-}2}$: -7 ± 8% n.s. compared to $I_{hERG1\text{-}\Delta PY}$, Figure 2), thus confirming that the effect of Nedd4-2 on hERG1 is PY motif-dependent. We also observed that the overexpression of a catalytically inactive form of Nedd4-2, Nedd4-2C801S (22), did not change the peak current of hERG1 WT, -YA or -ΔPY mutants (-4 ± 8%, 5 ± 9% and -2 ± 12%, respectively, Figure 2A), providing evidence that the effects of Nedd4-2 are dependent on a functional HECT catalytic domain. We then compared the biophysical properties of hERG1 in the presence or absence of Nedd4-2 and found slight differences in these two conditions, as presented and discussed in the supplementary data file.

hERG1 interacts with Nedd4-2 via its PY motif. The biochemical interactions between hERG1 and Nedd4-2 were investigated by co-precipitation experiments (Figure 3). When expressed with hERG1 WT, Nedd4-2 was present in the fraction immunoprecipitated with the anti-hERG1 antibody (Co-IP, lane 3, Figure 3A and 3B), and simultaneously, hERG1 WT protein was found in the co-precipitated fraction after Nedd4-2-S-protein pull-down (Co-PD, lane 3, Figure 3A and 3B). In order to confirm the PY motif-dependent interaction of hERG1 and Nedd4-2, co-immunoprecipitation assays were conducted using mutant hERG1-YA and hERG1-ΔPY and the ubiquitin ligase Nedd4-2. Regarding the single tyrosine mutation of the PY motif, a small fraction of Nedd4-2 was still co-immunoprecipitated with hERG1-YA (Co-PD and Co-IP, lane 4, Figure 3A), thus confirming the results obtained in the patch clamp experiments. When hERG1-ΔPY and Nedd4-2 were co-expressed, no interaction between these two proteins was detected (Co-IP and Co-PD, lane 5, Figure 3B), providing further evidence to the role of Nedd4-2 in the regulation of hERG1 via its PY motif.

Nedd4-2 promotes specific down-regulation of functional hERG1 at the plasma membrane. We investigated whether the decrease of I_{hERG1} could be due to a depletion of hERG1 protein at the plasma membrane. Initially we quantified the total level of hERG1 protein with or without co-expression of the ubiquitin ligase. Western blots of hERG1 protein in total HEK293 lysates (Figure 4) revealed that Nedd4-2 co-expression specifically decreased the fully glycosylated (fg) or mature form of hERG1 observed at 155 kDa (23); whereas the lower band at 135 kDa, known as the core-glycosylated (cg) or non mature form (23), was not changed upon Nedd4-2 co-expression. The quantification of the mature form of hERG1 was decreased by ~40% in the presence of Nedd4-2 (64 ± 8% *vs* 100 ± 4% for hERG1 alone); whereas the quantification of the non mature form was unchanged (93 ± 14% *vs* 100 ± 7% for hERG1 alone, *left panels* of Figure 4B and 4C). To confirm the down-regulation of the functional form of hERG1 by Nedd4-2, we quantified the amount of hERG1 localized at the plasma membrane by cell surface biotinylation assays. As previously shown, the biotinylated fraction demonstrated that cell surface channels are mainly constituted of the mature hERG1, but also non-mature proteins (Figure 4A) (23). We found that the number of channels at the plasma membrane was significantly reduced in the presence of the Nedd4-2 ubiquitin ligase (for mature hERG1: 66 ± 1% with Nedd4-2 *vs* 100 ± 5% for hERG1 alone; for non mature hERG1: 69 ± 6% with Nedd4-2 *vs* 100 ± 5% for hERG1 alone *right panels* of Figure 4B and 4C). These findings most likely underlie the effect of Nedd4-2 on I_{hERG1}.

hERG1 is ubiquitylated by Nedd4-2. Considering the findings that the ubiquitin ligase enzyme Nedd4-2 interacts with the hERG1 PY motif (Figure 2), we hypothesized that hERG1 could be a substrate for Nedd4-2. Two different approaches

were used to test this hypothesis. First we used the S5A protein, a proteasomal subunit which displays high affinity to ubiquitylated proteins (24), in order to determine the level of ubiquitylation of hERG1. Ubiquitylated protein fractions were precipitated by pull-down experiments using GST-S5A fusion proteins. Anti-hERG1 antibody was then used to detect ubiquitylated hERG1 in the Western blots (Figure 5A). The second approach was the immunoprecipitation of hERG1 (Figure 5) from HEK293 cells transiently expressing the channel with or without Nedd4-2. Western blot analyses were then performed using either an anti-hERG1 antibody (IP, Figure 5B) or an anti-ubiquitin antibody to reveal the immunoprecipitated proteins (IP, Figures 5C and D). These two complementary methods enabled us to confirm that hERG1 was most likely directly ubiquitylated by Nedd4-2, since Nedd4-2 co-expression dramatically increased the ubiquitylation of the channel. To determine the specificity of the ubiquitylation of hERG1 by Nedd4-2 we used enzymatically deficient Nedd4-2-C801S and two other members of the ubiquitin ligase Nedd4-family, Nedd4-1 and WWP2. As illustrated in Figure 5B, neither Nedd4-2C801S nor the other ligases had an effect on the basal ubiquitylation of hERG1.

Finally, we investigated the type of ubiquitylation chains promoted by Nedd4-2 ubiquitin ligase. We co-expressed hERG1 with or without Nedd4-2, and WT or mutant ubiquitins bearing an HA-tag (Figure 6). Mutant ubiquitin-K0 encodes for the ubiquitin protein in which the seven lysine residues are mutated into arginine, resulting in the inability to form a ubiquitin chain. Mutants K48 and K63 represent ubiquitin proteins for which only lysine 48 or 63 are available for chain formation, since the other lysine residues are mutated. Conversely, mutants K48R and K63R are ubiquitin proteins with mutation on only lysine 48 or 63, respectively. After hERG1 immuno-precipitation (Figure 6), global ubiquitylation of the channel was evidenced by western blotings against ubiquitylated proteins (Figure 6C), and integration of ubiquitin mutants was assessed by immunoblots against the HA-tag (Figure 6D). First, we observed that the pattern of hERG1 ubiquitylation by the different mutants is similar to that of the global pattern of ubiquitylation. However, co-transfection of hERG1 with Nedd4-2 and ubiquitin WT enhanced ubiquitylation of the channel, suggesting that under these conditions the availability of free ubiquitin in HEK293 cells is limited. Finally, we quantified the addition of tagged ubiquitins, WT or mutant, in presence of Nedd4-2. Ubiquitylation obtained with the WT ubiquitin was arbitrarily fixed at 100 (Figure 6E). A statistical analysis test was used to compare ubiquitylation obtained with mutants versus the wild-type peptide. We observed reduced Nedd4-2-dependent ubiquitylation of the channel with the K0 mutant, suggesting that Nedd4-2 may add chains of ubiquitin and not multiple mono-ubiquitins. However, the basal signal obtained with the K0 mutant argues in favor of endogenous multiple mono-ubiquitylation of the channel. Ubiquitylation levels obtained with the K48 mutant were similar to those obtained with the K0 mutant, suggesting that ubiquitin chains added by Nedd4-2 may not be K48-linked. Furthermore, the ubiquitylation of hERG1 by Nedd4-2 with the K48R mutant is similar to the ubiquitylation obtained with the WT ubiquitin, confirming that the residue 48 of ubiquitin is not involved in ubiquitin-chain formation dependent on Nedd4-2. Ubiquitylation of the channel by the K63 mutant showed a similar ubiquitylation pattern as that seen with the mutant K0, indicating that chains added by Nedd4-2 are not K63 chains. Contrary to the K48R results, residue lysine 63 appears to be involved in the Nedd4-2-dependent ubiquitylation of hERG1, as the level of channel ubiquitylation is low when this residue is mutated (with mutant Ub K63R). Altogether, these results suggest that Nedd4-2 promotes the addition of mixed chains of ubiquitin, linked by their respective K63s, and that another non-determined lysine may also be implicated. The possibility that Nedd4-2 is responsible for the addition of pure K63-ubiquitin chains to hERG1 was also excluded by performing Western blots with an antibody that specifically recognized K63-ubiquitin chains upon hERG1 co-immunoprecipitation; no hERG1 K63-ubiquitylation signal was detected after Nedd4-2 co-transfection (data not shown).

DISCUSSION

The major findings of this study are that 1) hERG1 interacts via its PY motif with the ubiquitin ligase Nedd4-2, 2) this interaction

promotes the down-regulation of the functional form of the channel at the plasma membrane through the addition of K63-Kx-ubiquitin chains to the channel, and 3) I_{hERG1} is strongly decreased by Nedd4-2 catalytic-dependent activity.

Interaction of hERG1 with Nedd4-2 via its PY motif. The hERG1 PY motif is a highly conserved sequence across species lines (Figure 1), highlighting its crucial role in the regulation of the hERG1 channel at the cell surface. The PPxYxxΦ sequence harbored by hERG1 is similar to the sequence of voltage-gated sodium channels (Na_Vs) (25) and ENaC channels (26), which have been shown to interact with Nedd4-2. It is, however, different from the LPxY motif present in the potassium channel KCNQ1, which is known to interact with ubiquitin ligases of the Nedd4/Nedd4-like family. In contrast to other cardiac ion channels (21), the tyrosine of the hERG1 PY motif plays a less important role in the interaction with Nedd4-2. We found that after single mutation of this tyrosine, hERG1-YA mutant still interacts with Nedd4-2, although to a lesser extent than the WT channel. The interaction of hERG1 with the ubiquitin-protein ligase was completely disrupted after the full canonical PPxY motif was mutated into alanine, e.g. hERG1-ΔPY. Surprisingly, in a previous study Rougier *et al.* found only a weak affinity of the hERG1 PY motif with the WW binding domains of Nedd4-2 (21). These contradictory results argue in favor of an important role of the tridimensional conformation of the PY motif of hERG1 in the interaction with Nedd4-2. Indeed, in the study of Rougier and co-workers only 10 amino acids were used to establish the affinity between the PY motif and the WW binding domains of Nedd4-2. Moreover, in its functional three-dimensional conformation, hERG1 is a homotetramer comprising four PY motifs, while Nedd4-2 harbors four WW domains. It is possible that several PY motifs of hERG1 interact with several WW domains of Nedd4-2 simultaneously.

Degradation of the functional form of hERG1 by Nedd4-2. Western blot analyses of hERG1 in a heterologous expression system revealed two main forms of the channel, the mature or fully glycosylated form and the non-mature or core-glycosylated form. We found that in the whole-cell lysates, only the fully glycosylated form of the channel was down-regulated upon Nedd4-2 co-expression, whereas the levels of the core-glycosylated form remain unaltered. At the cell surface, both forms were found decreased by Nedd4-2. These results point to a subcellular-dependent effect of Nedd4-2. Rougier *et al.* presented experimental evidence showing that Nedd4-2 decreased the plasma membrane density of the cardiac sodium channel $Na_V1.5$ by accelerating its internalization rate (21). Similar results have also been presented for ENaC channel ubiquitylation by Nedd4-2 (27). Altogether, these results suggest specific Nedd4-2-dependent degradation of the functional hERG1 channel localized at the plasma membrane.

hERG1 ubiquitylation by Nedd4-2. This study demonstrates that Nedd4-2 promotes K63-Kx-ubiquitin chain addition to the channel. To our knowledge, the type of ubiquitylation mediated by Nedd4-2 has only been investigated in one previous publication (28), which described a different mechanism of ubiquitylation in which Nedd4-2 added chains of four ubiquitin K63-linked to the dopamine transporter DAT. There is also discrepancy regarding of the size of the ubiquitin chains added, as in this study we observed ubiquitin smears that indicated that different sizes of ubiquitin chains can be added to hERG1.

Down-regulation of hERG1 channel and its implication in vivo. hERG1 encodes the pore-forming subunit of the rapidly activating-delayed rectifier K^+ channel (I_{Kr}) in the heart, which is crucial for the repolarization phase of the cardiac AP. Our results show that the ubiquitin ligase Nedd4-2 down-regulates I_{hERG1} measured in a mammalian cell line. The main limitation of our study is the lack of *in vivo* support, however, Nedd4-2 associated pathologies and *in vivo* evidence of voltage-gated cardiac ion channel ubiquitylation have been provided. For example, defective ubiquitylation of ENaC subunits by Nedd4-2 is responsible for Liddle's syndrome (28) and the overexpression of Nedd4-2 WT (14) or catalytically inactive mutant in guinea pig cardiomyocytes leads to alterations of KCNQ1-mediated slowly activating-delayed rectifier K^+ currents, I_{Ks} (12). It has been reported that the serum and glucocorticoid inducible kinase 3 (SGK3) upregulates I_{hERG1} by increasing protein levels in the plasma membrane, without affecting

the K^+ channel activating kinetics (29). SGK3 has previously been shown to up-regulate KCNQ1/KCNE1 (30), the other key K^+ channel involved in cardiac repolarization. Both SGK3 and SGK1 are kinases expressed in the cardiac tissue, and mRNA levels of SGK3 are particularly high in mouse hearts (31) (32). SGK3 appears to be constitutively expressed and regulated, whereas SGK1 is more sensitive to transcriptional regulation (33) (34). In their study, Maier and co-workers concluded that SGK3 down-regulation of hERG1 is not achieved through direct phosphorylation of the K^+ channel, but might result from the phosphorylation and inactivation of Nedd4-2 which decreases substrate affinity and ubiquitylation (29). Such regulation of ion channel cell surface expression has already been reported for ENaC, in which SGK1 was found to phosphorylate Nedd4-2 resulting in elevated amount of channels at the membrane (35). Our observations suggest that Nedd4-2 could be the involved in SGK3-dependent mechanism of hERG1 regulation, though direct evidence of Nedd4-2 phosphorylation by SGK3 is still pending.

In conclusion, the results of the present work indicate that ubiquitylation of hERG1 by the ubiquitin ligase Nedd4-2 is a potentially constitutive physiological mechanism for the regulation of hERG1 channel membrane density and that it contributes to the regulation of cardiac repolarization.

REFERENCES

1. Sanguinetti, M. C., and Tristani-Firouzi, M. (2006) *Nature* **440**, 463-469
2. Sanguinetti, M. C., Jiang, C., Curran, M. E., and Keating, M. T. (1995) *Cell* **81**, 299-307
3. Brugada, R., Hong, K., Dumaine, R., Cordeiro, J., Gaita, F., Borggrefe, M., Menendez, T. M., Brugada, J., Pollevick, G. D., Wolpert, C., Burashnikov, E., Matsuo, K., Sheng Wu, Y., Guerchicoff, A., Bianchi, F., Giustetto, C., Schimpf, R., Brugada, P., and Antzelevitch, C. (2004) *Circulation* **109**, 30-35
4. Anderson, C. L., Delisle, B. P., Anson, B. D., Kilby, J. A., Will, M. L., Tester, D. J., Gong, Q., Zhou, Z., Ackerman, M. J., and January, C. T. (2006) *Circulation* **113**, 365-373
5. Abriel, H., and Staub, O. (2005) *Physiology* **20**, 398-407
6. Hershko, A., and Ciechanover, A. (1998) *Annual Review of Biochemistry* **67**, 425-479
7. Komander, D. (2009) *Biochemical Society Transactions* **037**, 937-953
8. Chen, Z. J., and Sun, L. J. (2009) *Molecular Cell* **33**, 275-286
9. Ikeda, F., and Dikic, I. (2008) *EMBO Reports* **9**, 536-542
10. Staub, O., Gautschi, I., Ishikawa, T., Breitschopf, K., Ciechanover, A., Schild, L., and Rotin, D. (1997) *EMBO Journal* **16**, 6325-6336
11. van Bemmelen, M. X., Rougier, J. S., Gavillet, B., Apotheloz, F., Daidie, D., Tateyama, M., Rivolta, I., Thomas, M. A., Kass, R. S., Staub, O., and Abriel, H. (2004) *Circulation Research* **95**, 284-291
12. Jespersen, T., Membrez, M., Nicolas, C. S., Pitard, B., Staub, O., Olesen, S. P., Baro, I., and Abriel, H. (2007) *Cardiovascular Research* **74**, 64-74
13. Staub, O., and Rotin, D. (2006) *Physiological Reviews.* **86**, 669-707
14. Abriel, H., Loffing, J., Rebhun, J. F., Pratt, J. H., Schild, L., Horisberger, J.-D., Rotin, D., and Staub, O. (1999) *The Journal of Clinical Investigation* **103**, 667-673
15. Staub, O., and Rotin, D. (1996) *Structure* **4**, 495-499
16. Huibregtse, J. M., Scheffner, M., Beaudenon, S., and Howley, P. M. (1995) *Proceedings of the National Academy of Sciences of the United States of America* **92**, 2563-2567
17. Nalefski, E. A., and Falke, J. J. (1996) *Protein Science* **5**, 2375-2390
18. Persaud, A., Alberts, P., Amsen, E. M., Xiong, X., Wasmuth, J., Saadon, Z., Fladd, C., Parkinson, J., and Rotin, D. (2009) *Molecular Systems Biology* **5**
19. Vandenberg, J. I., Varghese, A., Lu, Y., Bursill, J. A., Mahaut-Smith, M. P., and Huang, C. L.-H. (2006) *American Journal of Physiology* **291**, C165-175
20. Flores, S. Y., Loffing-Cueni, D., Kamynina, E., Daidie, D., Gerbex, C., Chabanel, S., Dudler, J., Loffing, J., and Staub, O. (2005) *Journal of the American Society of Nephrology* **16**, 2279-2287
21. Rougier, J. S., van Bemmelen, M. X., Bruce, M. C., Jespersen, T., Gavillet, B., Apotheloz, F., Cordonier, S., Staub, O., Rotin, D., and Abriel, H. (2005) *American Journal of Physiology* **288**, C692-701

22. Scheffner, M., Nuber, U., and Huibregtse, J. M. (1995) *Nature* **373**, 81-83
23. Phartiyal, P., Jones, E. M. C., and Robertson, G. A. (2007) *Journal of Biological Chemistry* **282**, 9874-9882
24. Layfield, R., Tooth, D., Landon, M., Dawson, S., Mayer, J., and Alban, A. (2001) *Proteomics* **1**, 773-777
25. Fotia, A. B., Ekberg, J., Adams, D. J., Cook, D. I., Poronnik, P., and Kumar, S. (2004) *Journal of Biological Chemistry* **279**, 28930-28935
26. Staub, O., Abriel, H., Plant, P., Ishikawa, T., Kanelis, V., Saleki, R., Horisberger, J.-D., Schild, L., and Rotin, D. (2000) *Kidney International* **57**, 809-815
27. Abriel, H., Loffing, J., Rebhun, J. F., Pratt, J. H., Schild, L., Horisberger, J. D., Rotin, D., and Staub, O. (1999) *The Journal of Clinical Investigation* **103**, 667-673
28. Vina-Vilaseca, A., and Sorkin, A. (2010) *Journal of Biological Chemistry* (in press)
29. Maier, G., Palmada, M., Rajamanickam, J., Shumilina, E., Bohmer, C., and Lang, F. (2006) *Cellular Physiology and Biochemistry* **18**, 177-186
30. Embark, H. M., Bohmer, C., Vallon, V., Luft, F., and Lang, F. (2003) *Pflugers Archiv* **445**, 601-606
31. Kobayashi, T., Deak, M., Morrice, N., and Cohen, P. (1999) *Biochemical Journal* **344 Pt 1**, 189-197
32. Waldegger, S., Barth, P., Raber, G., and Lang, F. (1997) *Proceedings of the National Academy of Sciences of the United States of America* **94**, 4440-4445
33. Lang, F., and Cohen, P. (2001) *Science Signaling STKE* **2001**, re17
34. Brennan, F. E., and Fuller, P. J. (2000) *Molecular and Cellular Endocrinology* **166**, 129-136
35. Debonneville, C., Flores, S. Y., Kamynina, E., Plant, P. J., Tauxe, C., Thomas, M. A., Munster, C., Chraibi, A., Pratt, J. H., Horisberger, J. D., Pearce, D., Loffing, J., and Staub, O. (2001) *EMBO Journal* **20**, 7052-7059
36. Henke, G., Maier, G., Wallisch, S., Boehmer, C., and Lang, F. (2004) *Journal of Cellular Physiology* **199**, 194-199
37. Perrin, M. J., Subbiah, R. N., Vandenberg, J. I., and Hill, A. P. (2008) *Progress in Biophysics and Molecular Biology* **98**, 137-148
38. Benson, M. D., Li, Q. J., Kieckhafer, K., Dudek, D., Whorton, M. R., Sunahara, R. K., Iniguez-Lluhi, J. A., and Martens, J. R. (2007) *Proceedings of the National Academy of Sciences of the United States of America* **104**, 1805-1810

FOOTNOTE

* The work was supported by grants of the Swiss National Science Foundation to HA (310030_120707). We are grateful to Maria Essers and Sophie Roy for their expert technical assistance. We thank Dr. Allison Felley Jacquemont and Dr. Jean-Sébastien Rougier for their thorough reading of the manuscript and helpful comments.

The abbreviations used are:
AP, Action Potential; EGTA, ethylene glycol tetra-acetic acid; GST, Gluthatione-S-transferase; HEK293, Human Embryonic Kidney 293 cells; HEPES, 4-(2-hydroxyethyl)-1-piperazineethanesulfonic acid; hERG1, human ether-à-gogo-related gene 1; HP, Holding Potential; I_{hERG1}: hERG1 current; IPTG, Isopropyl β-D-1-thiogalactopyranoside; Nedd4-2, neural precursor cell expressed developmentally down-regulated 4-2; LQTS, Long QT Syndrome; PBS, Phosphate Buffer Saline; SUMO: small ubiquitin-like modifier protein; $V_{0.5}$, voltage of half maximal activation or inactivation.

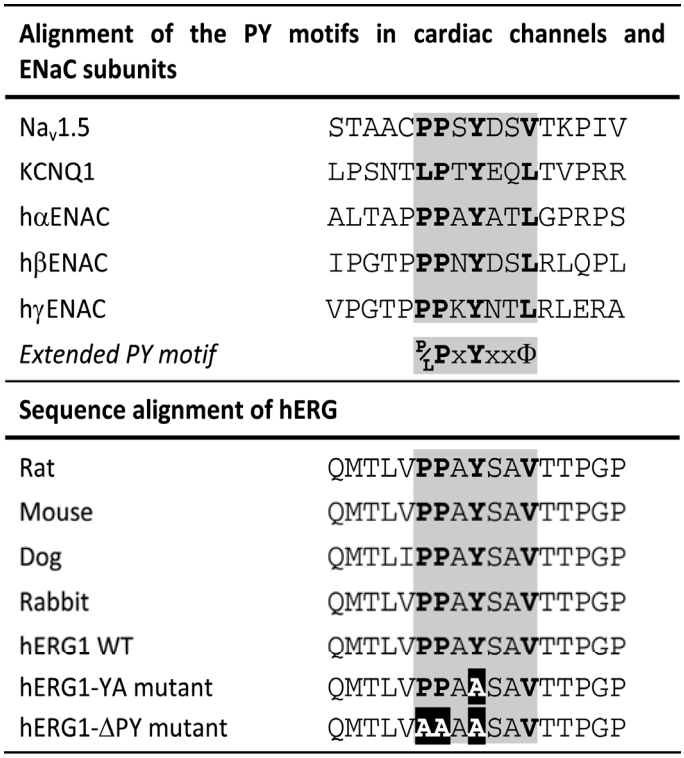

Figure 1. Alignment of extended PY motifs of cardiac ion channels (Nav1.5 and KCNQ1) and ENaC subunits. Extended PY motif is presented in bold characters, where L is a leucine, P is a proline, Y is a tyrosine, x any amino acid, and Φ is a hydrophobic amino acid. Sequence alignments of the C-terminal peptide sequence of *KCNH2* (hERG1-WT) show (similar to Nav1.5, KCNQ1 and ENaC) a conserved extended PY motif in the distal C-terminus in five different animal species using *T-Coffee* software (www.ch.embnet.org/software/TCoffee.html). Human *KCNH2* PY-motif mutants, referred to as hERG1-YA and -ΔPY, are presented with residues highlighted with black squares.

Albesa, Sintra Grilo et al., Figure 2

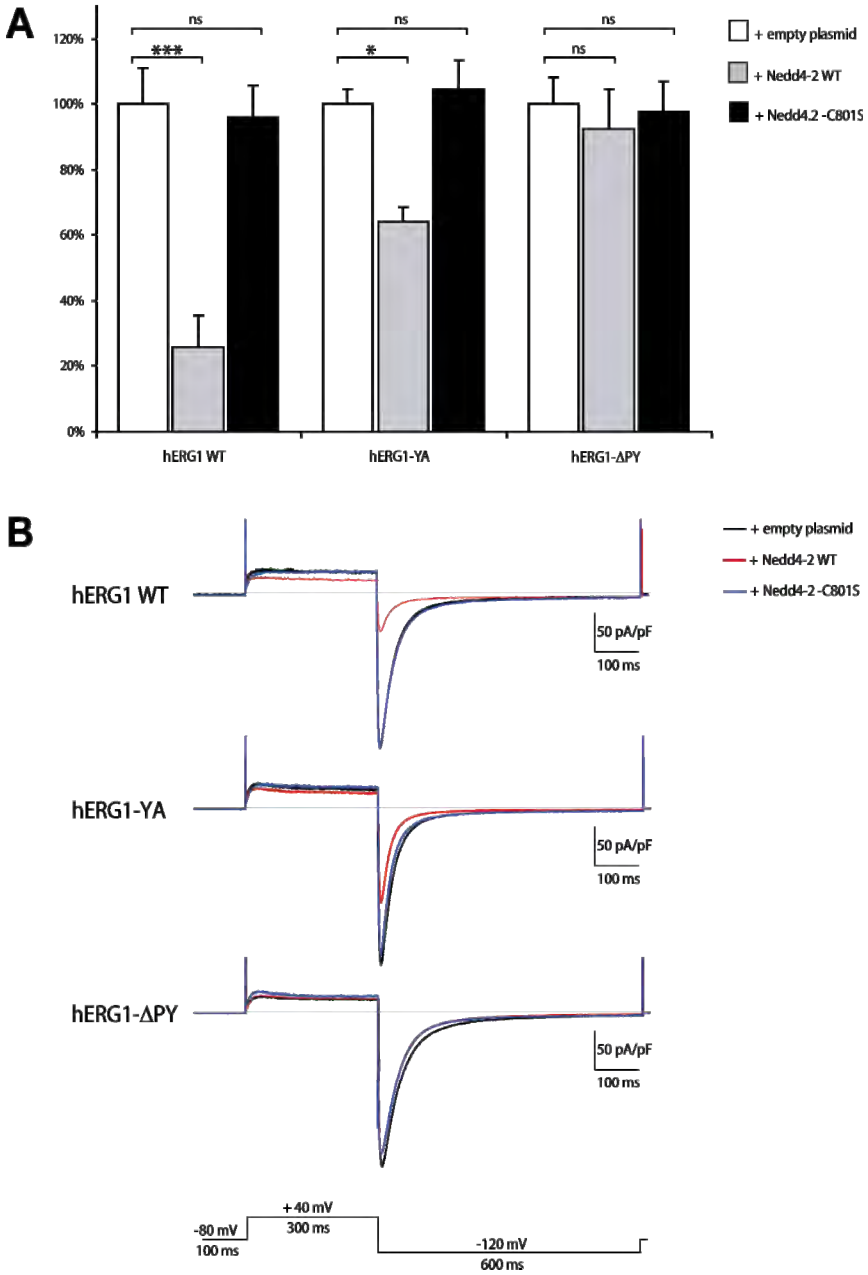

Figure 2. Current density changes observed in HEK293 cells transiently expressing hERG1 WT, YA or -ΔPY mutants in the presence or not of Nedd4-2 or Nedd4-2-C801S. (**A**) Peak tail current density (pA/pF) at -120 mV, normalized to hERG1 condition as presented in (**B**). Significant (*, P<0.05; ***, P<0.001) or non-significant differences (n.s.) versus hERG1 alone obtained after a one-way ANOVA analysis followed by Dunnett's post-test for n=14-23 cells in at least 3 independent experiments. (**B**) Current traces of hERG1 WT, YA and -ΔPY mutants, in presence or absence of Nedd4-2 WT or -C801S. Peak tail current amplitudes were obtained in whole cell configuration according to the protocol presented in inset and were normalized to cell capacitance (pA/pF).

Albesa, Sintra Grilo et al., Figure 3

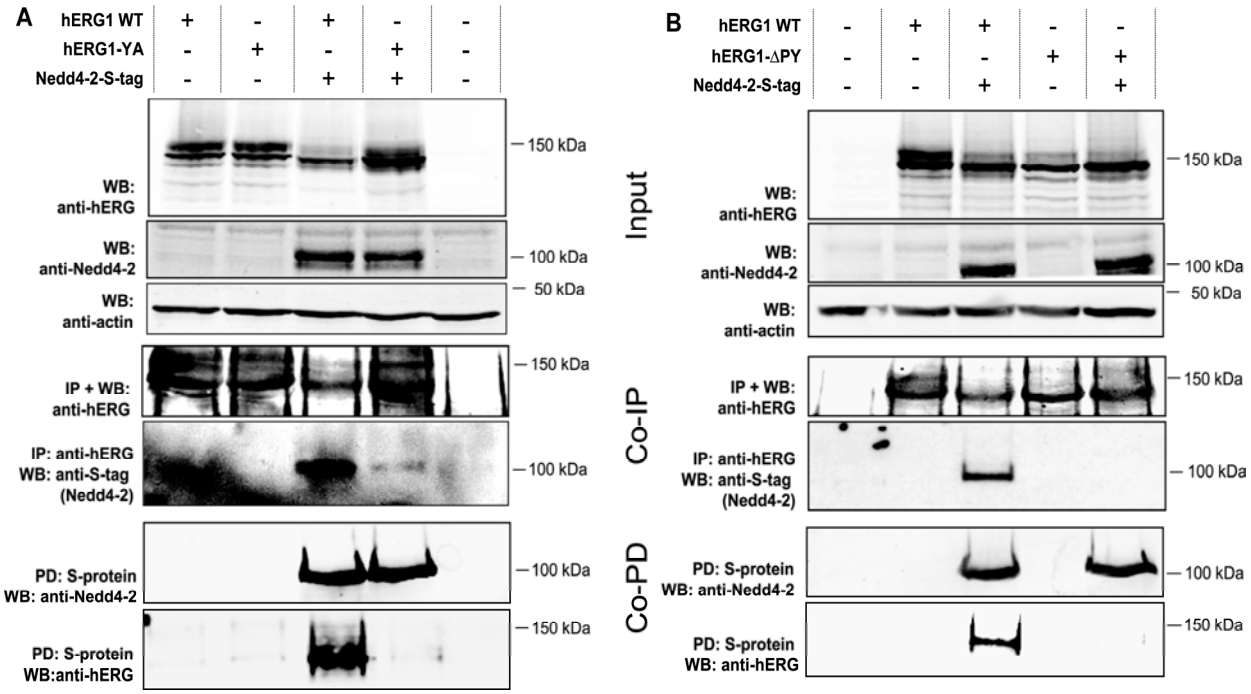

Figure 3. The protein interaction between hERG1 WT and Nedd4-2 is partially disrupted by hERG1-YA mutation and abolished with hERG1-ΔPY mutant. hERG1 channel interacts via its PY motif with Nedd4-2 ubiquitin ligase. (**A**) *Upper panels*: Input signals confirm the expression of hERG1-WT, hERG1-YA and Nedd4 2-S-tag, as well as equal loading by actin band intensity. *Middle panels*: Co immunoprecipitated Nedd4-2-S-tag (Co-IP) after hERG1 immunoprecipitation (IP) show interaction of Nedd4-2 protein with hERG1 WT and, to a lesser extent, with hERG1-YA mutant. *Lower panels*: Co-precipitated hERG1 (Co-PD) after Nedd4-2-S-tag pull-down precipitation (PD) with biotinylated S-protein shows intense signal for hERG1 WT and a weak band of co-precipitated hERG1-YA protein. (**B**) Same experiments as in (**A**) realized with hERG1-ΔPY in place of hERG1-YA mutant, where interaction between hERG1 and Nedd4-2-S-tag is revealed by co-immunoprecipitation and co-precipitation assays, but not with the total PY motif mutant hERG1-ΔPY.

Albesa, Sintra Grilo et al., Figure 4

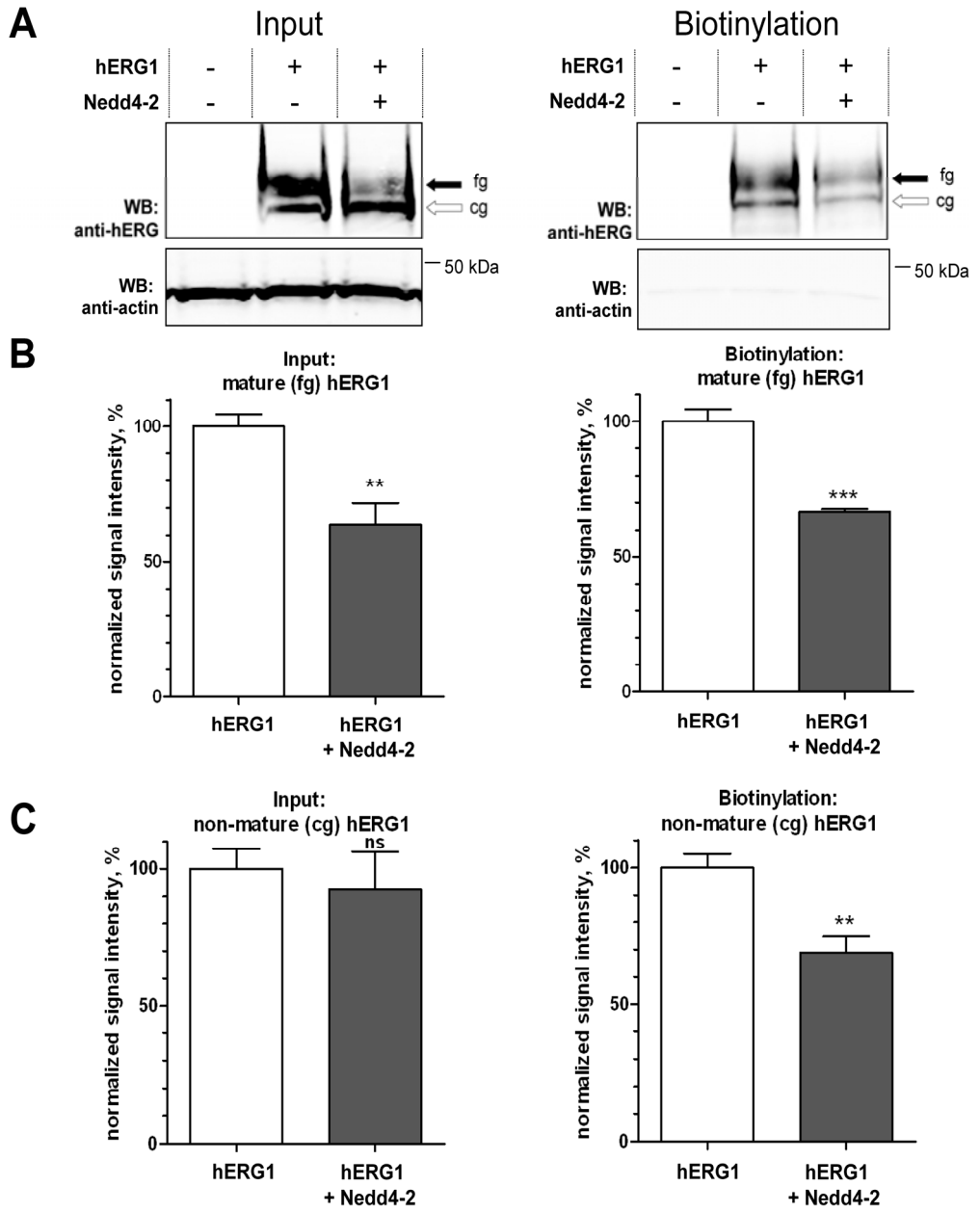

Figure 4. hERG1 mature form is down-regulated by Nedd4-2. (**A**) Western blot of a representative cell surface biotinylation assay on HEK293 cells transiently expressing hERG1-WT alone or with Nedd4-2 WT. hERG1 protein is revealed in its two forms: mature or fully glycosylated (fg) band at 155 kDa and non-mature band (cg, core-glycosylated) at 135k Da. Total lysates of cells (Input) and the biotinylated fractions (Biotinylation) are presented with actin control. (**B**) and (**C**) Quantification of mature and non-mature hERG1 bands, respectively, in repeated biotinylation assays as presented in (**A**), showing that total lysates of cells (Input) present decreased amount of mature hERG1 WT upon Nedd4-2 co-transfection, while the non-mature form remains unchanged. In the biotinylated fraction (Biotinylation), both hERG1 forms are decreased in the presence of Nedd4-2 compared to hERG1 WT alone. Statistical significance was tested with a two-tailed Student's t-test ($P<0.01$,**; $P<0.001$, ***; ns, non significant).

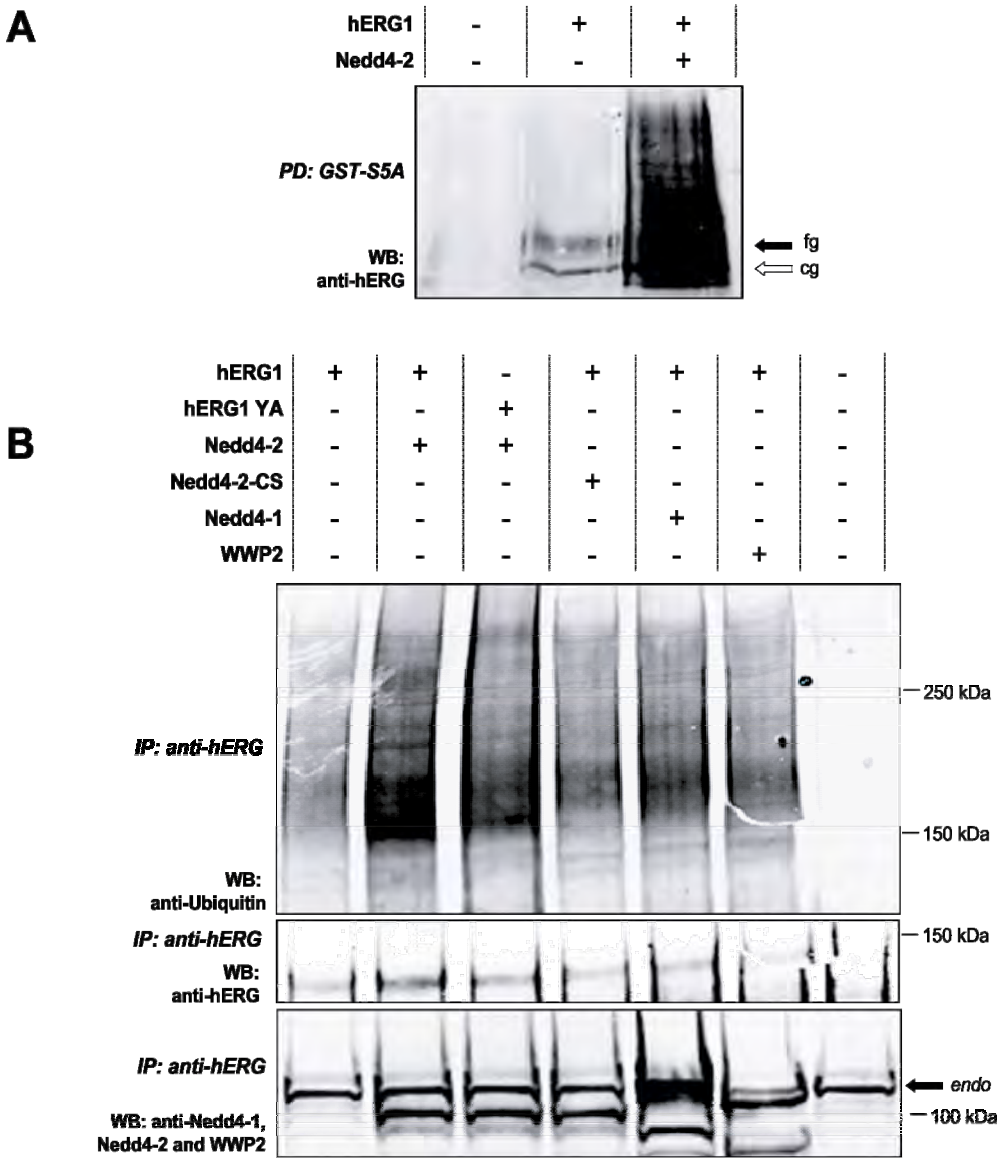

Figure 5. Ubiquitylation of hERG1 is specifically increased upon Nedd4-2 enzymatic activity. (**A**) Direct ubiquitylation of hERG1 by Nedd4-2 was confirmed with a Western blot against hERG1 protein after precipitation with a GST-S5A fusion protein of all ubiquitylated proteins recognized by the proteasomal S5A subunit. The amount of ubiquitylated hERG1 proteins is dramatically increased in Nedd4-2 overexpressing condition. Both mature (fg, 155 kDa) and non mature (cg, 135 kDa) forms of hERG1 protein are clearly seen in control condition only; whereas a smear of bands with higher molecular weights is observed when Nedd4-2 is co-expressed. (**B**) Ubiquitylation of hERG1 was assessed with an antibody recognizing all ubiquitylated proteins after hERG1 immunoprecipitation. Increased ubiquitylation of hERG1 is observed only with Nedd4-2, but not with the catalytically inactive mutant Nedd4-2-C801S (CS), nor with two other members of the Nedd4/Nedd4-like family, i.e. Nedd4-1 and WWP2. Expression of the three ubiquitin ligases was assessed in the cell lysates (upper panel, Input). Endogenous E3s of HEK293 cells are also detected and the main signal is identified with the grey arrow (endo).

Albesa, Sintra Grilo et al., Figure 6

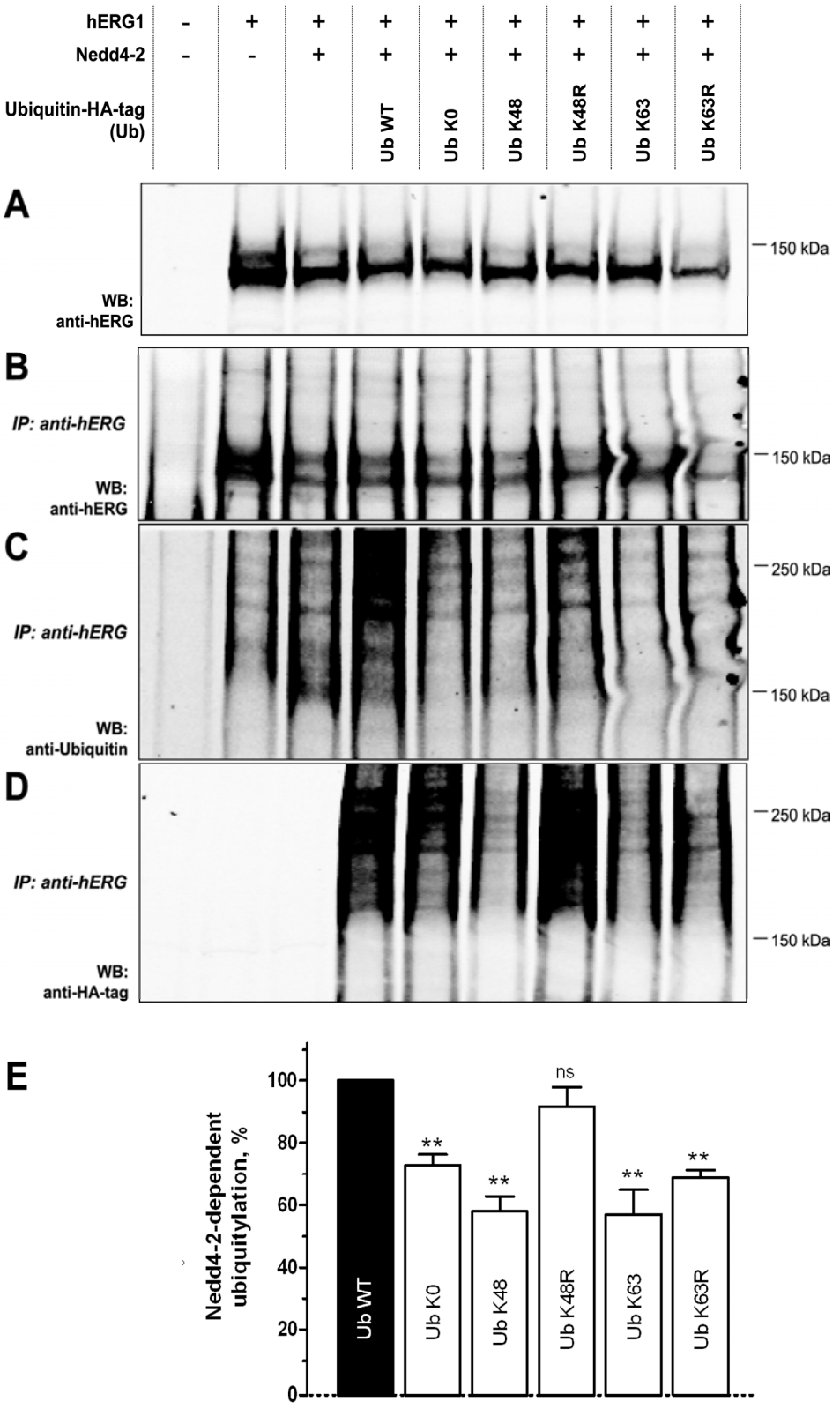

Figure 6. hERG1 protein is ubiquitylated by Nedd4-2 ubiquitin ligase with a pattern of mixed K63- and Kx-ubiquitin chains.

NB: see following page for complete legend.

Figure 6. hERG1 protein is ubiquitylated by Nedd4-2 ubiquitin ligase with a pattern of mixed K63- and Kx-ubiquitin chains. Different HA-tagged ubiquitin peptides were transiently expressed in HEK293 cells co-expressing wild type hERG1 and Nedd4-2 proteins. hERG1 was immunoprecipitated (input (**A**), IP (**B**)) and ubiquitylation of the K+ channel was assessed with two antibodies: (**C**) anti-HA-tag recognizing overexpressed ubiquitins (upper panel of IP) and (**D**) FK2 recognizing all ubiquitylated proteins (middle panel of IP). Overexpressed wild type ubiquitin (Ub WT) presents a ubiquitylation pattern of hERG1 protein similar to endogenous ubiquitin. When all lysines of ubiquitin are mutated to arginine (Ub K0), preventing formation of any chains, ubiquitylation of hERG1 is comparable to basal levels. When all lysine residues except K48 and K63 are mutated to arginine (Ub K48 and Ub K63, respectively) or when only lysine K63 is mutated to arginine (Ub K63R), only basal ubiquitylation is observed; whereas the single mutation of lysine K48 to arginine (Ub K48R) still presents important ubiquitylation of hERG1, ruling out any K48-ubiquitin chain addition by Nedd4-2. (**E**) Signal quantification from three different Western blots as presented in (**D**). Statistical significance was tested with a one-way Anova followed by a Dunnett's multiple comparison test vs Ub WT ($P<0.01$,**; ns, non significant).

Nedd4-2 dependent ubiquitylation and regulation of the cardiac potassium channel hERG1

Maxime Albesa[1‡], Liliana Sintra Grilo[1, 2‡], Bruno Gavillet[3], and Hugues Abriel[1]

[1] Department of Clinical Research, University of Bern, Switzerland [2] Pharmacochemistry, School of Pharmaceutical Sciences, University of Geneva, University of Lausanne, Switzerland [3] Department of Pharmacology, University of Lausanne, Switzerland

[‡]These authors contributed equally to this study

Running title: Ubiquitylation of hERG1 by Nedd4-2

Address correspondence to: Dr. Hugues Abriel, MD PhD, University of Bern, Department of Clinical Research, Murtenstrasse, 35, 3010 Bern, Switzerland, Phone: +41-31-6320928, Fax: +41-31-6320946, e-mail: Hugues.Abriel@dkf.unibe.ch

SUPPLEMENTARY RESULTS

Nedd4-2 modifies hERG1 biophysical properties. To control if the observed decrease in K^+ current was the result of an alteration of the biophysical properties of hERG1, we analyzed the macroscopic I_{hERG1}, WT and mutants, in presence and absence of Nedd4-2 WT or catalytically inactive mutant (C801S). Voltage-dependence of activation and steady-state inactivation are presented in Supplementary Figure 1. Statistical analyses find no significant differences for $V_{0.5}$ of activation and inactivation between all tested conditions. However, the presence of Nedd4-2 tends to shift towards hyperpolarizing voltages both $V_{0.5}$ of activation (~-4 mV) and inactivation (~-8 mV) in hERG1 WT and YA mutant, whereas this tendency is not seen with hERG1 ΔPY. Similarly, Nedd4-1-C801S does not present a trend to alter voltage-dependence of activation or steady-state inactivation. Kinetics of activation and inactivation of I_{hERG1} were also analyzed in alone or in presence of Nedd4-2 WT. Time constant of activation displayed, at potentials between -30 and +10mV, a significant decrease of ~50% and ~40% for hERG1 WT and YA mutant, respectively, when co-expressed with the WT ubiquitin ligase ($P<0.05$, *; $P<0.01$, **; in Supplementary Figure 2A). Conversely, no change in activation kinetics is observed regarding the complete PY motif mutant (hERG1-ΔPY) or regarding deactivation kinetics for all tested conditions (Supplementary Figure 2A and 2B). Since inactivation kinetics is an essential feature of the hERG1 channel, time constants for recovery from inactivation, fast and slow inactivations were analyzed as described in the Methods section. Fast inactivation is significantly accelerated – smaller time constant values – at potentials comprised between -50 and +10 mV when compared to hERG1 conditions without Nedd4-2 ($P<0.05$, *, in Supplementary Figure 3A). This is observed for currents elicited by hERG1 WT and YA mutant. As regards the ΔPY mutant of hERG1, no change in activation kinetics is seen at any of the tested voltages. Time constants of slow inactivation produced the same pattern of sensitivity in presence of Nedd4-2 for hERG1 WT and YA mutant, though differences observed are not always statistically significant. Slow inactivation appears to be faster for hERG1 WT and YA mutant in presence of ubiquitin ligase, but no difference is seen upon Nedd4-2 co-expression for the mutant lacking the PY motif (Supplementary Figure 3B).

SUPPLEMENTARY DISCUSSION

Decrease of hERG1 currents and alteration of biophysical properties by Nedd4-2. Electrophysiological measurements of peak tail currents of hERG1 showed that I_{hERG1} is strongly reduced in presence of Nedd4-2. Down-regulation of K^+ currents required the catalytic activity of the ubiquitin ligase, since when the active cysteine of the Nedd4-2 HECT domain was replaced by a serine (Nedd4-2-C801S mutant) no decrease of current was observed. Effect of Nedd4-2 on I_{hERG1} was shown to be also depending on the PY motif integrity. Mutation of a single residue (hERG1-YA) still conferred ability to Nedd4-2 to decrease significantly the current, while total deletion of the consensus PY motif (hERG1-

ΔPY) abolished the effect of the ubiquitin ligase. Analysis of biophysical properties also revealed small but significant changes upon Nedd4-2 co-transfection. Activation curves of hERG1 WT and –YA appeared shifted towards hyperpolarizing potentials in presence of Nedd4-2, though not significant with the statistical analysis employed. Increased number of open channels at a more negative voltage concomitant with accelerated activation would surprisingly result in increased I_{hERG1}. On the other hand, leftward shift in inactivation curve and faster inactivation of the same hERG1 WT and YA channels would conversely produce a decrease of measured K^+ currents. The resultant effect of these opposite alterations cannot be easily assessed; it would require a mathematical modeling of the hERG1 channel activity, which was beyond the scope of this study. However, it is noteworthy that hERG1 biophysical properties are affected by Nedd4-2, because it is, to our knowledge, the first consistent report of modulation of ion channel activity by direct ubiquitylation. With regard to $Na_v1.5$ (1) and KCNQ1 (2), no changes in the analyzed channel biophysical properties were observed upon Nedd4-2 overexpression. The potassium channel $K_v1.3$, up-regulated by serum glucocorticoid inducible kinase 1 (SGK1), was shown to be partially reversed by Nedd4-2 (3). Interestingly in Henke's study, $V_{0.5}$ of activation is slightly affected, in opposite directions, by Nedd4-2 and SGK1. Moreover, inactivation was significantly accelerated by co-expression of $K_v1.3$ with Nedd4-2 and was slowed by the co-expression of SGK1 (3). Gating kinetics of hERG1 involve complex interactions of segments and helices of the channel (4). It might be speculated that covalent addition of ubiquitin chains to the hERG1 channel not only regulates the amount of functional channels at the cell surface, but also affects, in a steric or electrostatic manner, the normal gating of the channel. For instance, it has been shown that disruption of the ubiquitin-related post-translational SUMO modification of cardiac $K_v1.5$ channel leads to altered inactivation (5). However, the dominant effect of Nedd4-2 on the I_{hERG1} properties is mainly illustrated by the decrease number of ion channel protein and reduced peak K current observed under the present experimental conditions.

REFERENCES

1. van Bemmelen, M. X., Rougier, J. S., Gavillet, B., Apotheloz, F., Daidie, D., Tateyama, M., Rivolta, I., Thomas, M. A., Kass, R. S., Staub, O., and Abriel, H. (2004) *Circulation research* **95**, 284-291
2. Jespersen, T., Membrez, M., Nicolas, C. S., Pitard, B., Staub, O., Olesen, S. P., Baro, I., and Abriel, H. (2007) *Cardiovascular research* **74**, 64-74
3. Henke, G., Maier, G., Wallisch, S., Boehmer, C., and Lang, F. (2004) *J Cell Physiol* **199**, 194-199
4. Perrin, M. J., Subbiah, R. N., Vandenberg, J. I., and Hill, A. P. (2008) *Prog Biophys Mol Biol* **98**, 137-148
5. Benson, M. D., Li, Q. J., Kieckhafer, K., Dudek, D., Whorton, M. R., Sunahara, R. K., Iniguez-Lluhi, J. A., and Martens, J. R. (2007) *Proceedings of the National Academy of Sciences of the United States of America* **104**, 1805-1810

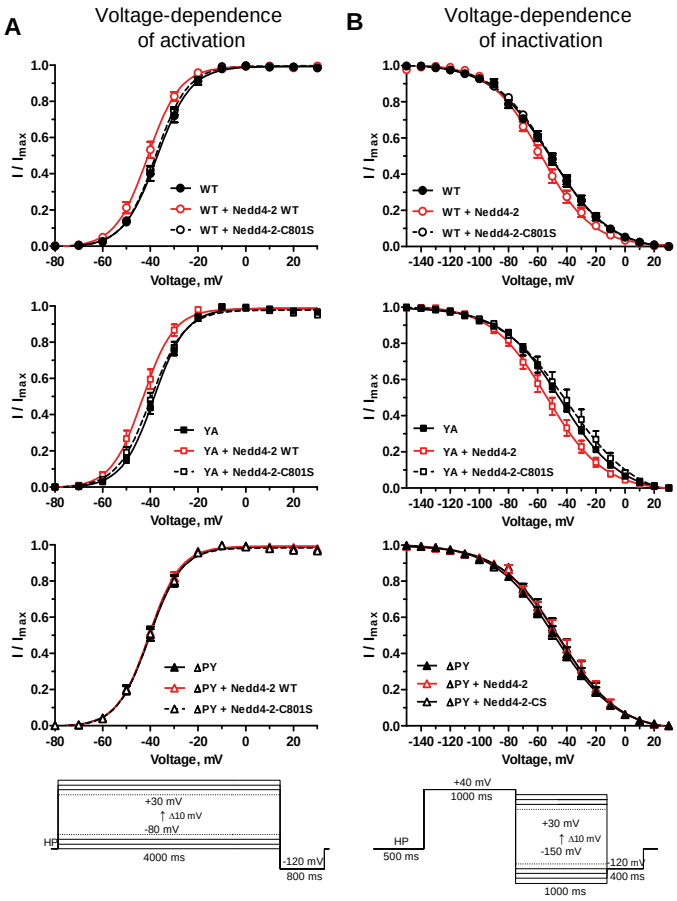

Supplementary Figure 1: Kinetics of activation and voltage-dependence of activation and steady-state inactivation.

(A) Voltage-dependence of activation and steady-state inactivation show no significant difference between tested conditions. Tendency (statistically non significant) towards hyperpolarizing shift of $V_{0.5}$ of activation is observed in presence of Nedd4-2 for hERG1 WT and YA mutant, but not with hERG1-ΔPY or catalytically inactive Nedd4-2-C801S ($V_{0.5,WT}$: -37.2 ± 0.5 mV *vs* $V_{0.5,WT+Nedd4\text{-}2}$: -41.1 ± 0.4 mV; $V_{0.5,YA}$: -38.5 ± 0.4 mV *vs* $V_{0.5,YA+Nedd4\text{-}2}$: -43.2 ± 0.6 mV; $V_{0.5,\Delta PY}$: -40.4 ± 0.4 mV *vs* $V_{0.5,\ \Delta PY+Nedd4\text{-}2}$: -40.8 ± 0.4 mV).

(B) Same trend towards negative shift in $V_{0.5}$ of steady-state inactivation is observed in presence of Nedd4-2 for hERG1 WT and YA mutant, but not with hERG1-DPY nor catalytically inactive Nedd4-2-C801S ($V_{0.5,WT}$: -50.9 ± 0.7 mV *vs* $V_{0.5,WT+Nedd4\text{-}2}$: -57.4 ± 0.8 mV; $V_{0.5,YA}$: -43.6 ± 0.5 mV *vs* $V_{0.5,YA+Nedd4\text{-}2}$: -53.4 ± 1.1 mV; $V_{0.5,\Delta PY}$: -47.6 ± 1.0 mV *vs* $V_{0.5,\ \Delta PY+Nedd4\text{-}2}$: -45.4 ± 1.4 mV). Protocols for voltage-dependence of activation and steady-state inactivation are presented in insets (A) and (B), respectively. Both activation (A) and steady-state inactivation (B) curves were analyzed for statistical significance with a one-way ANOVA followed by a Bonferroni's multiple comparison test.

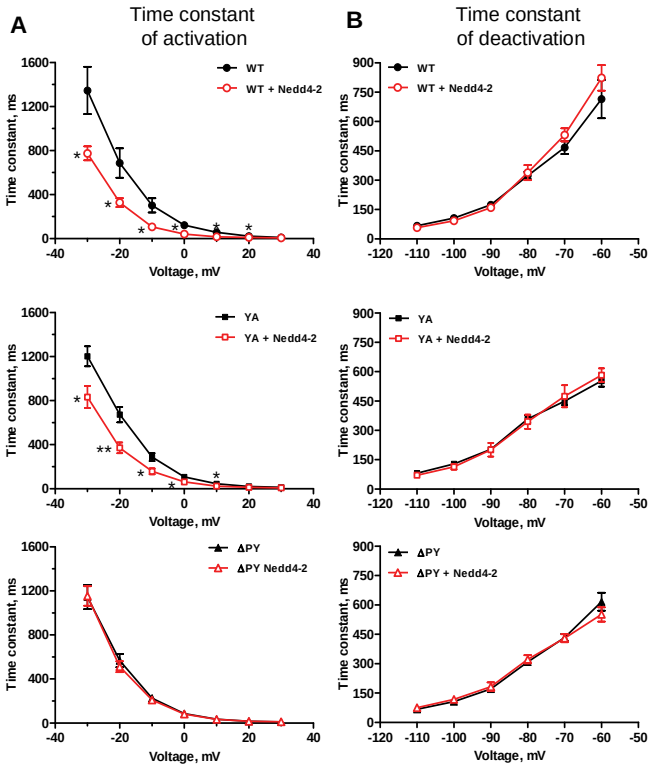

Supplementary Figure 2: Activation and deactivation kinetics of hERG1 WT, -YA and -ΔPY in presence of Nedd4-2.

(A) Time constant of activation obtained during depolarizing step of protocol shown in inset of Suppl. Fig. 1A. Time constant of activation is significantly faster in presence of Nedd4-2 for hERG1 WT and YA mutant ($P<0.05$, *; $P<0.01$, **), but not for PY-motif deleted mutant hERG1-ΔPY.

(B) Time constants of deactivation show no significant changes with or without Nedd4-2 for the three tested hERG1 channels. Deactivation kinetics were measured by fitting decay of tail current in protocol as presented in Suppl. Fig. 1B.

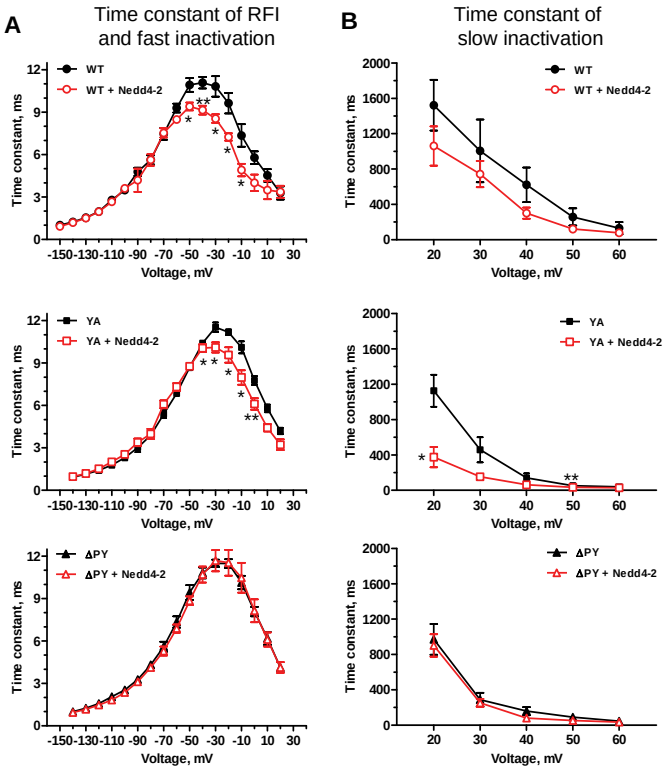

Supplementary Figure 3: Kinetics of recovery from inactivation (RFI), fast and slow inactivations, obtained from protocols presented in insets of Suppl. Fig. 1A and 1B.
(A) Time constant of fast inactivation is significantly faster at voltages between -40 and +10 mV ($P<0.05$, *; $P<0.01$, **) for hERG1 WT and YA mutant in presence of Nedd4-2, but not for hERG1-ΔPY mutant. Fast inactivation kinetics were measured during initial part of tail current of protocol presented in inset of Suppl. Fig.1B
(B) Time constant of slow inactivation tends to be faster for hERG1 WT and YA mutant in presence of Nedd4-2, but not for hERG1-ΔPY mutant. Significant difference is between hERG1-YA with and without Nedd4-2 ($P<0.05$, *; $P<0.01$, **). Slow inactivation kinetics were measured by fitting decay of current during depolarizing steps of protocol presented in inset of Suppl. Fig 1A.

II.C. Complementary discussion

In the present study, we demonstrated that hERG1 is downregulated by Nedd4-2. Downregulation is dependent on the catalytic activity of Nedd4-2 for substrate ubiquitylation, and on the integrity of the PY motif at the C-terminus of hERG1 for interaction. Contrary to previous studies (Rougier *et al.* 2005; Jespersen *et al.* 2007), mutation of the tyrosine of the PY motif into alanine (YA) was not sufficient to completely disrupt the interaction and the negative regulation of hERG1 channels at the cell surface. However, though the difference is not statistically significant, the equivalent YA mutation in KCNQ1 produced currents lower than control upon Nedd4-2 coexpression (Jespersen *et al.* 2007). Similarly to hERG1, KCNQ1 is a tetrameric channel, thus four *extended PY motifs* are potentially presented to the E3s, whereas $Na_v1.5$ channel bears a unique WW binding motif. Rougier *et al*. (2004) measured the interaction affinity of Nedd4-2 WW domains with C-terminal peptides of hERG1 and $Na_v1.5$ (KCNQ1-derived peptide was not studied). Results showed that affinity of the hERG1-derived PY peptide was low, though it apparently bound to all four WW domains of Nedd4-2, while $Na_v1.5$ peptide interacted essentially with the most C-terminal WW domain (Rougier *et al.* 2005). Taken together, it might be suggested that multiple interactions of Nedd4-2 WW domains with PY motifs of hERG1 compensate the low affinity by a cooperative effect, *i.e.* binding of one WW domain to a PY motif facilitates the interaction of a second WW domain-PY motif couple and so on, so that a single mutation does not totally abolish the synergetic interaction. This interpretation remains purely speculative, as no experiments addressing this possibility have been performed.

One important point brought by this study is the type of ubiquitylation undergone by hERG1 upon Nedd4-2 coexpression. The use of ubiquitin mutants that reveal the main lysine (K) linkages allowed us to suggest that hERG1 channels are modified with mixed K63 and undefined lysine (Kx) chains. To gain further insight in the composition of the chains, the whole set of ubiquitin mutants should be tested concomitant with mass spectrometry characterization. *In vitro* ubiquitylation is known to be promiscuous, and chains of alternating linkages can be formed readily.

It is currently difficult to estimate the abundance of mixed-linkage ubiquitin *in vivo* (Komander 2009). In 2003, a first large-scale analysis of ubiquitylated proteins in yeast also identified ubiquitin chains with mixed linkages (K29 and K33), although in a low proportion compared with mono-ubiquitylation or different types of homotypic chains (reviewed in Ikeda & Dikic 2008). Nevertheless, using a similar approach to ours, Ben-Saadon *et al*. (2006) discovered that the formation of mixed-linkage ubiquitin chains (K6/K27/K48) was implicated in the activation of the *Polycomb protein Ring1B* ligase complex, which modifies histones in mammalian cells. To our knowledge, we present the first report of mixed ubiquitin chains in a membrane ion channel. As regards hERG1, Nedd4-2-dependent mixed ubiquitylation drives the mature channels towards degradation, as suggested by the general decrease in intensity of the 155-kDa band. The two major cellular pathways of degradation are the proteasomal and the lysosomal pathways. As mentioned earlier, K48-poly-ubiquitylation is usually the sorting signal for the proteasomal degradation, whereas it seems not the case for K63-linked chains (Komander 2009). Moreover, *in vitro* experiments showed that ubiquitylated *troponine I* with mixed-linkage is more resistant to pure 26S proteasomes than when modified by homogeneous chains (Kim *et al.* 2007). This information, along with previous results on membrane hERG1 density regulation (Chapman *et al.* 2005; Guo *et al.* 2009; Massaeli *et al.* 2010), suggests that hERG1 K^+ channel is internalized in early endosomes and then targeted to lysosomal degradation. Use of lysosome and 26S proteasome inhibitors would allow for confirmation of the main degradation pathway involved. As hERG1 channels produce good results with cell surface biotinylation assay, a pulse-chase experiment with labeling of surface ion channels could inform on both the rate of internalization and the fate of hERG1 ubiquitylated upon Nedd4-2 activity. Indeed, the time-scale of analyses (48 h post transfection) reflects a steady-state situation, while investigation of initial effect might be more instructive, with or without inhibitors of the degradation pathways.

It is noteworthy to remind that hERG1 presents basal ubiquitylation (refer to Fig. 5 and 6), which is in line with the idea that ubiquitylation is a versatile system, and that type of ubiquitylation, subcellular localization of the process and specificity of

the enzymes determine the fate. Guo *et al*. (2009) demonstrated that hERG1 was downregulated upon overnight exposure to low $[K^+]_e$. We reproduced this experiment (data not shown), incubating cells expressing hERG1 WT and mutant ΔPY channel in normal medium and medium devoid of K^+. Although technical problems prevented from clear conclusions, it seems that hERG1-ΔPY is similarly downregulated in conditions of low $[K^+]_e$. Therefore, hERG1 ubiquitylation promoted by low potassium is independent on the presence of the canonical PY motif.

As regards the results presented in *Publication 1*, if we assume that current amplitude is directly proportional to the amount of proteins at the cell surface – as it was shown, for instance, by Massaeli *et al*. (2010) –, there is a discrepancy between our tail-current results and surface protein quantification. Indeed, in presence of the ubiquitin ligase, the decrease of membrane hERG1 protein is about 40% compared to without Nedd4-2, whereas I_{hERG1} is decreased by ~75% in the same conditions. We described in the supplementary document that Nedd4-2-dependent ubiquitylation modifies hERG1 biophysical properties and affects oppositely activation and inactivation gating processes. As discussed in the supplementary section of *Publication 1*, the resultant of these alterations in physiological conditions cannot be easily assessed. Nevertheless, assuming that the overall biophysical effect is a reduction of I_{hERG1} would bring an explanation to the protein-current discrepancy. These findings should be further investigated.

As pointed out earlier, a steady-state seems achieved at the time of analyses between internalization/degradation and hERG1 proteins newly arrived at the surface. This is exemplified in the cell surface biotinylation experiment (refer to Fig. 4, *Publication 1*): the total lysates, *internal pool*, and the biotinylated cell fractions, *membrane pool*, present similar ratios of mature hERG1 without:with Nedd4-2 (in both cases about 100:60). The deubiquitylation pathway could also be involved in the steady-state regulation of hERG1, as it may be implicated in the regulation of many cardiac ion channels. Fakitsas *et al.* (2007) demonstrated that ENaC channels were also deubiquitylated *via* a specific DUB enzyme called USP2-45.

However, very little is known about this specific pathway and future studies are necessary.

In a recent review, Rougier *et al*. (2010) addressed the increasing importance of another reversible post-translational modification of proteins known as *SUMOylation*. Covalent addition/subtraction of the protein modifier SUMO, which stands for *small ubiquitin-related modifier*, appears also involved in multiple regulatory events. As mentioned in the supplementary discussion of *Publication 1*, it has been shown that disruption of SUMOylation of cardiac $K_v1.5$ channel leads to altered inactivation (Benson *et al.* 2007), which supports the idea that modification of a ion channel by a peptide, including ubiquitin chains, can modulate the activity. SUMOylation of cardiac ion channels and its physiological significance have only been investigated recently. However, several targets, such as $K_v2.1$, TWIK, TRPM4 and the above-mentioned $K_v1.5$, have already been identified (reviewed in Rougier *et al*. 2010). Therefore, it would be interesting to assess possible SUMO-dependent modulations of hERG channel activity or cell surface density in further studies.

Remarkably, the regulation of an additional cardiac ion channel by an E3 of the Nedd4 family strengthens the hypothesis that Nedd4-2 ubiquitin ligase is an important selective modulator of ion channels membrane density. The relevance of these findings in normal and abnormal cardiac physiology remains speculative. The complexity of the ubiquitylation system is the major hindrance to a better knowledge in this field. Moreover, ubiquitylation is finely interwoven with the other important post-translational modification, *i.e.* phosphorylation. Regarding hERG1, PKA-dependent phosphorylation sites have been identified in its cytoplasmic N- and C-termini, and cAMP/PKA-mediated phosphorylation was shown to decrease I_{hERG1} and I_{Kr} (Cui *et al.* 2000; Karle *et al.* 2002), though diverging results were also published (see I.C.3.b). It is also worth mentioning that phosphorylation of hERG1 offers a new binding site to the scaffolding protein 14-3-3 (isoform ε). Kagan and McDonald (2005) demonstrated that 14-3-3ε binds on both N- and C-termini of the channel, therefore protecting the protein modification against phosphatases activity. Surprisingly, the interaction of 14-3-3ε with hERG1 led to increased currents

explained by faster activation kinetics (Kagan & McDonald 2005). Interestingly too, Nedd4-2, but not Nedd4-1, bears three phosphorylation sites that can be phosphorylated by the cAMP/PKA pathway or by the *serum- and glucocorticoid-induced kinase* (SGK) (reviewed in Snyder 2009). It has been shown that in the phosphorylated state, Nedd4-2 is unable to bind to ENaC, so that the channels remain at the cell surface and sodium absorption is enhanced (Snyder *et al.* 2002). The interaction is impeded due to binding of 14-3-3ε/β to the phospho-residues (Snyder 2009). If this holds true for hERG1 ion channel, a short β-adrenergic stimulation would result in decrease of I_{hERG1} (I_{Kr} in the heart) through the channel phosphorylation, but chronic adrenergic stimulation would favor an increase of hERG1-mediated currents through interactions of 14-3-3ε with the channel (increased currents) and with Nedd4-2 ligase (preventing decreased density of membrane hERG1 channels). This would be in agreement with the trigger effect in LQT2 of auditory stimuli and emotional stress, and less due to sports exercise (where adrenergic stimulation is progressive). Moreover, as discussed in the presented manuscript, hERG1 currents and plasma membrane abundance has been shown to be upregulated by the isoform 3 of SGK (Maier *et al.* 2006) and Lang's group demonstrated that SGK3 was also involved in the upregulation of other K_v channels, namely K_v1.3 (Henke *et al.* 2004) and KCNQ1/KCNE1 (Embark *et al.* 2003). It is noteworthy to mention that both SGK3 (Gamper *et al.* 2002) and Nedd4-2 are endogenously expressed in the cell model used for our experiments (HEK293), thus maybe masking in part the effect of Nedd4-2. Nevertheless, these results support the idea of a complex interplay of SGK- (phosphorylation-) and Nedd4-2-(ubiquitylation)-dependent regulation of hERG1 K^+ channel cell surface levels. Important pieces of the puzzle are falling into place, although a lot of research, mainly in *in vivo* models, is needed to understand the tight regulation of cardiac currents and I_{Kr} in physiological conditions, and to ultimately unveil their implications in acquired LQTS.

Part III:
Congenital LQTS and KCNH2 mutations

III. Characterization of congenital LQTS type 2 mutations

III.A. Introduction

III.A.1. Genetic transmission of LQTS

As mentioned in the *Background* section, the inherited character of LQTS was suggested long before molecular screening became available. When about 50 years ago Jervell and Lange-Nielsen reported on four brothers suffering from congenital deafness and important QT prolongation (whereas parents were asymptomatic), they proposed an autosomal-recessive mode of inheritance for the disease. In opposition, the other characterized form of LQTS, *i.e*. the Romano-Ward syndrome, is essentially transmitted as a dominant trait. In other words, a mutation present in a single allele is sufficient to cause the disease. Nevertheless, Priori *et al*. (1998) reported the case of a consanguineous family in which heterozygous carriers of the *KVLQT1* mutation (the parents) were asymptomatic, whereas the homozygous carrier (the son) presented prolonged QT interval and history of syncope, without hearing loss. This was the first report of recessive form of RWS and indicated that homozygous mutations on *KVLQT1* gene do not invariably produce the auditory phenotype of JLNS (Priori *et al.* 1998). Another difference lies in the fact that the RWS is much more heterogeneous in terms of genes affected (so far, 12 different genes *versus* 2 genes for JLNS), thus the severity of the disease varies considerably as well as the penetrance. Penetrance represents the probability for an individual with an affected genotype to manifest the clinical signs of the disease, and it has important implications for clinical management (Priori *et al.* 1999). Genotype–phenotype correlations, demonstrated in clinical and experimental studies, have enabled to stratify risk and to effectively treat patients with some defined types of long QT syndromes (Shimizu 2005). For the sake of brevity, the characteristics of the three main types of *c*LQTS and respective triggers for TdP will not be repeated, as well as the type-specific pharmacological treatment of this syndrome (see I.B.1.a). Nevertheless, attention should be drawn to the fact that the LQTS is generally a monogenic disorder, though compound mutations might occur. Westenskow and

colleagues (2004) analyzed the phenotypic and genotypic information of LQTS probands and found that up to 7.9% carried two mutations in the tested genes causing LQT1/2/3 and LQT5/6. The double mutation was found either in the same or two different genes. The authors demonstrated that loss of channel function was additive, thus explaining the more severe phenotype in probands with two mutations compared to only one and were 3.5-fold more likely to have cardiac arrest (Westenskow *et al.* 2004). Fodstad *et al*. (2006) identified six compound mutations in a Finnish population study of documented or suspected LQTS, with the HERG R176W mutation being always the second component of the pair. Their data provided some evidence that the R176W mutation may confer an additional QTc-prolonging and symptom risk for the carriers (Fodstad *et al.* 2006). Electrophysiological properties of the heterozygous expression of hERG-R176W were in general similar to WT, despite acceleration of deactivation kinetics. This hERG variant alone may cause a *forme fruste* LQTS. Most interestingly, it was present among Finnish control DNA with a frequency of about 1% (Fodstad *et al.* 2006). The group of Grunnet and co-workers (2005) also reported about a family with compound mutations on *KCNH2* and *KVLQT1* genes, and characterized them electrophysiologically. In this particular case, the hERG-R328C mutation (located in the N-terminus) appeared to have no impact on the elicited current, whereas the KCNQ1-R591H mutation leads to dramatic reduction of current. The phenotype of the two mutations together was explained by the decrease of I_{Ks} (Grunnet *et al.* 2005). In this particular case, carrying two mutations did not lead to more severe symptoms as concluded by Westenskow and colleagues, but observations are consistent with the additive-effects hypothesis. Moreover, these results clearly illustrate that genetic identification of a variant in the genes causing LQTS is not sufficient to deduce the clinical phenotype. Risk has already been shown to be gene-dependent, as patients who have mutations in *SCN5A* have a higher risk of sudden death than patients with LQT1- or LQT2-mutations (reviewed in Perrin *et al*. 2008). These findings add further evidence to the important intragenic variation of the clinical severity of *KCNH2* mutations.

III.A.2. Location and coding type of LQT2 mutations

There are several coding types of mutations found in the *KCNH2* gene: missense, nonsense, in-frame or frameshift deletion/insertion, and splice site mutations. Missense mutations are point mutations that result in a single amino acid change within the protein. Nonsense mutations generate a stop codon that truncates the protein. Insertion and deletion mutations may be in-frame or cause a shift in the reading frame (frameshift) that changes the grouping of nucleotide bases into codons. Finally, splice site mutations may alter splicing of the mRNA. Recently, Shimizu *et al*. (2009) investigated the effect of location/topology and coding type of *KCNH2* mutations on the clinical phenotype and on a large study population (858 subjects with 162 distinct mutations). They first characterized the coding type mutations and found that missense mutations of the K^+ channel accounted for ~60% of total mutations and frameshift mutations for ~25% (**Figure 14**). In a previous study regarding *KVLQT1* mutations, missense mutations accounted for even more, *i.e.* up to 81%. Location of the LQT1- and LQT2-mutations also differed. In the cohort of 600 LQT1 patients, the majority of mutations were found in transmembrane region (~70%), whereas in the LQT2 study the mutations are evenly distributed between the

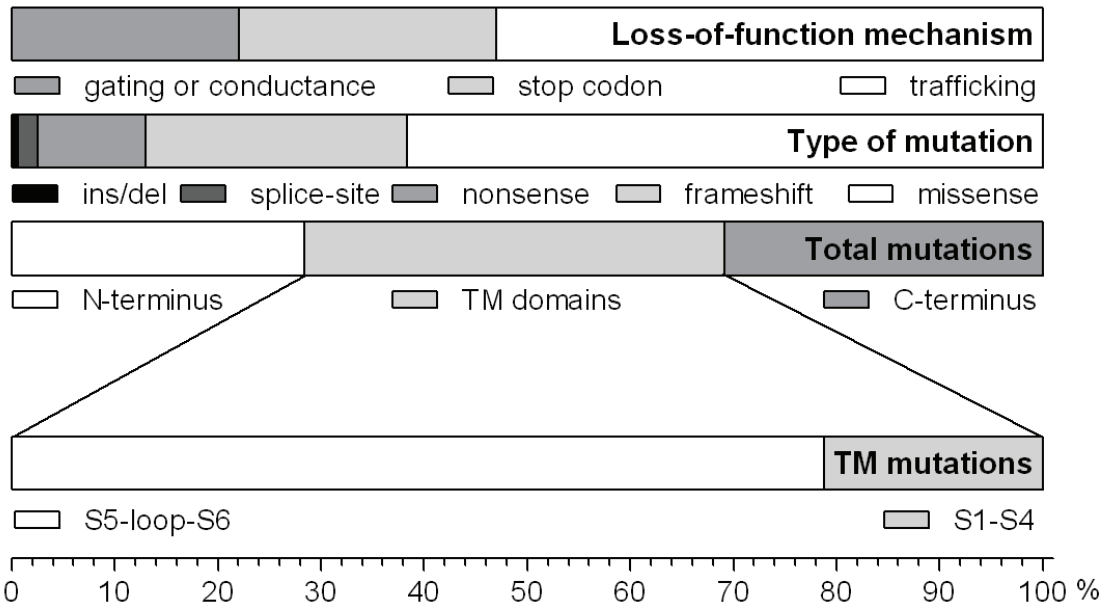

Figure 14 : Summary of location, coding type and loss-of-function mechanism of *KCNH2* mutations with respective percent representation.

Based on the results published by Shimizu *et al.* (2009) and Perrin *et al.* (2008).

N-terminus, transmembrane (TM) domains, and the C-terminus (**Figure 14**). Interestingly, most of the TM-domain mutations reside in the pore-forming region (S5-loop-S6) rather that in the S1-S4 domains (**Figure 14**) (Shimizu *et al.* 2009).

III.A.3. Risk stratification and treatment

The major contribution of Shimizu and colleagues is the evaluation of risk of first cardiac event or SCD by multiple variable analyses, including the type and the location of the mutation, and other risk predictors (*e.g.* QTc length, gender). In the study we refer to (Shimizu *et al.* 2009), a missense mutation in the pore-forming transmembrane domains is at significantly higher risk for a cardiac event that in any other region, as previously reported by Moss *et al.* (2002). The fact that patients with missense mutations in the pore region have a more severe phenotype may be explained because missense mutations are expected to cause *dominant-negative effects*. Indeed, a missense mutation in one allele can generate a defective hERG subunit that will retain in the ER and target to degradation the entire ion channel. Since hERG is a tetramer and a single mutant α-subunit may confer complete dysfunction, this may result in up to 93% reduction in hERG current (reviewed in Perrin *et al*. 2008). Regarding patients with non-missense mutations (mostly frameshift/ nonsense), they were surprisingly found at higher risk than subjects with missense mutations in the C-terminal region (Shimizu *et al.* 2009). As previously reported, patients with longer QTc intervals and females after puberty presented higher hazard ratio than individuals with shorter QTc values and male gender.

Moreover, the study of Shimizu *et al*. (2009) confirmed the efficacy of β-blockers as a first-line therapy in LQT2-patients (risk of first cardiac event decreased by 63%), and suggested more prophylactic use of such treatment. However, β-blocker was associated with less protection in the prevention of lethal events compared to first cardiac events, indicating that additional treatment may be considered in high-risk patients (Shimizu *et al.* 2009). Despite the great progress that has been made in understanding the basis of this syndrome, precise risk stratification in LQTS is still a weak point in defining appropriate treatment, especially for silent-gene carriers. Many individuals may carry a LQTS-mutation and be phenotypically silent, whereas

other family members present severe symptoms. This low penetrance of LQTS is problematic since family members that are silent gene carriers are unexpectedly at risk of generating affected offspring and developing TdP if exposed to QT-prolonging drugs (Priori *et al.* 1999). Besides, 30% to 40% of sudden deaths occur at the first cardiac event (Khan 2002a). Genetic screening of relatives of an identified proband, remains the only means of prevention that could decrease this percentage. Moreover, risk assessment is a major clinical dilemma as the recommended treatment for high risk *versus* low risk patients is different. The former are treated with an ICD while the later are likely to respond to β-blocker therapy alone (Perrin *et al.* 2008). Subjecting a young asymptomatic patient to long-term β-blockade therapy or to ICD treatment may reveal problematic. Moreover, while an ICD is undoubtedly effective in converting ventricular fibrillation to sinus rhythm and saving lives, an ICD does not reduce the risk of recurrences of TdP and may deliver unpleasantly frequent shocks to patients, thus causing a negative impact (Nademanee 2009).

Accurate risk stratification of a LQTS patient is the cornerstone for the optimal choice of therapy and converging efforts will enable to achieve it. In this sense, analysis of the functional effects of a mutation in order to fully understand the pathogenic impact and severity of the disease is crucial, because only then can appropriate clinical management proceed (Grunnet *et al.* 2005).

III.A.4. Mechanisms involved in the loss of function of hERG

The number of reported mutations on *KCNH2* has been continuously increasing to more than 500 mutations at the time of writing, most of them causing long QT syndrome by loss of function (*www.HGMD.cf.ac.uk*). As introduced earlier (see I.C.3), the extent of hERG current in a cardiomyocyte is determined by three parameters: the total number of channels at the cell surface (*N*), the probability that a given channel is open (*Po*) and the single channel conductance (*g*). Mutations in hERG may result in loss of function by four mechanisms that impair: synthesis at transcription and/or translation levels (class 1), trafficking from the ER to the plasma membrane (class 2), gating (class 3) or ion permeation (class 4). A simplified summary of biochemical and functional features of the different mutation classes of the hERG

channel is presented in **Figure 15**. It would be outside the scope of this work to list of all characterized mutations, but we would like to present a concise example for each mechanism.

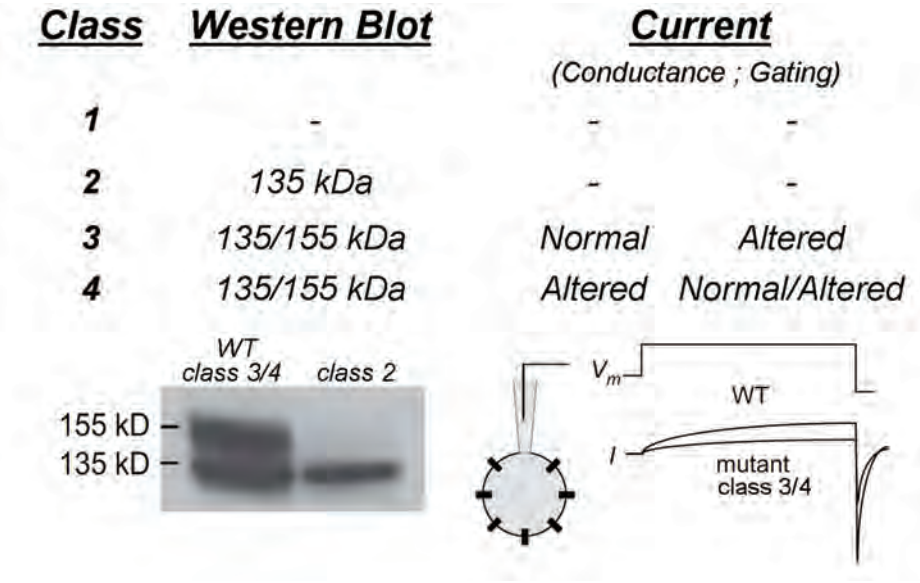

Figure 15 : Summary of biochemical and functional characteristics of hERG channel loss-of-function mechanisms. Adapted from (Perrin *et al.* 2008)

Class 1: no hERG protein is detected in Western Blot and similarly no current is measured with the patch-clamp technique. ***Class 2***: only the 135-kDa band is observed for the mutant in Western Blot and no functional current is detected. ***Class 3***: both 135-kDa and 155-kDa bands are detected in the Western Blot similary to WT hERG. Single channel conductance is not affected, but gating is altered. ***Class 4***: Western blot signal for class 3 mutant is indistinguishable from WT hERG. Ion channel conductance is decreased and gating may also be altered.

III.A.4.a. Defective synthesis (class 1)

Approximately 25% of all reported hERG mutations result in premature stop codons (**Figure 14**). If transcribed, such mutations would produce truncated proteins (single letter code: X). Kupershmidt *et al*. (2002) described the W1001X C-terminus truncated mutant of hERG, and they reported that truncated proteins were present at the cell surface and elicited reduced currents. When co-transfected in heterologous expression systems with WT hERG cDNA, this mutation caused a dominant negative effect, which was expected to result in a severe phenotype. In fact, W1001X mutation carriers present with a mild LQT2 phenotype. It is

noteworthy to mention that cells have developed a way to eliminate mRNAs that contain premature termination codons using a mechanism called *nonsense-mediated mRNA decay* (NMD). Gong and co-workers (2007) investigated the possibility that frameshift/nonsense mutations leading to premature stop codons more than 50-55 nucleotides upstream of the 3'-most exon-exon junction are controlled by NMD. Involvement of NMD in reduction of hERG W1001X transcripts was confirmed by *in vitro* experiments (Gong *et al.* 2007). In the studied case, by eliminating abnormal mRNA transcripts, NMD prevents the production of W1001X truncated proteins that could act in a dominant negative manner. The physiological role of NMD could be to convert the dominant-negative effect into *haploinsufficiency*[7], which would explain the mild form of LQTS of W1001X carrier patients (Gong *et al.* 2007). Importantly, NMD requires introns; the common use of cDNAs to characterize a truncated hERG mutant (as performed by Kupershmidt *et al.* 2002) would therefore not allow assessing NMD effects.

III.A.4.b. Defective trafficking (class 2)

According to Anderson and colleagues, most LQT2 mutations reduce hERG current by a trafficking-deficient mechanism. Indeed, the authors analyzed 34 missense LQT2-mutations and found that 28 (80%) of these channels resulted in a trafficking-deficient phenotype (Anderson *et al.* 2006). The same proportion applied to the results of Shimizu *et al*. (2009) allows us to say that approximately 50% of all LQT2 mutations depend on a class 2 mechanism (**Figure 14**).

Since ion channels are highly structured transmembrane proteins, a single missense mutation may result in its misfolding. Correct protein folding is checked by the ER quality-control machinery, and proteins failing this exam typically remain in the ER where the ERAD machinery recognizes and translocates them to the cytosol for degradation. As mentioned earlier, some hERG mutants, namely G601S and Y611H, have been reported to be under ERAD control (Ficker *et al.* 2003; Gong *et al.* 2005). The complexity of the cellular chaperones and ERAD pathway are not yet

[7] Deletion of one allele when the normal phenotype requires two alleles. The single copy of the gene is incapable of providing sufficient protein as to assure normal function.

understood, but important recent findings have improved our knowledge. First, different chaperone proteins appear to be involved in hERG folding. Initial reports suggest that cytosolic heat shock proteins Hsp70 and Hsp90 play a key role, as both chaperones interact with the immature form of WT hERG in the ER and interact even more with the G601S mutant (Ficker *et al.* 2003). Many chaperone molecules that are present on luminal side of ER (*e.g.* calnexin), as well as FK506-binding protein 38 (also known as FKBP38), appeared to interact to facilitate proper folding (Walker *et al.* 2007). Recently, Walker *et al*. (2009) also pointed out the involvement of Hsp40 co-chaperones and the chaperone-dependent E3 ubiquitin ligase CHIP in the degradation pathway of hERG. This was demonstrated by the ability of different human Hsp40 co-chaperones to reduce hERG trafficking efficiency. The export process seems also dependent on the presentation of ER-exit signals (diacidic motifs) concomitant with masking of the C-terminal RxR motif, which is an ER-retention signal (reviewed in Perrin *et al.* 2008). Thus, a mutation that affects interaction of hERG domains, and *e.g*. prevents masking of the RxR motifs, would result in the protein being retained in the ER (Kupershmidt *et al.* 2002).

A Western blot analysis of a class 2 hERG mutant, such as G601S or Y611H, results typically in a single band of core-glycosylated proteins with no expression of the fully-glycosylated form (**Figure 15**). A trafficking-defective mutant, as the name implies, might also be caused by failure in checkpoints encountered later in the way to the cell surface. As mentioned before, a membrane-bound protein follows the secretory pathway through pre-Golgi, Golgi apparatus and post-Golgi vesicles. Since hERG undergoes mature-glycosylation in the Golgi cisternae, it means that for all compartments prior to it, the protein will be observed with 135 kDa (refer to **Figure 6B**, page 26). While the ER export process is poorly understood, even less is known about hERG and Golgi checkpoints. Roti *et al*. (2002) identified an interacting partner for hERG, GM130, which is a Golgi-associated protein involved in vesicular transport. The authors proposed that the cytoplasmic C-terminus of hERG participates in the binding or targeting of hERG-containing vesicles within the Golgi *via* its interaction with GM130 (Roti *et al.* 2002). LQT2 mutations in the C-terminus could disrupt such interaction and impair trafficking. Nevertheless, this has never been reported, maybe

because the upstream ER-quality control is highly efficient. Regarding the single 135-kDa band, one may also argue that it may reflect defective N-glycosylation of the hERG mutant. However, Gong *et al.* (2002) demonstrated that unglycosylated α-subunits were still detected at the cell surface and could elicit a smaller although functional current.

Interestingly, in cystic fibrosis, several drugs are able to correct the trafficking-deficient phenotype of the *cystic fibrosis transmembrane conductance regulator* (CFTR) deletion mutant, ΔF508. Similarly, *pharmacological chaperones* were tested to rescue hERG defective-trafficking mutants. Zhou *et al*. (1999) were the first to show that trafficking could be rescued by incubating cells with a common hERG channel blocker, *E-4031*, or at a lower temperature. Anderson *et al*. (2006) showed that most of their trafficking-defective mutants had their fully-glycosylated form and channel function rescued by at least one of the measures employed: i) reduced temperature, ii) hERG channel blocker (E-4031) or iii) thapsigargin, a sarcoplasmic/ endoplasmic reticulum Ca^{2+}-ATPase inhibitor.

III.A.4.c. Defective gating (class 3)

Altered gating characteristics can lead to reduced hERG currents due to two main mechanisms. The first mechanism is reduced activation and includes all modifications that lead to decreased activating currents, which may be i) slower activation kinetics, ii) accelerated deactivation kinetics, or iii) shift in the voltage-dependence of activation to more depolarized voltages. The fast C-type inactivation is, as previously mentioned, fundamental for I_{Kr} characteristics. Thereby, if (iv) inactivation is further enhanced due to a *KCNH2* mutation, it will reduce the flow through the open channels owing to a faster conformation change into the non-conducting state. Nakajima *et al*. (1998) described this mechanism on different LQT2-mutants identified at the time. The authors noticed that co-expressing hERG-V630L with WT α-subunits decreased the K^+ channel current by ~80% (Nakajima *et al.* 1998). Heterozygous-mimicked expression of hERG V630L produced a significant decrease in channel conductance and an important hyperpolarizing shift in voltage (-20 mV) in the steady-state inactivation curve (Nakajima *et al.* 1998). Importantly,

many mutations, including V630L, were characterized in *Xenopus* oocytes. Contrary to mammalian cells, frog oocytes are maintained at temperatures of ~17°C and, consequently, trafficking-defects may be masked by low-temperature rescue. It is probable that a hERG mutation affects both trafficking and gating/single conductance. Indeed, the LQT2-mutation R534C was described by the group of Nakajima to shift the voltage-dependency of activation as well as kinetics of activation and deactivation (Nakajima *et al.* 1999), whereas Anderson *et al*. (2006) demonstrated later that the same hERG-R534C mutant, tested in mammalian HEK293 cells, presented a trafficking-defective phenotype rescued by low-temperature incubation.

III.A.4.d. Defective ion permeation (class 4)

Mutations in the vicinity of the selectivity filter of the hERG channel are likely to result in altered ionic selectivity and/or altered single channel conductance (Perrin *et al.* 2008). The atomic structure of the bacterial KcsA K^+ channel, that shares the most similarities with hERG pore-region, revealed that the SF is a tube of ~12 Å in length produced by four conserved sequences, one on each channel subunit (Valiyaveetil *et al.* 2004). The signature sequence of hERG selectivity filter differs from most K^+ channels in what a Phe is between the two conserved Gly ($_{626}$G-F-G$_{628}$). Nevertheless, these signature peptides direct four sequential backbone carbonyl oxygen atoms towards the pore to ensure the selectivity and rapid flow of K^+ ions across the cell membrane. Many naturally occurring mutations have been reported in the very conserved SF sequence (*www.fsm.it/cardmoc*), but not all have been characterized. Mutation of the capital glycine into serine, G628S, was already reported by Curran *et al*. (1995) in the paper revealing the liability of hERG for *c*LQTS. In this seminal publication, the authors already foreseen that a mutation in the SF could induce important loss of hERG function, since when a similar substitution was introduced into a K_v1 channel, potassium ion selectivity was lost (Curran *et al.* 1995). Later, Zhou *et al*. (1998a) confirmed in HEK293 cells that the mutant channels were expressed at the cell surface and processed similarly to WT hERG, however they were not functional, because the mutation disrupted ion permeation.

III.B. Publication 2 (submitted to *Annals of Noninvasive Electro-cardiology*)

Patient with syncope and LQTS carrying a mutation in the PAS domain of the hERG1 channel: a case report and mutation characterization

Although the number of identified mutations in the *KCNH2* gene is impressive, it does not account for all the cases of QTc interval prolongation. As mentioned previously, the three major types of LQTS differ by the severity of the outcome or the appropriate treatment. Moreover, some mutations have been reported to be silent and harmless (Anson *et al.* 2004), including the mutation hERG R328C located in the N-terminus (Grunnet *et al.* 2005), while other polymorphisms are kept silent until a drug reducing I_{Kr} is taken and unveils the mutation. Paulussen *et al*. (2004) reported among other LQTS-linked polymorphisms the single amino acid substitution P347S in hERG: the baseline QTc of the proband was normal (440 ms), but it was highly prolonged during concomitant *cisapride* administration (640 ms). In the presence of a hERG channel blocker, the reduced repolarization reserve caused by the polymorphism may render individuals more susceptible to acquired LQTS (Paulussen *et al.* 2004). Therefore, it is important to screen an LQTS patient and relatives for mutations in the putative genes, as well as characterize the mutation when identified. Moreover, a toxicological screening should be undertaken whenever possible, in order to reveal potential drug-induced symptoms.

The present publication sought to identify the molecular determinants responsible for the phenotype of a young patient who presented with syncope and prolonged QT intervals.

Contribution to the study:

In this study, I generated the point mutation described in the proband and characterized it biochemically (in parallel with S. Roy) and electrophysiologically in HEK293 cells. I was in charge of the cell culture, preparation and transfection for most experiments, with the kind help of S. Roy for biochemical assays. In addition to that, I wrote the first version of the following manuscript.

Patient with syncope and LQTS carrying a mutation in the PAS domain of the hERG1 channel

Liliana Sintra Grilo, MSc Pharm,*,** Jürg Schläpfer, M.D.,† Florence Fellmann, M.D., Ph.D.,‡ Hugues Abriel M.D., Ph.D.*

From the *Department of Clinical Research, University of Bern, Bern, Switzerland; **School of Pharmaceutical Sciences, University of Geneva, University of Lausanne, Geneva, Switzerland; †Service of Cardiology, University Hospital, Lausanne, Switzerland; and ‡Service of Medical Genetics, University Hospital, Lausanne, Switzerland.

* Address for reprints: Hugues Abriel, M.D., Ph.D., Department of Clinical Research, University of Bern, Murtenstrasse 35, 3010 Bern, Switzerland, Fax:+41316320946, Phone: +41316320998, E-mail: Hugues.Abriel@dkf.unibe.ch

This work was supported by grants of the CardioMet Centre of the Faculty of Biology and Medicine (CardioGene grant 2007-2009), University of Lausanne, and the Swiss National Science Foundation (310000-120707 to HA).

Running title: PAS-domain mutation in hERG1

Abstract

We report the case of a woman with syncope and persistently prolonged QTc intervals. Screening of congenital-LQTS genes revealed that she was an heterozygous carrier of a novel *KCNH2* mutation, c.G238C. Electrophysiological and biochemical characterizations unveiled the pathogenicity of this new mutation, displaying a 2-fold reduction in protein expression and current density due to a maturation/trafficking-deficient mechanism. The patient's LQTS phenotype can be fully explained by this observation. Since future pharmacological treatments may offer clinical benefits for some type 2 LQTS patients, this study stresses the importance of performing genetic analyses and mutation characterization when there is a suspicion of congenital LQTS.

Introduction

Congenital Long QT Syndrome (LQTS) is a genetic disorder primarily resulting from mutation-induced loss-of-function of cardiac ion channels or mutations in channel-associated proteins, and characterized by the electrocardiographic finding of QT interval prolongation and T wave abnormalities.[1] This syndrome affects an estimated 1 in 2,500 people[2] and typically presents with syncope, seizures or sudden death. Congenital LQTS types are named depending on the gene affected. There are currently 12 types reported and among them 5 encode potassium channel subunits.[3] *KCNQ1* and *KCNH2* genes encode voltage-gated potassium channels essential for the repolarizing currents (I_{Ks} and I_{Kr}) of the cardiac action potential and thus its duration. They are the most common genes mutated in congenital LQTS, type1 (LQT1) and 2 (LQT2), respectively. Nearly 300 LQT2-mutations have been reported in *KCNH2,* the gene encoding the hERG1 protein. Recently, several mutations in the amino-terminus PAS-domain were reported, all showing defective maturation and/or trafficking of hERG1 channels to the cell membrane as well as reduced channel currents.[4-8]

In the present study, we report the case of a young woman with syncope and a persistently prolonged QTc interval. Screening of congenital-LQTS genes revealed that she was a heterozygous carrier of a yet-undescribed *KCNH2* mutation in the PAS domain. Electrophysiological and biochemical characterizations unveiled the pathogenicity of this new mutation and highlighted the importance of trafficking-deficient mechanisms affecting PAS-domain mutations of hERG1.

Case presentation

A 20-year-old female of Caucasian origin was referred to our hospital after having 2 episodes of syncope. The first syncopal event occurred 10 months prior with clonical-type movements, but without tongue bite or urinary loss. No cardiac assessment was performed at that time. The second episode occurred a few days prior to presentation. According to the patient's report a short malaise preceded a 5-minute long fainting period, but no one witnessed the event. Both episodes were postprandial, while the patient was at rest and without adrenergic stimulation. Outpatient cardiac evaluation showed a prolonged QT interval, QTc values of 536 ms to 575 ms, and variations in T-wave morphology. Echocardiography revealed very mild mitral valve regurgitation with no evidence of valvular prolapse. Cardiac assessment upon admission to our hospital confirmed the prolonged QT interval (Figure 1, QT= 560 ms) and showed bifid T waves in precordial leads. The results of ergometry exercise testing were in the normal range. A congenital form of LQTS was suspected and the patient was started on beta-blocker treatment (metoprolol, 25 mg daily), with no further episodes reported since.

The diagnosis of congenital LQTS was followed by the genetic screening of the main genes known to be involved in LQTS. *KCNQ1* and *SCN5A* had no abnormal variants, but a new heterozygous point mutation was found in *KCNH2* (c.G238C, p.A80P).

The first degree family history revealed that the patient's parents and two siblings were in good health. The enlarged family history showed only one case of a relatively premature and undetermined death (a great-uncle), reported to be due to a myocardial infarction. Cardiac evaluation of the father and the sister of the proband showed no ECG abnormalities, and no further molecular evaluations were performed. However, it is important to mention that family members may be genetically affected but asymptomatic, and that β-blockers can be effective at reducing sudden cardiac death in patients with a molecular LQTS analysis and normal QT interval.[9]

Methods

A complete version of the methods is presented in supplementary file 1.

Results and Discussion

The patient's ECG recorded at admission is consistent with LQTS, and more specifically LTQ2 because of the characteristic bifid T wave morphology.[10] Genetic screening of the proband for the three main LQTS genes revealed the presence of a heterozygous point mutation in *KCNH2,* with no

abnormal variants in *KCNQ1* or *SCN5A*. The *KCNH2* c.G238C mutation translates into the p.A80P mutation at the protein level, which affects a residue of the PAS domain of the hERG1 channel. The PAS domain is a highly structured domain in the amino-terminus of the hERG1 channel. It interacts with the core of the channel and is involved in the regulation of the deactivation rate.[7] Due to its important packing of β-sheets anḍ α-helices, the amino-terminus of hERG1 could be crystallized and is available in the Protein Data Bank (pdb entry: 1byw), which enabled us to precisely locate the residue affected in the largest α-helix of the PAS domaiṇ (αC). Proline is different from other amino acids because of its distinctive cyclic structure that locks the dihedral angle, providing important conformational rigidity. Such a mutation in an α-helix may disrupt the proper folding of the amino-terminus. The misfolded protein may be recognized and degraded by the cellular quality-control machinery.

Generation of the hERG1-A80P mutant allowed for its characterization at the electrophysiological and biochemical levels. Patch-clamp technique in whole cell configuration was used to measure the current density in CHO cells transiently expressing wild-type (WT) and mutant hERG1 channels (Figure 2A). When compared with hERG1-WT condition (100% ± 10% in Figure 2A), the heterozygous-mimicking condition (hERG1-WT/A80P) elicited only half of the tail current at -120mV (52% ± 11%), whereas complete hERG1-A80P elicited almost no current (4% ± 2%). These results are consistent with a loss of function of the hERG1-A80P mutation. Protein expression was assessed using Western blot analysis (Figure 2B), where hERG1-WT protein appears with a double signal: a lower band at 135kDa (non-mature form) and a higher band at 155kDa (fully glycosylated and mature form). Functional channels at the cell surface are constituted with fully glycosylated subunits. There was a clear decrease of the fully glycosylated band in the heterozygous-mimicking condition (46% ± 5% of hERG1-WT 155kDa band), and no signal was observed for the A80P-mutant homozygous condition (0.6% ± 2.8% of hERG1-WT 155kDa band). These results are in line with the functional assay of current measurement. Interestingly, the non-mature band was still present for the homozygous-mutant condition. The signal intensity for the 135kDa band of hERG1-A80P was 22% ± 6% of hERG1-WT, and heterozygous condition presented intermediate intensity values of 66% ± 7% (Figure 2B). Expression patterns of the hERG1-A80P protein allows us to conclude that the mutant channel is biosynthesised and expressed in the endoplasmic reticulum (ER), although to a lesser extent than the wild type, as seen by the weaker 135kDa band. Further maturation in the Golgi

complex, where the final glycosylation takes place, is not possible since the protein may be recognized and destroyed by the ER-associated degradation pathway. Chen and co-workers[11] described a similar mutation, p.A78P, which showed accelerated deactivation but no decrease in current. Their PAS mutant, however, was electrophysiologically characterized in Xenopus oocytes. It has been shown that mutant proteins can be rescued and delivered to the plasma membrane after incubation at reduced temperatures, which are used when working with Xenopus oocytes.[12] Thus, it remains possible the A78P mutation exhibits defective trafficking in mammalian cells as seen with A80P. Pharmacological chaperones, usually channel blockers, also have the ability to rescue hERG1 mutants. Pharmacological rescue is not only domain-dependent (e.g. cNBD mutations are not rescued), but also mutation-dependent. The PAS-domain mutant T65P[4] was rescued with E4031 and cisapride incubations, but a 7-amino-acid duplication in the PAS domain[8] was not rescued upon astemizole treatment. According to Anderson and colleagues,[13] abnormal protein trafficking is the most common mechanism for decreased ionic current caused by *KCNH2* mutations. Improved knowledge on chemical chaperone binding sites and the rescue mechanisms of protein trafficking might lead to the development of specific pharmacological chaperones for the treatment of LQT2. We propose that suspect cases of congenital LQTS should be systematically screened for mutations in the known culprit genes.

Conclusion

We identified a 20-year-old woman with LQTS carrying a previously undescribed hERG1 PAS-domain heterozygous mutation. This mutation proved to be pathogenic, as co-expression of WT and mutant alleles in mammalian cells led to a ~50% decrease of the hERG1 protein at the cell surface as well a decrease in its current. The patient's LQTS phenotype may be fully explained by theses observations. This additional mutation in the PAS domain, leading to impaired channel maturation and trafficking, emphasizes this zone as a non-pore mutational "hot-spot". It is of critical importance to perform genetic analyses upon suspicions of congenital LQTS in the hopes of future pharmacological treatments.

Abbreviations

WT: wild type; LQTS: Long QT Syndrome; LQT1 : Long QT Syndrome type 1; LQT2 : Long QT Syndrome type 2; ECG : Electrocardiogram; cNBD : cyclic Nucleotide Binding Domain

Consent

Written informed consent was obtained from the patient for publication of this case report and accompanying images. The genetic investigation conformed to the principles outlined in the Declaration of Helsinki, and the research protocol was approved by the ethics committee of the Faculty of Biology and Medicine of the University of Lausanne.

Acknowledgements

Authors thank Sophie Roy for her help with the biochemistry assays and Dr. Francine Thonney and Séverine Arcioni for their molecular analysis of the LQTS genes.

References

1 Shimizu W. The long QT syndrome: therapeutic implications of a genetic diagnosis. Cardiovasc Res 2005 August 15;67(3):347-56.

2 Ackerman MJ. Cardiac channelopathies: it's in the genes. Nat Med 2004 May;10(5):463-4.

3 Markiewicz-Loskot G, Moric-Janiszewska E, Mazurek U. The risk of cardiac events and genotype-based management of LQTS patients. Ann Noninvas Electro 2009 January;14(1):86-92.

4 Paulussen A, Raes A, Matthijs G, Snyders DJ, Cohen N, Aerssens J. A novel mutation (T65P) in the PAS domain of the human potassium channel HERG results in the long QT syndrome by trafficking deficiency. J Biol Chem 2002 December 13;277(50):48610-6.

5 Shushi L, Kerem B, Goldrait M, Peretz A, Attali B, Medina A, Towbin JA, Kurokawa J, Kass RS, Benhorin J. Clinical, genetic, and electrophysiologic characteristics of a new pas-domain HERG mutation (M124R) causing long QT syndrome. Ann Noninvas Electro 2005;10(3):334-41.

6 Rossenbacker T, Mubagwa K, Jongbloed RJ, Vereecke J, Devriendt K, Gewillig M, Carmeliet E, Collen D, Heidbuchel H, Carmeliet P. Novel Mutation in the Per-Arnt-Sim Domain of KCNH2 Causes a Malignant Form of Long-QT Syndrome. Circulation 2005 March 1;111(8):961-8.

7 Morais Cabral JH, Lee A, Cohen SL, Chait BT, Li M, MacKinnon R. Crystal structure and functional analysis of the HERG potassium channel N terminus: a eukaryotic PAS domain. Cell 1998 November 25;95(5):649-55.

8 Sintra Grilo L, Pruvot E, Grobθty M, Castella V, Fellmann F, Abriel H. Takotsubo cardiomyopathy and congenital long QT syndrome in a patient with a novel duplication in the Per-Arnt-Sim (PAS) domain of hERG1. Heart Rhythm 2010 February;7(2):260-5.

9 Sauer AJ, Moss AJ, McNitt S, Peterson DR, Zareba W, Robinson JL, Qi M, Goldenberg I, Hobbs JB, Ackerman MJ, Benhorin J, Hall WJ, Kaufman ES, Locati EH, Napolitano C, Priori SG, Schwartz PJ, Towbin JA, Vincent GM, Zhang L. Long QT syndrome in adults. J Am Coll Cardiol 2007 January 23;49(3):329-37.

10 Zareba W. Genotype-specific ECG patterns in long QT syndrome. J Electrocardiol 2006 October;39(4 Suppl):S101-S106.

11 Chen J, Zou A, Splawski I, Keating MT, Sanguinetti MC. Long QT Syndrome-associated Mutations in the Per-Arnt-Sim (PAS) Domain of HERG Potassium Channels Accelerate Channel Deactivation. J Biol Chem 1999 April 9;274(15):10113-8.

12 Ficker E, Thomas D, Viswanathan PC, Dennis AT, Priori SG, Napolitano C, Memmi M, Wible BA, Kaufman ES, Iyengar S, Schwartz PJ, Rudy Y, Brown AM. Novel characteristics of a misprocessed mutant HERG channel linked to hereditary long QT syndrome. Am J Physio Heart Circ Physiol 2000;279(4):H1748-H1756.

13 Anderson CL, Delisle BP, Anson BD, Kilby JA, Will ML, Tester DJ, Gong Q, Zhou Z, Ackerman MJ, January CT. Most LQT2 mutations reduce Kv11.1 (hERG) current by a class 2 (trafficking-deficient) mechanism. Circulation 2006 January 24;113(3):365-73.

Figures

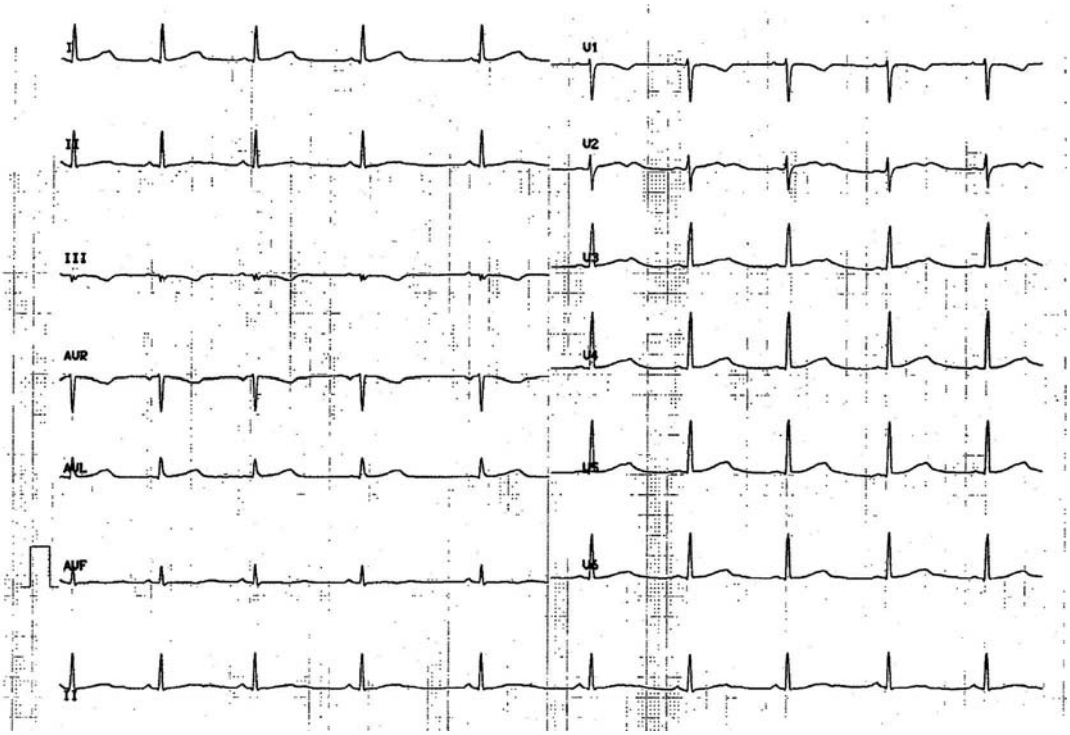

Figure 1.

12-lead ECG recorded at admission.

Sinus rhythm 58/min. PR: 140 ms. QRS : 80 ms, normal axis. Prolongation of QT interval with an obvious bifid T wave in precordial lead V2-V3, and a subtle bifid T wave in V4-V6. QTc : 560 ms

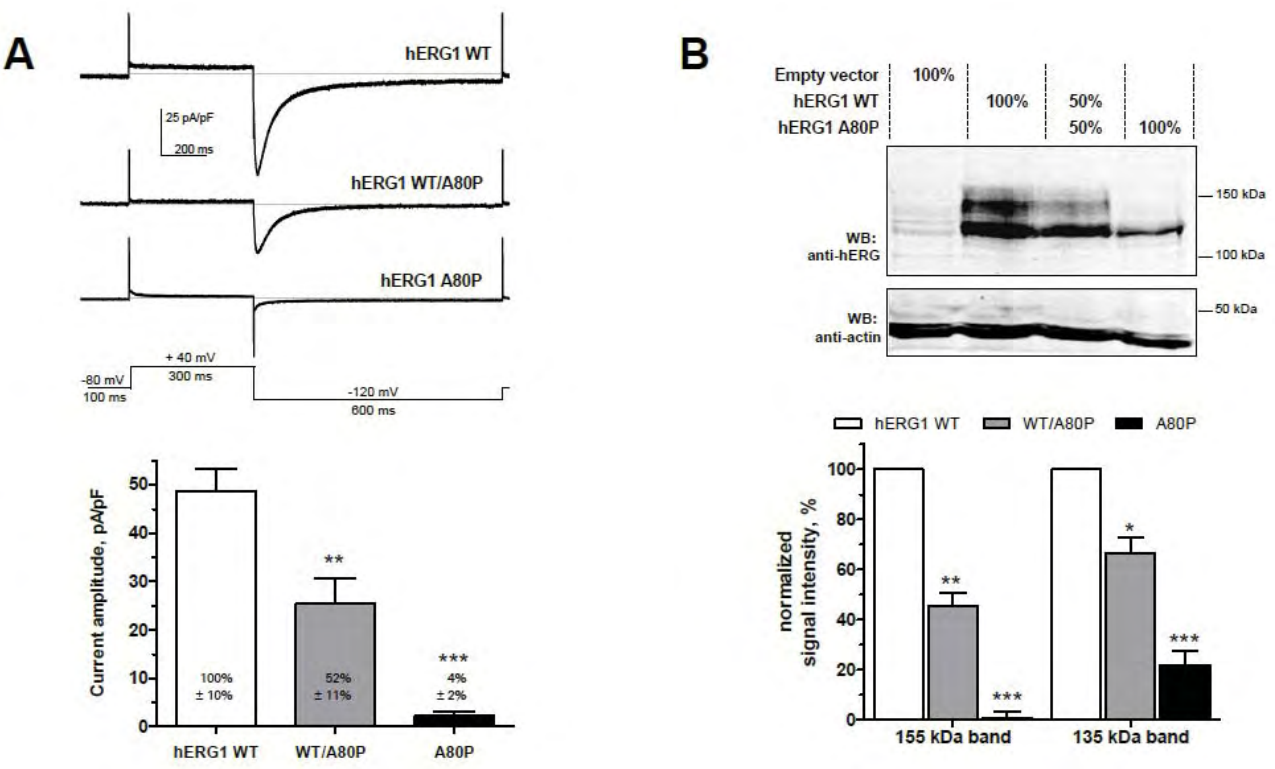

Figure 2.

Electrophysiological and biochemical characterization of hERG1-A80P mutant

(**A**) *Upper panel*: patch-clamp current recordings of hERG1-WT, heterozygous (hERG1-WT/A80P) and homozygous hERG1-A80P mutant obtained in whole cell configuration according to the depicted protocol.

Lower panel: Quantification of -120-mV peak tail currents of hERG1-WT, heterozygous (hERG1-WT/A80P) and homozygous hERG1-A80P mutant for n=12-18 cells per condition and at least 3 independent experiments.

(**B**) *Upper panel*: Protein expression of hERG1-WT, heterozygous (hERG1-WT/A80P) and homozygous hERG1-A80P mutant with western blot analyses.

Lower panel: Fully glycosylated (mature, 155kDa band) and core-glycosylated (non-mature, 135kDa band) protein quantification of hERG1-WT, heterozygous (hERG1-WT/A80P) and homozygous hERG1-A80P mutant upon 3 independent experiments.

Supplementary Methods

Genetic and molecular investigations – Genomic DNA was extracted from peripheral lymphocytes. All coding exons of *KCNQ1*, *KCNH2*, *SCN5A* were amplified by polymerase chain reaction, using primers designed in intronic flanking sequences according to gene sequences. All amplicons were directly sequenced in both directions and compared to reference sequences.

Plasmids and mutagenesis – The cDNA encoding hERG1 (gift of Dr. R.S. Kass, Columbia University, NY) was cloned into pcDNA3.1-(+)Zeo (Invitrogen AG, Basel, Switzerland) vector as previously described 1. The mutant hERG1-A80P construct was engineered with the mutation using appropriate primers and the Quick change II XL site-directed mutagenesis kit (Stratagene, Basel, Switzerland). Sequence integrity was confirmed by complete sequencing of the cDNA.

Electrophysiological procedures – CHO cells were used for all electrophysiological measurements 44-56 hours after transient transfection, which included a cDNA encoding the CD8 antigen, allowing for the identification of transfected cells by using anti-CD8 beads (Invitrogen, Basel, Switzerland). Patch-clamp recordings in whole-cell configuration were performed using an internal solution containing (mmol/L) KCl 145; EGTA 10; $MgCl_2$ 1; HEPES 5; and Mg^{2+}-ATP 5, pH 7.3 with KOH; and an external solution NaCl 140; KCl 5; $CaCl_2$ 2; $MgCl_2$ 1; HEPES 20; and glucose 5, pH 7.4 with NaOH. Pipette resistance was in the range of 2.0–3.5 MΩ. Measurements were carried out using an Axopatch 200B amplifier (Axon Instruments, Union City, CA), and were performed at room temperature (25±1°C). To study current amplitude, peak tail currents were measured at -120 mV. Voltage was stepped from a holding potential (HP) of -80 mV to +40 mV for 300 ms, followed by repolarization to -120 mV for 600 ms. To avoid bias of measurements, mean current measured in CHO cells transfected with empty plasmid was subtracted to the current values of all hERG1 conditions.

Western blot analyses – HEK293 cells were transiently transfected with hERG1-WT and/or hERG1-A80P cDNA 48 hours prior to collection. Cells ware lysed with lysis buffer containing (mmol/L) HEPES 50 pH 7.4, NaCl 125, $MgCl_2$ 1,5, EGTA 1 pH 8, and 8.7 % glycerol, 1% Triton X-100, 24 mg N-ethylmaleimide and 1 tablet of Complete® protease inhibitors cocktail (Roche Diagnosis, Mannheim, Germany). Cell lysates were homogenized at 4°C for 45

minutes and spun at 16,000 x g for 15 minutes. From the supernatant containing solubilized proteins, 60 ul of sample was boiled 5 minutes with 5 x SDS-PAGE loading buffer, and analyzed in 7% PAGE. For Western blots, antibodies against carboxy-terminus of hERG1 were purchased from Alomone (APC-062, Jerusalem, Israel) and antibodies against actin from Sigma Chemical (A2066, Sigma Aldrich, Buchs, Switzerland).

Data analyses and statistics – Electrophysiological data were analyzed using pClamp software, version 10 (Axon Instruments, Union City, CA). Western blots were scanned and semi-quantified with Odyssey infrared imaging system and software, version 2.1 (LI-COR, Lincoln, NE), respectively. The statistical significance of the differences between means was determined by two-tailed Student *t*-test using GraphPad Prism software, version 5 (GraphPad Softwares, La Jolla, CA). $P<0.05$ was considered statistically significant. Data are presented as means ± standard error of the means.

Reference

1 Eap CB, Crettol S, Rougier JS, Schlapfer J, Sintra GL, Deglon JJ, Besson J, Croquette-Krokar M, Carrupt PA, Abriel H. Stereoselective block of hERG channel by (S)-methadone and QT interval prolongation in CYP2B6 slow metabolizers. Clin Pharmacol Ther 2007 May;81(5):719-28.

III.C. Publication 3 (*Heart Rhythm Journal*)

Takotsubo cardiomyopathy and congenital LQTS in a patient with a novel duplication in the Per-Arnt-Sim (PAS) domain of hERG1

Takotsubo[8] *cardiomyopathy* (TTCM), also referred to as *stress cardiomyopathy*, *transient apical ballooning* or more romantically *broken heart syndrome*, is a disorder associated with transient left ventricular dysfunction. This syndrome, originally described in Japan in the 1990's, may be divided into acute, subacute (2-12 days after the attack), and chronic phases (Ito *et al.* 2005). The attack is characterized by symptoms including acute chest pain and dyspnea, and it is found predominantly in postmenopausal women (~80%). The symptoms might mimic an acute myocardial infarction, although with no signs of coronary artery obstruction on angiography (Nef *et al.* 2010). Assessment of the left ventricular function in patients with TTCM reveals *apical ballooning* and ventricular hypokinesia with the preservation of basal contraction. Moreover, electrocardiogram changes are frequent and include ST-segment elevation, evolution of marked T-wave inversion, and prolongation of the QT interval (Behr & Mahida 2009). These features all appear to resolve with time.

The precise pathophysiological mechanism of Takotsubo cardiomyopathy is unknown, though emotional or physical stress are known as the main triggers (Samuelov-Kinori *et al.* 2009). No large studies have confirmed the etiology of stress cardiomyopathy, so determining the underlying cause has so far not been possible. Several pathological mechanisms have been proposed, including coronary artery vasospasm, coronary microcirculation dysfunction, obstruction of the left ventricular outflow tract, and catecholamine overload (Nef *et al.* 2010). Data suggest that substantially elevated plasma catecholamine levels seen in TTCM patients seem particularly relevant, as it would result in adrenergic-based cardiac impairment.

[8] *Takotsubo* is the Japanese name for pots that fishermen use to catch octopus. In this syndrome, the left ventricle takes the shape of an octopus trap, with a round bottom and narrow neck.

Importantly, the prognosis of TTCM is considered as favorable (in-hospital disease-related mortality 2%; 4-year survival similar to control), although fatal complications, such as malignant arrhythmias and free wall rupture of the left ventricle, have been reported (Nef *et al.* 2010). The prevalence of prolonged QT interval among TTCM patients is significant in acute and subacute phases, ranging from 50-100% according to different case series (reviewed in Samuelov-Kinori *et al*. 2009). Although QT interval prolongation is frequent and might precede TdP, the later has rarely been reported in TTCM patients, with only 1-1.5% incidence of ventricular arrhythmia. Among the 20 case reports retrieved by Samuelov-Kinori *et al.* (2009) and Behr and Mahida (2009) of documented both TTCM and TdP, 7 patients were males (35%) and 13 were females (65%). This result contrasted with the female predominance of the Takotsubo cardiomyopathy and allowed the group of Samualov-Kinori to conclude that men with TTCM-associated QT interval prolongation are at higher risk for *Torsades de Pointes*. Remarkably too, Behr and Mahida (2009) noticed in their literature research that significant QT prolongation at other times than during the acute episode was present in 36% of included cases of TTCM and TdP. They suggested in these patients an underlying predisposition towards repolarization abnormality, or in other words a reduced *repolarization reserve* (Roden 1998). According to the authors, this could be a silent mutation implicated in *c*LQTS or polymorphisms that more subtly impair the repolarization reserve. These individuals may also have other predisposition abnormalities such as structural cardiac disease, metabolic disease or bradycardia (Behr & Mahida 2009).

In the following study, we reported the case of a woman who experienced acute phase of Takotsubo cardiomyopathy followed by TdP episodes. The pattern of electrophysiological changes motivated a genetic screening for congenital LQTS, and characterization of the genetic mutation at the functional level. In agreement with Behr and Mahida (2009), this additional case report supports a tight relationship between the two discussed cardiac syndromes.

Contribution to the study:

In the following study, I carried out the molecular biology experiments to generate the 21-bp in-frame duplication mutant as identified in the proband. I also analyzed channel expression using cell surface biotinylation assays and performed the rescue experiments with reduced temperature and incubation with astemizole drug. I was in charge of the cell culture, preparation and transfection for all experiments. Finally, I performed all electrophysiological experiments in CHO cells and contributed to the writing of the manuscript.

Takotsubo cardiomyopathy and congenital long QT syndrome in a patient with a novel duplication in the Per-Arnt-Sim (PAS) domain of hERG1

Liliana Sintra Grilo, MSc Pharm,*† Etienne Pruvot, MD,‡ Michel Grobéty, MD,¶ Vincent Castella, PhD,§ Florence Fellmann, MD, PhD,‖ Hugues Abriel, MD, PhD*‡

*From the *Department of Clinical Research, University of Bern, Bern, Switzerland, †School of Pharmaceutical Sciences, University of Geneva, University of Lausanne, Geneva, Switzerland, ‡Service of Cardiology, CHUV, Lausanne, Switzerland, ¶Clinique Cécil, Lausanne, Switzerland, §Forensic Genetics Unit, University Center of Legal Medicine, Geneva and Lausanne, Switzerland, and ‖Service of Medical Genetics, CHUV, Lausanne, Switzerland.*

Introduction

Delayed cardiac repolarization can be caused by mutations in cardiac channel subunit genes, resulting in different forms of the congenital long QT syndrome (LQTS),[1] or secondary to cardiac pathologies, such as the recently described Takotsubo cardiomyopathy.[2] LQTS is characterized by QT-interval prolongation on the ECG, reflecting cardiac action potential prolongation. Takotsubo cardiomyopathy[2] is a clinical syndrome characterized by transient ventricular wall-motion abnormalities and left ventricular dysfunction that primarily affects postmenopausal women.[3] Frequent ECG alterations include ST-segment elevation and/or T-wave inversion, with occasional clear QT-interval prolongation.[2,3] The etiology of Takotsubo cardiomyopathy is poorly understood. Patients often experience psychologically or physically stressful events prior to presentation, leading to the hypothesis that mechanical dysfunction results from catecholamine-dependent toxicity, as seen with reversible cardiomyopathies that occur in patients with pheochromocytomas.[4]

Both LQTS and Takotsubo cardiomyopathy are characterized by ECG repolarization abnormalities, but only recently have investigators questioned whether a causal relationship exists between the two syndromes. Three recent case reports describe patients in whom previously unrecognized congenital LQTS was unveiled after an acute episode of Takotsubo cardiomyopathy.[5–7]

KEYWORDS Congenital long QT syndrome; hERG1; KCNH2; Takotsubo cardiomyopathy; Voltage-gated potassium channel

ABBREVIATIONS LQTS = long QT syndrome; **PAS domain** = Per-Arnt-Sim domain; **WT** = wild type (Heart Rhythm 2010;7:260–265)

Supported by grants from the CardioMet Centre of the Faculty of Biology and Medicine (CardioGene Grant 2007-2009), University of Lausanne, and the Swiss National Science Foundation (Grant 310000-120707 to Dr. Abriel). **Address reprint requests and correspondence:** Dr. Hugues Abriel, Department of Clinical Research, University of Bern, Murtenstrasse, 35, 3010 Bern, Switzerland. E-mail address: Hugues.Abriel@dkf.unibe.ch. (Received July 7, 2009; accepted September 18, 2009.)

Here we report the case of a female patient with a history of syncope and torsades de pointes associated with prominent alterations in chest lead T waves and apical ventricular bulging, all suggestive of an acute Takotsubo cardiomyopathy. After near normalization of the ECG, congenital LQTS was diagnosed on the basis of QT prolongation. A mutation was found in the gene *KCNH2,* which encodes hERG1, the cardiac potassium channel responsible for the K^+ current I_{Kr}. The mutation was a novel in-frame duplication of seven amino acids in the Per-Arnt-Sim (PAS) domain located in the N-terminus of the channel. The purpose of this study was to demonstrate the pathogenicity of the novel hERG1 PAS-domain duplication by performing electrophysiological and biochemical investigations.

Methods

The methods are presented in the Online Supplementary Data.

Index case

The index case was a 37-year-old Russian woman of Caucasian origin who was admitted by the emergency service of the University Hospital of Lausanne, Switzerland, because of a sudden convulsive syncopal event. The patient was admitted during a period of stressful events for her, including surgery to remove uterine polyps performed abroad 9 days earlier. She had been prophylactically prescribed intravenous ceftriaxone for 5 days, followed by a single oral dose of 200 mg ketoconazole 5 days before the syncopal event. Physical examination was unremarkable except for an unusual bradycardia of 51 bpm. The patient had not experienced prior syncopal events and had no family history of sudden death. The ECG recorded at admission revealed QT-interval prolongation (QTc = 534 ms in lead V_2; Online Supplementary Figure 1A). Electrolyte levels were within the normal range (K^+ 3.7 mmol/L, total Ca^{2+} 2.15 mmol/L, total Mg^{2+} 0.82 mmol/L). Troponin I level was elevated within the first 48 hours after admission (peak 0.17 μg/L), suggesting myocardial involvement. Creatine kinase values

1547-5271/$ -see front matter doi:10.1016/j.hrthm.2009.09.026

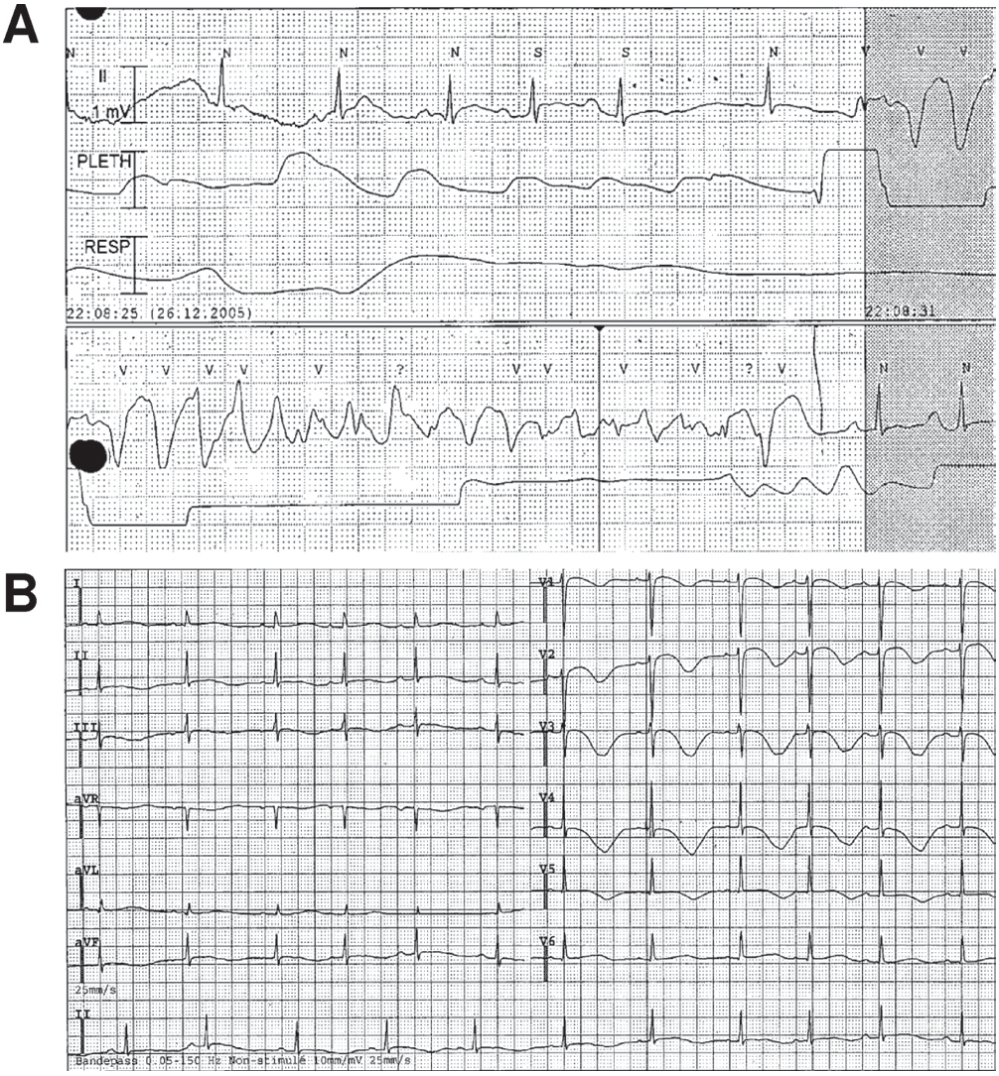

Figure 1 ECGs recorded at admission and during hospitalization. **A:** Strip ECG with torsades de pointes following variations in beat-to-beat QRS durations recorded a few hours after admission. **B:** ECG depicting negative T waves in leads V_1–V_5 with extreme QTc prolongation (QTc = 721 ms).

were normal. The patient was monitored overnight, during which time she had another spontaneous and self-limiting syncopal event. Figure 1A shows torsades de pointes preceded by sudden variations in beat-to-beat QRS intervals. Because an acquired form of LQTS was suspected, isoprenaline infusion was started immediately. Following the second event, the patient developed giant negative T waves with extreme prolongation of the QT interval on chest leads. Figure 1B shows a representative ECG (QTc interval = 721 ms in lead V_3). Echocardiography performed the same day revealed localized akinesia of the left ventricular apex with hyperkinesia of the basal and mid segments (Online Supplementary Figure 2). Coronary angiography performed 8 days after the event was unremarkable and showed normal left ventricular function, thus ruling out a transient ischemic arterial thromboembolic event. Cardiac magnetic resonance imaging performed 3 weeks after admission revealed normal size and thickness of both the right and left ventricles. Global function was normal without segmental alteration. First-pass myocardial perfusion was normal for the left ventricle. No pathologic staining was observed with late myocardial enhancement contrast technique. Echocardiography performed at the same time confirmed normalization of cardiac function. Based on these transient functional and structural alterations, a mild form of Takotsubo cardiomyopathy was suspected. Drug-induced LQTS was considered unlikely given the long time lag since ketoconazole administration. The possible proarrhythmic role of another drug could not be excluded because a toxicology screen had not been performed on admission. Upon cessation of isoprenaline infusion, atenolol 50 mg/day was prescribed. The patient was discharged from the hospital 10 days after admission. An ECG recorded 6 weeks after the patient presented to the emergency department is shown in Supplementary Figure 1B. Progressive reduction in the amplitude of the giant negative T waves as well as in the QT intervals (QTc interval = 526 ms in lead V_3) was seen. At 9-month follow-up, ECG was unremarkable (Figure 2A), with positive chest lead T waves and QT intervals at the upper limit of normal (QTc interval = 472 ms in lead V_3). Since then, the patient

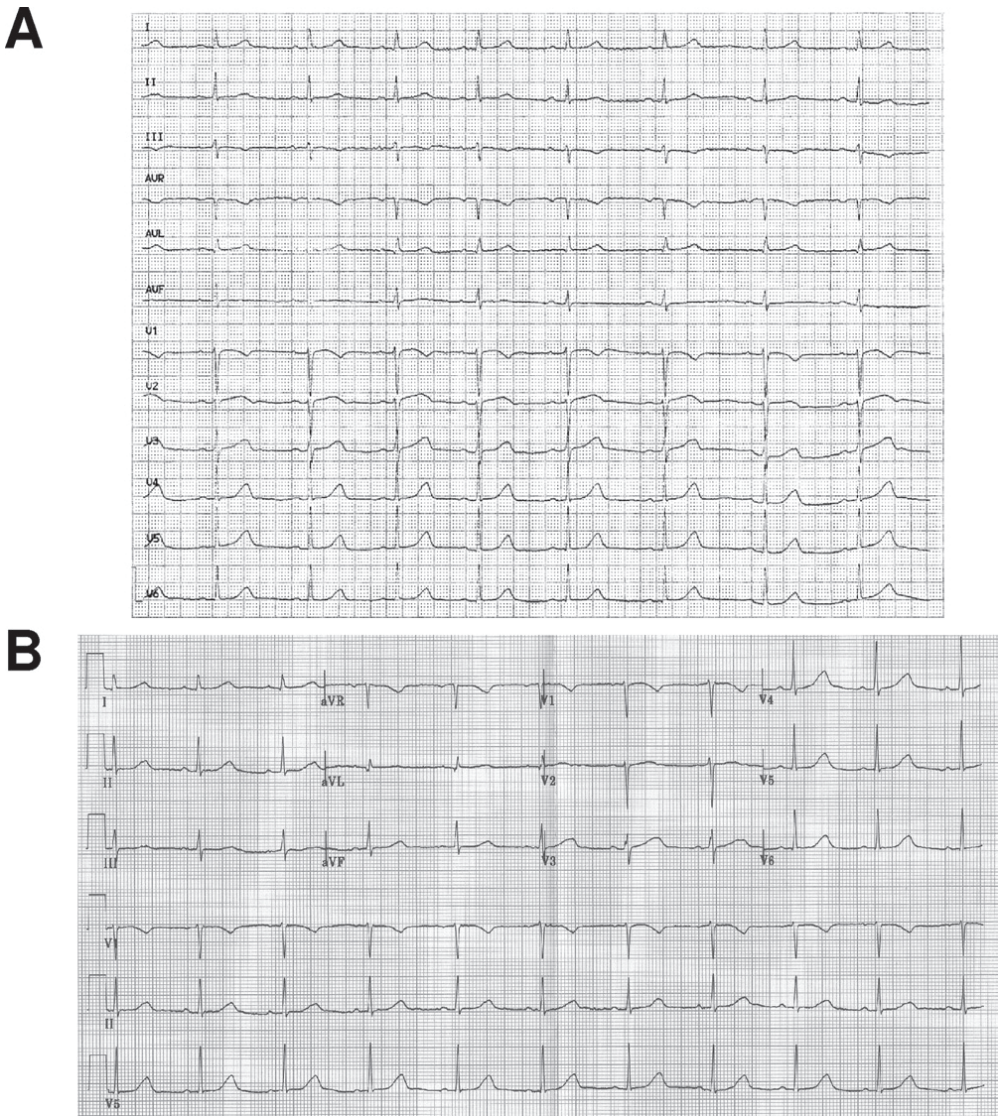

Figure 2 ECGs recorded after discharge from the hospital. **A:** ECG recorded 9 months after the event shows normal positive T waves in precordial leads and QTc at the upper limit of normal (473 ms). **B:** ECG recorded 2 years after the event shows QTc prolongation (495 ms).

has been treated with atenolol 50 mg/day with no further events (4-year follow-up at the time of this submission). ECG recordings recorded over the following years showed a pattern of LQTS (QTc interval = 495 ms, Figure 2B).

Results

Genetic analysis

The three most common LQTS genes (*KCNQ1*, *KCNH2*, *SCN5A*) were screened in the proband's DNA. We detected a novel heterozygous mutation in *KCNH2* (nc.343-363dup corresponding to p.V115-A121dup, Online Supplementary Figure 3A) leading to a 7-amino-acid duplication in the PAS domain of the hERG1 amino-terminus. No other abnormal variants were found in the two other genes. This duplication was not found in any of the 100 control cases screened in the laboratory of Dr. E. Zaklyazminskaya (Personal Communication, July 2009). These findings led to a diagnosis of congenital LQTS type 2. The 16-year-old son of the proband had a normal ECG and did not carry the abnormal variant. No further family analyses could be performed.

Electrophysiological characterization of mutant hERG1 channel

The duplication was located within the highly structured PAS domain of hERG1 (Online Supplementary Figure 3B), which is involved in the hERG1 deactivation process.[8] Naturally occurring mutations in this domain have been shown to affect the rate of deactivation.[9,10] For this reason, we investigated whether deactivation was altered by the duplication. The deactivation time constant was significantly reduced at −60 mV in both heterozygous-mimicking (~1.4×) and Dupl conditions (~2×) (Online Supplementary Figure 4A). The heterozygous condition displayed deactivation values between those of wild type (WT) and mutant. Similar differences were observed when the deactivation process was recorded at 37°C (data not shown).

Peak tail current amplitude of mutant channels was smaller than that of the control at all negative currents (Figures 3A and 3B and Online Supplementary Figure 4B). To ensure that the cellular expression system was not sat-

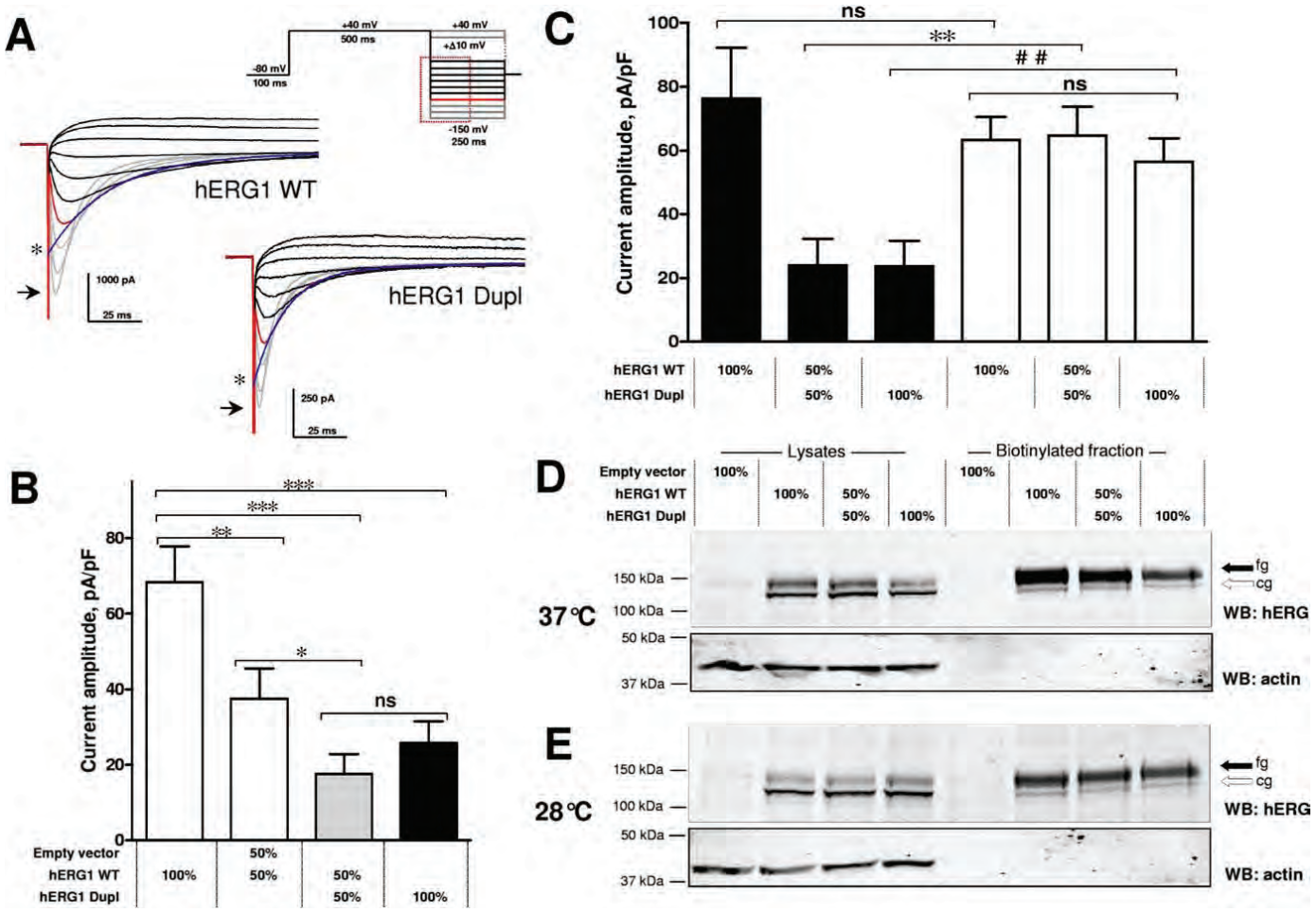

Figure 3 Decreased current amplitude observed for hERG1 Dupl mutant and rescue of both trafficking and function by incubation at lower temperatures. **A:** Representative recordings (protocol in **inset,** *red box* bounds the zone of represented traces) of hERG1 wild type (WT; **left**) and Dupl mutant (**right**). Fitting the deactivation part of tail current *(red trace)* with an exponential *(blue curve)* enables extraction of time constant (Tau of deactivation) and peak (*) tail current corrected for deactivation *(arrow)* at the beginning of the pulse. **B:** Normalized peak tail current amplitudes (pA/pF) at –120 mV corrected for deactivation as presented in panel A. Both heterozygous-mimicking and Dupl conditions display reduced current density compared with WT. Significant differences seen versus WT ($*P < .05$, $**P < .01$, $***P < .001$) but not significant (ns, $P > .05$) for heterozygous versus Dupl for n = 23–39 cells. **C:** CHO cells transfected with hERG1 WT or Dupl cDNAs in various ratios. Cells were cultured at normal (37°C, *black bars*) or low (28°C, *white bars*) temperature 36 hours prior to patch-clamp measurements as for panel B. Significant differences seen for heterozygous-mimicking (WT 50%: Dupl 50%) and hERG1 Dupl at 28°C versus 37°C ($**P < .01$, $^{\#\#}P < .01$) but not significant (ns, $P > .05$) for hERG1 WT at 28°C versus 37°C for n = 14–20 cells. With incubation at 28°C, no difference is observed between the three transfected conditions, representing a rescue of function of Dupl and heterozygous hERG1 channels. **D:** Western blot of a representative cell surface biotinylation assay on HEK293 cells transiently expressing hERG1 WT or Dupl mutant and maintained at normal culture temperature (37°C). Total lysates of cells show decreased amount of mature or fully glycosylated (fg) hERG1 Dupl compared with WT. The core-glycosylated form (cg) remains unchanged. In the biotinylated fraction, fully glycosylated hERG1 levels are decreased in heterozygous-mimicking and Dupl mutant condition compared with hERG1 WT. **E:** Western blot of a representative cell surface biotinylation assay on HEK293 cells transiently expressing hERG1 WT or Dupl mutant and maintained at a low temperature (28°C). This assay was performed in parallel to the assay shown in panel D. Total lysates of cells show no decreased amount of the mature or the nonmature form of hERG1 Dupl compared with WT. Rescue of cell surface levels of hERG1 mature form is observed in the biotinylated fraction where heterozygous-mimicking and Dupl mutant present signals similar to hERG1 WT. For panels D and E, protein loading was verified by anti-actin immunoblotting **(bottom rows).**

urated, I_{hERG1} was also recorded when half the amount of hERG1-channel plasmids was transfected (Figure 3B). As expected under these conditions, the recorded current was half that of the control condition (55% ± 12%). Figure 3B shows that both heterozygous-mimicking (–74% ± 8%) and Dupl (–64% ± 9%) conditions displayed a significant reduction in current density compared with WT ($P < .001$). Because the heterozygous-mimicking condition (gray column in Figure 3B) is significantly smaller than the control condition (50% empty vector + 50% hERG1 WT), a dominant negative effect can be inferred.

Reduced membrane expression of the mature form of the hERG1 duplication mutant

Cell surface biotinylation experiments were performed to assess whether decreased I_{hERG1} (Figure 3B) was caused by defective expression or trafficking of hERG1. Membrane proteins of HEK293 cells transiently expressing hERG1

WT, Dupl mutant, or both were tagged with biotin and collected with streptavidin-coated beads. Figure 3D shows a representative western blot of cell lysates and biotinylated fractions. Antibodies against hERG1 revealed two bands with molecular weights of approximately 135 and 150 kDa. The lower band corresponds to the core-glycosylated immature hERG1; the upper band corresponds to the fully glycosylated (fg) mature hERG1.[11] Total lysates (Figure 3D, left lanes, fg) showed gradually decreasing amounts of fully glycosylated hERG1 heterozygous (–12%) and Dupl (–35%) compared with WT, whereas the nonmature form remained unaffected. This effect was more pronounced in the biotinylated fraction (Figure 3D, right lanes, fg), where the mature hERG1 bands were decreased by 17% for heterozygous and 45% for Dupl conditions after quantification and normalization to the hERG1 WT signal. Upon quantification of three similar blots, total lysates showed that the mature hERG1 was decreased by 26% ± 13% and the nonmature form by 7% ± 10% in Dupl compared with the WT condition. Cell surface fraction quantification resulted in reduction of 38% ± 5% for the mature hERG1 and 7% ± 9% for the nonmature hERG1 Dupl condition compared with the WT signal.

Rescue of function and expression of the duplication mutant

Specific procedures, such as incubation with hERG1 inhibitors and reduction of incubation temperature, may partially rescue the trafficking defects of many LQT2 mutant channels,[12] including the PAS-located T65P.[10] Therefore, we tested rescue of function and expression of hERG1 duplication mutants with both electrophysiological experiments and biotinylation assays. Lowering the incubation temperature to 28°C for 36 hours partially rescued the deactivation-corrected peak current generated by hERG1 mutant channels (Figure 3C). No significant difference was observed for corrected current amplitudes of hERG1 WT at 37°C or 28°C (100% ± 22% vs 80% ± 9%, $P > .05$). Incubation at 28°C rescued the expression to 82% ± 12% for heterozygous and 72% ± 10% for the Dupl condition of the hERG1 WT 37°C control. Significant differences were seen between normal and low incubation temperatures for heterozygous-mimicking and Dupl conditions ($P < .01$). Incubation at 28°C abolished the differences between the three transfected conditions, representing a successful rescue of function of Dupl and heterozygous hERG1 channels (Figure 3C, white columns).

Cell surface biotinylation experiments were performed using transfected HEK293 cells maintained in parallel at either 28°C or 37°C in order to investigate the rescue of cell membrane hERG1 expression. Figure 3E shows a representative western blot of a biotinylation experiment performed with cells incubated for 36 hours at 28°C. The mature form of the mutant channel in both the lysates and the biotinylated fraction was comparable to the WT channel (Figure 3E). The intensity of the signal at 28°C is fainter than at 37°C, which may reflect a lower expression efficiency after transfection.

Discussion

In this report we present the case of a female patient with a history of syncopal episodes. Echocardiography and ECG changes were consistent with altered cardiac repolarization, leading to the diagnosis of Takotsubo cardiomyopathy. Genetic analyses performed based on the persistently prolonged QT interval revealed a novel duplication mutation in the PAS domain of hERG1. Familial analysis was performed only on the son of the proband, who had a normal ECG and did not carry the abnormal variant. All other relatives of the patient were living abroad and could not be tested for the mutation. Nevertheless, the pathogenicity of the duplication mutation of hERG1 is supported by our results. The electrophysiological and biochemical characterizations of the mutant channel suggest that the LQTS phenotype is largely due to the trafficking defect of the mutant protein and is partly due to mutation-induced hastening of deactivation kinetics. We also observed that the mutant channel trafficking defect is rescued upon incubation of cells at a reduced temperature.

LQTS and Takotsubo cardiomyopathy

LQTS and Takotsubo cardiomyopathy are both known to alter cardiac repolarization. Although unusual, their simultaneous occurrence has been reported in three recent case reports.[5–7] All three case reports presented a female patient with an acute episode of Takotsubo cardiomyopathy who displayed transient typical chest lead T wave inversion and a persistently prolonged QTc that was observed for several months following the acute episode. All three reports proposed that the acute Takotsubo episode unveiled a previously unrecognized congenital form of LQTS. The diagnosis of congenital LQTS could not be supported by genetic data in two of the three cases because either no analyses was performed [6] or no mutation was found in the LQTS genes that were screened.[5] Another important limitation to this proposal is that no ECG recordings could be obtained prior to the Takotsubo episode in the same two case reports.[5,6] However, in the third study by Wedekind et al,[7] analyses of ECG recordings from previous hospital stays identified clearly prolonged QT intervals on ECGs of the patient as well as of her daughter after subsequent screening of the family.

Based on these four case reports, one can speculate that patients with congenital LQTS may be more prone to develop Takotsubo cardiomyopathy. The pathogenic mechanisms underlying Takotsubo cardiomyopathy are poorly understood.[2] Among the possible alterations, it has been proposed that mechanical and electrical dysfunctions may be caused by epinephrine-induced toxicity occurring under stressful conditions.[13] Catecholamines are known to increase calcium entry into cardiomyocytes, mainly by stimulating the L-type calcium current. Intracellular calcium overload has been proposed to underlie ventricular dysfunc-

tion in stress cardiomyopathies.[2] The duration of the cardiac action potential determines how much calcium enters the myocytes during each contraction–relaxation cycle, so it is possible that a prolonged action potential duration, as seen in LQTS, exacerbates catecholamine-dependent intracellular calcium overloading. If this hypothesis is true, individuals with a reduced repolarization reserve, such as LQTS gene mutation carriers, patients taking hERG1-blocking drugs, or those with hypokalemia,[14] may have an increased risk for cellular calcium overload under such stressful conditions, rendering these individuals more susceptible to an acute cardiomyopathy. Finally, it may not be a coincidence that the four case patients were female; on average they have QTc values approximately 20 ms longer than in males, reflecting a longer action potential duration.[15]

The new and unusual in-frame duplication of 21 base pairs found in the highly structured PAS domain of hERG1 is discussed in the Online Supplementary Data.

Conclusion

We present the case of a female patient with Takotsubo cardiomyopathy in whom a previously undiagnosed congenital form of LQTS was discovered. Genetic analysis revealed an unusual duplication mutation in *KCNH2*. We showed that the LQTS phenotype is caused by defective maturation and/or trafficking of the mutant hERG1 protein, exertion of a dominant negative effect, and mutation-induced hastening of deactivation. A putative causal relationship between LQTS and Takotsubo cardiomyopathy is discussed. The mechanisms responsible for this proposed link have yet to be investigated.

Acknowledgments

We thank the patient and her family for their cooperation; Nathalie Deriaz and Sophie Roy for technical assistance; Dr. Carlo Rivolta for useful advice; and Dr. Allison Felley Jacquemont for thorough reading of the manuscript and helpful comments.

Appendix

Supplementary data

Supplementary data associated with this article can be found, in the online version, at 10.1016/j.hrthm.2009.09.026.

References

1. Rossenbacker T, Priori SG. New insights into the long-QT syndrome. Rev Esp Cardiol 2007;60:675–682.
2. Akashi YJ, Goldstein DS, Barbaro G, Ueyama T. Takotsubo cardiomyopathy: a new form of acute, reversible heart failure. Circulation 2008;118:2754–2762.
3. Pilgrim TM, Wyss TR. Takotsubo cardiomyopathy or transient left ventricular apical ballooning syndrome: a systematic review. Int J Cardiol 2008;124:283–292.
4. Nanda AS, Feldman A, Liang CS. Acute reversal of pheochromocytoma-induced catecholamine cardiomyopathy. Clin Cardiol 1995;18:421–423.
5. Mahida S, Dalageorgou C, Behr ER. Long-QT syndrome and torsades de pointes in a patient with Takotsubo cardiomyopathy: an unusual case. Europace 2009;11:376–378.
6. Sasaki O, Nishioka T, Akima T, et al. Association of Takotsubo cardiomyopathy and long QT syndrome. Circ J 2006;70:1220–1222.
7. Wedekind H, Muller JG, Ribbing M, et al. A fatal combination in an old lady: Tako-Tsubo cardiomyopathy, long QT syndrome, and cardiac hypertrophy. Europace 2009;11:820–822.
8. Morais Cabral JH, Lee A, Cohen SL, et al. Crystal structure and functional analysis of the HERG potassium channel N terminus: a eukaryotic PAS domain. Cell 1998;95:649–655.
9. Chen J, Zou A, Splawski I, Keating MT, Sanguinetti MC. Long QT syndrome-associated mutations in the Per-Arnt-Sim (PAS) domain of HERG potassium channels accelerate channel deactivation. J Biol Chem 1999;274:10113–10118.
10. Paulussen A, Raes A, Matthijs G, et al. A novel mutation (T65P) in the PAS domain of the human potassium channel HERG results in the long QT syndrome by trafficking deficiency. J Biol Chem 2002;277:48610–48616.
11. Phartiyal P, Jones EMC, Robertson GA. Heteromeric assembly of hERG 1A/1B channels occurs cotranslationally via amino-terminal interactions. J Biol Chem 2007;282:9874–9882.
12. Anderson CL, Delisle BP, Anson BD, et al. Most LQT2 mutations reduce Kv11.1 (hERG) current by a class 2 (trafficking-deficient) mechanism. Circulation 2006;113:365–373.
13. Wittstein IS, Thiemann DR, Lima JA, et al. Neurohumoral features of myocardial stunning due to sudden emotional stress. N Engl J Med 2005;352:539–548.
14. Roden DM. Long QT syndrome: reduced repolarization reserve and the genetic link. J Intern Med 2006;259:59–69.
15. Stramba-Badiale M, Locati EH, Martinelli A, Courville J, Schwartz PJ. Gender and the relationship between ventricular repolarization and cardiac cycle length during 24-h Holter recordings. Eur Heart J 1997;18:1000–1006.

JHRM-S-09-00883
Submitted to Heart Rhythm Journal
18 September 2009

Supplementary Data

Takotsubo cardiomyopathy and congenital LQTS in a patient with a novel duplication in the Per-Arnt-Sim (PAS) domain of hERG1

Liliana Sintra Grilo (1, 2), Etienne Pruvot (3), Michel Grobéty (4), Vincent Castella (5), Florence Fellmann, (6) and Hugues Abriel (1,3)

(1) Department of Clinical Research, University of Bern, Bern, Switzerland
(2) Pharmacochemistry, School of Pharmaceutical Sciences, University of Geneva, University of Lausanne, Switzerland
(3) Service of Cardiology, CHUV, Lausanne, Switzerland
(4) Clinique Cécil, Lausanne, Switzerland
(5) Forensic genetics unit, University Center of Legal Medicine, Geneva and Lausanne, Switzerland.
(6) Service of Medical Genetics, CHUV, Lausanne, Switzerland

Funding sources: Supported by grants of the CardioMet centre of the Faculty of Biology and Medicine (CardioGene grant 2007-2009), University of Lausanne, and the Swiss National Science Foundation (310000-120707 to HA).

Disclosures: None

Correspondence to:
Dr. Hugues Abriel, MD PhD
University of Bern, Department of Clinical Research
Murtenstrasse, 35, 3010 Bern, Switzerland
Phone: 41-31-6320928
Fax: 41-21-6930946
email: Hugues.Abriel@dkf.unibe.ch

Methods

Genetic and molecular investigations – Genomic DNA was extracted from peripheral lymphocytes. All coding exons of *KCNQ1*, *KCNH2* and *SCN5A* were amplified by polymerase chain reaction (PCR) using primers designed in intronic flanking sequences according to gene sequences (available upon request). All amplicons were directly sequenced in both directions and compared to reference sequences. The investigation conformed to the principles outlined in the Declaration of Helsinki, and the research protocol was approved by the ethics committee of the Faculty of Biology and Medicine of the University of Lausanne.

Plasmids and mutagenesis – cDNA encoding hERG1 (gift of Dr. R.S. Kass, Columbia University, NY) was cloned into pcDNA3.1-(+)Zeo (Invitrogen AG, Basel, Switzerland) vector as previously described [1]. Generation of the hERG1 duplication in the PAS domain was obtained through a long PCR protocol using the following sequences: 5'-**CTCGTTCTTCAC**AGCCCCATCCTCGTTCTTCACGGG-3' and 5'-**GATGGGGCT**GTCATCATGTTCATCC-3', respectively, as forward and reverse primers. Underlined characters represent complete matching bases of the sequence to duplicate. Bold letters stand for the inserted duplication sequences. The PCR product of the full plasmid was then blunt-ligated according to the instructions of the Rapid DNA Ligation Kit (Roche Diagnosis, Mannheim, Germany). Insertion of the 21 bases was confirmed and additional non-desired mutations were excluded by complete sequencing of the cDNA.

Cell culture – Chinese hamster ovary (CHO) cells were maintained in F12-GlutaMAX medium with 10% Fetal Bovine Serum (FBS), 1000 U/ml Penicillin, 1000 μg/ml Streptomycin and Glutamine 2 mM. For pharmacological rescue experiments, astemizole (Sigma Aldrich, Buchs, Switzerland) was added to the

medium by diluting a 10 mmol/L stock solution in di-methyl-sulfoxyde (DMSO) in order to achieve a final concentration of 5 μmol/L. Human embryonic kidney (HEK293) cells were cultured with DMEM medium supplemented with Glutamine 4 mM, FBS 10 % and gentamycine 20 μg/ml. For experiments requiring a lower incubation temperature, cells were transferred ~6 hours after transfection from 37℃ to 28℃ incubators and grown for 36 hours before pe rforming functional or expression assays. Plasmids, hERG1 wild type (WT) or mutant (Dupl), and empty vectors (pcDNA3.1-(+)Zeo), were transfected into CHO or HEK293 cells using Lipofectamine LTX reagent (Life Technologies Inc., Basel, Switzerland) according to the manufacturer's instructions.

Electrophysiological procedures – CHO cells were used for all electrophysiological measurements 44 to 52 hours after transient transfection with a cDNA encoding the CD8 antigen (*EBO-pCD-leu2*; American Type Culture Collection, Manassas, VA). Transfected cells were identified using Dynabeads coated with anti-CD8 monoclonal antibodies (Invitrogen, Basel, Switzerland). Patch-clamp recordings in whole-cell configuration were carried out using an internal solution containing (mmol/L) KCl 145; EGTA 10; $MgCl_2$ 1; HEPES 5; and Mg^{2+}-ATP 5, pH 7.3 with KOH; and an external solution containing NaCl 140; KCl 5; $CaCl_2$ 2; $MgCl_2$ 1; HEPES 20; and glucose 5, pH 7.4 with NaOH. Pipette resistance was in the range of 2.0–3.5 MΩ. Measurements were carried out using an Axopatch 200B amplifier (Axon Instruments, Union City, CA), and were performed at room temperature (25±1℃) or 37±1℃ using the temperature control system TC_2bip (Cell Micro Controls, Norfolk, VA) to heat the perfused solution. To study peak current amplitude, voltage was stepped from a holding potential (HP) of -80 mV to +40 mV (300 ms), followed by repolarization to -120 mV (600 ms). Peak tail currents were measured with correction for deactivation

at -120 mV, where the deactivation part of the peak tail current was fitted with a double exponential according to $f(t)= (A_1 \cdot e^{-t/Tau_{fast}})+(A_2 \cdot e^{-t/Tau_{slow}}) +C$. The corrected peak amplitude was measured using the extrapolated value at the start of the repolarizing step of -120 mV. Steady-state inactivation was obtained using a double-pulse protocol modified from [2]; an initial depolarizing pulse at +40 mV (500 ms), followed by a step pulse ranging from -150 to +40 mV, increasing by 10-mV increments, lasting for 250 ms and then back to HP. Deactivation kinetics were assessed using a similar protocol: an initial pulse was applied at +40 mV (500 ms), followed by a repolarization step (250 ms) in the range of -110 to -60 mV, increasing by 10-mV increments. Because deactivation traces at voltages of -110 mV and higher were better fitted monoexponentially, the time constant (Tau) of tail currents between -110 and -60 mV was obtained through fitting the deactivation part of the curve with $f(t)= (A_1 \cdot e^{-t/Tau})+C$. The activation curve was achieved by subjecting cells to depolarizing steps ranging from -80 to +40 mV (1000 ms), in 10-mV increments, before measuring tail currents at -120 mV (500ms). Boltzmann sigmoidal function was used to analyze activation and steady-state inactivation curves in current (I/I_{max}) versus membrane potential (V_m) plots and was expressed according to $I/I_{max}= 1/(1+\exp((V_{0.5}-V_m)/k)$ to determine the voltage of half maximal activation or inactivation ($V_{0.5}$) and the slope factor (k).

Cell surface biotinylation assay – HEK293 cells were transiently transfected with hERG1 WT or Dupl cDNA 48 hours prior to treatment with EZ-Link™ Sulfo-NHS-SS-Biotin (Pierce, Rockford, IL) at 0.35 mg/ml in PBS (Life Technologies Inc., Basel, Switzerland) for 30 minutes at 4℃. HEK293 cells we re then washed 3x with cold Glycine solution 200 mM (Sigma Aldrich, Buchs, Switzerland) in PBS and 1x in cold PBS. Cell lysates were spun at 16,000 x g for 15 minutes and the supernatants were

incubated for 2 hours at 4℃ with Steptavindin Seph arose beads (GE Healthcare, Uppsala, Sweden). The beads were subsequently spun and washed 5x with lysis buffer supplemented with 1% of PMSF 100 mM in isopropanol. Pelleted beads were then resuspended in 2.5 x SDS-PAGE loading buffer, boiled for 5 minutes, and analyzed in 7% PAGE. Antibodies against the C-terminus of hERG1 were purchased from Alomone (APC-062, Jerusalem, Israel).

Data analysis and statistics – Electrophysiological data were analyzed using pClamp software, version 10 (Axon Instruments, Union City, CA). Western blots were scanned and semi-quantified with Odyssey infrared imaging system and software, version 2.1 (LI-COR, Lincoln, NE). Statistical significance ($P<0.05$) of the differences between means was determined by two-tailed Student *t*-tests using GraphPad Prism software, version 5 (GraphPad Softwares, La Jolla, CA). Data are presented as means ± standard error of the means (SEM).

Supplementary Results

Electrophysiological characterization of the mutant hERG1 channel

We transiently expressed hERG1 WT and Dupl mutant channels in CHO cells in order to perform patch-clamp recordings in whole-cell configuration. hERG1 currents (IhERG1) were elicited using a double-pulse protocol (inset of Suppl. Fig. 4B). Kinetics of deactivation were assessed by fitting the deactivation part of tail currents from -110 to -60 mV with a monoexponential, enabling extraction of deactivation time constants (Suppl. Fig. 4A and 4B).

In order to eliminate bias on peak tail current amplitude estimation caused by faster deactivation, a bi-exponential fit of the curve was applied to the -120-mV repolarizing step. Fitted curves were extrapolated to the start of the repolarizing step, yielding peak tail current amplitudes corrected for deactivation

Other biophysical properties than deactivation kinetics of hERG1 WT and Dupl mutant channels were also investigated (Suppl. Fig. 5). A small, but significant, hyperpolarizing shift (-4.3±1.4mV) of activation $V_{0.5}$ was observed for the duplication mutant (Suppl. Fig. 5B). Activation kinetics (data not shown) were not different for the hERG1 WT and mutant and thus could not explain the shift of $V_{0.5}$. Steady-state inactivation curves showed no statistical differences (Suppl. Fig. 5C).

Reduced membrane expression of the mature form of the hERG1 duplication mutant

Even though fully glycosylated hERG1 was the predominant form in the biotinylated membrane fraction, some non-mature hERG1 was detected at the membrane surface. Once again, quantification of the corresponding signals (Fig. 3D, right lanes, cg)

showed no significant differences (92% and 105% of WT hERG1 signal for heterozygous and Dupl mutant, respectively).

Rescue of function and expression of the duplication mutant

Finally, to test the rescue effect of a hERG1 inhibitor, cells transiently expressing hERG1 WT or Dupl were cultured for 36 hours with or without astemizole (5 μmol/L). WB did not show any rescue using astemizole (data not shown).

Supplementary Discussion

An unusual mutation in the PAS domain of hERG1

The duplication is located within the highly structured PAS domain of hERG1 [3], which is arranged in a five-stranded antiparallel β-sheet (βA to βE) packed against a long strand of a coil and a single turn (Suppl. Fig. 3B). The β-sheet is flanked by α-helices (αA to αC) and packed against a 3_{10} helix (α'A). The N- and C-termini are positioned side by side in order to form the two central strands [3]. The amino-acid sequence that is duplicated is in the wild type channel between the βE - βD turn (Suppl. Fig. 3B). More than 290 mutations in *KCNH2* are listed in the database curated by Napolitano and Priori (*http://www.fsm.it/cardmoc/* 2004). Most of them are missense mutations, while only one is an in-frame duplication, also in the PAS domain [4]. No functional characterization of this duplication mutation has been performed. To our knowledge, this is the first characterization of such in-frame duplication mutation in hERG1. Our findings strongly suggest that the observed alterations in trafficking and biophysical properties of the mutant channel are involved in the pathogenic mechanisms underlying the LQTS phenotype. We cannot completely exclude, however, that mutations in other genes may also play a role in the LQTS phenotype, since no familial investigation could be performed and only three of the most prevalent LQTS genes were screened.

We also confirm that the PAS domain of hERG1 is an important "mutational hot-spot", as all of the naturally occurring mutations [5-8], such as the present duplication mutation, hasten the deactivation process and lead to a reduced repolarizing current during the AP. Gustina and Trudeau[9] recently showed that soluble recombinant N-terminus was able to restore normal deactivation in a truncated or PAS-domain

mutated hERG1 channel. Their results suggest that the LQTS-linked mutation (in their case R56Q) has a weaker interaction between the PAS domain and the core of the channel.

Importantly, the use of mammalian cell line expression systems enables discovery of temperature-sensitive trafficking phenotypes that may be missed when expressing such mutant channels in Xenopus oocytes at lower incubation temperatures [6]. We also show that the decreased current amplitude is partially explained by a reduced amount of the mature channel protein at the cell surface. Decreased single channel conductance caused by the duplication mutant may be possible based on the observed discrepancy between patch-clamp and biotinylation results (Dup mutant currents being only ~30% of hERG1 WT *vs*. ~60% of mature-form expression). As previously observed for several hERG1 channels bearing missense mutations [10, 11], our results show that the expression defect is rescued by lowering the incubation temperature but not with the use of a pharmacological agent (astemizole). The absence of pharmacological rescue has been previously reported for three cNBD-located mutants: hERG1 R752W, F805C, R823W[12].The molecular determinants of the biogenesis and trafficking of hERG1 are not well understood, but it has been proposed that the N-terminus may play an important role in the assembly of subunits [13]. It remains unclear whether the PAS domain also plays a role in the proper folding of the hERG1 channel, but our results suggest that alteration of the PAS structure may not only influence the biophysical properties of the channel, but also its biogenesis and/or trafficking.

Supplementary Figures

A

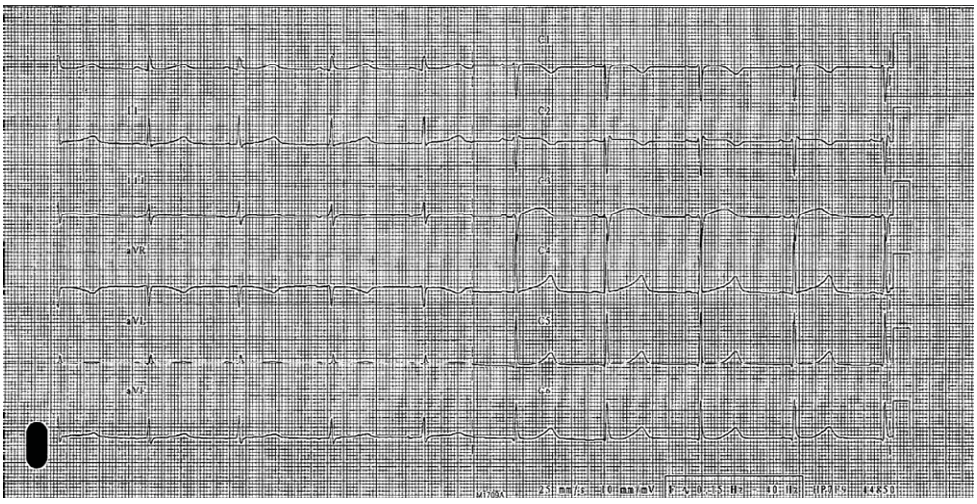

B

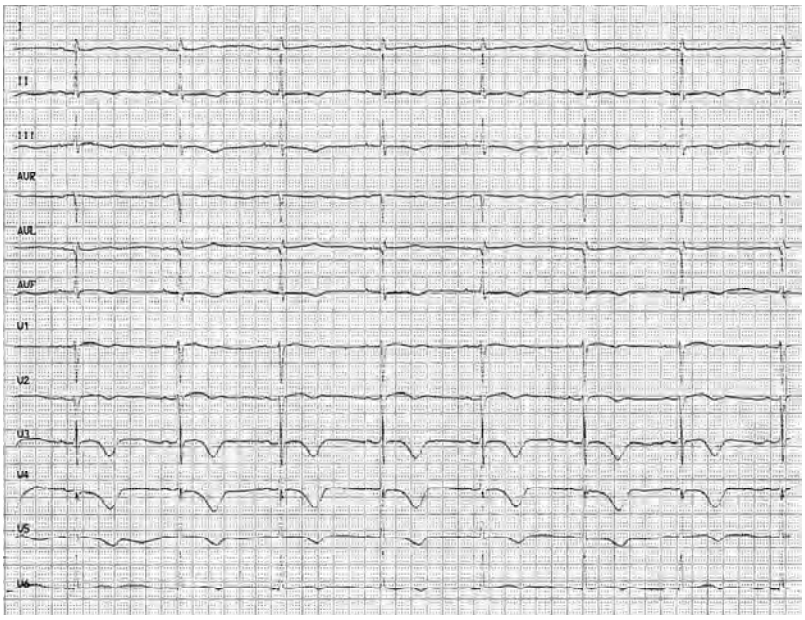

Supplementary Figure 1.

ECGs recorded at admission and after discharge from the hospital.

(A) ECG recorded at admission showing the QTc prolongation (QTc= 534 ms).

(B) ECG performed 6 weeks after the event showing the maintenance of giant negative T-waves in V1-V5, with mild reduction of the prolonged QTc (526 ms versus 721 ms in Fig. 1B).

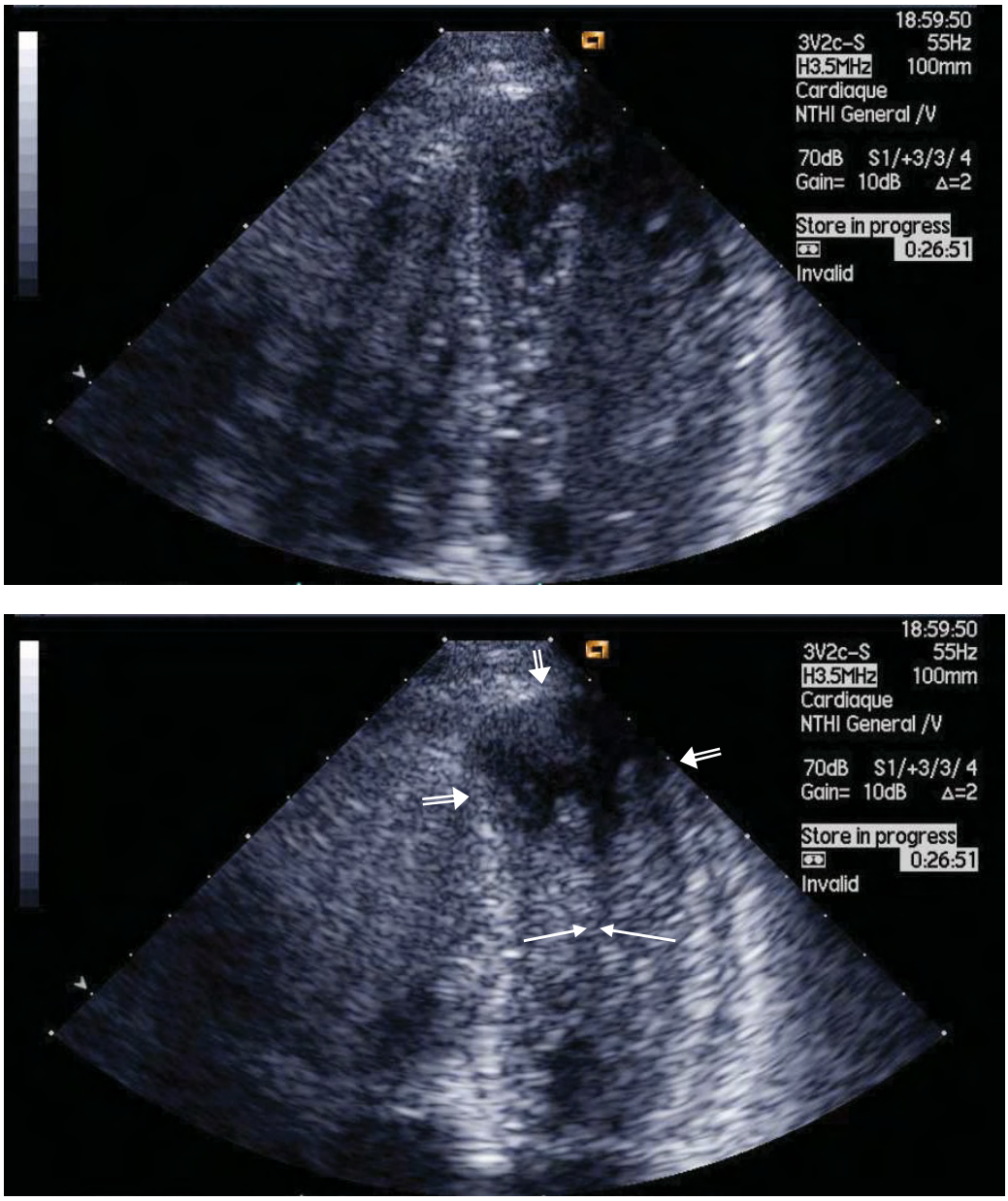

Supplementary Figure 2.

Two-chamber view echocardiography following emergency room admission. Top panel shows the left ventricle in diastole. Bottom panel shows hyperkinesis of the basal and mid segment (thin arrows) with localized akinesis and mild bulging of the left ventricle apex (double arrows) during systole suggestive of Takostubo cardiomyopathy.

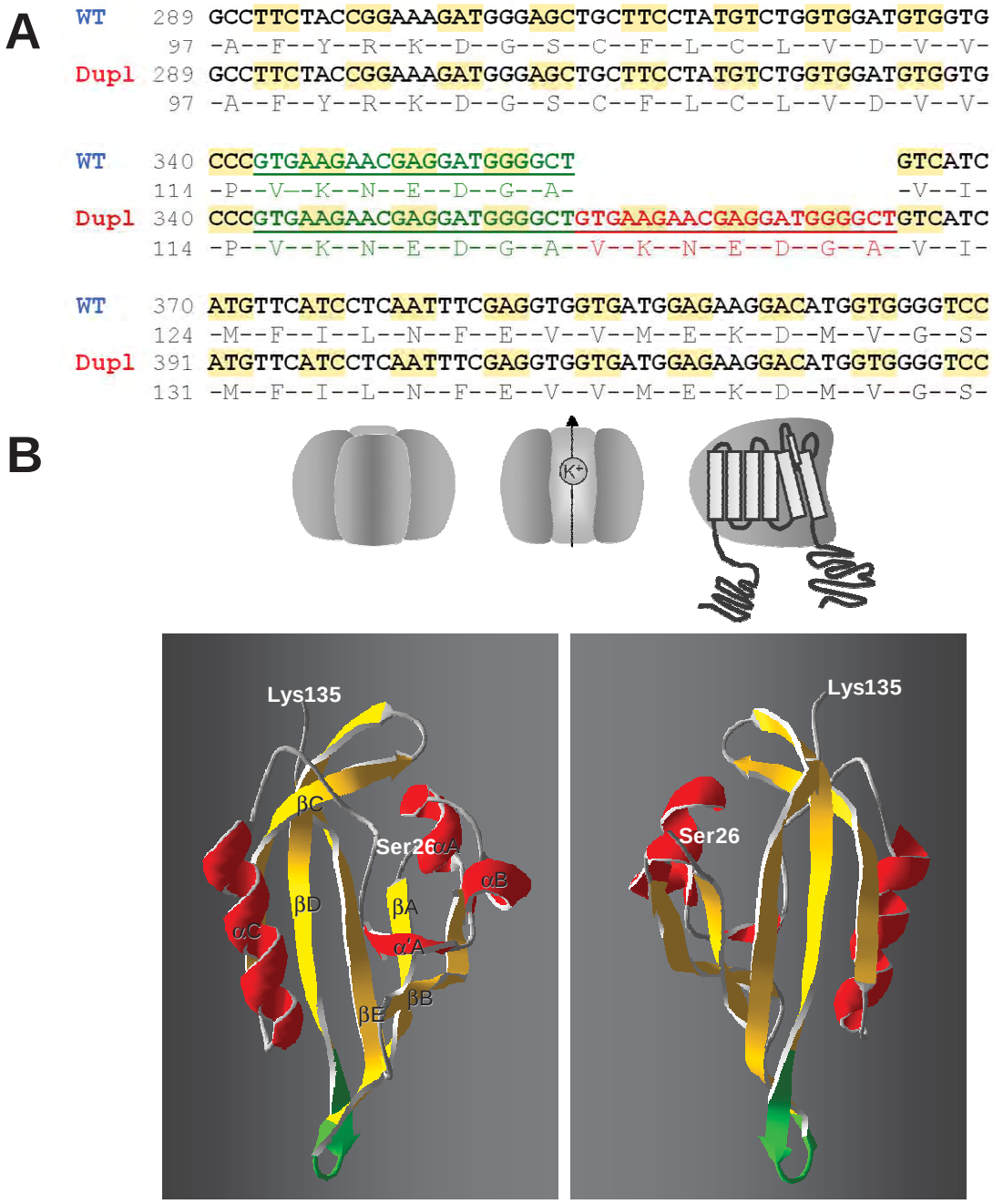

Supplementary Figure 3.

Presentation of hERG1 duplication mutant in PAS domain.

(A) Sequence of WT and Dupl hERG1 cDNA. The 21 base pair sequence (green) found duplicated in the proband is represented in blue.

(B) *Top*: cartoon of hERG1 tetramer (left panel) forming a central pore for K+ ions (middle panel) to pass through. Each subunit (right panel) is composed of six transmembrane domains.

Bottom: crystal structure of the N-terminal domain of hERG1 with PAS domain (pdb entry: 1byw) in front (left panel) and rear (right panel) view. α-helices are presented in red, β-sheets are shown in yellow and location of the 21-base-pair sequence is highlighted in green.

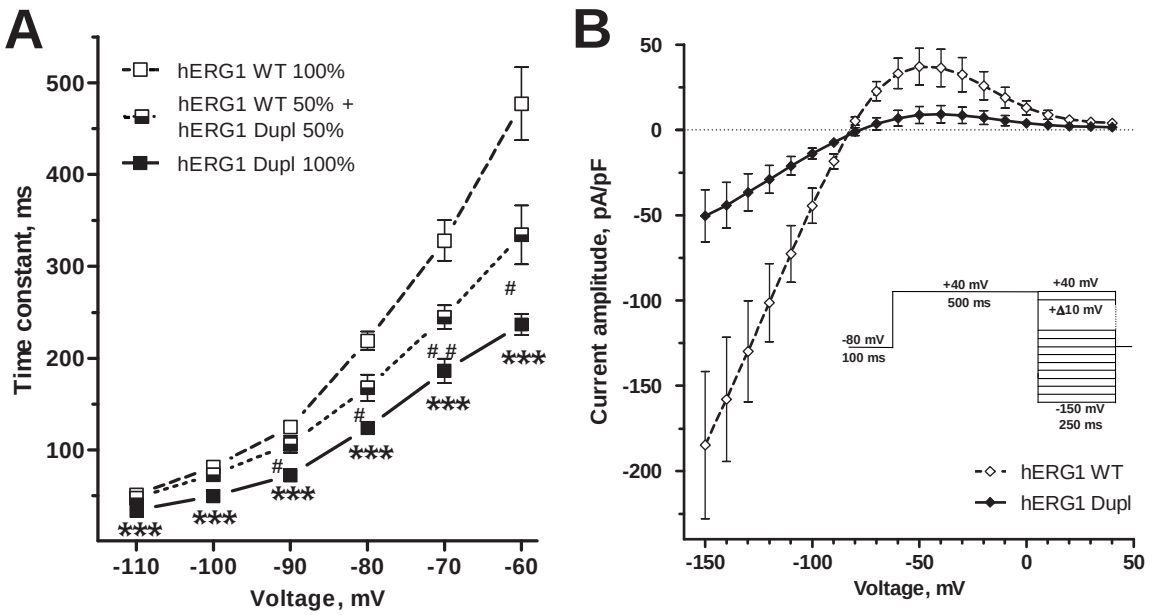

Supplementary Figure 4.

Biophysical changes observed in hERG1 Dupl mutant versus hERG1 WT.

(A) Time constant (Tau) of deactivation for hERG1 WT 100%, heterozygous-mimicking condition (WT 50%: Dupl 50%) and Dupl 100%. Tau is faster in both heterozygous-mimicking and Dupl conditions compared to WT. Significant differences for heterozygous versus WT (#, P<0.05; ##,P<0.01) and Dupl versus WT (***, P<0.001) for n=7-18 cells.

(B) Tail current-voltage relationship for hERG1 WT and Dupl mutant obtained by plotting peak tail currents of the second pulse (see inset) to the voltage applied.

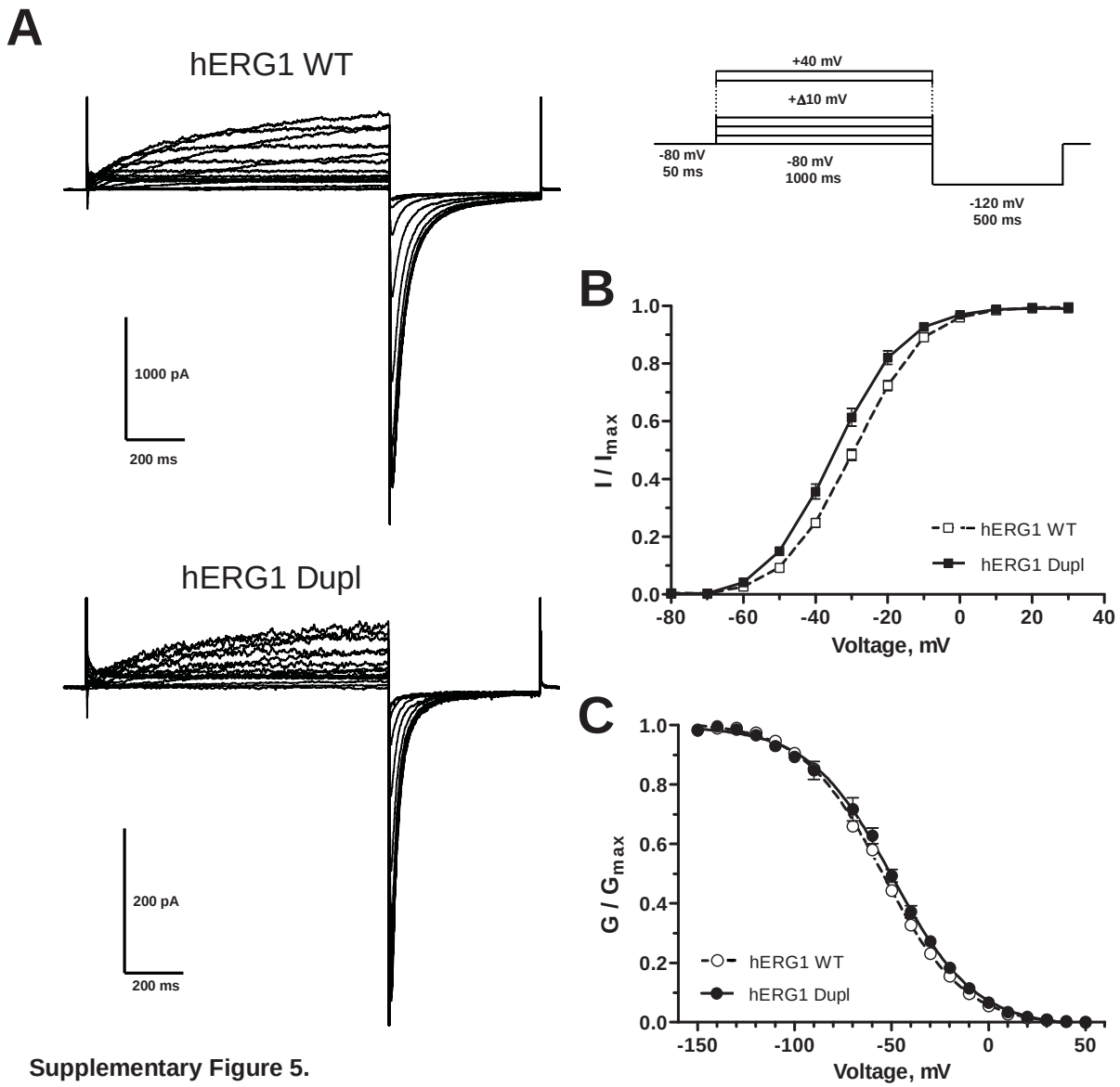

Supplementary Figure 5.

Voltage-dependence of hERG1 WT and Dupl mutant currents in activation and steady-state inactivation.

(A) Representative recordings of hERG1 WT (upper panel) and Dupl (lower panel). Protocol used to elicit currents is presented in inset.

(B) Activation curves obtained from curves as presented in (A). Dashed or continuous lines represent best fit of the Boltzmann relationship to the data. The V0.5 for hERG1 WT and Dupl are -30.3±0.9 mV and -34.6±1.1 mV, respectively (**, *P*<0.01) for n= 15-19 cells.

(C) Steady-state inactivation curves were obtained through protocol presented in inset of Figure 4A, with voltages of second pulse ranging from -150 mV to +50 mV. Dashed or continuous lines represent best fit of the Boltzmann relationship to the data. The V0.5 for hERG1 WT and Dupl are -54.0±1.4 mV and -49.8±1.9 mV, respectively (ns, *P*>0.05) for n= 9-14 cells.

References to the Supplementary Data

1. Eap CB, Crettol S, Rougier J-S et al. Stereoselective block of hERG channel by (S)-methadone and QT interval prolongation in CYP2B6 slow metabolizers. *Clin Pharmacol Ther* 2007;81(5):719-28.

2. Vandenberg JI, Varghese A, Lu Y et al. Temperature dependence of human Ether-a-go-go Related Gene (hERG) K+ currents. *Am J Physiol Cell Physiol* 2006;291(1):C165-75.

3. Morais Cabral JH, Lee A, Cohen SL et al. Crystal structure and functional analysis of the HERG potassium channel N terminus: a eukaryotic PAS domain. *Cell* 1998;95(5):649-55.

4. Larsen LA, Andersen PS, Kanters J et al. Screening for mutations and polymorphisms in the genes KCNH2 and KCNE2 encoding the cardiac HERG/MiRP1 ion channel: implications for acquired and congenital long Q-T syndrome. *Clin Chem* 2001;47(8):1390-5.

5. Paulussen A, Raes A, Matthijs G et al. A Novel Mutation (T65P) in the PAS Domain of the Human Potassium Channel HERG Results in the Long QT Syndrome by Trafficking Deficiency. *J Biol Chem* 2002;277(50):48610-6.

6. Chen J, Zou A, Splawski I, Keating MT, Sanguinetti MC. Long QT syndrome-associated mutations in the Per-Arnt-Sim (PAS) domain of HERG potassium channels accelerate channel deactivation. *J Biol Chem* 1999;274(15):10113-8.

7. Rossenbacker T, Mubagwa K, Jongbloed RJ et al. Novel mutation in the Per-Arnt-Sim domain of KCNH2 causes a malignant form of long-QT syndrome. *Circulation* 2005;111(8):961-8.

8. Shushi L, Kerem B, Goldmit M et al. Clinical, genetic, and electrophysiologic characteristics of a new PAS-domain HERG mutation (M124R) causing Long QT syndrome. *Ann Noninvasive Electrocardiol* 2005;10(3):334-41.

9. Gustina AS, Trudeau MC. A recombinant N-terminal domain fully restores deactivation gating in N-truncated and long QT syndrome mutant hERG potassium channels. *Proc Natl Acad Sci U S A* 2009.

10. Zhou Z, Gong Q, January CT. Correction of defective protein trafficking of a mutant HERG potassium channel in human long QT syndrome. Pharmacological and temperature effects. *J Biol Chem* 1999;274(44):31123-6.

11. Anderson CL, Delisle BP, Anson BD et al. Most LQT2 Mutations Reduce Kv11.1 (hERG) Current by a Class 2 (Trafficking-Deficient) Mechanism. *Circulation* 2006;113(3):365-73.

12. Ficker E, Dennis A, Kuryshev Y, Wible BA, Brown AM. HERG channel trafficking. *Novartis Found Symp* 2005;266:57-69.

13. Phartiyal P, Jones EMC, Robertson GA. Heteromeric assembly of hERG 1A/1B channels occurs cotranslationally via amino-terminal interactions. *J Biol Chem* 2007;282(13):9874-82.

III.D. Complementary discussion

In this section, we described two newly identified *KCNH2* mutations located in the N-terminal PAS domain of hERG1 subunit. Both mutations result in loss of function of hERG1 due to the major class 2 mechanism. In the literature, some hERG1 trafficking mutants reported to exert a dominant-negative suppression of I_{hERG1} when co-expressed with WT subunits (*e.g*. A651V, Ficker *et al*. 2000), while others showed co-dominance (*e.g*. K28E, Rossenbacker *et al*. 2005) or even haploinsufficiency (*e.g*. G601S, Anderson *et al*. 2006). As regards the characterized mutations, hERG1 A80P clearly denotes of a total loss of function of the mutant proteins, which do not associate with WT subunits at the cell surface; this results in haploinsufficiency. In contrast, the V115-A121dup (Dupl) mutant shows a dominant-negative effect on the heteromeric hERG1 channel current. In both cases, the functional current elicited through hERG1 channels was importantly reduced in the heterozygous-mimicking condition (approx. -50% and -70%, for WT/A80P and WT/Dupl mutant, respectively) and could explain the clinical phenotype of the proband. Interestingly, one could envisage that complete lack of expression would be more deleterious than partial expression of one allele. This will depend on the dominance or not of the mutated α-subunit on hERG1 channel function as well as the extent of loss of function. As mentioned earlier, if a single mutated α-subunit is able to retain the tetrameric K^+ channel in the ER and target it to degradation, this may results in up to 93% reduction in hERG1 current (Perrin *et al.* 2008). This highlights the fact that the final effect of a mutation cannot be assessed by simple genetic identification (*e.g*. missense *vs* in-frame insertion) and global localization of the mutation (*e.g.* here, in the N-terminus). Nevertheless, the PAS domain of hERG1 has been crystallized, which allows us to make some assumptions regarding the precise localization of the studied mutations. As described by Morais Cabral *et al.* (1998), the PAS domain is a $\alpha+\beta$ protein – thus highly structured – with a five-stranded antiparallel β-sheet (βA to βE) packed against a long ordered "vine" composed of coil and a single turn of 3_{10} helix (α'A). The antiparallel sheets are decorated on two sides by α-helices (αA to αC) as depicted in Suppl. Figure 3B (*Publication 3*). As regards the Dupl mutant, we

already mentioned that the sequence that is duplicated is present at the turn between the βE-βD strands, whereas the Ala80 is located in the αC helix. As the insertion of seven residues is a repetition of sequence and occurs in a more flexible region (turn), it might disturb less the general conformation of the PAS domain and be able to fool the quality control machinery, whereas a single substitution in the α-helix into proline, which is a structurally rigid residue, can have more drastic consequences.

Table 5 : Discrepancy between quantification of hERG1 mature form and whole-cell currents measured. According to the general equation $I = N \cdot Po \cdot g$, we may hypothesize that the difference is due to impaired single channel conductance, *e.g.* caused by symmetry problems in heteromeric channels.

hERG1 channel	***I*** **(whole-cell patch-clamp)**	=	***N*** **(mature form in Biotinylation)**	·	***Po · g*** ***(not assessed experimentally)***
100 % WT 	100 %	=	100 %	x	***100 %***
Mainly 50:50 	~ 25 %	=	~ 80 %	x	***~ 33 %***
100 % Dupl 	~ 25 %	=	~ 55 %	x	***~ 50 %***

Another intriguing point to mention is the discrepancy between the reduction of hERG1 channels at the cell surface in presence of Dupl subunits and the respective decrease of current. For the sake of demonstration, results are summarized in **Table 5**. Indeed, whole-cell current measurements (*I*) clearly denote a dominant-negative effect, as the heterozygous-mimicking condition is not significantly different from the total Dupl mutant. On the contrary, the protein density of hERG1 (*N*) appears to be determined by the stoichiometric expression of WT and Dupl subunits. In other words, ER retention/degradation of the channel – if we assume this mechanism takes place for the Dupl mutant – is proportional to the number of Dupl subunits in the hERG1 tetramer (*N*). Therefore, according to the equation $I = N \cdot Po \cdot g$ (see I.C.3), we may hypothesize that the difference lies in the $Po \cdot g$ parameters. Accelerated

deactivation kinetics in presence of Dupl subunits decrease the open probability (*Po*) of K^+ channels during the repolarization phase. Nevertheless, based on our experiments, this is not sufficient to explain the heterozygous discrepancy. We speculate that single channel conductance (*g*) is also affected by the mutation, and differently in homo- or heterotetramers of Dupl subunits. hERG1 channels are not a simple juxtaposition of four α-subunits: their transmembrane domains of the pore region intercross like a "bouquet" with a rotational symmetry. Moreover, it is recognized that different regions of hERG1 interact dynamically during the AP, as mentioned for the PAS domain and the S4-S5 linker. If a mutated subunit causes a steric hindrance (*e.g*. at the intracellular entrance of the pore) that disturbs the delicate symmetry (**Table 5**), it might have repercussions in the flow of K^+ ions. In contrast, if all subunits are identical (all Dupl mutant), it may conserve an adequate rotational symmetry and have less impact on ion flow (**Table 5**). Recording single ion channel currents may permit to verify this hypothesis.

It is capital to mention that the biochemical and electrophysiological characterization of both *KCNH2* mutations is highly relevant for the clinical management of the patients and their offsprings carrying the mutation. More generally, defining the mechanism of loss-of-function mutation is essential for future specific treatments. Indeed, Anderson *et al*. (2006) demonstrated that 68% of trafficking-deficient LQT2-mutations could undergo correction by one or more of the conditions tested (*i.e*. incubation at 27°C, with hERG1 channel blocker or with *thapsigargin*). In contrast, several mutant KCNQ1 channels (LQT1) have shown to be trafficking deficient and yet failed to respond to low-temperature correction or drug rescue (Balijepalli *et al.* 2010). Thus, the significant functional recovery of LQT2-mutations with a class 2 mechanism makes this phenotype a promising target for therapeutic intervention (Walker *et al.* 2009). In the presented cases, only the Dupl mutant was tested for rescue, successfully with the decrease of incubation temperature but not with the hERG1 high-affinity blocker *astemizole*. In the above-mentioned study of Anderson *et al*. (2006), mutations in the N-terminus and cNBD appeared to be non correctable. In later publications, PAS-domain mutants such as T65P and K28E showed rescue of expression in presence of the hERG1 blocker *E-4031* (Paulussen *et al.* 2002; Rossenbacker *et al.* 2005). Our current understanding

of pharmacological rescue is limited and it is therefore still considered as both drug- and mutation-specific.

In a recent review, Balijepalli and colleagues (2010) summarized the therapeutic strategies under investigation for correcting the trafficking-deficient phenotype. Since the influential work of Zhou and co-workers a decade ago, in which they rescued the hERG1 N470D mutant by incubating cells at reduced temperature and with hERG1 channel blockers, multiple approaches have been identified for increasing I_{hERG1} including incubation with *glycerol* or *thapsigargin*, or even the addition of specific second mutations (Balijepalli *et al.* 2010). Small molecules that rescue loss-of-function mutations are sometimes referred to as *correctors* or *pharmacological chaperones*, and are at the moment the most promising option for treatment.

However, questions arise regarding specificity and sensitivity of the of trafficking and function salvage. Indeed, drugs that act to fool the quality control mechanisms for mutant hERG1 channels, if they lack specificity, may also do the same for other proteins that must be retained because of misfolding. Moreover, the extent of rescue required is not known for hERG1 channels, whereas restoring transport of the ΔF508 CFTR mutant to 5 to 30% of WT level was suggested to ameliorate clinical symptoms (Balijepalli *et al.* 2010). On the other hand, if the rescue of LQT2-mutant is too high, the overcorrection could potentially lead to a SQTS. The other important issue is that, at the moment, most available pharmacological chaperones block the hERG channel. Naturally, the use of such compounds is not possible in patients with *c*LQTS. Therefore, the authors of the above-mentioned review (Balijepalli *et al.* 2010) call for uncoupling the hERG1 channel block from the pharmacological rescue. Ficker *et al*. (2002) studied the class 2 G601S mutant and showed that the potency of current block by drugs and rescue of expression varied in parallel. Moreover, by mutating a supplementary residue in the drug-binding site (F656C), both *astemizole* blockade and pharmacological rescue of hERG1-G601S-F656C were impaired. In addition, higher concentrations were generally required for pharmacological rescue than for block. Nevertheless, Rajamani and colleagues (2002) tested *terfenadine* – a

high-affinity blocker of hERG channels – and its metabolite, *fexofenadine,* on hERG1 trafficking-defective mutants. Fexofenadine is a less potent inhibitor of hERG1 current; nevertheless, it remarkably succeeded in restoring N470D and G601S channels at the cell surface without current inhibition. Moreover, half-maximal rescue concentration was ~350-fold lower than the half-maximal current block concentration (Rajamani *et al.* 2002). Unfortunately, pharmacological rescue is mutation-dependent, and the V822M mutant was insensitive to fexofenadine. The same approach was attempted by Ficker and colleagues (2002) using *astemizole* and *norastemizole* metabolite, but norastemizole did not rescue G601S expression.

One may also wonder about the impact of restoring expression of the mutated channel. Owing to the tetrameric structure of hERG channel and the dominant-negative effect of most missense mutations, complete absence of expression of the mutant allele might be less deleterious than co-expression of a mutation with important gating and/or permeability alterations. In their study regarding the premature stop codon mutant hERG W1001X, Gong *et al*. (2007) suggested that the physiological role of *nonsense-mediated mRNA decay* could be to convert a dominant-negative effect into haploinsufficiency. Moreover, Balijepalli *et al*. (2010) also pointed out the importance of assessing *in vitro*, and in adequate cellular models, the identified LQT2 mutation. Indeed, in case of a class 2 mechanism leading to haploinsufficiency, channel activators (see I.C.3.b) may have higher benefits than corrector drugs.

The number of identified LQT2 mutations is notable and still increasing. Characterization of all mutations is not easily feasible or sensible, since no adequate therapeutic response is currently available. Nevertheless, biophysical understanding of mutations associated with severe phenotypes is essential for the patients and relatives, for their clinical management and potential future treatment. Research on pharmacological chaperones and activators is on progress, but parallel work is still required, such as studies on ion channel biogenesis or screening of molecule libraries for different modalities of rescue (Balijepalli *et al.* 2010). These new approaches should permit the development of therapeutic interventions targeting protein synthesis and trafficking to treat congenital LQTS.

Part IV:
Stereoselective block of hERG channel and drug-induced LQTS

IV. Drug-induced LQTS and stereoselective block of hERG

IV.A. Introduction

IV.A.1. Drug block of hERG channel

A continuously growing number of non-class III antiarrhythmic agents have been shown to prolong cardiac repolarization, thus predisposing to *Torsades de Pointes* arrhythmias and sudden cardiac death. As already mentioned, drug-induced LQTS is considered the most frequent cause of withdrawal or relabeling of marketed drugs in the last decade (Roden 2004). Drugs with proven lengthening of the QT interval or definite association with TdP are common (see list on *www.QTdrugs.org*) and were estimated, in a study dating a decade ago, to comprise approximately 2-3% of all drug prescriptions (De Ponti *et al.* 2000).

Almost all drugs that prolong the QT interval involve the hERG channel. One notorious exception is *alfuzosin*, a selective antagonist of postsynaptic α1-adrenergic receptors (located in the prostate and bladder), which is prescribed for management of benign prostatic hyperplasia. Lacerda *et al*. (2008) demonstrated that alfuzosin prolonged APD at clinically relevant concentrations by significantly increasing the $Na_v1.5$-mediated current. Block of hERG current usually accounts for >95% of drug-induced delayed repolarization, although disrupting hERG protein trafficking has also been reported. Some drugs, such as *arsenic trioxide*, *geldamycin* or *pentamidine*, were shown to impair the normal trafficking of hERG channel and to reduce thereby its density at the cell surface (reduction of *N*, see I.C.3) without blocking I_{hERG} (reviewed in Wible *et al*. 2005). Other drugs, including *fluoxetine*, *ketoconazole* or *thioridazine*, present combined effects of hERG current inhibition and disruption of protein trafficking (Wible *et al.* 2005; Rajamani *et al.* 2006; Takemasa *et al.* 2008). Although Wible *et al.* (2005) reported this mechanism for ~40% of hERG channel blockers tested, IC_{50} for disruption of trafficking was generally orders of magnitude higher than IC_{50} of block.

IV.A.1.a. Molecular determinants of hERG channel block

The wide variety of drugs of different class and structure that inhibit the hERG current is unique among ion channels. The first insights on the reason why hERG is so promiscuous came about a decade ago. Based upon the assumption that the block of hERG occurred in the cavity of the channel (**Figure 16**), like many blockers of Na^+ and Ca^{2+} channels, Mitcheson *et al*. (2000a) used alanine-scanning mutagenesis of hERG pore-helix and S6 domain to define binding sites for *MK-499*, a potent methanesulfonanilide blocker of the K^+ channel. Three channels with missense mutations located in the S6 domain (G648A, Y652A, and F656A) were hardly inhibited by MK-499 compared to WT channels (Mitcheson *et al.* 2000a). Remarkably, based on a *homology model* of the hERG channel, these aromatic residues were predicted to line the pore cavity. In addition, three channels with a mutation located in the base of the pore-helix (T623A, S624A, and V625A) and one located in the S6 domain (V659A) were also less sensitive to MK-499 (Mitcheson *et al.* 2000a). Similar reductions in potency of block were obtained with Y652A and F656A mutants for *terfenadine* and *cisapride*, as well as many other compounds (reviewed in Stansfeld *et al*. 2007). Mitcheson's group brought further evidence to the intra-cavity block of hERG by rather large molecules like methanesulfonanilide drugs. Using the hERG D540K channel that has the unusual property of opening in response to hyperpolarization, they confirmed that MK-499 blocked hERG in the inner vestibule, as MK-499 was trapped by closure of the activation gate (Mitcheson *et al.* 2000b). The ability of HERG (WT and D540K) channels to trap MK-499, despite its large size, suggests that the vestibule of this channel is larger than other well studied K_v1 (*Shaker* family) channels. On the contrary to other voltage-gated K^+ channels (K_v1-K_v4), hERG lacks the Pro-x-Pro sequence in the S6 domain that has been proposed to cause a sharp bend in the S6 helices and reduce the volume of the channel cavity (Mitcheson *et al.* 2000a). Altogether, these results set the residues lining the pore (especially Tyr652 and Phe656) as major structural determinants for the hERG current block.

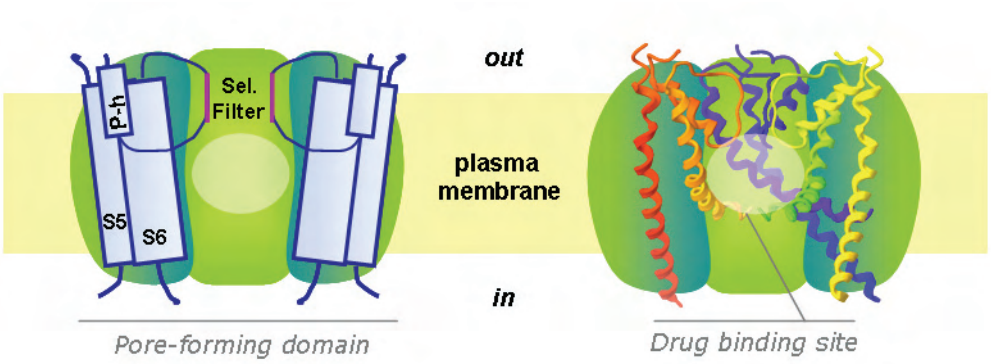

Figure 16 : Located binding region (pale circle) for drugs blocking the hERG channel in the cavity.

Schematic (*left*) and ribbon representation (*right*) of the hERG channel presenting the general *drug binding site* in the cavity created by the *pore-forming domain*, *i.e*. transmembrane domains (S5, S6), pore-helix (P-h) and selectivity filter (Sel. Filter) of four α-subunits. For clarity, only three subunits are depicted.

Importantly, although the upper part of the inner cavity appears as the major binding site for hERG blockers (**Figure 16**), some drugs are likely to block the channels at different sites. The macrolide antibiotic *erythromycin* is associated with risk of drug-induced LQTS as it demonstrated to inhibit hERG currents at clinically relevant concentrations (Duncan *et al.* 2006). Because the antibiotic structure is exceptionally large, it was expected to block the channel differently. Indeed, Y652A mutation did not significantly alter hERG current block by erythromycin, indicating that Tyr652 is not important for blockade. As regarded hERG F656A channel, the mutation resulted in only weak attenuation of the inhibition (Duncan *et al.* 2006). The authors also presented computer models of the channel in open and closed state, in which they docked the macrolide drug. In their open-state model, erythromycin could make several direct contacts with F656, but not with Y652, because the large size of the drug restricted its ability to move further up into the inner cavity. Interestingly, erythromycin was unable to fit into their closed-state channel model (Duncan *et al.* 2006).

For smaller molecules, such as the selective-serotonin re-uptake inhibitor *fluvoxamine*, the S6 mutations Y652A and F656A and the pore-helix mutant S631A only partially attenuated the block at concentrations causing profound inhibition of

WT hERG (Milnes *et al.* 2003a). In their work, Milnes and co-workers suggested that fluvoxamine action on hERG involves a binding site that is distinct from that previously described. Scorpion toxin peptides can also block potently the hERG current, though in an unusual manner. One such toxin named *ergtoxin* has been shown, using chimeras and mutants of hERG channels, to have molecular determinants of block in the extracellular S5-P linker region (Pardo-Lopez *et al.* 2002). Another scorpion toxin, known as *BeKm-1*, blocks the hERG current from the extracellular side. Because of the toxin is large and positively charged, it probably does not access its site of action from inside the cell and is unlikely to cross the plasma membrane easily. Milnes *et al*. (2003b) analyzed the block mechanism of BeKm-1 and concluded that the peptide blocks hERG preferentially at the closed state.

IV.A.1.b. Characteristics of hERG channel block

The molecular mechanisms that underlie hERG channel block are crucial to understand why a particular compound produces drug-induced LQTS. As mentioned earlier, structural determinants of hERG block have been identified in the inner cavity of the channel (considered as the general binding site), although other particular determinants of binding have been assessed. Importantly too, the magnitude of hERG current blockade, and thus QT interval prolongation and risk of TdP, is known to be a *dose-dependent adverse effect*. It is therefore important to have a large safety margin between the free plasma concentrations attained during the clinical use and the IC_{50} of I_{hERG}/I_{Kr} block, also known as the *therapeutic window*. In the work of Redfern *et al*. (2002), the investigators sought to determine a value for predicting risk of TdP in clinical use derived from cardiac electrophysiological data (*in vitro* and *in vivo*). Based upon a literature review that compiled complete information on 52 QT-prolonging drugs, the authors concluded that a 30-fold margin between maximal effective therapeutic plasma concentrations and hERG IC_{50} may be adequate for drugs currently undergoing clinical evaluation. Obviously margins should reflect disease severity and medical need. For example, a 10-fold margin might be acceptable for drugs used in diseases that are lethal if untreated (*e.g.* cancer or severe infectious disease), but a margin of 100-fold or higher might be

required in the case of less serious diseases (*e.g.* seasonal rhinitis) (Redfern *et al.* 2003).

Drug blockade of hERG was shown to be *state-dependent*, in other words a compound preferentially blocks the channel in one of the three conformations (closed, open and inactivated). Initial studies of Mitcheson *et al*. (2000b) have shown that *MK-499* methanesulfonanilide drug blocked hERG channels only when these were depolarized, suggesting that opening of the S6 helices is required for blockade in an open and/or inactivated state. However, block of hERG by *dofetilide*, another class III antiarrhythmic agent, needs an intact C-type inactivation process for high-affinity drug binding, thus suggesting that inactivation promotes hERG channel block (Ficker *et al.* 1998). Other drugs, such as the already mentioned *BeKm-1*, *ketoconazole* or *amiodarone*, have been proposed to inhibit hERG currents at a closed state (reviewed in Thomas *et al*. 2004).

Some low-affinity hERG channel ligands present an enhanced block in response to increasing membrane depolarizations; this property is known as *voltage-dependence* of block. Conversely, high-affinity blockers exhibit little or no voltage-dependent block. Although models have been proposed to explain this phenomenon (reviewed in Thomas 2004), the molecular mechanisms are yet to be resolved.

Under clinical conditions, some drugs increase AP duration and refractoriness to the greatest extent at slow heart rates; this property is known as *reverse use-dependence* (or *frequency use-dependence*). Since bradycardia increases the risk of TdP initiation in the presence of prolonged QT interval, reverse use-dependence is an unfavorable effect. Indeed, this property has been implicated in the proarrhythmic effects of various class III agents, including *E-4031*, *dofetilide* (Hondeghem & Snyders 1990), and has been demonstrated with various I_{Kr}-blocking agents such as *cisapride* or *sotalol* (Potet *et al.* 2001). *Amiodarone*, conversely, exhibits stronger current inhibition at higher heart rates (*e.g*. tachycardia), which is a beneficial property in the antiarrhythmic treatment (Thomas *et al.* 2004).

IV.A.2. Molecular Modeling

It is noteworthy to mention that Mitcheson and co-workers (2000a) presented in their influential work a *homology model* of the hERG pore region and suggested it could be used as a starting point to develop a virtual screening tool. Indeed, *in silico* methods possess the potential to identify and filter-out from further development the compounds that are likely to block hERG channels. In computational drug design, modeling studies follow two strategies that depend on the information available. If experimental data exist only for the molecules displaying activity towards the target, a so-called *ligand-based approach* is taken and QSAR (Quantitative Structure-Activity Relationship) models are derived. If biostructural information about the protein target is available (*e.g.* 3D structures or even validated protein sequences), a *target-based approach* can be pursued and in this case docking models can be built (Recanatini *et al.* 2005). In the field of hERG channel blocking drugs, *pharmacophoric* (ligand-based) studies aim at determining the physicochemical features associated with the channel block and at predicting blocking potential of compounds. Partial homology models (*target-based*) have been built and used as working tools to interpret experimental studies (Recanatini *et al.* 2005). Despite Mitcheson's prediction, a decade of research in the field did not succeed in accurately predicting cardiotoxicity of unrelated compounds using a target-based virtual screening. However, pharmacophoric features of hERG blockers have emerged and *in silico* models for hERG liability achieved some goals among structurally related compounds.

With regard to pharmacophores for hERG-blocking compounds, as far as we know, Morgan and Sullivan (1992) undertook the first structure-activity relationship study with class III antiarrhythmics. Although hERG responsibility was at the time not yet pointed out, the authors were able to depict a pharmacophoric scheme (**Figure 17a**) containing important structural characteristics associated with AP prolongation. In 2002, two 3D-QSAR models for hERG channel inhibition were independently proposed by Ekins *et al*. and Cavalli *et al.* (**Figure 17b** and **c**, respectively). The similarities of the two pharmacophores are remarkable, all the more that they were based on different sets of blockers and computational tools. The "general hERG

pharmacophore" built by Ekins consisted in one ionisable feature (basic nitrogen) and four hydrophobic centers, which are not necessarily simultaneously present. In Cavalli's model, almost the same features appeared, but designated differently (reviewed in Recanatini *et al.* 2005). Based on a series of *sertindole* analogs, Pearlstein proposed the "drain-plug" pharmacophoric model, which consisted in a "handle" and a "body" (**Figure 17e**), which fitted the previous knowledge on sertindole structural bases of block (Pearlstein *et al.* 2003). Later, Aronov studied the importance of hydrogen-bond acceptors in hERG-blocking compounds as well as a 3D model for uncharged hERG blockers. Using cross-validation runs, the authors (Aronov & Goldman 2004) obtained three consistent pharmacophore hypothesis (**Figure 17f**-**h**). Two models (**f**-**g**) were in good agreement with Cavalli's (**c**), and the third model (**h**) placed a hydrogen-bond acceptor as essential feature. Although the typical published pharmacophore models contain a basic nitrogen or a positively charged center, compounds devoid of this feature (*e.g*. *ketoconazole*) may also block hERG. Aronov (2006) published a six-point model comprising hydrophobic/aromatic features and hydrogen-bond acceptors (**Figure 17d**), which would enable for identification of non-charged hERG blockers.

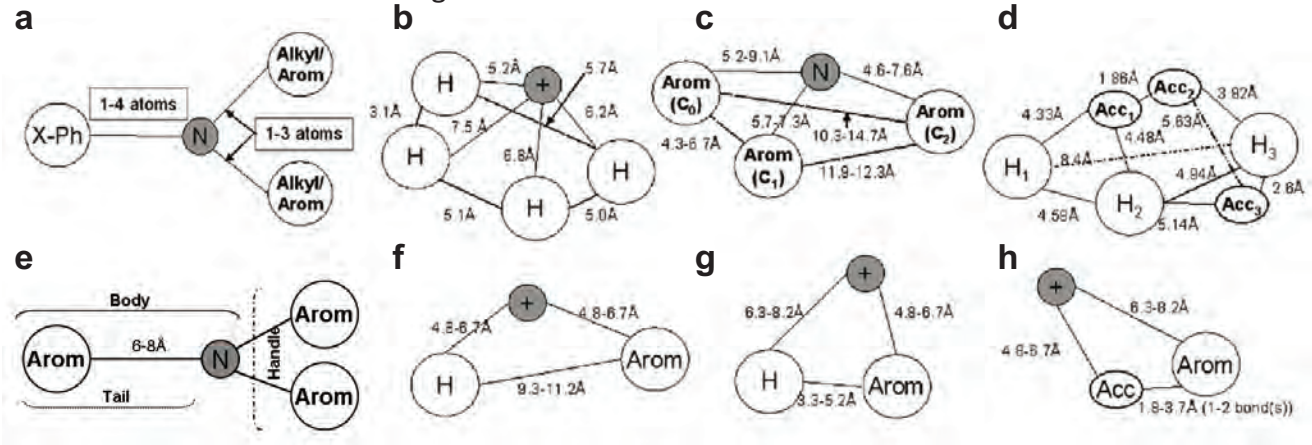

Figure 17 : Schematic illustration of 3D pharmacophoric models for hERG channel blockers. Figure modified from (Thai & Ecker 2007).

a-**c**: Early published pharmacophoric models (Morgan, Jr. & Sullivan 1992; Ekins *et al.* 2002; Cavalli *et al.* 2002), **d**: 3D six-point pharmacophoric model for neutral/uncharged hERG blockers (Aronov 2006), **e**: "drain-plug" pharmacophoric model with *handle* and *tail* (Pearlstein *et al.* 2003). **f**-**h**: three hypotheses of the three-point pharmacophoric model (Aronov & Goldman 2004).

Abbreviation: *N* or *(+)*: basic nitrogen or positive charged atom; *X-Ph*: phenyl ring; *H*: hydrophobic/aromatic feature; *Arom*: aromatic feature; *Acc*: H-bond acceptor.

No experimental determination of the hERG structure has been disclosed up to date. Therefore, most of our understanding of the hERG channel is inferred from X-ray and NMR structures of bacterial K^+ channels or the mammalian $K_v1.2$ channel, of which the pores are architecturally related. Based on this, it seems rational to use these crystal structures as *templates* to model the hERG K^+ channel (Thai & Ecker 2007). However, depending on the template used partial homology models of hERG – partial, because only the pore-forming domain is modeled – may be in a closed state (crystals of KcsA, KirBac1.1) or in an open state (crystals of KvAP or MthK), as exemplified in **Figure 18**. Homology models of hERG allowed to verify, as suggested with mutagenesis studies, that side chains of Tyr652 and Phe656 (on the S6 helix) are facing the interior of the conduction pathway. These multiple aromatic side chains (eight per channel) are arranged in two concentric rings, with the "tetrade" of Phe656 closer to the intracellular entry of the pore, and the four Tyr652 residues being closer to the pore-helix and SF. As reviewed by Thai and Ecker (2007), the first homology models presented essentially hERG in the closed state. Then, fully open or partially open models (originated from the closed state crystal structure KcsA) appeared with promising results. The various degrees of pore opening in structures was used to derive intermediate states of the helix motion, since Gly648 was recognized as the "hinge" for bending S6 by overlay of KcsA and MthK structures (reviewed in Thai & Ecker 2007). Homology models can be used as working tools to interpret electrophysiological and mutagenesis studies. Moreover, as the hERG promiscuous binding region has been identified, homology models appear suitable for *docking studies*, which are computational techniques that explore the possible binding modes of a substrate to a given binding site. Here again, early docking studies aimed at interpreting interactions between drug and hERG channel, such as the "drain-plug" hypothesis of Pearlstein *et al*. (2003). Later, docking studies using a series of structurally related compounds (*e.g*. *sertindole* analogs in Farid *et al*. 2006) showed good correlation (R^2 = 0.95) between ligand binding energy predicted by fitness function and experimental IC_{50} values. In a previous publication, using almost the same set of sertindole analogs, but through a different approach, Österberg and Aqvist (2005) also obtained a good correlation between binding free energies from their simulations *versus* experimental IC_{50} values. Problems arise when a larger

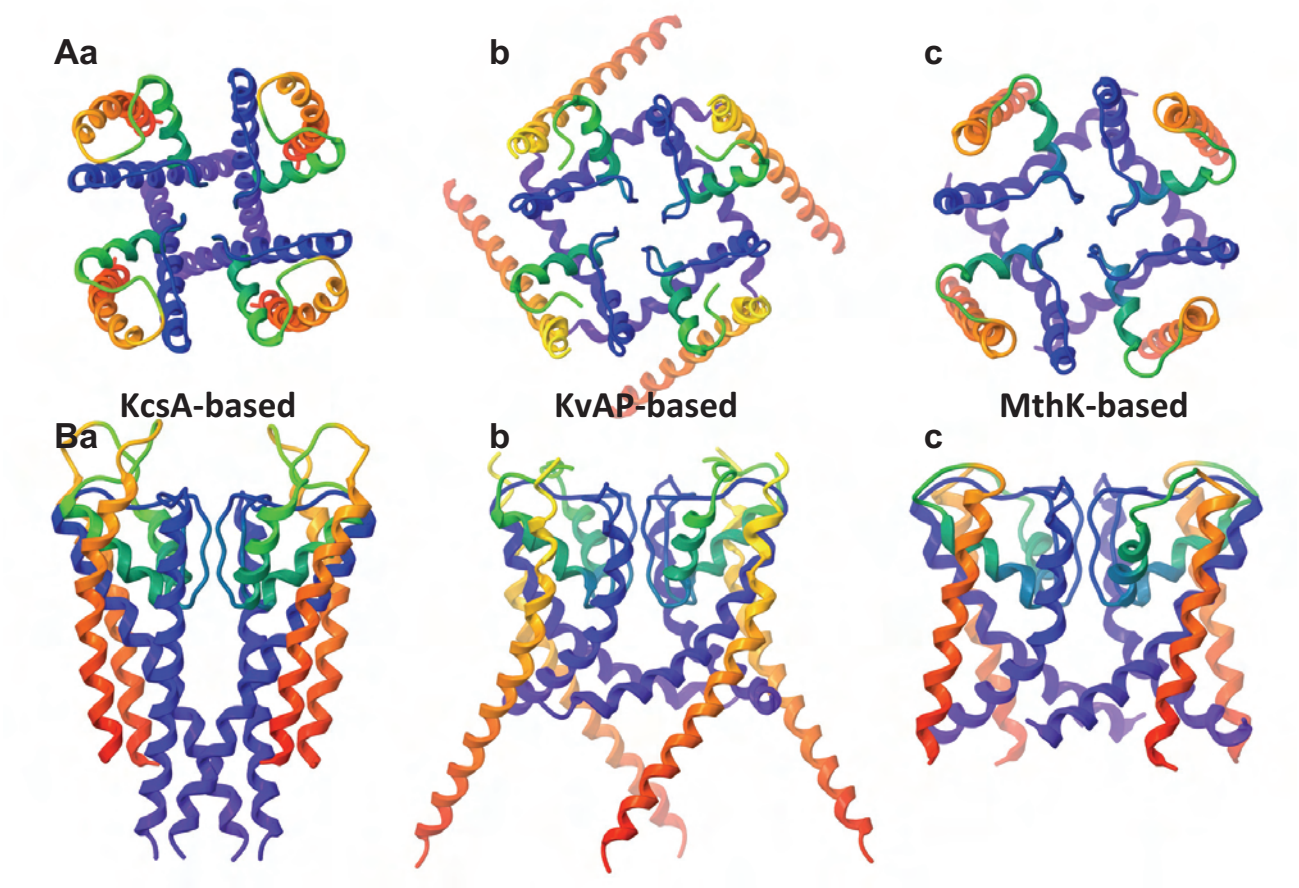

Figure 18 : Partial homology models based on different K^+-channel templates.

View from the extracellular side (**A**, through the pore axis) or lateral view (**B,** through the plasma membrane plane). The ribbon representation shows *S5 helix* (red-orange), *pore-helix* (green), *selectivity filter* (thin tube) and *S6 helix* (blue) for all homology models. The **KcsA** template (**a**) generates a closed conformation model of hERG (Stansfeld *et al.* 2007), while sequence alignment with the **KvAP** crystal(**b**) produces the open hERG homology model (Farid *et al.* 2006). A "more open" homology structure can be obtained with the **MthK** bacterial crystal (**c**) (Imai *et al.* 2009).

dataset of less chemically related molecules is used. As pharmaceuticals of widely varying structure have been shown to interact with hERG and should be studied, target-based virtual screening is not reasonable nowadays to filter out cardiotoxic drug candidates. Better results appeared to come from QSAR studies using consensus approaches (O'Brien & de Groot 2005), though controversy exists about this strategy (Hewitt *et al.* 2007). A consensus scoring scheme combines multiple models and multiple approaches in order to increase the predictive power (Thai & Ecker 2007). In a recent publication, Doddareddy *et al*. (2010) presented ligand-

based *in silico* models to qualitatively classify chemical structures into hERG blockers and compounds devoid of such activity. The authors validated experimentally the models using 50 unrelated structures predicted "*hERG blockers*" and 10 predicted "*non-hERG blockers*". Their models performed well in predicting non-hERG blockers as all the ten predicted non-hERG blockers were indeed found to be inactive in the assay. However, biological evaluation of the 50 predicted blockers found only 18 that produced more than 50% (set as threshold) displacement of radiolabelled *astemizole* binding to cell membranes expressing the hERG channel, which represents a large proportion of false positives in their models (Doddareddy *et al.* 2010).

Remarkably, direct *lead optimization* of the hERG liability has been seen with success for some molecules responding to the pharmacophore models. As a case in point, the introduction of a carboxylic moiety to *terfenadine* (IC_{50} ~50 nM, ClogP 6.07) gave rise to *fexofenadine* (IC_{50} ~20 μM, ClogP 1.96), which has a safer cardiologic profile. Indeed, many QSAR reports displayed a series-dependent correlation between hERG potency and lipophilicity (reviewed in Thai & Ecker 2007). In a review by Jamieson *et al*. (2006), the authors present series of compounds with structural alterations that successfully decreased the hERG liability. These can be i) discrete or more significant structural modifications of the template, the above-mentioned ii) control of the lipophilicity (logP), iii) attenuation of basic character of the nitrogen (pKa), as well as iv) formation of zwitterions (Jamieson *et al.* 2006).

It is noteworthy that the hERG-blockade property is only an imprecise surrogate biomarker for the proarrhythmic risk of a drug – for instance, a potent hERG blocker such as *verapamil* is not associated with potentially lethal TdP. As the hERG pharmacophore is quite widespread in the chemical space of "druggable" compounds, it would be preferred that *in silico* initial filtering did not discard pharmacologically useful compounds but gave an alert. Furthermore, six *in vitro* and *in vivo* assays are commonly used in preclinical studies to verify torsadogenic liability (including Purkinje fiber APD or Langendorff assays, binding or patch-clamp assays, and ECG animal assays), and these tests can evaluate more accurately the complex effect of a compound on QT interval. Nevertheless, computational tools have

contributed, and are still, to a remarkable understanding of the structure of the channel as well as ligand-channel interactions, and provide insights on structure-activity relationships.

IV.A.3. Chiral drugs and stereoselectivity

A chiral molecule is a type of molecule whose structure lacks an internal plane of symmetry and has a non-superimposable mirror image (**Figure 19**). Most often, the cause of *chirality* – from the Greek word *cheir* for hand – is the presence of an asymmetric atom. A chiral molecule and its mirror image are named *enantiomers*, and different methods are used to distinguish them. One method differentiates enantiomers according to the direction of rotation of polarized light: (+) or *d* for dextrorotatory, and (-) or *l* for levorotatory. An equimolar mixture of a pair of enantiomers is termed *racemate* and it does not exhibit optical activity. Another naming system specifies the absolute chemical configuration: (S)- or (R)-isomers, referring respectively to the left (*sinister*) and right (*rectus*) orientation of groups at the chiral center. A third nomenclature, also based on absolute configuration, uses the letters L and D, and is nowadays almost restricted to sugars (*e.g.* D-fructose) or amino acids (*e.g.* L-alanine) (Tucker 2000).

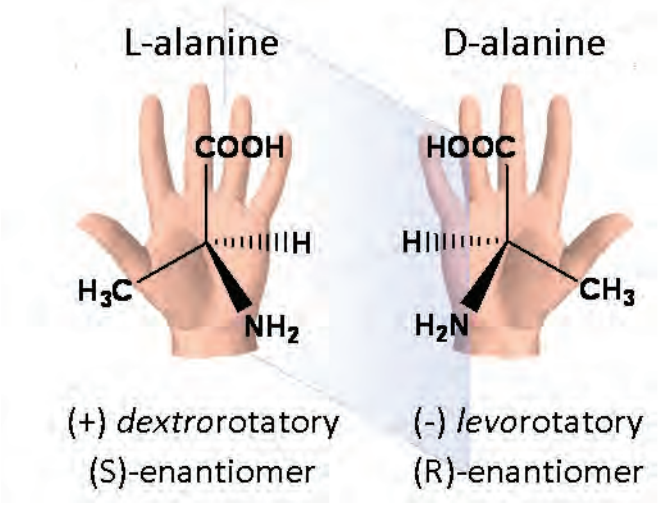

Figure 19 : A chiral molecule and its different names: the amino acid *alanine*.
The "left-handed" molecule (L-alanine or (S)-alanine) is presented with its mirror image, the "left-handed" molecule (D-alanine or (R)-alanine). The optical activity (*dextro*- or *levo*rotatory) cannot be deduced from the structure.

Except for their ability to rotate polarized light in opposite directions, enantiomers have identical chemical and physical properties. However, in the presence of other chiral molecules or environment, enantiomers will behave differently. Enantiomers of a compound may taste or smell differently, and may have different effects as drugs. These effects reflect the chirality inherent in biological systems, since the main "building blocks", like amino acids or sugars, are chiral. Chirality often introduces a marked selectivity, and often specificity, in drug action (Tucker 2000). *Stereoselectivity* is consequently the preferential interaction of one enantiomer molecule with a biological target. Since many commonly used drugs are racemates, differentiation of the relative contribution of each enantiomer to the overall drug action, which includes stereoselective pharmacokinetics and pharmaco-dynamics, is essential. While one enantiomer is responsible for the activity of interest, its paired enantiomer could be partially or equally active, inactive or have an antagonist effect. It may also have a separate activity that could be desirable or not (Caner *et al.* 2004).

IV.A.3.a. Stereoselectivity and ion channels

Receptors, such as β-adrenergic receptors, often display marked stereoselectivity in agonist or antagonist activity (Popp *et al.* 2004). As regards ion channels, which may be taken as particular pharmacologic receptors (Triggle 1996), different stereoselective blockers have also been identified. The levorotatory *chromanol 293B* was demonstrated to be nearly 7-fold more potent than its (+)-form in the block of KCNQ1/KCNE1 current (Yang *et al.* 2000). *Verapamil* was the first L-type calcium channel blocker available for the treatment of angina pectoris, hypertension and supraventricular arrhythmias, and it is still widely used as a racemic mixture in the management of these conditions. Although they possess a similar spectrum of pharmacological effects, its two enantiomers differ in their pharmacokinetic and pharmacodynamic properties. (S)-verapamil is more potent than (R)-verapamil to block $I_{Ca,L}$, but it is also preferentially metabolized during the hepatic first-passage and has a greater volume of distribution (Busse *et al.* 2006). Interestingly, dihydropyridine molecules, another class of calcium channels modulators, present

marked stereoselectivity in their action. Whereas the enantiomer (*S)-Bay K 8644* is a potent activator of L-type Ca^{2+} channels, the (*R)-Bay K 8644* acts as an antagonist (Triggle 1996). Moreover, the stereoselective effect may be *state-dependent*, which is a feature unique to ion channels. This phenomenon is clearly seen with (S)-Bay K 8644, which shows an activator property at polarized membrane potentials and an antagonist property at depolarized levels (reviewed in Triggle 1996).

Bupivacaine, a local anesthetic drug belonging to the amino amide group, also displays a stereoselective effect on its main targets, the voltage-gated sodium channels. Although some studies demonstrated that the potency and duration of local anesthesia *in vivo* were the same for levo-(S)- as for dextro-(R)-bupivacaine (Kanai *et al.* 1999), *in vitro* observations indicated that the (R)-enantiomer is more potent to block neuronal sodium channels (Lee-Son *et al.* 1992). Accidental intravascular injection or the use of high concentrations of local anesthetics can produce profound systemic effects, especially in the central nervous and cardiovascular systems. Valenzuela and co-workers studied the potential block of cardiac channels and putative differences between enantiomers. Both cardiac $Na_v1.5$ and $K_v1.5$ were inhibited by the bupivacaine local anesthetic with the (R)-form being in both cases a more potent blocker (Valenzuela *et al.* 1995a; Valenzuela *et al.* 1995b). Altogether, these results spoke in favor of the use of levo-(S)-bupivacaine for a better cardiovascular safety.

IV.A.3.b. Stereoselectivity and QT interval prolongation

Although an impressive number of reports about drugs blocking I_{hERG} can be found in the literature, the potential stereoselective contribution has been scarcely investigated. Among the few publications existing, it is worth mentioning the work of Yang *et al.* (2000) in which enantiomers of *chromanol 293B* showed no difference in the hERG current, whereas a 7-fold stereoselectivity was observed in KCNQ1/KCNE1 current block. Likewise, *verapamil* enantiomers that block the L-type Ca^{2+} channels also block the hERG K^+ channels, but they presented equal potency of inhibition when tested in *Xenopus* oocytes (Waldegger *et al.* 1999). The first demonstration of stereoselective block of the hERG channel – not QT interval prolongation or APD – is

due to Gonzalez and co-workers (2002). The authors, using a heterologous expression system, revealed that *levo-(S)-bupivacaine* was more potent at blocking I_{hERG} than *dextro-(R)-bupivacaine*, which is remarkably the inverse stereoselectivity observed in other cardiac channels (Gonzalez *et al.* 2002). The same observation was made for *ropivacaine*, a structurally related anesthetic differing only by the size of the N-substituent (Siebrands *et al.* 2005).

Other enantiomers of drugs have been reported to prolong differently AP or QT interval durations, though, to the best of our knowledge, stereoselective involvement of hERG has not yet been demonstrated.

Jurkiewicz and co-workers (1996) studied the effects of the class III antiarrhythmic agent *RP58866* and its (S)-enantiomer, named *terikalant*, on outward K^+ currents in guinea pig ventricular myocytes. RP58866 and terikalant potently blocked the I_{Kr}, with IC_{50} of 22 and 31 nM, respectively (Jurkiewicz *et al.* 1996). The difference reported is small and might not be relevant; studies of hERG current block by the (R)-enantiomer may validate the possible stereoselectivity of block. The reason why the (R)-enantiomer was not tested is because terikalant is considered as the active enantiomer of RP58866. Escande *et al*. (1992) demonstrated that RP58866 and terikalant lengthened the AP in a comparable manner, while the (R)-isomer produced a 3-fold lower effect at the same concentration. Indeed, as the racemate is a 1:1 mixture of enantiomers, the pure active enantiomer would be expected to exert a larger effect. The fact that equal concentrations of racemic and pure (S)-form present similar effects on APD brings additional evidence to a diverse modulation by RP58866 enantiomers of various cardiac channels determining the APD.

Disopyramide is a class Ia antiarrhythmic drug marketed as a racemic mixture since 1977. In a study by Vanhoutte and co-workers (1991), both (R)- and (S)-enantiomers of the antiarrhythmic agent were tested on the guinea-pig papillary muscle. At physiological K^+ concentrations and pacing, 20 μM of (S)-disopyramide significantly increased APD by ~20%, while it was diminished by ~5% in the presence of the same concentration of (R)-disopyramide. Nevertheless, controversy exists concerning enantioselective effects on sodium channel – the intended clinical target

of disopyramide – for which both absence and higher block by the (R)-form have been reported (reviewed in Vanhoutte *et al*. 1991). Nevertheless, at lower concentrations (2 μM), APD was still significantly increased by (S)-disopyramide but not modified by the (R)-form, thus excluding the contribution of I_{Na}-block effects (Vanhoutte *et al.* 1991). Importantly, this drug has been associated with *di*LQTS and TdP events (Kimura *et al.* 1994; Hirose *et al.* 2008). Meanwhile, disopyramide was demonstrated to block I_{hERG} at clinically relevant concentrations (IC_{50} <10 μM) and this action was proposed to constitute the molecular basis for the proarrhythmic effect (Paul *et al.* 2001). Investigation of a preferred block of I_{hERG}/I_{Kr} by disopyramide enantiomers would be very instructive and might lead to reconsider the safety of racemic administration.

Similar observations have been reported for *terodiline*, a drug used to treat incontinence. Terodiline was developed as a mixed antimuscarinic (effect of the (R)-terodiline) and Ca^{2+} channel blocker (effect of (S)-terodiline), and both enantiomers were considered to contribute to the beneficial effects of the racemic drug on the urinary bladder (Martin *et al.* 2006). This antispasmodic drug appears to be one of the drugs withdrawn from the market after it was linked to serious tachyarrhythmias and QT interval prolongation, but also bradycardia and AV-dissociation (Hartigan-Go *et al.* 1996). Taken together, description of the adverse effects points towards excessive delay of ventricular repolarization. In 1996, *i.e.* shortly after Sanguinetti *et al.* (1995) described hERG as encoding the I_{Kr} channel, Hartigan-Go and colleagues studied the cardiovascular and electrocardiographic effects of both (R)- and (S)-terodiline on healthy volunteers. Interestingly, both racemic (single dose of 200 mg) and (R)-terodiline (100 mg) significantly increased QTc interval and QRS duration, while pure (S)-enantiomer (100 mg) did not affect QTc values (Hartigan-Go *et al.* 1996). Although (S)-terodiline plasma concentrations were higher than for the (R)-form, the authors demonstrated that pharmacokinetics were not sufficient to account for the differences in ECGs. Hartigan-Go and colleagues (1996) concluded that QT prolongation with racemic terodiline administration was imputable exclusively to the (R)-enantiomer. Later, racemic terodiline was demonstrated to block I_{Kr} and I_{hERG} at clinically relevant concentrations

(Jones *et al.* 1998; Martin *et al.* 2006). However, as far as we know, no publication tried to assess the stereoselective effect of terodiline on hERG channels.

The last example is the antimalarial drug *halofantrine*. This drug is effective in the treatment of uncomplicated chloroquine-resistant *Plasmodium falciparum* malaria. However, it has been associated with QT interval prolongation and arrhythmias in patients without known underlying cardiac abnormalities (Mbai *et al.* 2002). Halofantrine accumulates extensively upon daily administration and shows high intersubject pharmacokinetic variability. However, in the clinical study of Abernethy *et al.* (2001), the steady-state plasma concentration of (+)-halofantrine exceeded the concentration of (-)-halofantrine by about 2-fold. The correlation between plasma concentration and QT interval appeared to be stronger for (+)- than (-)-halofantrine for all but one patient, which may be consistent with increased cardiotoxic potential of the (+)-isomer (Abernethy et al. 2001). In addition to the pharmacokinetic difference, halofantrine produced a stereoselective block of delayed rectifier potassium currents in isolated feline myocytes, with the (+)-enantiomer reducing the most K^+ currents (Wesche *et al.* 2000). Mbai *et al.* (2002) confirmed the contribution of halofantrine and its major liver metabolite on the block of hERG (IC_{50}s at the nM range), but the authors did not assess separately the enantiomers

IV.A.4. Pharmacogenetics

In drug-induced LQTS, a number of “silent” mutations and polymorphisms have been found associated with an increased vulnerability for this disease. Furthermore, there is also evidence that differences in drug metabolism, caused by functional polymorphisms in drug-metabolizing enzyme genes, may be a risk factor for drug-induced QT interval prolongation. Inter-individual differences in pharmacokinetics (PK) and pharmacodynamics (PD) are assessed by *pharmacogenetics studies*, which search for genetic causes of a variable drug response. *Pharmacogenomics* – although the terms are often used interchangeably – is a different research area, which aims at identifying at the genome level disease genes and new drug-response markers, such as drug targets or disease pathways (Ingelman-Sundberg 2001). In this sense,

identification of different LQTS-causing genes or drugs that produce QT-prolongation by interfering with the hERG channel belong to the pharmacogenomic field.

The pharmacological action of a chemical in the organism is generally considered as the combined effect of both the PK and the PD. As mentioned above, metabolism, which is a distinct step in the PK process, has demonstrated important genetic variability, and cytochromes P450 (CYP) isoenzymes – essential to catalyze, during phase I, the oxidation of endogenous molecules or xenobiotics – have been extensively studied. Many different human *CYP* genes exist; however, the most important are *CYP2C9*, *CYP2D6* and *CYP3D4* genes, since their gene products account for 60-70% of all phase I metabolism of clinically important drugs (Ingelman-Sundberg 2001). Mutations in the *CYP* genes can generate enzymes with abolished, reduced, altered or increased activity. The phenotype of a CYP enzyme can be easily tested by administering a specific substrate, *e.g*. *debrisoquine* for CYP2D6, and measuring the metabolite-to-parent drug ratio in the urine. Individuals that present a low ratio have reduced activity of the enzyme and are called *slow metabolizers* (SMs) in order to differentiate them from *extensive metabolizers* (EMs). *Perhexiline* and *thioridazine* are examples of drugs that depend on the CYP2D6 activity and act on hERG channel (reviewed in Roden & Viswanathan 2005). Walker *et al*. (1999) studied the block of I_{hERG} by perhexiline, an antianginal agent known to cause QT interval prolongation and TdP. Interestingly, IC_{50} values were above the clinical plasma concentrations usually observed. Nevertheless, authors proposed, as 8-10% of Caucasians and Black individuals are CYP2D6 SMs, that these patients may be especially prone to having high plasma concentrations of perhexiline with consequent susceptibility to adverse effects (Walker *et al.* 1999). Similarly, some drugs are able to convert *extensive metabolism* in a person into *slow metabolism* by interfering with the CYP pathway, thus possibly causing drug-drug interactions. The gastrointestinal prokinetic *cisapride* is another good example of high-affinity blocker of the hERG channel being substrate of the CYP3A4. Importantly, prolongation of QT interval along with severe cardiac outcomes have been reported after its concomitant administration with macrolide antibiotics such as *erythromycin* (Tierney *et al.* 1997), or with azole antifungal agents like *ketoconazole* (Michalets & Williams

2000). These drugs alone may prolong the QT interval by blocking I_{hERG}, but they are mainly responsible for a drastic increase of cisapride plasma concentration due to CYP3A4 inhibition. *Diltiazem* is a Ca^{2+} channel blocker with only weak effect on hERG channels (Zhang *et al.* 1999). Nevertheless, a possible interaction was reported under co-administration of cisapride and diltiazem, because this latter is a potent inhibitor of CYP3A4 (Thomas *et al.* 1998).

As regards pharmacogenetics at the PD level, Roepke and Abbott (2006) reviewed variations in genes, *KCNH2* but also other cardiac ion channel and associated genes, that predispose to acquired and drug-induced LQT2. Among hERG polymorphisms, the mutation R1047L presented effects insufficient to produce TdP alone. However, this mutation appeared to increase the torsadogenic risk in a 105-patient cohort under *dofetilide* (Sun *et al.* 2004). Similarly, the hERG mutation M124T was found in several members of a family presenting with QT interval prolongation. Nevertheless, only the two family members that took cholesterol-lowering drug *probucol* experienced TdP (reviewed in Roepke & Abbott 2006). The variant of hERG K897T is maybe the best studied case and it emerged as a genetic modifier of LQTS, even though discrepancies are observed between studies. In a study of middle-aged Finnish individuals, this relatively common hERG variant (up to 25% of individuals depending on ethnicity) was associated with significantly increased QTc intervals in women but not men (reviewed in Roepke & Abbott 2006). Similar conclusions of higher risks for women harboring this polymorphism were presented in another study (Linna *et al.* 2006). At the electrophysiological level, Paavonen *et al*. (2003) observed changes in inactivation and deactivation properties, as well as a reduced current density. Conversely, other studies found that current elicited through hERG-K897T channels were indistinguishable from WT I_{hERG} (Anson *et al.* 2004). Recently, Gentile and co-workers (2008) showed that this mutation creates a new phosphorylation site that inhibits channel activity. Moreover, Crotti and co-workers (2005) highlighted the fact that this common *KCNH2* polymorphism may modify the clinical expression of another latent LQT2 mutation. In their family report, while carriers of the hERG A1116V mutation were asymptomatic (some exhibited transient

mild QTc prolongation), the relative who also carried the K897T polymorphism on the non-mutant allele experienced severe cardiac events (Crotti *et al.* 2005).

Polymorphisms of other ion channels, such as the putative β-subunits of hERG channels have been mentioned earlier to influence drug block (see I.C.3.b). The T8A polymorphism of MiRP1 (encoded by *KCNE2*) was found in a patient who developed prolonged QTc after taking the antibiotic *sulfamethoxazole* (Sesti *et al.* 2000). The T8A polymorphism occurs at a frequency of 1.6% in Caucasian Americans but appears absent in African Americans (Roepke & Abbott 2006). Sesti and co-workers (2000) showed that hERG channels co-expressed with MiRP1-T8A in CHO cells were 4-fold more sensitive to sulfamethoxazole than when co-expressed with WT MiRP1. In contrast to T8A, the MiRP1-Q9E polymorphism is found at a frequency of 3% in African Americans, but appears absent in Caucasians in the USA. This variant was originally identified in a woman who developed TdP after treatment with *clarithromycin* antibiotic. Further studies demonstrated that MiRP1-Q9E impairs hERG channel gating, although this is tolerated by the majority of carriers (reviewed in Roepke & Abbott 2006). Remarkably, a common polymorphism in *SCN5A* has been described with only subtle effects on sodium channel function, but which may predispose carriers to LQTS. Even if about 13% of Africans and African Americans carry the S1103Y allele, most carriers will never experience *Torsades de Pointes*. However, $Na_v1.5$-S1103Y may be a molecular marker for the prediction of arrhythmia susceptibility in these populations in the context of additional risk factors, such as certain medicine use (Splawski *et al.* 2002).

Careful use of hERG blockers with respect to the patient's genetic background – regarding both PK and PD – may be possible in the future if a cheap and rapid genetic screening of desired genes becomes feasible. Importantly also, the inter-ethnic distribution of polymorphisms can be manifest and thus has to be taken into account when dealing with drugs that possibly affect repolarization.

IV.B. Publication 4 (*Clinical Pharmacology and Therapeutics*)

Stereoselective block of hERG channel by (S)-methadone and QT interval prolongation in CYP2B6 slow metabolizers

Methadone is a synthetic analgesic drug, primarily a μ-agonist with pharmacological properties similar to *morphine*, though lacking some of the euphoric actions of the opium poppy alkaloid. Methadone (first synthesized in the 1930's) is thereby widely used in maintenance treatments (or MMTs) in order to reduce illicit opioid misuse, but also for chronic pain, generally when other opioids are ineffective or poorly tolerated. Methadone is a chiral drug with an asymmetrical carbon in its structure. Although in most countries the drug is administered as a racemic mixture of (R)- and (S)-methadone, the (R)-enantiomer accounts for most if not all of the opioid effects (Eap *et al.* 2002). Indeed, *in vitro* competitive binding experiments (*versus* labeled *naloxone* in rat brain homogenates) have shown that the necessary concentration for binding of (R)-enantiomer was 10 times lower than that of (S)-methadone. Similarly, a 10-fold difference of affinity was found between the two enantiomers for purified μ_1 and μ_2 receptors. Finally, in human analgesia, (R)-methadone was about 50 times as potent as the (S)-form (reviewed in Eap *et al*. 2002). Despite these results, the use of racemate in MMTs was pursued, namely for the reason that only racemic methadone was available in the international market and because the racemate formulation was less costly than the pure (R)-enantiomer (Gaertner *et al.* 2008).

Recent studies have demonstrated that pharmacokinetics of methadone, mainly the metabolism step, was highly variable owing to genetic and environmental influences (Eap *et al.* 2002). In humans, methadone is extensively metabolized in the body, predominantly at the level of the liver and probably also intestinal cytochrome P450 isoenzymes. More precisely, CYP3A4 and CYP2B6 are the major isoforms involved in this synthetic opioid metabolism *in vivo*, with CYP2D6 contributing to a minor extent (Crettol *et al.* 2006). It is worth mentioning that stereoselective metabolism of methadone by CYP2B6 has been reported *in vitro*, with an estimated

1.8-fold preference towards (S)-methadone. Crettol and co-workers confirmed it *in vivo* assessing the influence of the *CYP2B6* *6/*6 genotype, a *slow metabolizer* status representing ~6% of Caucasians and Africans. These authors confirmed that CYP2B6 contributed to (S)-methadone metabolism and, to a lesser extent, to (R)-methadone metabolism, with the homozygous carriers of allele *6 showing higher (S)- and (R,S)-methadone plasma levels (Crettol *et al.* 2005; Crettol *et al.* 2006).

Importantly, a disproportionate number of unexpected deaths is seen in patients receiving methadone. Although many of these deaths are likely to be a result of respiratory depression, *Torsades de Pointes* are undoubtly a contributing factor (Wilcock & Beattie 2009). The number of reports of cardiac events under methadone treatment has been continuously increasing over the last decade (Sticherling *et al.* 2005; Valko *et al.* 2001; Ehret *et al.* 2006), thus rising strong suspicion about block of hERG. It was finally without surprise that methadone racemate was demonstrated to block hERG currents in transfected HEK293 cells with an IC_{50} of ~10 μM (reviewed in Eap *et al*. 2002).

However, in the light of the marked difference between the enantiomers in PK and PD, neither stereoselectivity of hERG blockade nor metabolic implications of the *CYP2B6* *6/*6 genotype were assessed in regard to methadone cardiac safety. The following publication aimed at answering these questions by means of both clinical and electrophysiological studies.

Contribution to the study:

In this study, I carried out the dose-response curves with methadone (enantiomers and racemate) at room temperature and 37°C, in parallel with J.-S. Rougier. I was in charge of the cell culture, preparation and transfection for my own experiments.

Stereoselective Block of hERG Channel by (*S*)-Methadone and QT Interval Prolongation in CYP2B6 Slow Metabolizers

CB Eap[1], S Crettol[1,8], J-S Rougier[2,8], J Schläpfer[3], L Sintra Grilo[2,4], J-J Déglon[5], J Besson[6], M Croquette-Krokar[7], P-A Carrupt[4] and H Abriel[2,3]

Methadone inhibits the cardiac potassium channel hERG and can cause a prolonged QT interval. Methadone is chiral but its therapeutic activity is mainly due to (*R*)-methadone. Whole-cell patch-clamp experiments using cells expressing hERG showed that (*S*)-methadone blocked the hERG current 3.5-fold more potently than (*R*)-methadone (IC_{50}s (half-maximal inhibitory concentrations) at 37°C: 2 and 7 μM). As CYP2B6 slow metabolizer (SM) status results in a reduced ability to metabolize (*S*)-methadone, electrocardiograms, *CYP2B6* genotypes, and (*R*)- and (*S*)-methadone plasma concentrations were obtained for 179 patients receiving (*R*,*S*)-methadone. The mean heart-rate-corrected QT (QTc) was higher in CYP2B6 SMs (6/*6* genotype; 439 ± 25 ms; $n = 11$) than in extensive metabolizers (non **6/*6*; 421 ± 25 ms; $n = 168$; $P = 0.017$). CYP2B6 SM status was associated with an increased risk of prolonged QTc (odds ratio = 4.5, 95% confidence interval = 1.2–17.7; $P = 0.03$). This study reports the first genetic factor implicated in methadone metabolism that may increase the risk of cardiac arrhythmias and sudden death. This risk could be reduced by the administration of (*R*)-methadone.**

Methadone, a μ-opioid receptor agonist, is an effective drug for maintenance treatment in opioid-dependent patients and for pain treatment. Methadone is widely prescribed (~215,000 opioid-dependent patients and >275,000 patients treated for pain in the US[1]). Importantly, it can be predicted that the future number of patients being treated with methadone will increase due to its introduction into the World Health Organization (WHO) list of essential medicines in 2005.[2] Methadone is mainly administered as a chiral mixture of (*R*,*S*)-methadone. However, the μ-opioid receptor activation is mostly due to (*R*)-methadone.[3] Recently, torsades de pointes and sudden deaths have been described,[4–15] mainly, but not only,[12,14,15] in patients receiving high to very high doses of methadone, often administered for pain treatment, as well as for maintenance treatment.[6,8–11,15] Although the reported number of cardiac adverse events associated with the prescription of methadone may appear low compared with the total number of patients receiving this drug (in November 2005, 282 reports of heart rate and rhythm disorders were associated with methadone in the WHO adverse drug reactions database[13]), this is likely to be an underestimation because it is generally estimated that, in a voluntary reporting system, only one in 10 or even one in 100 events are ever reported.[12]

In the human heart, the hERG (human *ether-à-gogo* related gene) voltage-gated potassium channel mediates the rapidly activating delayed rectifier current, I_{Kr}.[16] The crucial role of hERG channels in repolarization and duration of the cardiac action potential has been exemplified by the numerous mutations in *KCNH2*, the gene encoding hERG. These mutations result in congenital long QT syndrome[16] and cause sudden death due to malignant ventricular arrhythmias (so-called torsades de pointes). Importantly, hERG can also be blocked by many structurally diverse drugs, including methadone,[17,18] causing a prolonged QT interval.[19,20]

[1]Unit of Biochemistry and Clinical Psychopharmacology, Centre for Psychiatric Neurosciences, University Department of Psychiatry-CHUV, Hospital of Cery, Prilly-Lausanne, Switzerland; [2]Department of Pharmacology and Toxicology, University of Lausanne, Lausanne, Switzerland; [3]Service of Cardiology, CHUV, Lausanne, Switzerland; [4]Unit of Pharmacochemistry, School of Pharmaceutical Sciences, University of Geneva, University of Lausanne, Geneva, Switzerland; [5]Phénix Foundation, Geneva, Chêne-Bougeries, Switzerland; [6]Unit of Drug Addiction, Centre Saint-Martin, University Department of Psychiatry-CHUV, Lausanne, Switzerland; [7]Division of Substance Abuse, Department of Psychiatry, University Hospitals of Geneva, Belle-Idée, Chêne-Bourg, Switzerland. Correspondence: CB Eap (chin.eap@chuv.ch) and H Abriel (Hugues.Abriel@unil.ch)

Received 24 October 2006; accepted 29 December 2006; published online 28 February 2007. doi:10.1038/sj.clpt.6100120

[8]These authors contributed equally to this study.

In humans, methadone metabolism is mediated by several cytochrome *P*450 (CYP) isozymes, mainly CYP3A4 and CYP2B6, and to a lesser extent CYP2D6,[21–25] the activities of which are genetically and environmentally determined.[21] Of special interest is the demonstrated *in vitro* stereoselectivity (~1.8-fold) of CYP2B6 toward (*S*)-methadone,[23] which was confirmed by *in vivo* data showing that CYP2B6 slow metabolizer (SM) status (with a **6/*6* genotype) is associated with high (*S*)- but not (*R*)-methadone plasma concentrations.[24,25] The *CYP2B6*6* allele is a haplotype that combines two single-nucleotide polymorphisms corresponding to alleles **4* and **9*.[26] The *CYP2B6 *6/*6* genotype represents about 6% of Caucasians and African-Americans.[24,25,27]

As methadone is a chiral drug, the first aim of this study was to investigate whether the block of hERG current (I_{hERG}) by methadone was stereoselective. In parallel, investigating a cohort of opioid-dependent patients, we also tested the hypothesis that a CYP2B6 SM status could be associated with a prolonged heart-rate-corrected QT (QTc) interval on the electrocardiogram (ECG).

RESULTS

Inhibition of the potassium channel hERG by the enantiomers of methadone

The I_{hERG} was recorded using HEK293 cells stably expressing hERG and by performing whole-cell patch-clamp experiments. Block of I_{hERG} was evaluated using a typical two-step protocol (**Figure 1a**, see insets). At 37°C, the steady-state block of tail I_{hERG} (−50 and −120 mV) by the two enantiomers of methadone (5 μM) was different: whereas (*S*)-methadone reduced I_{hERG} by ~65%, (*R*)-methadone inhibition was only ~40%. This difference in inhibition of

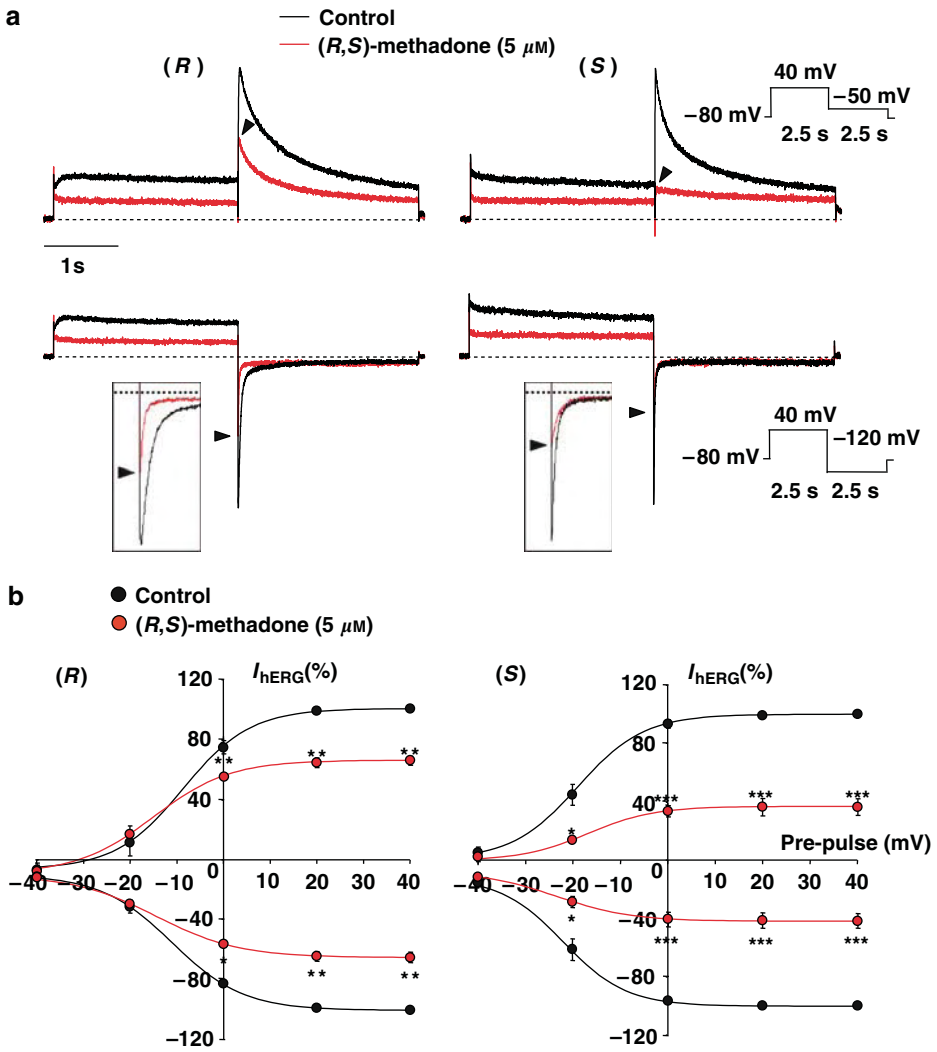

Figure 1 (**a**) Representative hERG current recordings measured at 37°C with 5 μM (*R*)- and (*S*)-methadone using the schematized protocols. The current traces were normalized to the maximum peak tail current after stepping to −120 or −50 mV without drug. Arrows show the peak tail current levels after drug block. (**b**) Current/voltage relationships showing normalized hERG outward and inward (tail currents at −50 and −120 mV, respectively) current before (black) and after (red) perfusion of (*R*)- or (*S*)-methadone; insets: magnification of the −120 mV representative tail currents; $N = 4$–5 cells per condition; $^{*}P < 0.05$; $^{**}P < 0.01$; $^{***}P < 0.001$.

I_{hERG} by methadone enantiomers was also present when analyzing the outward currents obtained during the conditioning pulses (**Figure 1a**), suggesting that, under these conditions, the current recordings were not significantly influenced by the endogenous HEK293 outward currents.[28] Moreover, **Figure 1b** illustrates that for all tested voltages, the (*R*)- or (*S*)-methadone-induced (5 μM) inhibition of the outward (−50 mV) and inward (−120 mV) tail currents was similar.

The concentration–response curves of I_{hERG} block at 37°C (**Figure 2**, filled symbols) show that (*R*)-methadone blocked I_{hERG} significantly less potently than (*S*)-methadone, whereas (*R*,*S*)-methadone block was intermediate. The obtained IC_{50}s (half-maximal inhibitory concentrations) were as follows: (*R*,*S*)-methadone: 3 μM; (*S*)-methadone: 2 μM; (*R*)-methadone: 7 μM (**Figure 2** and **Table 1**). At room temperature (RT), (*R*,*S*)-methadone blocked I_{hERG} with an IC_{50}s of 19 μM, whereas the IC_{50}s of (*S*)-methadone and (*R*)-methadone were 12 and 29 μM, respectively (**Figure 2**, empty symbols and **Table 1**). Thus, the recording temperature influences the I_{hERG} inhibition by methadone, and despite being less pronounced at RT, methadone-induced block of I_{hERG} is stereoselective under both conditions. Finally, we measured at 37°C the I_{hERG} block by 2-ethylidene-1,5-dimethyl-3,3-diphenylpyrrolidine (EDDP) and 2-ethyl-5-methyl-3,3-diphenyl-1-pyrroline (EMDP), the two main metabolites of methadone.[29] The inhibition was extremely weak and the estimated IC_{50}s were >250 μM for both substances (data not shown).

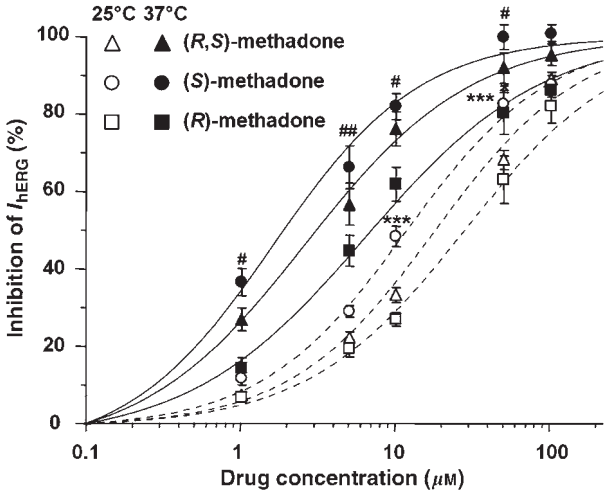

Figure 2 Concentration–response curves of hERG current block at 25°C and 37°C by methadone and its enantiomers. $N = 3$–10 cells per condition, $^{***}P < 0.001$ for (*S*)- versus (*R*)-methadone at 25°C, and $^{\#}P < 0.05$; $^{\#\#}P < 0.01$ (*S*)- versus (*R*)-methadone at 37°C; Bonferroni's post-test; see **Table 1** for the results of the fitted dashed and solid curves.

Table 1 IC_{50} values and Hill coefficients obtained with the fitting of the concentration–response data of methadone and its enantiomers induced block of I_{hERG} at 25°C and 37°C

		IC_{50} (μM)	Hill coefficient
RT	(*R*,*S*)-methadone	19	0.94
	(*S*)-methadone	12	0.94
	(*R*)-methadone	29	0.87
37°C	(*R*,*S*)-methadone	3	0.86
	(*S*)-methadone	2	0.95
	(*R*)-methadone	7	0.82

RT, room temperature. These values correspond to the dashed and solid curves of **Figure 2**.

QTc intervals, methadone plasma concentrations, and clinical data

In parallel, we investigated a cohort of patients in methadone maintenance treatment. A detailed description of the patients can be found in **Table 2**. Among the 179 included patients, all but nine subjects had been in treatment for at least 6 months at the time of inclusion, with the lowest duration of treatment in those nine patients being 2 months. Methadone plasma concentrations were in steady-state conditions in all but one patient, for whom a small change of methadone dose (9%) occurred 3 days before the inclusion. Detailed results of trough and peak methadone plasma concentrations and QTc intervals are shown in **Table 3**. The QTc intervals at trough were not significantly different from those at peak (mean difference: 0.74 ± 23 ms; $n = 164$; $P = 0.68$). Among the 179 patients with an ECG at trough, 16 patients (9%, 16 male subjects) had a prolonged QTc interval (>450 ms for male subjects and >470 ms for female subjects;[30] **Figure 3**, red dots), and 42 patients (26%, 35 male subjects) had a borderline QTc interval (not prolonged and >430 ms for male subjects and >450 ms for female subjects;[30] **Figure 3**, yellow dots).

A weak, albeit significant, correlation was observed between methadone daily dose and QTc at trough ($r = 0.19$, $P = 0.01$) and at peak ($r = 0.22$, $P = 0.005$). As expected, a higher correlation was observed between (*R*,*S*)-methadone plasma concentrations and QTc at trough ($r = 0.31$, $P < 0.00005$; **Figure 3**) and at peak ($r = 0.25$, $P = 0.0012$). Owing to the very strong correlation between (*R*)-methadone and (*S*)-methadone plasma concentrations ($r = 0.87$, $P < 10^{-18}$ at trough; $r = 0.91$, $P < 10^{-18}$ at peak), which can be explained by the broad range of methadone dose, it was not possible to differentiate directly the effect of (*S*)- versus (*R*)-methadone plasma concentrations on QTc interval (both (*R*)- and (*S*)-methadone plasma concentrations correlate significantly with QTc at trough and at peak, data not shown). Univariate analysis between QTc interval at trough and several risk factors indicated that trough (*R*,*S*)-methadone concentrations ($r = 0.31$, $r^2 = 0.097$, $P < 0.00005$; **Figure 3**), use of co-medications ($r = 0.18$, $r^2 = 0.034$, $P = 0.01$), methadone daily dose ($r = 0.19$, $r^2 = 0.036$, $P = 0.01$), CYP2B6 SM status ($r = 0.18$, $r^2 = 0.032$, $P = 0.02$), and serum calcium ($r = -0.15$, $r^2 = 0.023$, $P = 0.04$), were predictive of the QTc interval duration. Other variables, such as gender ($P = 0.35$), age ($P = 0.28$), serum potassium ($P = 0.42$), cocaine ($P = 0.45$), and alcohol consumption ($P = 0.51$), were not predictive of the QTc

Table 2 Detailed clinical description of the 179 included patients

	Mean ± SD	Range
Age (years)	36 ± 8	21–53
Methadone daily dose (mg)	145 ± 83	10–430
MMT duration (months)	61 ± 61	2–294
Methadone dose kept unchanged before inclusion (days)	211 ± 343	3–3271
	Number	**Percentage**
Gender (M/F)	139/40	78/22
Ethnicity (Caucasian/other)	172/7	96/4
Self-declared opiate consumption	22	12
Self-declared cocaine consumption	52	29
Self-declared cannabis consumption	108	60
Self-declared alcohol consumption[a]	67	37
Self-declared benzodiazepines consumption[b]	117	65
Patients taking concomitant medications[c]	153	85
Benzodiazepines	101	56
Antiepileptics	42	23
Antipsychotics	40	22
Non-selective serotonin reuptake inhibitor antidepressants	39	22
Selective serotonin reuptake inhibitors	35	20
Sedative-hypnotics	34	19
Drugs having a risk of causing torsades de pointes[d]	3	2
Drugs that could be associated with torsades de pointes and/or QT prolongation[d]	21	12
Drugs weakly associated with torsades de pointes and/or QT prolongation[d]	28	16

F, female; M, male; MMT, methadone maintenance treatment; SD, standard deviation. [a]Superior to 40 g/day for men and 20 g/day for women. [b]Regardless of whether or not prescribed. [c]Mean number of concomitant medications: 2.3 ± 1.6 per patient, range: 0–7. [d]According to the classification of ArizonaCERT (http://www.torsades.org, accessed 21 December 2005).

Table 3 Trough and peak methadone plasma concentrations and QTc intervals in MMT patients

	Mean ± SD	Range
Number of patients	179	
Trough (*R*,*S*)-methadone plasma concentrations (ng/ml)	445 ± 275	44–1591
Trough (*S*)-methadone plasma concentrations (ng/ml)	205 ± 138	25–742
Trough (*R*)-methadone plasma concentrations (ng/ml)	240 ± 146	19–874
Trough QTc interval (ms)	422 ± 25	360–485
Number of patients	164	
Peak (*R*,*S*)-methadone plasma concentrations (ng/ml)	717 ± 368	79–2252
Peak (*S*)-methadone plasma concentrations (ng/ml)	362 ± 193	47–1123
Peak (*R*)-methadone plasma concentrations (ng/ml)	355 ± 184	32–1129
Peak QTc interval (ms)	423 ± 23	375–474

MMT, methadone maintenance treatment; QTc, heart-rate-corrected QT interval; SD, standard deviation. All values are expressed as means ± SD and range.

interval duration. Multivariate analysis yielded a model including trough (*R*,*S*)-methadone concentrations ($P < 0.0005$), hypocalcemia (< 2.2 mmol/l; $P = 0.02$), use of co-medication ($P = 0.03$), and CYP2B6 status ($P = 0.05$) with a determination coefficient (r^2) of 0.17 ($n = 179$; $P < 0.00005$).

Although methadone plasma concentrations can only account for a small part of QTc variation, QTc measured at

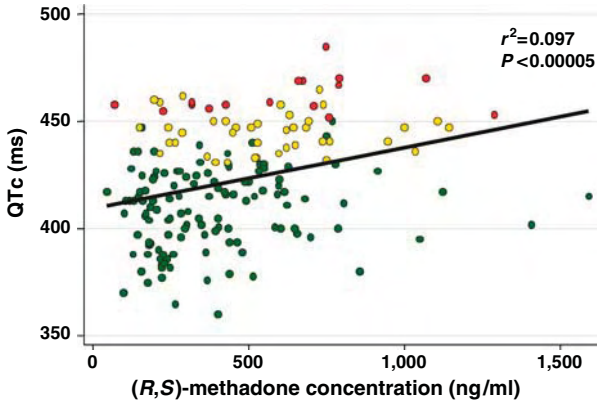

Figure 3 Representation of QTc intervals measured at trough versus trough (*R,S*)-methadone plasma concentrations. Red dots represent prolonged QTc intervals and yellow dots represent borderline QTc intervals, both as defined in the text. Green dots represent normal QTc values.

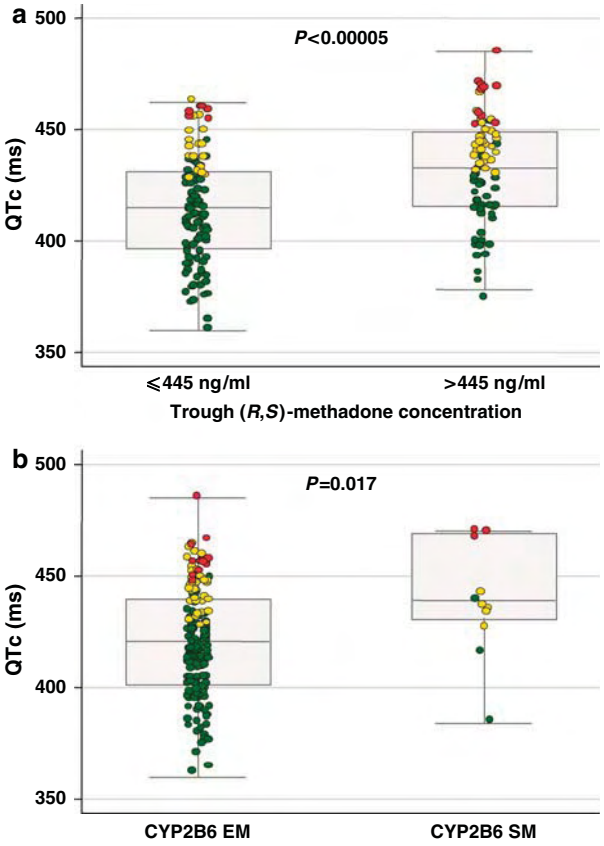

Figure 4 (**a**) Comparisons of QTc intervals measured at trough in patients with (*R,S*)-methadone plasma concentrations lower or equal to ($n = 105$) and higher ($n = 74$) than the mean value of the group (445 ng/ml). Medians and quartiles are shown for each group. Red dots represent prolonged QTc intervals and yellow dots represent borderline QTc intervals, both as defined in the text. Green dots represent normal QTc values. (**b**) Comparisons of QTc intervals measured at trough in CYP2B6 EMs (all non **6/*6* genotypes, $n = 168$) and in CYP2B6 SMs (**6/*6* genotype, $n = 11$). Medians and quartiles are shown for each group. Red dots represent prolonged QTc intervals and yellow dots represent borderline QTc intervals, both as defined in the text. Green dots represent normal QTc values.

trough in patients with (*R,S*)-methadone plasma concentrations superior to the mean value of the group (445 ng/ml) was 17 ms higher than in patients with plasma concentrations inferior to the mean value (432 ± 23 versus 415 ± 24 ms; $n = 105$ versus $n = 74$, respectively; $P < 0.00005$; **Figure 4a**). In addition, when comparing the patients with trough (*R,S*)-methadone plasma concentrations superior and inferior or equal to 600 ng/ml, the former presented significantly more frequently prolonged QTc intervals (9/45 (20%) versus 7/134 (5%); odds ratio (OR) = 4.5, 95% confidence interval ($CI_{95\%}$) = 1.6–12.6; $P = 0.003$). Similar results were obtained when grouping the patients with borderline or prolonged QTc intervals (OR = 4.4, $CI_{95\%}$ = 2.2–8.8; $P < 0.00005$).

In agreement with the results obtained with uni- and multivariate analyses, self-declared consumptions of illicit drugs and/or alcohol within the past 3 months did not have any significant effect on measured trough and peak QTc, nor did the results of opiate and cocaine urine analysis on the study day (data not shown). Although use of concomitant medication was found by the uni- and multivariate analyses to influence the QTc interval, the concomitant medications known to affect QTc interval were not differently distributed between the patients with and without prolonged QTc interval or with and without QTc intervals above the threshold used for classification as borderline (data not shown). Similarly, the concomitant medications known to inhibit or induce the main CYP isozymes involved in methadone metabolism, namely CYP3A4, CYP2B6, and CYP2D6[25] (as described in refs. 31–34), were not differently distributed between the patients with and without prolonged QTc interval or with and without QTc intervals above the threshold used for classification as borderline (data not shown).

QTc intervals and *CYP2B6* genotype

CYP2B6 genotyping of 179 patients showed an allelic frequency of 22% ($CI_{95\%}$ = 18–27%) for allele **6*, a similar value to that reported in a random German population of 215 subjects (26%).[35] The CYP2B6 SM status, corresponding to genotype **6/*6*,[24] was observed in 6% ($CI_{95\%}$ = 3–11%) of patients.

As detailed in **Table 4**, the mean QTc and (*S*)-methadone plasma concentrations at trough were higher in the CYP2B6 SMs than in the extensive metabolizers ((Ems), all non **6/*6* genotype). In particular, the mean QTc interval at trough for CYP2B6 SMs ($n = 11$) was 439 ± 25 ms, whereas it was 421 ± 25 ms in CYP2B6 EMs ($n = 168$; $P = 0.017$; **Figure 4b**). The trend was similar when considering the non-carriers of allele **6* ($n = 110$), the heterozygous ($n = 58$), and the homozygous ($n = 11$) carriers (mean QTc interval of 421 ± 24, 419 ± 27, and 439 ± 25 ms, respectively; $P = 0.052$). On the other hand, the (*R*)-methadone trough plasma concentrations were not significantly different between CYP2B6 SMs and EMs. As previously shown, the other *CYP2B6* genotypes analyzed, with alleles **5* and **7*, did not influence (*R,S*)-, (*R*)-, or (*S*)-methadone concentrations,[25]

Table 4 Influence of *CYP2B6* genotype on trough methadone plasma concentrations, QTc intervals, methadone dosing, and MMT duration

	CYP2B6 SMs	CYP2B6 EMs	*P*-value
Number (%)	11 (6%)	168 (94%)	
Trough (*R*,*S*)-methadone plasma concentrations (ng/ml)	643±307	432±268	0.013
Trough (*S*)-methadone plasma concentrations (ng/ml)	346±169	195±131	0.0004
Trough (*R*)-methadone plasma concentrations (ng/ml)	297±145	236±145	0.18
Trough QTc interval (ms)	439±25	421±25	0.017
Methadone daily dose (mg)	136±67	146±85	0.73
Treatment duration (months)	46±52	62±62	0.42

EMs, extensive metabolizers; QTc, heart-rate-corrected QT interval; SMs, slow metabolizers. All values are expressed as means±SD.

and they did not influence the QTc interval (data not shown). Allele **9* was always associated with allele **4* and could therefore be seen as a marker of allele **6*. The influence of allele **4* could not be considered alone because it was associated in most patients with allele **6*. Furthermore, the frequencies of prolonged (**Figure 4b**, red dots) or borderline (**Figure 4b**, yellow dots) QTc intervals were significantly higher in CYP2B6 SMs compared with EMs (for prolonged QTc intervals: 3/11 (27%) versus 13/168 (8%); OR = 4.5, $CI_{95\%}$ = 1.2–17.7; $P = 0.03$; for borderline or prolonged QTc intervals: 8/11 (73%) versus 50/168 (30%); OR = 6.3, $CI_{95\%}$ = 1.7–22.7; $P = 0.003$). Among the other CYPs that were previously found to significantly influence methadone plasma concentrations, namely CYP3A4 and CYP2D6,[25] none of the analyzed genotypes were found to significantly influence the QTc interval (data not shown).

No problems related to QTc interval prolongations were encountered during the clinical study. At inclusion, one patient had a previous medical history of prolonged QT (QTc of 610 ms measured during one episode), torsades de pointes, and syncope, which occurred before his inclusion in the study while receiving higher methadone doses than the 80 mg/day he received on the day of the study and in association with other risk factors (multiple co-medications, hypokalemia (3.2 mmol/l) measured during one episode of syncope with prolonged QTc interval). At inclusion, the following parameters were measured: QTc at trough, 469 ms; (*R*)-methadone, 325 ng/ml; (*S*)-methadone, 334 ng/ml; (*R*,*S*)-methadone, 659 ng/ml. The patient was genotyped during the study as being a CYP2B6 SM. Methadone was subsequently replaced by oral morphine, which resulted in a normalization of the QTc interval and the disappearance of episodes of syncope.

DISCUSSION

In this study, we found that the block of the hERG channel by methadone displays stereoselectivity, the (*S*)-enantiomer being more potent than (*R*)-methadone, which is the active form with regard to the μ-opioid receptor. In addition, comparison of the IC_{50} values for hERG current block measured at 37°C and at RT (25°C) indicated an important role of the recording temperature. The IC_{50} of (*R*,*S*)-methadone measured at RT was 19 μM, approximately two-fold higher than the 9.8 μM previously reported at RT,[17] whereas the IC_{50} measured in this study at 37°C was 3 μM. Methadone main metabolites, EDDP and EMDP, did not show any significant inhibition of I_{hERG} at 37°C, which confirms a previous result for EDDP at RT[17] and suggests that both metabolites are unlikely to contribute to the block of hERG during methadone treatment.

The IC_{50} value at 37°C for (*R*)-methadone (2166 ng/ml or 7 μM) is, respectively, nine- and sixfold higher than the mean trough and peak (*R*)-methadone plasma concentrations measured in this study (**Table 3**). Even considering the highest measured peak concentration of (*R*)-methadone (1129 ng/ml or 3.65 μM; **Table 3**), the IC_{50} value is still twofold higher. In animals, methadone has been shown to accumulate in the heart,[36,37] but it is currently not known whether this is also the case in humans. Assuming no accumulation, the cardiac concentrations of (*R*)-methadone would be below the IC_{50} value, whereas those of (*S*)-methadone could easily be close to, or even exceed, the IC_{50} value (2 μM) in patients treated with high doses and/or with a genetic deficiency in the metabolism of methadone.

Recently, CYP2B6 stereoselectivity toward (*S*)-methadone was demonstrated *in vitro*[23] and confirmed *in vivo*.[24,25] We thus demonstrated that a CYP2B6 SM status, associated with **6/*6* genotype, resulted in a reduced ability to metabolize (*S*)-methadone and was significantly associated with higher (*S*)-methadone plasma concentrations.[24,25] Therefore, the observed *in vitro* stereoselectivity of the hERG block led us to investigate whether CYP2B6 SM status could be associated with prolonged or borderline QTc interval.

Measured trough and peak QTc intervals and (*R*)-, (*S*)-, and (*R*,*S*)-methadone plasma concentrations displayed a wide variability. QTc intervals measured at peak were not significantly different from those measured at trough ($P = 0.68$). This observation is consistent with the moderate difference of methadone plasma concentrations between peak and trough under steady-state conditions. The proportion of *CYP2B6 *6/*6* genotype (SMs) in the study group was similar to the proportion recently reported in Caucasians.[35] The impact of commonly identified risk factors for developing torsades de pointes, such as female gender, hypokaliemia,

hypocalcemia, high drug concentrations, and drug interactions,[19] was evaluated by uni- and multivariate analyses of QTc intervals. Among them, (*R*,*S*)-methadone plasma concentrations, the use of at least one concomitant medication, and hypocalcemia showed a significant influence on QTc interval. The use of concomitant medications was further analyzed by grouping them according to the classification of QTc prolongation risk[38] and CYP inhibitory potential. The patients taking concomitant medications known to affect QTc interval or known to inhibit the main CYP isozymes involved in methadone metabolism did not have significantly more prolonged or borderline QTc intervals. This could possibly be due to the small number of patients classified in such groups. Surprisingly, female gender did not appear to influence QTc interval, but such a lack of influence of gender on QTc interval has also been found in a recent study,[15] with the small proportion of included female subjects (22%) possibly explaining this result.

Importantly, CYP2B6 SM status influenced the QTc interval in both uni- and multivariate analyses. Comparisons of QTc intervals between CYP2B6 SMs and EMs also yielded significant results, with the mean QTc interval being 18 ms longer in SMs than in EMs ($P = 0.017$). The impact of CYP2B6 SM status on QTc intervals could be expressed by an OR of 4.5 for prolonged QTc intervals and 6.3 for prolonged or borderline QTc intervals, whereas the impact of (*R*,*S*)-methadone plasma concentrations superior to 600 ng/ml could be expressed by an OR of 4.5 for prolonged QTc intervals and 4.4 for prolonged or borderline QTc intervals. We previously showed that CYP3A4 and CYP2B6 are the major CYP isoforms involved in methadone metabolism, with CYP2D6 contributing to a minor extent.[25] The finding that only CYP2B6 displayed a stereoselectivity in its activity[24,25] is in agreement with the present results that none of the analyzed genotypes, with the exception of *CYP2B6*, was found to significantly influence the QT interval.

In interpreting the *in vitro* results, we are aware that stereoselective block of hERG channels by (*S*)-methadone, demonstrated by measuring I_{hERG} using a heterologous expression system, may not encompass the complexity of the channels expressed *in situ*. However, these *in vitro* findings are well supported by the pharmacogenetic data showing that the genetically determined reduced ability to metabolize (*S*)-methadone via CYP2B6 is significantly associated with high (*S*)- but not (*R*)-methadone plasma concentrations and is also significantly associated with longer QTc interval. These data represent the first reported genetic factor resulting in altered methadone metabolism, which is associated with a potentially higher risk of severe cardiac arrhythmias and sudden death. As CYP2B6 SMs represent about 6% of Caucasians,[24] this genotype is of clinical relevance for (*R*,*S*)-methadone treatment. In interpreting the *in vivo* results, we acknowledge that, owing to the design of the study, the measure of methadone effect was the actual duration of the QT interval and not the real pharmacological effect, which is the change in QT interval from baseline (*i.e.*, before methadone treatment). This should be examined in future studies.

Considering the opioid agonist specificity of (*R*)-methadone, the significantly weaker inhibition of I_{hERG} by this enantiomer, the significant proportion of CYP2B6 SMs in the population, the availability of (*R*)-methadone in Germany, the potential twofold decrease of the necessary dose, and therefore the potential twofold decrease of methadone plasma concentrations, prospective clinical studies should be performed to investigate the putative safer cardiac profile of (*R*)-methadone. If these results are confirmed, and if (*R*)-methadone use becomes generalized, one can expect that this would greatly diminish the clinical concern of CYP2B6 SM status for cardiotoxicity during methadone treatment. It should be mentioned that methadone differs from morphine by an additional non-competitive antagonist activity at the *N*-methyl-D-aspartate receptor, an interesting property that allows attenuation and reversal of the development of tolerance to morphine without altering its analgesic properties.[39,40] Administration of the pure (*R*)-enantiomer would not abolish this property because a stronger inhibitory potency has been shown for this enantiomer (K_i of 3.4 and 7.4 μmol/l for (*R*)- and (*S*)-methadone, respectively[39]). In addition, inhibition of serotonin and norepinephrine uptake by methadone might also contribute to its antinociceptive activity.[41] Similarly, stronger inhibitory potential of (*R*)-methadone compared with (*S*)-methadone has been shown for serotonin (K_i of 0.014 and 0.992 μmol/l, respectively) and norepinephrine uptake (K_i of 0.702 and 12.7 μmol/l, respectively).[41]

As a word of caution, it is important to emphasize that methadone is a life-saving treatment for opioid-dependent patients. Until future prospective clinical studies confirm the safer cardiac potential profile of (*R*)-methadone, and in this case, until the pure enantiomer is available in countries other than in Germany, the present findings should in no way limit the use of the racemate when clinically indicated. Rather, these findings should encourage careful consideration of appropriate dosing and clinical monitoring. Finally, the present report suggests that stereoselectivity in hERG current blockade should be more often considered in the field of drug-induced prolonged QT interval. To our knowledge, stereoselective block of hERG has only been reported for two drugs studied at RT (bupivacaine and ropivacaine).[42,43] As one-fourth of all marketed drugs are sold as racemates,[44] chiral drugs known to induce prolonged QT interval should be re-evaluated with regard to possible stereoselective hERG blocking properties. This could ultimately lead to the finding of safer drugs.

METHODS

Cellular electrophysiology. Whole-cell patch-clamp experiments were performed with HEK293 cells stably expressing hERG. cDNA encoding hERG (gift of Dr RS Kass, Columbia University) was cloned into pcDNA3.1-Zeo (Invitrogen AG, Basel, Switzerland)

vector. The plasmid was transfected into HEK293 cells using Lipofectamine® (Invitrogen AG) in order to establish a clonal cell line using 400 μg/ml Zeocin® (Invitrogen AG). The selected HEK–hERG cells were maintained with 100 μg/ml Zeocin®. Patch-clamp recordings in whole-cell configuration were carried out using an internal solution containing (mmol/l) KCl 110; EGTA 5; $MgCl_2$ 1; $CaCl_2$ 1; HEPES 10; and Mg-ATP 5, pH 7.2 with KOH; external solution NaCl 130; $CaCl_2$ 2; $MgCl_2$ 1.2; KCl 5; HEPES 10; and glucose 5, pH 7.4 with NaOH.

The resistance of the pipettes was 1.7–2.5 MΩ. Measurements were made using a MultiClamp 700A amplifier (Axon Instruments, Union City, CA) and were performed at either RT (25 ± 1°C) or 37 ± 1°C, using a temperature control system TC2bip (Cell Micro Controls, Norfolk, VA) to heat the perfused solution. To study drug action, tail currents were measured at −50 or −120 mV in the absence or presence of different drug concentrations. Control current values were first obtained by superfusing the cells with drug-free solutions, and the inhibition values were obtained after the currents reached a steady state when superfused with solutions containing the drugs. Membrane voltage was stepped from a holding potential of −80 to +40 mV for 300 ms followed by repolarization to −120 mv for 600 ms. No leak subtraction was performed. The interval between pulses was 500 ms. Three criteria were used to determine data acceptability: (1) seal resistance greater than 1 GΩ; (2) access resistance ⩽5 MΩ; and (3) apparent rundown of test pulse current amplitude <2.5% per minute. Electrophysiology data were analyzed using pClamp8 (Axon Instruments). The current steady-state values before and after drug application were used to calculate the percentage of current inhibited. The values of the outward or inward current were determined during the peak I_{hERG} at –50 or −120 mV steps, respectively. Data were fit using OriginPro7.5 to the formula: block in % = (1−1/(1 + ((drug)/IC_{50})^n))100, where n is the Hill coefficient and IC_{50} the drug concentration at half-maximal inhibition. Using the same experimental protocol at 37°C, astemizole, one of the most potent hERG blockers, inhibited hERG with an IC_{50} of 1.1 nM, which is very similar to the 1.3 nM reported previously[45] (data not shown).

Drugs. (*R*,*S*)-methadone HCl was obtained from Hänseler (Herisau, Switzerland). (*R*)- and (*S*)-methadone HCl were obtained from Hoechst AG (Frankfurt am Main, Germany). EDDP and EMDP were purchased from Alltech (Socochim, Basel, Switzerland). Astemizole was obtained from Sigma (Steinheim, Germany). Stock solutions (1 mg/ml in H_2O for methadone, 100 mM in methanol for EDDP and EMDP and 10 mM in dimethyl sulfoxide for astemizole) were stored at −20°C. Appropriate concentrations were prepared daily by diluting stock solution into extracellular solution. For EDDP and EMDP, the highest final concentration of methanol present during the experiments was less than 0.1%, a concentration that does not influence the results (data not shown). For astemizole, the highest final concentration of dimethyl sulfoxide present during the experiments was less than 0.0001%, a concentration that does not influence the results (data not shown).

Study design and patients. The protocol of this multicenter (Lausanne, Geneva) pharmacogenetic study was described in other reports showing the effect of *CYP2B6*, of other CYP isoforms, and of *ABCB1* genotypes and phenotypes on methadone plasma concentrations and response to treatment.[24,25] Among the patients included in the previous report,[25] ECGs were obtained for 200. For technical reasons, several ECGs were not interpretable and blood could not be obtained for all patients and, therefore, we only obtained measured QT interval and methadone plasma concentration for 179 genotyped patients at trough (before the intake of methadone). Among those 179 patients, QT interval measurement and methadone plasma concentration were obtained at peak (4 h after methadone intake, approximately at the maximum plasma concentration) in 164 patients. Only data from those 179 and 164 patients were used subsequently. ECG recordings were performed using a standard 12-lead digital recording apparatus. The trough methadone samples were taken for 179 patients (139 male patients) on average 23.1 ± 3.9 h (range: 12–37 h) after the last dose. The peak samples were taken for 164 patients (128 male patients) on average 4.1 ± 0.2 h (range: 3.6–5.2 h) after the last methadone dose. ECGs were recorded in all cases just before or after the blood samplings. Written informed consent was obtained from all patients (as well as for the genetics analyses) and the study was approved by the Local Ethics Committees.

Genotyping and methadone analysis. *CYP2B6* genotyping (for the detection of alleles **4*, **5*, **6*, **7*, and **9*) was performed by real-time polymerase chain reaction as described previously.[24] For *CYP2D6*, alleles **3*, **4*, and **6* were analyzed by commercialized assays (Applied Biosystems; TaqMan® Pre-Developed Assay Reagents for Allelic Discrimination; product nos. 4312554, 4312555, and 4312556) following the manufacturer's instructions. *CYP2D6* gene deletion (allele **5*) and duplication/multiplication (allele **xN*) were analyzed by quantitative real-time polymerase chain reaction and long polymerase chain reaction, respectively, as described previously.[46,47] *CYP3A4*1B* genotype was determined as described previously.[25]

The concentrations of (*R*,*S*)-, (*R*)-, and (*S*)-methadone in the plasma samples and in the stock solutions used for the *in vitro* experiments were measured by *LC-MS* as described previously.[24]

Data and statistical analysis. Data from the *in vitro* study are presented as means ± SE of the mean. Data from the pharmacogenetic study are presented as means ± SD and range. The statistical significance of the differences between means was determined by two-tailed unpaired Student's *t*-test or one-way analysis of variance, followed by Bonferroni's multiple comparison test for the *in vitro* study. A $P \leqslant 0.05$ was considered statistically significant. All pharmacogenetic analyses, including Pearson correlation, regression, χ^2 test and determination of OR with $CI_{95\%}$, were performed with Stata 8.2 (StataCorp, College Station, TX). QTc interval was calculated using Bazett's formula, $QTc(ms) = QT(ms)/\sqrt{RR}$ interval, with RR interval expressed in seconds. ECGs were read by a senior cardiologist specializing in arrhythmias (JS) in blind conditions. The measured QTc intervals were classified as prolonged for QTc superior to 450 ms for male subjects and 470 ms for female subjects and as borderline for QTc not measured as prolonged but superior to 430 ms for male subjects and 450 ms for female subjects.[30]

ACKNOWLEDGMENTS

We thank Mr J Spagnoli for supervising the statistical analyses and Mrs M Brocard, Mrs N Cochard, Mrs A-C Aubert, Mrs L Koeb, and Mrs M Brawand for analyzing the samples of the pharmacogenetic study. We are grateful to the nurses and medical staff of the different centers where the pharmacogenetic study was conducted for their help in the recruitment of patients. We also thank the editorial assistance of Mrs V Sari and Mrs K Powell Golay, Dr T-D Morisberger and Dr S Kellenberger for their useful comments on this manuscript. This work was supported by grants from the Swiss National Science Foundation (632-66149.01 to HA and 3200-065427.01 to CBE) and the Swiss Federal Office of Public Health (02.001382 to CBE). Part of this work was presented as an oral communication at the International Conference on Pharmacogenetics (28–30 June 2006 in Changsha, China), a satellite meeting of the 15th World Congress of Pharmacology (IUPHAR 2006), and at the annual meeting of the Swiss Society of Pharmacology and Toxicology (5–6 October 2006 in Lausanne, Switzerland).

CONFLICT OF INTEREST

The authors declared no conflict of interest.

1. American Association for the Treatment of Opioid Dependence. Public policy statement on office-based opioid agonist treatment. *AATOD'S Policies*. http://www.aatod.org/pdfs/ASAM_Policy_Comm_March_05_2.pdf (2005). Accessed 31 August 2005.
2. World Health Organization. WHO model list of essential medicines, http://www.who.int/medicines/publications/essentialmedicines/en/index.html (2005). Accessed 15 March 2006.
3. Kristensen, K., Christensen, C.B. & Christrup, L.L. The mu1, mu2, delta, kappa opioid receptor binding profiles of methadone stereoisomers and morphine. *Life Sci.* **56,** L45–L50 (1995).
4. Sticherling, C., Schaer, B.A., Ammann, P., Maeder, M. & Osswald, S. Methadone-induced Torsade de pointes tachycardias. *Swiss Med. Wkly.* **135,** 282–285 (2005).
5. Bittar, P. *et al.* Methadone, induced long QTc and "torsade de pointe". *Forum. Med. Suisse.* Suppl 8: 36S (2002).
6. Walker, P.W., Klein, D. & Kasza, L. High dose methadone and ventricular arrhythmias: a report of three cases. *Pain* **103,** 321–324 (2003).
7. De Bels, D., Staroukine, M. & Devriendt, J. Torsades de pointes due to methadone. *Ann. Intern. Med.* **139,** E156–E-156 (2003).
8. Gil, M. *et al.* QT prolongation and torsades de pointes in patients infected with human immunodeficiency virus and treated with methadone. *Am. J. Cardiol.* **92,** 995–997 (2003).
9. Krantz, M.J. *et al.* Torsades de pointes associated with very-high-dose methadone. *Ann. Int. Med.* **137,** 501–504 (2002).
10. Sala, M., Anguera, I. & Cervantes, M. Torsade de pointes due to methadone. *Ann. Intern. Med.* **139,** W64 (2003).
11. Piguet, V., Desmeules, J., Ehret, G., Stoller, R. & Dayer, P. QT interval prolongation in patients on methadone with concomitant drugs. *J. Clin. Psychopharmacol.* **24,** 446–448 (2004).
12. Pearson, E.C. & Woosley, R.L. QT prolongation and torsades de pointes among methadone users: reports to the FDA spontaneous reporting system. *Pharmacoepidemiol. Drug Saf.* **14,** 747–753 (2005).
13. World Health Organization. Methadone—cardiac vigilance recommended. *WHO Pharm. Newslett.* **5,** 3. http://www.who.int/medicines/publications/pn2005_5.pdf (2005). Accessed 27 December 2005.
14. Violand, C. & Piguet, V. Méthadone et risque dose-dépendant de prolongation de l'intervalle QT et de torsade de pointes—informations importantes pour les professionnels de la santé. *Swimedic J.* **1,** 19–20. http://www.swissmedic.ch/files/pdf/01_2004.pdf (2004). Accessed 27 December 2005.
15. Ehret, G.B. *et al.* Drug-induced long QT syndrome in injection drug users receiving methadone high frequency in hospitalized patients and risk factors. *Arch. Intern. Med.* **166,** 1280–1287 (2006).
16. Sanguinetti, M.C., Jiang, C., Curran, M.E. & Keating, M.T. A mechanistic link between an inherited and an acquired cardiac arrhythmia: HERG encodes the IKr potassium channel. *Cell* **81,** 299–307 (1995).
17. Katchman, A.N. *et al.* Influence of opioid agonists on cardiac human ether-a-go-go-related gene K+ currents. *J. Pharmacol. Exp. Ther.* **303,** 688–694 (2002).
18. Kornick, C.A. *et al.* QTc interval prolongation associated with intravenous methadone. *Pain* **105,** 499–506 (2003).
19. Abriel, H. *et al.* Molecular and clinical determinants of drug-induced long QT syndrome: a iatrogenic channelopathy. *Swiss Med. Wkly.* **134,** 685–694 (2004).
20. Sanguinetti, M.C. & Mitcheson, J.S. Predicting drug-HERG channel interactions that cause acquired long QT syndrome. *Science* **26,** 119–124 (2005).
21. Eap, C.B., Buclin, T. & Baumann, P. Interindividual variability of the clinical pharmacokinetics of methadone: implications for the treatment of opioid dependence. *Clin. Pharmacokinet.* **41,** 1153–1193 (2002).
22. Kharasch, E.D., Hoffer, C., Whittington, D. & Sheffels, P. Role of hepatic and intestinal cytochrome P450 3A and 2B6 in the metabolism, disposition, and miotic effects of methadone. *Clin. Pharmacol. Ther.* **76,** 250–269 (2004).
23. Gerber, J.G., Rhodes, R.J. & Gal, J. Stereoselective metabolism of methadone N-demethylation by cytochrome P4502B6 and 2C19. *Chirality* **16,** 36–44 (2004).
24. Crettol, S. *et al.* Methadone enantiomer plasma levels CYP2B6, CYP2C19 and CYP2C9 genotypes, and response to treatment. *Clin. Pharmacol. Ther.* **78,** 593–604 (2005).
25. Crettol, S. *et al.* ABCB1 and cytochrome *P*450 genotypes and phenotypes: influence on methadone plasma levels and response to treatment. *Clin. Pharmacol. Ther.* **80,** 668–681 (2006).
26. Human Cytochrome *P*450 (CYP) Allele Nomenclature Committee. *Allele Nomenclature for Cytochrome P450 enzymes*. http://www.cypalleles.ki.se. Accessed 30 November 2006.
27. Klein, K. *et al.* Genetic variability of CYP2B6 in populations of African and Asian origin: allele frequencies, novel functional variants, and possible implications for anti-HIV therapy with efavirenz. *Pharmacogenet. Genomics* **15,** 861–873 (2005).
28. Delisle, B.P. *et al.* Intragenic suppression of trafficking-defective KCNH2 channels associated with long QT syndrome. *Mol. Pharmacol.* **68,** 233–240 (2005).
29. Sullivan, H.R. & Due, S.L. Urinary metabolites of dl-methadone in maintenance subjects. *J. Med. Chem.* **16,** 909–913 (1973).
30. European Agency for the Evaluation of Medicinal Products. Committee for Proprietary Medicinal Products. The assessment of the potential for QT interval prolongation by non-cardiovascular medicinal products. CPMP/986/96. http://www.emea.eu.int/pdfs/human/swp/098696en.pdf (1997). Accessed 27 December 2005.
31. Division of Clinical Pharmacology, Indiana University. Cytochorme *P*450 drug-interaction table. http://medicine.iupui.edu/flockhart/table.htm. Accessed 30 November 2006.
32. Service de Pharmacologie et Toxicologie cliniques, Hôpitaux Universitaires de Genève Tables des interactions médicamenteuses et cytochromes P450. http://extranot.hcuge.ch/QuickPlace/pharmacoclin/Main.nsf/h_Index/09791F9D326CDDB8C1256C68005AA5A9/$file/cytP450.pdf.?OpenElement. Accessed 30 November 2006.
33. Bruce, R.D., Altice, F.L., Gourevitch, M.N. & Friedland, G.H. Pharmacokinetic drug interactions between opioid agonist therapy and antiretroviral medications: implications and management for clinical practice. *J. Acquir. Immune Defic. Syndr.* **41,** 563–572 (2006).
34. Walsky, R.L., Astuccio, A.V. & Obach, R.S. Evaluation of 227 drugs for *in vitro* inhibition of cytochrome P450 2B6. *J. Clin. Pharmacol.* **46,** 1426–1438 (2006).
35. Lang, T. *et al.* Extensive genetic polymorphism in the human CYP2B6 gene with impact on expression and function in human liver. *Pharmacogenetics* **11,** 399–415 (2001).
36. Misra, A.L., Mule, S.J., Bloch, R. & Vadlamani, N.L. Physiological disposition and metabolism of levo-methadone-1-3 H in non-tolerant and tolerant rats. *J. Pharmacol. Exp. Ther.* **185,** 287–299 (1973).
37. Swanson, B.N., Gordon, W.P., Lynn, R.K. & Gerber, N. Seminal excretion, vaginal absorption, distribution and whole blood kinetics of *d*-methadone in the rabbit. *J. Pharmacol. Exp. Ther.* **206,** 507–514 (1978).
38. Arizona Center for Education and Research on Therapeutics. QT drug lists, http://www.torsades.org. Accessed 21 December 2005.
39. Gorman, A.L., Elliott, K.J. & Inturrisi, C.E. The *d*- and *l*-isomers of methadone bind to the non-competitive site on the *N*-methyl-D-aspartate (NMDA) receptor in rat forebrain and spinal cord. *Neurosci. Lett.* **223,** 5–8 (1997).
40. Ebert, B., Andersen, S. & Krogsgaard-Larsen, P. Ketobemidone, methadone and pethidine are non-competitive *N*-methyl-D-aspartate (NMDA) antagonists in the rat cortex and spinal cord. *Neurosci. Lett.* **187,** 165–168 (1995).
41. Codd, E.E., Shank, R.P., Schupsky, J.S. & Raffa, R.B. Serotonin and norepinephrine uptake inhibiting activity of centrally acting analgesics: structural determinants and role in antinociception. *J. Pharmacol. Exp. Ther.* **274,** 1263–1270 (1995).
42. Siebrands, C.C., Schmitt, N. & Friederich, P. Local anesthetic interaction with human ether-a-go-go-related gene (HERG) channels: role of aromatic amino acids Y652 and F656. *Anesthesiology* **103,** 102–112 (2005).

43. Gonzalez, T. *et al.* Effects of levobupivacaine, ropivacaine and bupivacaine on HERG channels: stereoselective bupivacaine block. *Br. J. Pharmacol.* **137,** 1269–1279 (2002).
44. Caldwell, J. Do single enantiomers have something special to offer? *Hum. Psychopharmacol. Clin. Exp.* **16,** S67–S71 (2001).
45. Tarantino, P., Appleton, N. & Lansdell, K. Effect of trazodone on hERG channel current and QT-interval. *Eur. J. Pharmacol.* **510,** 75–85 (2005).
46. Schaeffeler, E., Schwab, M., Eichelbaum, M. & Zanger, U.M. CYP2D6 genotyping strategy based on gene copy number determination by TaqMan real-time PCR. *Hum. Mutat.* **22,** 476–485 (2003).
47. Løvlie, R., Daly, A.K., Molven, A., Idle, J.R. & Steen, V.M. Ultrarapid metabolizers of debrisoquine: characterization and PCR-based detection of alleles with duplication of the CYP2D6 gene. *FEBS. Lett.* **392,** 30–34 (1996).

IV.C. Publication 5 (in preparation)

Electrophysiological and molecular modeling investigation of the hERG channel's stereoselective block by bupivacaine enantiomers

As mentioned previously, stereoselectivity in the block of hERG channel has been scarcely studied. The first report of two enantiomers blocking differently the hERG current is attributed to Gonzalez *et al*. (2002) for the anesthetic drug *bupivacaine*. At the same concentration, levo-(S)-bupivacaine was reported to inhibit more I_{hERG} than the dextro-(R)-enantiomer in electrophysiological experiments. As a point of fact, bupivacaine isomers already demonstrated to inhibit selectively Na_v1 and $K_v1.5$ channels, though with reversed enantiomeric preferences (see IV.A.3.a).

On the other hand, in an attempt to understand the molecular determinants of block and accurately estimate the hERG liability of a molecule, most if not all pharmaceutical companies and laboratories generate their own homology models. Companies that can afford patch-clamp measurements of a series of compounds have therefore a consistent database of IC_{50}s of compounds to challenge their model. The lack of homogeneous data (non standardized conditions, protocol, temperature or expression model) for determining *e.g*. a drug concentration for half-maximal inhibition of hERG is indeed a major hurdle for academic development of ligand- and target-based *in silico* models.

The general idea of the present work is to combine both approaches. Initially, the patch-clamp technique was used to obtain (in similar conditions) measurements of current inhibition of the WT channel and hERG with mutated residues (previously identified as required for the binding), and therefore assess the potential stereoselective effect. Then, based on the reliable results retrieved, bupivacaine enantiomers would be submitted to docking to the hERG channel cavity. For that, we intended to rely on – but also challenge – an already existing hERG model, for which atom coordinates were made publicly available. Based upon an online literature research, three recently published homology models (Farid *et al.* 2006; Stansfeld *et*

al. 2007; Imai *et al.* 2009) were meticulously evaluated (*e.g.* crystal template used, consistency of docking results, quality of the model, computational strategy employed) and considered as a potential target for the docking studies involving bupivacaine enantiomers. With the present publication, we sought to improve the comprehension of the molecular requirements for the stereoselective block of hERG channel by bupivacaine using complementary viewpoints.

Contribution to the study:

In this study, I subcloned the hERG-encoding cDNA of all mutants into mammalian expressing vectors (pcDNA3.1(+)Zeo). I assisted the generation and antibiotic-resistance selection (performed by M. Nenniger-Tosato) of clonal HEK293 cells stably expressing the hERG mutants by TaqMan and electrophysiological selection. I also measured the hERG current inhibition by the different forms of bupivacaine in WT and mutated channels. I was in charge of the cell culture, preparation and transfection for all experiments.

I also performed most of the molecular modeling experiments, under the direct supervision of A. Daïna (docking, selection of parameters and constraint, binding mode analysis). In addition to that, I wrote the first version of the following manuscript.

Electrophysiological and molecular modeling investigation of the hERG channel's stereoselective block by bupivacaine enantiomers

Liliana Sintra Grilo[†‡], *Pierre-Alain Carrupt*[†], *Hugues Abriel*[‡], *and Antoine Daina*[†*]

[†]School of Pharmaceutical Sciences, University of Geneva, University of Lausanne, Switzerland

[‡]Department of Clinical Research, University of Bern, Switzerland

[*] To whom correspondence should be addressed: Antoine Daina, PhD Address: School of Pharmaceutical Sciences, University of Geneva, Quai Ernest-Ansermet 30, 1211 Geneva 4, Switzerland. Phone: +41 22 3793365, Fax: +41 22 3793360, E-mail: antoine.daina@unige.ch

[a] Abbreviations: AP, action potential; cLQTS, congenital long QT syndrome; diLQTS, drug-induced long QT syndrome; ECG, electrocardiogram; ES, extracellular solution; GB/SA, modified Generalized Born/Surface Area model; HEK293, human embryonic kidney 293 cells; hERG, human *ether-à-gogo* related gene; IC_{50}, half-maximal inhibitory concentration; $I_{hERG,}$ rapid component of the delayed; I_{Kr}, rapid component of the delayed rectifier potassium current; K_v channels, voltage-gated potassium channels; $MHBP_{do/ac}$, Molecular Hydrogen Bonding Potentials for donor and acceptor capacity; rmsd, root mean square deviation; WT, wild-type.

ABSTRACT

The hERG voltage-gated potassium channel mediates the cardiac I_{Kr} current, which is crucial for the duration of the cardiac action potential. Undesired block of the channel by certain drugs may prolong the QT interval and increase the risk of malignant ventricular arrhythmias. Although the molecular determinants of hERG block have been intensively studied, not much is known about its stereoselectivity. Levo-(S)-bupivacaine was the first drug reported to have a higher affinity to block hERG than its enantiomer. This study strives to understand the principles underlying the stereoselectivity of bupivacaine block with the help of mutagenesis analyses and molecular modeling simulations. Electrophysiological measurements of mutated hERG channels allowed for the identification of residues involved in bupivacaine binding and stereoselectivity. Docking and molecular mechanics simulations for both enantiomers of bupivacaine and terfenadine (a non-stereoselective blocker) were performed inside an open-state model of the hERG channel. The predicted binding modes enabled a clear depiction of ligand-protein interactions. Estimated binding affinities for both enantiomers were consistent with electrophysiological measurements. A similar computational procedure was applied to bupivacaine enantiomers towards two mutated hERG channels (Tyr652Ala and Phe656Ala). This study confirmed, at the molecular level, that bupivacaine stereoselectively binds the hERG channel. These results help lay the foundation for structural guidelines to optimize the cardiotoxic profile of drug candidates *in silico*.

MANUSCRIPT TEXT

Introduction

The human *Ether à-go-go* Related Gene channel (hERG[a]) plays a central role in the repolarization phase of the cardiomyocyte action potential (AP), where it is responsible for the rapid component of the delayed rectifier potassium current (I_{Kr}), which determines AP duration.[1] hERG is a voltage-gated potassium channel (K_v) that consists of four identical α-subunits (Fig. 1A) encoded by the *KCNH2* gene. Many loss-of-function mutations in the *KCNH2* gene (~300 listed on www.fsm.it/cardmoc) are responsible for causing *congenital Long QT Syndrome* (cLQTS), a genetic disorder characterized by a prolonged QT interval on the ECG due to reduced repolarizing currents.[2] Lengthening of the QT interval is linked to potentially lethal ventricular arrhythmias named *Torsades de Pointes.*[3]

Numerous structurally diverse drugs, such as antifungal ketoconazole,[4] antipsychotic chlorpromazine[5] and prokinetic cisapride,[6] may unintentionally block the hERG channel, leading to the *drug-induced Long QT Syndrome* (diLQTS).[7] This rare, yet serious adverse effect, led to the withdrawal of several drugs from the market, and raised the awareness of hERG toxicity in the health and pharmaceutical fields. Concomitantly, research involving the hERG channel and the block of potassium channel determinants dramatically increased. No solved crystal structure of hERG has been made publicly available, at the time of writing this manuscript. Nevertheless, according to hydropathy plots and sequence similarity with other K_v channels, it may be proposed that each α-subunit is composed of six membrane-spanning helices (transmembrane domains S1-S6) and intracellular N- and C-termini. Enough information exists to reliably construct homology models of the pore-forming domain of hERG, consisting of transmembrane helix S5, the pore helix and selectivity filter (SF) and the S6 transmembrane domain (Fig. 1A). Most drugs are thought to block the channel inside its

unusually large pore cavity.[8] Unlike other K_v channels, hERG lacks a Pro-X-Pro kink motif in the S6 helices that restrict inner cavity size.[9] The propensity of numerous and structurally diverse drugs to block the hERG channel is also due to the presence of aromatic residues (Tyr652 and Phe656) in the S6 domain that are known to interact with drugs. These amino acids are present in hERG and related *ether à-go-go* channels, but not in other K_v channels.[10] Mutation of one of these residues into alanine was initially reported to dramatically affect the block of hERG by MK-499, a methanesulfonanilide antiarrhythmic drug,[8] and was later observed for many other compounds.[11, 12] In addition to these two aromatic residues, other amino acids have been reported to affect drug block in mutagenesis studies (reviewed in [13]).

Although molecular determinants of hERG block have been intensively studied, not much is known about its stereoselectivity.[14-18] Levo-(S)-bupivacaine (Fig. 1B), a widely used anesthetic, was the first drug reported to be more potent than its enantiomer (~2 fold) at blocking hERG currents.[15-17] The work presented here focuses on bupivacaine and terfenadine, another drug with an asymmetric carbon atom (Fig. 1B). Terfenadine shares structural similarities with bupivacaine, and is also a potent hERG blocker.[19, 20] Both structures have a piperidine ring N-substituted by an alkyl chain. Moreover, one of the terfenadine aromatic rings is at a comparable distance from the basic nitrogen compared to the *o,o*-dimethylphenyl of bupivacaine. Terfenadine was employed as an anti-histaminic drug until its adverse effects on hERG[21] and QT prolongation[22] led to its withdrawal from the market. In notable contrast to bupivacaine, putative stereoselective block of the hERG channel has never been reported for terfenadine.

We present here the stereoselective block of the hERG channel, analyzed with a double approach involving electrophysiological experiments and molecular modeling simulations. First, the inhibition of the hERG current by bupivacaine enantiomers was evaluated using the whole-cell patch clamp technique on cells expressing wild-type or selected mutant channels.

In a second step, the block of hERG channels by bupivacaine was then studied using a fine-tuned structure-based methodology involving flexible docking, coupled with molecular mechanics treatments in order to rationalize the stereoselective binding at the molecular level.

Results

Current block of wild-type and mutated hERG channels by bupivacaine enantiomers

Patch-clamp studies of bupivacaine perfusion on HEK293 cells expressing wild-type (WT) hERG channels show a clear stereoselective block of the measured K^+ current, with the levo-(S)- blocking more than the dextro-(R)-enantiomer (Fig. 2A). Inhibition values of the racemate are in-between those of the two enantiomers, and are significantly different from those of levo-(S)-bupivacaine. The dose-response data were mathematically described by Hill functions and the concentrations of half-maximal inhibition (IC_{50}) obtained for racemate and levo-(S)-isomer (32 ± 3 μM and 13 ± 1 μM, respectively) are in agreement with previous estimations[16], as presented in Table 1. As expected, dextro-(R)-bupivacaine has less affinity to block the hERG current (I_{hERG}), with an estimated IC_{50} of 84 ± 5 μM. Inhibition values of racemate and dextro-(R)-bupivacaine were not altered when currents were measured at 37°C (data not shown).

In addition to the aromatic residues Tyr652 and Phe656 in the S6 helix, other amino acids important for high- and low-affinity drug binding to the hERG channel were identified by mutagenesis analyses. Based on published data reporting alanine scanning analyses of 20 drugs known to bind the K^+ channel,[13] as well as comprehensive work on racemic bupivacaine block [23], we selected 7 amino acids individually mutated to alanine (Ala, A) in order to assess the stereoselective determinants of block. Three residues – Thr623 (T), Ser624 (S) and Val625 (V) – are located at the base of the selectivity filter, whereas the remaining four – Gly648 (G), Tyr652 (Y), Phe656 (F) and Val659 (V) – line the pore cavity on the S6

helix (inset, Fig. 3A). A preliminary screen of current block of the mutants was performed using 1 mM of bupivacaine. As previously noted by Siebrands and Friederich[23], some hERG mutants were low-expressing and required higher concentrations of extracellular K^+ to elicit larger inward tail currents. Several studies have confirmed that inhibition of hERG channels by bupivacaine is not affected by changes of external potassium levels when tail currents are measured at -120 mV[23, 24]. Similarly to WT hERG channels, mutants Y652A, F656A, and V659A elicited sufficient currents with 5 mM K^+ (ES5, see *Experimental section*). Increased potassium (ES20) was needed for mutants S624A, V625A, G648A and (ES60) for T623A. In a former study on these mutants,[23] only G658A needed a 20-mM K^+ solution. Mutated hERG current traces (Fig 3A) and properties are in agreement with formerly published studies.[23, 26, 27]

According to the differences in enantiomeric block observed at a concentration of 1 mM, mutants of the K^+ channel can be classified as having: i) stereoselective block retained, ii) stereoselective block abolished or iii) stereoselective block reversed when compared to the WT channel (Fig 3B). Channels mutated at the base of the selectivity filter behave like WT channels in presence of bupivacaine enantiomers, with significantly higher block produced by the (S)-enantiomer. hERG Y652A and V659A channels belong to the second group and have similar current block by the enantiomers. Finally, reversed stereoselectivity of bupivacaine block was seen for G648A and F656A mutants. Though local anesthetic concentration used was high, all mutated hERG channels had reduced current inhibition by bupivacaine compared to WT channels, with pronounced effects on F656A and V659A channels (Fig. 3A and 3B). The Y652A mutant was surprisingly not among the residues with the most current inhibition by bupivacaine. Dose-response curves of the mutants confirmed the loss of stereoselective block for Y652A (Fig. 2B), as well as the significantly higher block of F656A by dextro-(R)-bupivacaine (Fig. 2C). The IC_{50} of block for the racemate is increased ~10- and

30-fold compared to WT for mutants in position 652 and 656, respectively (Table 1). Hill slope (k) values for Y652A mutant are significantly higher than that of the WT channel (Table 1), and can explain why a minimal decrease in inhibition is observed at 1 mM, whereas an important difference is seen at lower concentrations (Fig. 2D). This emphasizes the importance of testing different drug concentrations in order to accurately assess mutagenesis effects.

Binding modes of terfenadine enantiomers in wild-type hERG

Redocking of (S)-terfenadine in the chosen homology model was performed to calibrate the entire molecular modeling workflow prior to the docking of bupivacaine enantiomers. Parameters leading to the best overlap between the (S)-terfenadine solution and the native pose adopted in the model of Farid et al.[28] are described in the *Experimental section*. The block of hERG by terfenadine has not been previously reported to be stereoselective. Docking of (R)-terfenadine was concurrently performed in order to assess whether this can be interpreted at the molecular level. Selected docking solutions are presented in Figure 4A and show superimposed binding modes for both terfenadine enantiomers over the (S)-terfenadine, as found in Farid's homology model, with a remarkable overlap of all poses. Location of the chiral center allows only minor conformational and positional changes between (R)- and (S)-enantiomers, primarily resulting in a flip of the hydroxyl group and rotation of the *tert*-butylphenyl end. Nevertheless, this aromatic group keeps its general location inside the hERG binding site, where it is involved in aromatic interactions with the residue Phe656. As expected by the constraint applied during docking runs, the protonated nitrogen of both enantiomers closely interacts with Ser624 by donating a hydrogen to the side chain oxygen. The converging binding mode predicted for both enantiomers (Fig. 4A) is consistent with the absence of stereoselectivity for the binding of terfenadine within the K^+ channel pore.

Force field post-processing of the docked ligands resulted in the final predicted binding modes presented in Fig. 4B and 4C (solid stick representation). Molecular mechanics optimization of (S)-terfenadine inside the binding site only slightly affected the raw docking solutions. Three of the four intermolecular hydrogen bonds displayed in Farid's binding mode are found in our predicted binding mode for (S)-terfenadine (Suppl. Fig. 1). Moreover, regarding (S)-terfenadine and the residues chosen for our mutagenesis studies, the same contributions are observed in Farid's homology model and ours: four α-subunits are involved with the contribution of all Ser624 and Tyr652, and two Thr623 and Phe656 (Suppl. Fig. 1). Importantly, the aromatic residues of hERG participate in π-π interactions with terfenadine. Farid et al.[28] reported four such interactions in their model. In their published binding mode (Suppl. Fig. 1A) one phenyl group could create aromatic interactions with both Tyr652 and Phe656 of the same subunit. It is important to note that inter-ring distance measurements clearly show that the aromatic stabilizing contribution is considerably higher for Phe656 than Tyr652. In neglecting this Tyr652, as in our predicted binding mode, all remaining π–π interactions in Farid's model are recovered (Fig. 5B and Suppl. Fig. 1B). In the optimized binding mode of the (R)-enantiomer, the diphenylmethanol substituent stays in its general location, but the piperidine and the *tert*-butylphenyl of (R)-terfenadine are displaced because the butanol linker finds favorable interactions lower in the binding site. Interestingly, only one hydrogen bond remains (Fig. 5A, tertiary alcohol and side chain of Ser649), and the interaction previously found in GOLD solutions between the basic nitrogen and Ser624 is lost. The loss of hydrogen bonding would support higher binding affinity for the (R)-enantiomer of terfenadine, but the calculated free energy of binding for the (R)- and (S)-terfenadine was not significantly different with a Δ(ΔG) of -0.70 kcal/mol (Table 2). The loss of the (R)-enantiomer's strong polar interaction is likely counterbalanced by the hydrophobic interactions with one additional Phe656 residue (subunit III, Fig. 5), as well as additional

stabilizing π-stackings due to a better relative position of aromatic partners. Altogether, the overall computational results support the absence of stereoselective affinity of terfenadine enantiomers for the hERG channel.

Binding modes of bupivacaine enantiomers in wild-type hERG

After validation of our modeling strategy with terfenadine, the same methodology was used for the docking of dextro-(R)- and levo-(S)-bupivacaine towards the vestibule of the hERG channel. To ensure that results were not biased by the hydrogen bond constraint, we simultaneously generated docking solutions without constraint. As this constraint was used to limit protein symmetry issues and facilitate the rmsd cluster analysis of solutions, convergence of the best docking solutions was sought out for both conditions. Binding modes obtained for bupivacaine enantiomers, in the presence or absence of constraint, were all located perpendicularly to the pore axis in the same region of the cavity. Most ligands in the study by Farid et al.[28] as well as our bupivacaine solutions, were positioned just beneath the selectivity filter. Superimposition of the terfenadine and bupivacaine binding modes highlights some previously described pharmacophoric features:[29-31] the aromatic rings (*o,o*-dimethylphenyl group of bupivacaine and one phenyl ring of terfenadine) and the piperidine basic nitrogen show reasonably good overlap. The most striking difference between the GOLD solutions of dextro-(R)- and levo-(S)-bupivacaine is the opposite orientation of the butyl chain (Suppl. Fig. 2A). As described above, our modeling strategy involved post-docking optimization of the ligand inside the channel. Therefore, docking solutions of bupivacaine enantiomers underwent force field treatment, resulting in binding modes that were not significantly different from the original docking solutions (Suppl. Fig. 2B). When comparing optimized solutions of enantiomers, dextro-(R)-bupivacaine binding modes (with or without the constraint) have a good superimposition of the aromatic group,

while other features are poorly overlapped, namely the amide group, the piperidine ring and its N-alkyl substituent (Suppl. Fig. 2B). The optimized poses of levo-(S)-bupivacaine both with and without constraint are well superimposed. This is also true for the charged nitrogen that is expected to be pharmacophoric and could be involved in hydrogen bonding. Conversely, the (R)-enantiomer optimized poses demonstrate clear discrepancy in the localization of the piperidine ring (Suppl. Fig. 2B). The convergence of the levo-(S)-bupivacaine binding modes, before and after AMBER optimization, suggests that hydrogen bonding with Ser624 is indeed relevant for the (S)- but not the (R)-enantiomer of bupivacaine.

The final optimized binding modes of bupivacaine, originated from docking solutions without constraint, were analyzed considering pore residues that interact with the ligand, i.e. those with their atoms in a 5-Å shell. Good contacts between the ligand and near residues (see *Experimental section*) are displayed in Figure 6, allowing for identification of amino acids involved in drug recognition. Residues Tyr652 and Phe656 are well-known molecular determinants of drug block, and this study highlights their contribution to bupivacaine binding. It is to note that Tyr652 of all four α-subunits are involved in good contacts with levo-(S)-bupivacaine, whereas only three participate in dextro-(R)-bupivacaine recognition. Residues of α-subunit I do not participate in dextro-(R)-bupivacaine binding, except for a slight contribution of Ser624 (Fig. 6A), whereas Thr623, Ser624, Ser649 and Tyr652 contribute to polar and steric contacts (with possibly minor hydrophobic contribution) with the (S)-enantiomer. Residues Ser624, Ser649 and Tyr652 (subunits II and III) are found in both binding modes. Additional steric and hydrophobic contributions of Thr623 (II) and Phe656 (III) are also observed in both binding modes (Fig. 6). Subunit IV also displays common residues for both enantiomers, most importantly Tyr652 that allows for parallel-displaced π-stacking interaction with the *o,o*-dimethylphenyl group. This α-subunit (IV) also

has three residues at the base of the selectivity filter – Leu622, Thr623 and Ser624 – that contribute to both hydrophobic and polar interactions. Remarkably, Ser624 of subunit IV enables the formation of a hydrogen bond with levo-(S)-bupivacaine, the side chain hydroxyl being the donor and the amide carbonyl acting as acceptor. Regarding bupivacaine (R)-enantiomer, this Ser624 is too far to form a hydrogen bond.

In contrast to terfenadine, no evident hydrogen bond between the basic nitrogen of the (R)- or (S)-bupivacaine and the oxygen of Ser624 was retrieved in our final optimized binding modes, even though this would have been favored by the applied docking constraint. This can be explaned by bupivacaine's geometry. The representation of hydrogen-bonding properties by computing the Molecular Hydrogen Bonding Potentials (MHBPs) on the solvent accessible surface around bupivacaine binding conformations allows for quantitative depiction of both donor and acceptor capacity (respectively $MHBP_{do}$ and $MHBP_{ac}$ for levo-(S)-bupivacaine on Fig. 7C, dextro-(R)-bupivacaine not shown). When intramolecular forces are not considered, the piperidine protonated nitrogen bears an expected moderate donating potential for creating a hydrogen bond with a hypothetical acceptor partner in the proteic environment (yellow dots on Fig. 7C, *upper right panel*). However, when taking intramolecular forces into account, the binding conformation for levo-(S)-bupivacaine displays an internal interaction between the piperidine protonated nitrogen and one electronic lone pair on the carbonyl oxygen of the amide (Fig. 7B and 7C, *lower panel*). For bupivacaine enantiomers, the hydrogen-bond donor capacity is largely decreased by this intramolecular electrostatic non-bonded force (lack of dots at the vicinity of the protonated nitrogen in Fig. 7C, *lower right panel*), while this is not the case for terfenadine. Careful inspection of the virtual bupivacaine-hERG complexes unveiled the role of the electrostatic interactions between the carbonyl group and Ser624 residues. In the case of the dextro-(R)-bupivacaine binding mode, all four Ser624 create a crown-shaped hydrogen-bond network involving side-chain hydroxyls and backbone

carbonyls, with an additional good contact between Ser624 (subunit III) and the amide carbonyl of the ligand (Fig. 7A). Regarding the (S)-enantiomer, intermolecular hydrogen bonding – between the hydroxyl hydrogen of Ser624 (IV) and the second lone pair of the amide oxygen – is more favorable than the intra-protein hydrogen bonding of serine residues (Fig. 7B). $MHBP_{ac}$ also indicates that one lone pair of the amide carbonyl is intramolecularly consumed, whereas the second theoretically remains available for electrostatic interactions (Fig. 7C, *lower left panel*). The geometrical criteria defining the existence of the hydrogen bond interaction are of capital significance. In Maestro 8.5, the default hydrogen bond cut-off distance is 2.5 Å, which is in agreement with high energy interactions, but might be too restrictive in some cases. Indeed, if the cut-off distance is set as 3.5 Å, which considers also hydrogen bonds of intermediate energy, additional hydrogen bonds are revealed. For levo-(S)-bupivacaine, the contacts involving the carbonyl of the amide and the charged nitrogen with residues Ser624 (red dashed lines in Fig. 7B) are promoted to hydrogen bonds. Similarly, the good contact between the amide carbonyl of dextro-(R)-bupivacaine and the hydrogen of Ser624 hydroxyl side chain (red dashed lines in Fig. 7A) is interpreted as a hydrogen bond. These results support more favorable binding of the (S)-enantiomer inside the hERG WT cavity than the (R)-form.

The difference in the molecular recognition, the contribution of one additional subunit together with enhanced hydrogen-bonding network, is a central piece in the molecular modeling explanation for the higher current block experimentally described for levo-(S)-bupivacaine. Contrary to terfenadine, free energy of binding calculations predicted the (S)-enantiomer-hERG complex to be more stable than the complex with the (R)-enantiomer with a difference of 3.71 kcal/mol (Table 2). These results reveal a stereoselective binding of bupivacaine within the channel, with levo-(S)-bupicavaine showing higher affinity than the dextro-(R)-form.

Binding modes of bupivacaine enantiomers in hERG Y652A and F656A mutants

Our modeling strategy was applied likewise to the hERG mutants Y652A and F656A. For the F656A mutant, binding modes of bupivacaine enantiomers are located in the same cavity region as in the hERG WT pore. Global conformation of both enantiomers is comparable to that of the WT, particularly for the *o,o*-dimethylphenyl groups, since Tyr652 (subunit IV) still allows for parallel-displaced π-interaction with the aromatic moiety of bupivacaine (Fig. 8A). Unlike the docking solutions obtained in the WT channel, the α-subunits I, II and IV predominantly interact with both bupivacaine enantiomers, with only a slight contribution from subunit III. On three of the α-subunits (I, II and IV), serine residues (in position 624 and 649), Tyr652 and an adjacent Ala653, along with Thr623 on subunit IV, appear to be implicated in important steric contacts with both enantiomers of bupivacaine, involving to a certain extent hydrophobic contributions (Fig. 8A). For other amino acids implicated in molecular recognition, only slight differences are observed between the predicted binding modes for both enantiomers, such as minor hydrophobic contributions of Ser649 (III) and Ala653 (II) for (S)-bupivacaine binding versus Leu622 (IV) and Ser624 (II) for the dextro-(R)-formbupivacaine. As side-chain volume of alanine is much reduced likened to the one of phenylalanine, it proves of interest to examine closer the steric changes. A cross-sectional view of the cavity solvent-accessible surface (Fig. 9) allows for assessment of shape variations; Phe to Ala mutation in position 656 widens the intracellular part of the vestibule, and subsequent rearrangement of adjacent amino acids rebuilds the upper vestibule into a cone. Bupivacaine enantiomers would, therefore, be sterically hindered from placement at the top of the cavity (Fig. 9C), as is seen with the WT channel (Fig. 9B). Due to favorable interactions with Tyr652 and the enlarged volume below this residue, the binding modes of bupivacaine enantiomers in the F656A channel are shifted downwards, but conserving the aromatic moiety as is found in the WT channel. Displacement of the amide carbonyl and

protonated piperidine nitrogen lower in the binding site precludes any favorable polar interaction, as is seen inside the WT cavity with residues Ser624, which is consistent with the decreased affinity observed experimentally. The binding modes of bupivacaine enantiomers in the F656A cavity, as well as the free energy of binding calculations ($\Delta(\Delta G)$= -0.15 kcal/mol, Table 2), do not suggest stereoselectivity in favor of dextro-(R)-bupivacaine.

Docking solutions obtained with the constraint for the Y652A mutant of hERG channel were clearly less homogenous than those without, indicating that its use yields an inappropriate bias for this mutated structure. Optimized final binding modes of bupivacaine, originated without constraint, reveal unexpected locations inside the cavity; bupivacaine molecules are lateral and not perpendicular to the pore axis, thus involving only two out of the four α-subunits (Fig. 8B). Variations in the solvent-accessible surface indicate that Tyr to Ala mutations extend the upper part of the binding site by opening side pockets. These pockets allow suitable accommodation of the N-butyl substituent of both enantiomers (Fig. 9D). Unlike other presented cases, both enantiomers have satisfactory overlap of all carbon atoms and do not present opposite orientations of the butyl chain. Analyses of binding modes indicate that phenylalanine residues in position 656 are crucial for stabilizing cation-π (subunit I) and T-shaped π-π (subunit IV) interactions with both enantiomers (Fig. 8B). Contrary to the hERG F656A channel, mutated residues Ala652 are involved in hydrophobic interactions, mainly with the butyl chain. Some residues are involved in recognition of both enantiomers, including both hydrophobic and polar intermolecular forces, notably Thr623, Ala653 and the aforementioned Ala652 and Phe656 on subunit I, as well as Ser624, Leu646, Ser649 and Ala653, and Ala652 and Phe656 on subunit IV (Fig. 8B). Moreover, the residue Phe656 is implicated in the hydrophobic and aromatic stabilization of the *o,o*-dimethylphenyl ring. Differences observed laid in minor contributing residues, such as Ser649 (I), Leu622 and Met645 (IV) for the (R)-enantiomer, and Thr623 (IV) for the levo-(S)-bupivacaine. Similar

docking poses and interacting residues let infer that there is no major difference in binding between the bupivacaine forms. Considering the estimated free energy of binding (Table 2), (R)- and (S)-enantiomers have similar values of ΔG, being different by less than 1 kcal/mol and regarded as negligible. Altogether, the molecular modeling results support the absence of stereoselectivity of the bupivacaine enantiomers for the Y652A mutant of hERG channel.

Discussion

The raised concern about diLQTS impelled knowledge of structural determinants of hERG block; nevertheless, little is known about the stereoselective block of the delayed repolarizing potassium channel.[14-18] We present here an electrophysiological and molecular investigation of the hERG channel's stereoselective block by bupivacaine enantiomers.

Through the use of the patch clamp technique on HEK293 cells expressing wild-type hERG channels, we confirmed the stereoselective block of hERG currents by levo-(S)-bupivacaine, as was originally described by Gonzalez and co-workers.[15] Our results show that levo-(S)-bupivacaine is ~7 times more potent at inhibiting I_{hERG} than its dextro-(R)-enantiomer. Levo-(S)-bupivacaine was commercialized because it was demonstrated to be a safer local anesthetic than its racemic mixture.[32] The purpose of this study is not to question the use of this enantiomer in anesthesiology, but rather to identify the molecular determinants that govern the stereoselective block of the hERG channel.

Prior to bupivacaine investigation, the computational strategy was validated by redocking the (S)-terfenadine enantiomer towards the described homology model. The difficulty of this particular docking case was due to the symmetrical nature of the ligands, as well as the tetrameric structure of the hERG channel, introducing rotational symmetry. The multiplication of different docking poses, representing identical binding modes due to the symmetry of the binding cavity, was overcome by adding a slight constraint favoring

hydrogen-bond formation with one Ser624 residue. The predicted binding mode of the (S)-terfenadine is similar to that published by Farid et al.,[28] though obtained by truly unrelated modeling techniques. Estimations of ΔG values provided supplementary evidence for the equal affinity of terfenadine enantiomers to the hERG binding site, which is consistent with the absence of reported stereoselective block.

Siebrands and Friederich[23] previously presented an electrophysiological study on the structural requirements of hERG block by racemic bupivacaine. Their conclusions were that all tested mutations – affecting residues Thr623, Ser624, Val625, Gly648, Tyr652 and Phe656 – reduced the inhibition of hERG currents by bupivacaine. We demonstrated that the valine residue in position 659 mutated to alanine (V659A) also importantly decreases the sensitivity to current block by bupivacaine. Based on these results, we measured the current inhibition of hERG channel mutants, which permitted their classification according to the relative potency of block by bupivacaine enantiomers.

The mutation of residues near the selectivity filter (positions 623, 624 and 625) retained the same stereoselectivity of bupivacaine block as the WT channel. Interestingly, Siebrands and Friederich[23] described a significant contribution of these three amino acids to the interaction with bupivacaine. Our predicted binding modes of levo-(S)- and dextro-(R)-bupivacaine within the WT channel vestibule show how Ser624 and Thr623 directly interact with the ligand through electrostatic contacts, but not Val625. The V625A mutation could indirectly affect bupivacaine binding through local changes of the shape and properties of the SF. The importance of the hydrophilic volume at the selectivity filter entrance has been previously highlighted in a study by Farid et al.[28], in which they stated that a “propeller-shaped” hydrophilic volume accepted basic groups of blockers to form electrostatic interactions with Ser624, instead of a generally accepted cation-π interaction with Tyr652. The importance of this serine residue for binding was confirmed in Kamiya et al.[33],

where it was shown that the mutation S624A significantly decreased terfenadine block of hERG. With respect to the retained stereoselectivity, it appears that the polar residues at the base of the SF are necessary for binding but not determinant for enantiomeric recognition, meaning that the roots of stereoselective block reside in other amino acids.

Two mutated residues abolished enantiomer differences of I_{hERG} block – Tyr652 and Val659 – and two others led to the reversal of stereoselectivity of the current block – Gly648 and Phe656. Tyr652 and Phe656 are close enough to the bupivacaine ligands to directly interact, but residues in positions 648 and 659 are not within a 5 Å distance. Considering G658A, mutation of glycine to alanine should not drastically change the volume of the side chain. Importantly, Gly648 was long thought to be the glycine hinge that enables bending of the S6 and opening of the hERG channel[10, 34] because it is located close to the Pro-X-Pro motif conserved in K_v channels.[35] This is a matter of debate as the detailed work by Hardman and colleagues[27] revealed that, conversely to what was expected, glycine residues are not required for flexibility, but rather for the tight packing of the S6 helix. Their results showed that substitution of Gly648 shifted the gating equilibrium to favor the open state. Siebrands and Friederich[23], however, reported that G648A was continuously opened. Taking together these findings, even a small change of side-chain volume at position 648 might affect packing and intra-helical interactions, and could explain the indirect involvement of this amino acid in drug binding. It is noteworthy that the nearby residue Ser649 appears important for electrostatic interactions with both terfenadine and bupivacaine enantiomers. Previous observations[28] suggested that aromatic side-chains at position 652 and 656 are highly sensitive to variation in the backbone conformation of Gly648 between their closed versus open model – the latter model serving as the basis for our target-based study. Conformational and gating changes might also account for the effect of V659A on bupivacaine enantiomer block. Mutation of this residue dramatically reduced the deactivation rate.[8] Consequent

impairment in drug trapping[36] could explain the reduced sensitivity of this mutant to many drugs,[13] including bupivacaine.

Finally, the aromatic residues Tyr652 and Phe656 were shown to be critical for both the affinity of binding and the stereoselectivity of block. Predicted binding modes of bupivacaine enantiomers (Fig. 6) highlighted the contribution of Tyr652 (subunit IV) to a highly favorable π-interaction with both (R)- and (S)-ligands. On subunit III, Phe656 appears to interact equally with both enantiomers through hydrophobic contacts. Discrepancy between interacting residues is seen in the number of α-subunits involved (four for levo-(S)- and only three for dextro-(R)-bupivacaine), of which the main stabilizing hydrophobic/aromatic good contacts involve tyrosines. The crucial role of Tyr652 and Phe656 aromatic residues in drug binding has long been attributed to formation of π-stacking interactions with aromatic rings, as well as cation-π interactions with the basic group of the ligand.[12, 26] Farid et al.[28] and Zachariae et al.[37] assign the importance of these protruding amino acids to their concentric arrangement in the cavity allowing for multiple aromatic and/or hydrophobic interactions with various combinations of Tyr652 and Phe656 side-chains. A striking observation considering all the bupivacaine enantiomer docking poses and refined virtual complexes is the systematic overlay of the *o*,*o*-dimethylphenyl group. This electron-rich aromatic appears to be very favorably stabilized by much electron-poorer rings, such as side chains of phenylalanine and especially tyrosine. This is likely an important pharmacophoric feature of hERG channel affinity. Moreover in our binding models, hydrogen bond formation between the Ser624 hydroxyl and the carbonyl of the (S)-enantiomer emphasizes the binding affinity difference. It is worth to mention that the hydrophilic volume at the entrance of the SF, which favors polar interactions with the amide carbonyl and to a lesser extent with the basic nitrogen, obliges bupivacaine enantiomers to adopt poses with opposite orientation of the alkyl chain. Such a

constraint of positioning is not seen for terfenadine due to the small size, flexibility and amphiprotic nature of hydroxyl substituent on the asymmetric carbon.

Molecular docking studies towards Y652A and F656A mutants proved to be insightful. Expected changes in side-chain volume lead to the reshaping of the hERG binding site. In the case of the F656A mutation, bupivacaine enantiomers adopt a diagonal binding mode, though globally similar to those observed for the hERG WT since important aromatic interactions with tyrosine side-chains are effective. Electrostatic interactions with Ser624 are no longer observed since the oblique positioning of enantiomers moves away the amide carbonyl of bupivacaine. Residues identified as creating good contacts with bupivacaine are noticeably the same for both enantiomers. This is consistent with the equivalent predicted free energy of binding, but not with the patch clamp results, which revealed a slight but significant reversal of stereoselectivity for the F656A channel. However, IC_{50} values of enantiomers presented only a ~1.25-fold difference and reside in the mM range. In other words, our molecular strategy fails in retrieving a tiny difference between two poor blockers of the hERG current, which, in addition, may not be clinically relevant.

Remarkably, binding modes of the bupivacaine ligands in the Y652A channel appear to be completely unlike that previously predicted in the WT and the F656A mutant. The major role of aromatic residues is disclosed by the retrieved binding modes. In the absence of Tyr652 residues, which are strong determinants of binding in the WT channel, the ligand finds other favorable interacting partners in the promiscuous hERG vestibule. Due to the reduction of side-chain volume, new openings in the cavity allow for the accommodation of the butyl chain of (R)- and (S)-enantiomers, furthermore stabilized by hydrophobic interactions with the introduced Ala652. Phe656 appears to be an important feature for bupivacaine binding in Y652A cavity due to aromatic contributions (T-shaped and cation-π interactions). Altogether, the similar interacting residues in binding modes, the negligible

differences in calculated free energies of binding and the comparable I_{hERG} block strongly support the abolishment of bupivacaine stereoselectivity in hERG Y652A. Extension of the binding site, coupled with lateral positioning of the ligands, leaves a large passage (~8-10 Å) between the intracellular side and the SF. Interestingly, Hill slope values are significantly higher for the inhibition of Y652A than WT and F656A hERG currents. This suggests that another molecular mechanism of block may be involved, such as the hypothetical accommodation of two molecules in the larger mutant cavity.

Another remarkable question raised by the positioning of the ligands in the cavities is the direct relationship between the affinity of binding and the potency of I_{hERG} block. Binding mode analyses in the WT hERG cavity show that the bupivacaine enantiomers are perpendicular to the pore axis, and that, along with important recognition forces with near SF residues, it transforms the molecule into a good "physical plug" which blocks the flow of K^+ ions. Moreover, bupivacaine molecules showed very favorable interactions in the Y652A cavity (ΔG), suggesting a high affinity of binding. At the level of IC_{50} of current block, values for the racemate are almost 10 times higher than that of the WT channel. As aforementioned, despite an important affinity of binding, the lateral positioning of the ligands in the Y652A cavity might still allow some current flow. Almost perpendicular positioning of the molecules is retrieved for the binding modes in the F656A mutant, but affinity of binding appears weaker than in the WT or Y652A cavities, rendering it an unstable plug against the K^+ current. Altogether, the physical obstruction coupled with the estimated binding affinity determines the block potency of the hERG channels by ligands.

Conclusion

Our dual-approach study strives to understand the molecular determinants underlying the stereoselectivity of hERG block by bupivacaine. Validation of our computational strategy

using terfenadine, a chiral hERG blocker not reported to be stereoselective, was an important prerequisite of our work. Aromatic residues Tyr652 and Phe656, already known as crucial structural determinants for a majority of hERG blockers, were shown to be responsible for stereoselective differences in binding and block of the repolarizing K^+ channel. Polar residues located at the base of the selectivity filter, namely Ser624 and Thr623, also importantly contribute to bupivacaine recognition. The contribution of one additional α-subunit of the hERG channel for binding, together with the enhanced hydrogen-bonding network, is a central part of the molecular explanation for the higher current block experimentally observed for levo-(S)-bupivacaine. Molecular modeling results increased our understanding of the blocking effects of bupivacaine enantiomers on hERG WT channels. Similar *in silico* investigations were carried out with the hERG channel mutants Y652A and F656A. In both cases, binding modes and negligible differences in free energy of binding between the bupivacaine enantiomers can explain the experimental results obtained with the patch clamp technique.

The final convergence of results, obtained from the computational investigation of enantiomeric block in an environment with rotational symmetry and the electrophysiological measurements of wild-type and mutated hERG channels, speak in favor of the effectiveness of our target-based strategy. Nevertheless, a more detailed understanding of the structural basis of binding could be acquired by studying structurally-related molecules with experimental values of block. In this perspective, the present work lays a robust foundation for a structure-based design approach to address hERG-related cardiotoxic problems currently faced during drug development.

Experimental Section

Electrophysiology

Drugs

Racemic (R,S)-bupivacaine hydrochloride was obtained from Sigma-Aldrich and levo-(S)-bupivacaine hydrochloride was purchased from Brunschwig AG (Basel, Switzerland). Dextro-(R)-bupivacaine was kindly supplied by Cristália Ltd. (Itapira, SP, Brazil). Stock solutions (40 mM) were prepared in electrophysiological external solution ES5 (see *Patch clamp* section) and aliquots were kept at -20°C. Final dilutions of bupivacaine were prepared daily.

Patch clamp

HEK293 cells were used 48 h after transient transfection with calcium phosphate technique using plasmid pcDNA3.1-(+)Zeo-hERG wild-type (WT), as previously described[14]. hERG mutants (gift from Dr. J. S. Mitcheson, University of Leicester, UK) were isolated from pSP64-hERG, subcloned into pcDNA3.1-(+)Zeo and the cDNA of final constructs was fully sequenced. Mutated hERG plasmids were transfected, similarly to WT plasmids, into HEK293 cells. Patch-clamp recordings in whole-cell configuration were carried out using an internal solution containing (mmol/L) KCl (145), EGTA (10), $MgCl_2$ (1), Mg-ATP (5) and HEPES (5), pH 7.30 with KOH. Three different K^+-concentration external solutions, or ES, were used according to the current amplitude on the hERG channels. All ES contained (mmol/L) $MgCl_2$ (1), $CaCl_2$ (2), D-Glucose (5) and HEPES (20), and pH 7.40 with NaOH. Differences between ES60, ES20 and ES5 were in K^+ and Na^+ concentrations, with KCl (60) and NaCl (85), KCl (20) and NaCl (125), and KCl (5) and NaCl (140), respectively. Measurements were carried out using an Axopatch 200B amplifier (Axon Instruments, Union City, CA), and were performed at room temperature (25±1°C) or 37±1°C, using a temperature control system TC2bip (Cell Micro Controls, Norfolk, VA) to heat the perfused solution.

Constant flow (~250 µl/min) of perfusion was achieved with hydrostatic pressure. Voltage was stepped from a holding potential of -80 mV to +40 mV for 300 ms, followed by repolarization to -120 mV for 600 ms, applied at a frequency of 1.5Hz. To study current amplitude, peak tail currents were measured at -120 mV under perfusion of vehicle (I_{max}) followed by perfusion of enantiomer or racemic bupivacaine diluted in the same ES (I_{drug}) until steady-state was achieved. Inhibition was expressed as percent of inhibition compared to vehicle values of current (I_{max}/I_{drug}). Dose-response curves of inhibition were fitted by a Hill function described as:

$$y = \frac{100}{1+10^{(\log IC_{50} - x)\cdot k}} \qquad \text{Equation 1}$$

where y is the normalized current (% inhibition), x is the log of concentration, IC_{50} is the concentration producing half maximal inhibition and k is the Hill slope.

Electrophysiological data are presented as mean ± standard error of the mean (SEM), and n indicates the number of cells treated per condition. Statistical significance ($P<0.05$) was tested using a two-sided Student's t-test.

Molecular modeling

Selection and preparation of hERG target structures

Different publicly available homology models of the hERG channel were considered and meticulously evaluated as potential targets for the present computational studies. One of the published structures, based on the bacterial KvAP crystal (pdb entry:1orq), was provided by Farid et al.[28] and selected for two main reasons: i) the open conformation of the template channel appears suitable for drug binding and ii) it was built with the ligand (S)-terfenadine as an integral part of the structure using the so-called *induced-fit docking* protocol, which involves successive steps of Glide docking and Prime protein modeling.[38] Furthermore, this tridimensional structure was used by the authors as a docking target for binding mode

prediction of well-characterized hERG blockers, including terfenadine, cisapride, sertindole, ibutilide and clofilium. The previous study yielded converging binding modes for all mentioned ligands, which added confidence to the poses obtained.

In the present study, i) all hydrogen atoms were added to the protein residues of the model by the procedure embedded in the BIOPOLYMER module of Sybyl 8.0 (Tripos Associates, Inc., St-Louis, MO), ii) (S)-terfenadine was removed, and iii) the remaining hERG structure was employed as input target (referred to as hERG WT) for docking simulations, without any further refinement or optimization.

For the generation of the mutated hERG structures (hERG Y652A and F656A), all four Tyr652 or Phe656 residues were mutated into alanine in the aforementioned hERG WT homology model using the BIOPOLYMER mutation tool provided within Sybyl 8.0. In order to correct for side chain reorganization at the vicinity of the manually-introduced mutation, hERG Y652A and F656A were subjected to slight conjugate gradient minimization by the Sander module of AMBER 10[39] within the FF99SB force field, including implicit solvation according to the modified generalized Born model (GB/SA) developed by Onufriev et al.[40]

Preparation of terfenadine and bupivacaine ligand structures

Both enantiomers of terfenadine **(**i.e. 1-(4-*tert*-butylphenyl)-4-[4-[hydroxyl-di(phenyl)methyl]piperidin-1-yl]butan-1-ol) and both enantiomers of bupivacaine (i.e. 1-butyl-N-(2,6-dimethylphenyl)piperidine-2-carboxamide) were modeled with a protonated piperidine nitrogen, a formal charge of +1 and Gasteiger & Marsili partial atomic charges[41] within the Sybyl 8.0 environment. A first energy minimization was performed in the Tripos Force Field. Geometrical uncertainty about the piperidine rings stressed the need for deeper conformational searches using Spartan '06 (Wavefunction Inc, Irvine, CA). Cationic structures of terfenadine and bupivacaine were submitted to Monte Carlo (MC) analyses according to the semi-empirical AM1 molecular orbital theory. Selected geometries were then optimized at

HF/3-21G(*) level of theory. The lowest energy conformer of each compound was used as input ligand for GOLD docking towards hERG.

Automated flexible molecular docking

Molecular docking studies were carried out with the GOLD engine version 4.0 (CCDC Software Ltd., Cambridge, UK). The binding site was defined following the description of Stansfeld et al.[13], i.e. all protein atoms within 20Å from the natural K^+ ion S_{cav}. K^+ ions are not explicitly included in the hERG structure we used, therefore, coordinates were retrieved from the crystal subunit of KcsA including K^+ ions (pdb entry: 1k4c). The selectivity filter backbone was overlaid on our protein target and coordinates of potassium K3005 (corresponding to $S_{cav)}$ were set as the center of the binding site.

Three independent docking simulations, each calling for twenty solutions per ligand, were run in parallel according to the GOLD genetic algorithm default parameters. Ligands were considered as flexible and protein as rigid, except all hydroxyl and amine moieties. Moreover, on each subunit, the whole side chain of tyrosine at position 652, which is crucial for binding and can easily adapt its orientation, was considered as fully flexible according to the rotamer library available in GOLD 4.0. The dispersion of docking poses due to the rotational symmetry of the tetrameric target rendered examination and assessment of their goodness of fit difficult. For the sake of limiting this dispersing effect, a slight constraint favoring hydrogen-bonding with Ser624 of one specific subunit was applied, in accordance with the observations of Farid et al..[28]

The GoldScore fitness function with default parameters was employed for first evaluation and ranking of the sixty docking solutions returned for each ligand. Further criteria were applied to select one or a few more docking poses to be submitted to post-docking treatment: i) the population of clusters of solutions based on rmsd on heavy atoms, and ii)

detailed visual inspection of intermolecular interactions involving *a priori* important pharmacophoric features, particularly the protonated nitrogen, the amide group and the aromatic rings.

Molecular mechanics post-docking optimization and binding affinity prediction

The estimated best virtual complexes, i.e. the selected docking solutions (according to the above-mentioned criteria) inside their corresponding hERG structure, were submitted to molecular mechanics treatment within the AMBER 10 environment. This post-docking procedure implied the traditional all-atom AMBER force field for the protein atoms, the GAFF force field and semi-empirical AM1-BCC charges for the ligand atoms, together with implicit solvation model terms. The protocol, adapted from Graves et al.[42], consists of three main steps where only the ligand is allowed to move inside the rigid protein channel: i) a 100-steps minimization with a conjugate gradient method, ii) a Langevin molecular dynamics of 3000 steps at constant temperature of 300K, and iii) a second minimization identical to i). The procedure, besides geometry optimization and refined binding mode prediction, leads to an approximation of ligand affinity for the hERG channel by estimating the free energy of binding (ΔG), according to the Equation 2:

$$\Delta G = E_{binding} = E_{complex} - (E_{protein} + E_{ligand}) \qquad \text{Equation 2}$$

where $E_{complex}$, $E_{protein}$, E_{ligand} are the solvated internal energies of the complex, the protein and the ligand, respectively, as computed by the force fields enriched by implicit solvation terms according to the GB/SA model of Onufriev et al.[40] and the LCPO algorithm[43] term accounting for surface area.

Analysis of binding mode and intermolecular recognition

Geometries and intermolecular interactions within the optimized virtual complexes were visually analyzed using computer graphic facilities and with the help of Maestro 8.5 measurement tools (Schrödinger, LLC, Portland, OR). “Good contacts” were defined as atom

radius ratio cutoff of 1.3 Å. Hydrogen bond distance cut-off was set as 2.5 Å between both partner atoms; the minimum angles are set as 120° and 90 for donor and acceptor atoms, respectively.

A deeper exploration of the ligands' hydrogen-bonding properties was achieved by an in-house tool called Molecular Hydrogen Bonding Potentials (MHBPs). MHBPs include two molecular interaction fields to model hydrogen-bonding donor ($MHBP_{do}$) and acceptor ($MHBP_{ac}$) capacities of conformations in the three-dimensional space. One of the advantages of this methodology is that it relies on an atomic fragmental system of donor (α) and acceptor (β) values, determined experimentally and not solely on geometrical considerations. It allows a precise and quantitative determination of the repartition of hydrogen bonding properties around the molecule as measured in various solvents. Theoretical and technical details about MHBPs are given elsewhere.[44,45] For the specific purpose of assessing the balance between intramolecular and intermolecular hydrogen bonding capacities of (R,S)-bupivacaine, $MHBP_{do}$ and $MHBP_{ac}$ were computed twice on a solvent accessible surface around the predicted binding conformations. Intramolecular forces were neglected during the first computation, but taken into account during the second.

ACKNOWLEDGMENT

The authors thank E. Favre (School of Pharmaceutical Sciences, Geneva, Switzerland) for her kind help and fruitful discussions regarding modeling, and M. Nenniger-Tosato (Department of Pharmacology and Toxicology, Lausanne, Switzerland) for the technical assistance in cell culture. We are also grateful to Dr. A. Felley Jacquemont for her thorough reading of the manuscript. We acknowledge Cristália Ltd. for generously supplying the pure (R)-enantiomer of bupivacaine and Dr. J. S. Mitcheson for the pSP64-hERG mutant constructs. The work was supported by grants of the Swiss National Science Foundation to H. Abriel (310030_120707). Part of this work was presented as a poster communication at the annual Fall Meeting of the Swiss Chemical Society (September 4th 2009, Lausanne, Switzerland). The poster was awarded a prize and the authors were invited to present their preliminary results in the special issue of the journal of the Swiss Chemical Society (Chimia).[46]

SUPPORTING INFORMATION AVAILABLE

Supplementary Figure 1: Optimized binding mode of (S)-terfenadine in hERG WT channel versus Farid's model.

Supplementary Figure 2: Selected docking solutions (GOLD) of bupivacaine enantiomers retrieved with or without constraint and binding modes of these poses after molecular mechanics optimization (AMBER) in the hERG WT channel.

TABLES

Table 1: Parameters derived from the Hill fit of the dose-response data of inhibition of hERG channels, WT and Y652A or F656A mutants.

		levo-(S)-bupivacaine	**racemic (R,S)-bupivacaine**	**dextro-(R)-bupivacaine**
hERG WT	IC_{50} (μM) ± SEM	13 ± 1 13 ± 1 [a]	32 ± 3 22 ± 2 [a]	84 ± 5 n.d.
	Hill slope ± SEM	0.44 ± 0.03 0.85 ± 0.07 [a]	0.53 ± 0.04 0.91 ± 0.06 [a]	0.61 ± 0.03 n.d.
Y652A	IC_{50} (μM) ± SEM	278 ± 12 83 ± 3 [a]	265 ± 13 95 ± 5 [a]	276 ± 12 n.d.
	Hill slope ± SEM	1.02 ± 0.05 1.11 ± 0.05 [a]	1.03 ± 0.06 1.21 ± 0.07 [a]	1.00 ± 0.05 n.d.
F656A	IC_{50} (μM) ± SEM	1013 ± 84 n.d.	866 ± 57 n.d.	758 ± 42 n.d.
	Hill slope ± SEM	0.75 ± 0.05 n.d.	0.77 ± 0.04 n.d.	0.83 ± 0.05 n.d.

[a] : data obtained on Chinese Hamster Ovary (CHO) cells, from reference [16].

n.d. = not determined

Table 2: Calculated Gibbs free energy of binding (ΔG, kcal/mol) within the AMBER 10 environment, including implicit solvation and surface terms for the different docked ligands within the hERG structure and estimated binding energy difference ($\Delta G_{(R)\text{-form}} - \Delta G_{(S)\text{-form}} = \Delta(\Delta G)$, kcal/mol).

	Ligand	(ΔG), kcal/mol	Δ(ΔG), kcal/mol
hERG WT	(R)-terfenadine	-26.73	-0.70 **(S)=(R)**
	(S)-terfenadine	-26.03	
	dextro-(R)-bupivacaine	-17.14	+3.71 **(S)>(R)**
	levo-(S)-bupivacaine	-20.85	
Y652A	dextro-(R)-bupivacaine	-23.07	-0.76 **(S)=(R)**
	levo-(S)-bupivacaine	-22.31	
F656A	dextro-(R)-bupivacaine	-16.72	-0.15 **(S)=(R)**
	levo-(S)-bupivacaine	-16.57	

REFERENCES

1. Sanguinetti, M. C.; Jiang, C. G.; Curran, M. E.; Keating, M. T. A mechanistic link between an inherited and an acquired cardiac-arrhythmia - Herg encodes the I-Kr potassium channel. *Cell* **1995,** *81*, 299-307.

2. Curran, M. E.; Splawski, I.; Timothy, K. W.; Vincent, G. M.; Green, E. D.; Keating, M. T. A molecular basis for cardiac arrhythmia: HERG mutations cause long QT syndrome. *Cell* **1995,** *80*, 795-803.

3. Sanguinetti, M. C.; Tristani-Firouzi, M. hERG potassium channels and cardiac arrhythmia. *Nature* **2006,** *440*, 463-469.

4. Dumaine, R.; Roy, M. L.; Brown, A. M. Blockade of HERG and Kv1.5 by ketoconazole[1]. *J. Pharmacol. Exp. Ther.* **1998,** *286*, 727-735.

5. Thomas, D.; Wu, K.; Kathöfer, S.; Katus, H. A.; Schoels, W.; Kiehn, J.; Karle, C. A. The antipsychotic drug chlorpromazine inhibits HERG potassium channels. *Brit. J. Pharmacol.* **2003,** *139*, 567-574.

6. Mohammad, S.; Zhou, Z. F.; Gong, Q. M.; January, C. T. Blockage of the HERG human cardiac K+ channel by the gastrointestinal prokinetic agent cisapride. *Am. J. Physio. Heart Circ. Physiol.* **1997,** *273*, H2534-H2538.

7. Roden, D. M. Drug-induced prolongation of the QT interval. *N. Engl. J. Med.* **2004,** *350*, 1013-1022.

8. Mitcheson, J. S.; Chen, J.; Lin, M.; Culberson, C.; Sanguinetti, M. C. A structural basis for drug-induced long QT syndrome. *Proc. Natl. Acad. Sci. USA* **2000,** *97*, 12329-12333.

9. Mitcheson, J. S. Drug binding to HERG channels: evidence for a 'non-aromatic' binding site for fluvoxamine. *Brit. J. Pharmacol.* **2003,** *139*, 883-884.

10. Sanguinetti, M. C.; Mitcheson, J. S. Predicting drug-hERG channel interactions that cause acquired long QT syndrome. *Trends Pharmacol. Sci.* **2005,** *26*, 119-124.

11. Sanchez-Chapula, J. A.; Navarro-Polanco, R. A.; Culberson, C.; Chen, J.; Sanguinetti, M. C. Molecular determinants of voltage-dependent human ether-a-go-go related gene (HERG) K^+ channel block. *J. Biol. Chem.* **2002,** *26*, 23587-23595.

12. Fernandez, D.; Ghanta, A.; Kauffman, G. W.; Sanguinetti, M. C. Physicochemical features of the hERG channel drug binding site. *J. Biol. Chem.* **2004,** *279*, 10120-10127.

13. Stansfeld, P. J.; Gedeck, P.; Gosling, M.; Cox, B.; Mitcheson, J. S.; Sutcliffe, M. J. Drug block of the hERG potassium channel: insight from modeling. *Proteins: Struct. Funct. Bioinf.* **2007,** *68*, 568-580.

14. Eap, C. B.; Crettol, S.; Rougier, J. S.; Schläpfer, J.; Sintra Grilo, L.; Déglon, J. J.; Besson, J.; Croquette-Krokar, M.; Carrupt, P. A.; Abriel, H. Stereoselective block of hERG channel by (S)-methadone and QT interval prolongation in CYP2B6 slow metabolizers. *Clin. Pharmacol. Ther.* **2007,** *81*, 719-728.

15. Gonzalez, T.; Arias, C.; Caballero, R.; Moreno, I.; Delpon, E.; Tamargo, J.; Valenzuela, C. Effects of levobupivacaine, ropivacaine and bupivacaine on HERG channels: stereoselective bupivacaine block. *Brit. J. Pharmacol.* **2002,** *137*, 1269-1279.

16. Siebrands, C. C.; Schmitt, N.; Friederich, P. Local anesthetic interaction with human ether-a-go-go-related gene (HERG) channels. *Anesthesiology* **2005,** *103*, 102-112.

17. Friederich, P.; Solth, A.; Schillemeit, S.; Isbrandt, D. Local anaesthetic sensitivities of cloned HERG channels from human heart: comparison with HERG/MiRP1 and HERG/MiRP1T8A. *Brit. J. Anaesth.* **2004,** *92*, 93-101.

18. Waldegger, S.; Niemeyer, G.; Mörike, K.; Wagner, C. A.; Suessbrich, H.; Busch, A. E.; Lang, F.; Eichelbaum, M. Effect of verapamil enantiomers and metabolites on cardiac K^+ channels expressed in xenopus oocytes. *Cell. Physiol. Biochem.* **1999,** *9*, 81-89.

19. Rampe, D.; Roy, M. L.; Dennis, A.; Brown, A. M. A mechanism for the proarrhythmic effects of cisapride (Propulsid): high affinity blockade of the human cardiac potassium channel HERG. *FEBS Lett.* **1997,** *417*, 28-32.

20. Crumb, W. J. Loratadine blockade of K^+ channels in human heart: Comparison with terfenadine under physiological conditions. *J. Pharmacol. Exp. Ther.* **2000,** *292*, 261-264.

21. Roy, M. L.; Dumaine, R.; Brown, A. M. HERG, a primary human ventricular target of the nonsedating antihistamine terfenadine. *Circulation* **1996,** *94*, 817-823.

22. Pinney, S. P.; Koller, B. S.; Franz, M. R.; Woosley, R. L. Terfenadine increases the Qt interval in isolated guinea-pig heart. *J. Cardiovasc. Pharmacol.* **1995,** *25*, 30-34.

23. Siebrands, C. C.; Friederich, P. Structural requirements of human ether-a-go-go-related gene channels for block by bupivacaine. *Anesthesiology* **2007,** *106*, 523-531.

24. Limberis, J. T.; Su, Z.; Cox, B. F.; Gintant, G. A.; Martin, R. L. Altering extracellular potassium concentration does not modulate drug block of human ether-a-go-go-related gene (hERG) channels. *Clin. Exp. Pharmacol. Physiol.* **2006,** *33*, 1059-1065.

25. Zhou, Z. F.; Gong, Q. M.; January, C. T. Correction of defective protein trafficking of a mutant HERG potassium channel in human long QT syndrome - Pharmacological and temperature effects. *J. Biol. Chem.* **1999,** *274*, 31123-31126.

26. Perry, M.; Stansfeld, P. J.; Leaney, J.; Wood, C.; de Groot, M. J.; Leishman, D.; Sutcliffe, M. J.; Mitcheson, J. S. Drug binding interactions in the inner cavity of HERG channels: molecular insights from structure-activity relationships of clofilium and ibutilide analogs. *Mol. Pharmacol.* **2006,** *69*, 509-519.

27. Hardman, R. M.; Stansfeld, P. J.; Dalibalta, S.; Sutcliffe, M. J.; Mitcheson, J. S. Activation gating of hERG potassium channels - S6 glycines are not required as gating hinges. *J. Biol. Chem.* **2007,** *282*, 31972-31981.

28. Farid, R.; Day, T.; Friesner, R. A.; Pearlstein, R. A. New insights about HERG blockade obtained from protein modeling, potential energy mapping, and docking studies. *Bioorg. Med. Chem.* **2006,** *14*, 3160-3173.

29. Morgan T.K., J.; Sullivan, M. E. An overview of class III electrophysiological agents: A new generation of antiarrhythmic therapy. In *Prog.Med.Chem.*; Ellis, G. P.; Luscomb, D. K. Eds.; Elsevier Science Publishers, Amsterdam, 1992; pp 65-108.

30. Pearlstein, R. A.; Vaz, R. J.; Kang, J.; Chen, X. L.; Preobrazhenskaya, M.; Shchekotikhin, A. E.; Korolev, A. M.; Lysenkova, L. N.; Miroshnikova, O. V.; Hendrix, J.; Rampe, D. Characterization of HERG potassium channel inhibition using CoMSiA 3D QSAR and homology modeling approaches. *Bioorg. Med. Chem. Lett.* **2003,** *13*, 1829-1835.

31. Cavalli, A.; Poluzzi, E.; De Ponti, F.; Recanatini, M. Toward a pharmacophore for drugs inducing the long QT syndrome: insights from a CoMFA study of HERG K^+ channel blockers. *J. Med. Chem.* **2002,** *45*, 3844-3853.

32. Bardsley, H.; Gristwood, R.; Baker, H.; Watson, N.; Nimmo, W. A comparison of the cardiovascular effects of levobupivacaine and rac-bupivacaine following intravenous administration to healthy volunteers. *Br. J. Clin. Pharmacol.* **1998,** *46*, 245-249.

33. Kamiya, K.; Niwa, R.; Morishima, M.; Honjo, H.; Sanguinetti, M. C. Molecular determinants of hERG channel block by terfenadine and cisapride. *J. Pharmacol. Sci.* **2008,** *108*, 301-307.

34. Rajamani, R.; Tounge, B. A.; Li, J.; Reynolds, C. H. A two-state homology model of the hERG K^+ channel: application to ligand binding. *Bioorg. Med. Chem. Lett.* **2005,** *15*, 1737-1741.

35. Labro, A. J.; Raes, A. L.; Bellens, I.; Ottschytsch, N.; Snyders, D. J. Gating of shaker-type channels requires the flexibility of S6 caused by prolines. *J. Biol. Chem.* **2003,** *278*, 50724-50731.

36. Mitcheson, J. S.; Chen, J.; Sanguinetti, M. C. Trapping of a methanesulfonanilide by closure of the HERG potassium channel activation gate. *J. Gen. Physiol.* **2000,** *115*, 229-239.

37. Zachariae, U.; Giordanetto, F.; Leach, A. G. Side chain flexibilities in the human ether-a-go-go related gene potassium channel (hERG) together with matched-pair binding studies suggest a new binding mode for channel blockers. *J. Med. Chem.* **2009,** *52*, 4266-4276.

38. Sherman, W.; Day, T.; Jacobson, M. P.; Friesner, R. A.; Farid, R. Novel procedure for modeling ligand/receptor induced fit effects. *J. Med. Chem.* **2006,** *49*, 534-553.

39. Case, D. A.; Darden, T. A.; Cheatham, T. E.; Simmerling, C. L.; Wang, J.; Duke, R. E.; Luo, R.; Crowley, M.; Walker, R. C.; Zhang, W.; Merz, M.; Wang, B.; Hayik, S.; Roitberg, G.; Seabra, G.; Kolossváry, I.; Wong, K. F.; Paesani, F.; Vanicek, J.; Wu, X.; Brozell, S. R.; Steinbrecher, T.; Gohlke, H.; Yang, L.; Tan, C.; Mongan, J.; Hornak, V.; Cui, G.; Mathews, D. H.; Seetin, M. G.; Sagui, C.; Babin, V.; Kollman, P. A. AMBER. [10]. 2008. University of California, San Francisco.

40. Onufriev, A.; Bashford, D.; Case, D. A. Exploring protein native states and large-scale conformational changes with a modified generalized born model. *Proteins:Struct,Funct,Bioinf* **2004,** *55*, 383-394.

41. Gasteiger, J.; Marsili, M. Iterative partial equalization of orbital electronegativity: a rapid access to atomic charges. *Tetrahedron* **1980,** *36*, 3219-3222.

42. Graves, A. P.; Shivakumar, D. M.; Boyce, S. E.; Jacobson, M. P.; Case, D. A.; Shoichet, B. K. Rescoring docking hit lists for model cavity sites: Predictions and experimental testing. *J. Mol. Biol.* **2008,** *377*, 914-934.

43. Weiser, J.; Shenkin, P. S.; Still, W. C. Approximate atomic surfaces from linear combinations of pairwise overlaps (LCPO). *J. Comput. Chem.* **1999,** *20*, 217-230.

44. Rey, S.; Caron, G.; Ermondi, G.; Gaillard, P.; Pagliara, A.; Carrupt, P. A.; Testa, B. Development of molecular hydrogen bonding potentials (MHBPs) and their application to structure permeation relations. *J. Mol. Graphics Model.* **2001,** *19*, 521-535.

45. Rey, S.; Carrupt, P. A.; Testa, B. The hydrogen-bond: Computational approaches and applications to drug design. *Ann. Pharm. Fr.* **2002,** *60*, 386-396.

46. Grilo, L. S.; Carrupt, P. A.; Daina, A. Stereoselective block of hERG channel by bupivacaine scrutinized at molecular level. *Chimia* **2010,** *64*, 165-169.

FIGURES

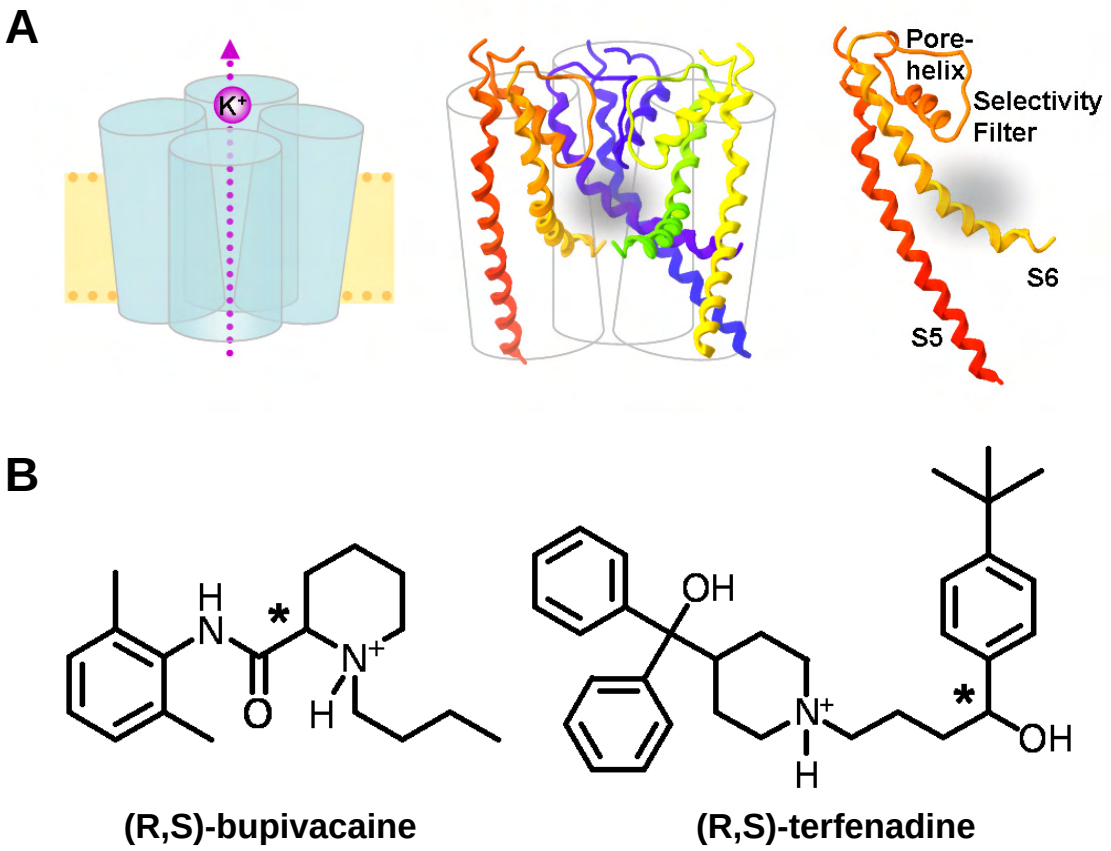

Fig. 1: Structure of hERG channel and blocking drugs.
(**A**) Cartoon depicting the tetrameric structure of hERG voltage-gated potassium channel (*left*). For clarity, only three subunits are presented in order to show the pore-constituting unit (*middle*), which is formed by S5 and S6 transmembrane domains, the pore-helix and the selectivity filter (*right*). (**B**) Chemical structures of hERG blockers (R,S)-bupivacaine and (R,S)-terfenadine, protonated as at physiological pH and with chiral center marked with an asterisk. Both structures encompass a piperidine ring N-substituted by an alkyl chain, and one aromatic ring within similar distance from the basic nitrogen.

Figure 1, Sintra Grilo *et al*.

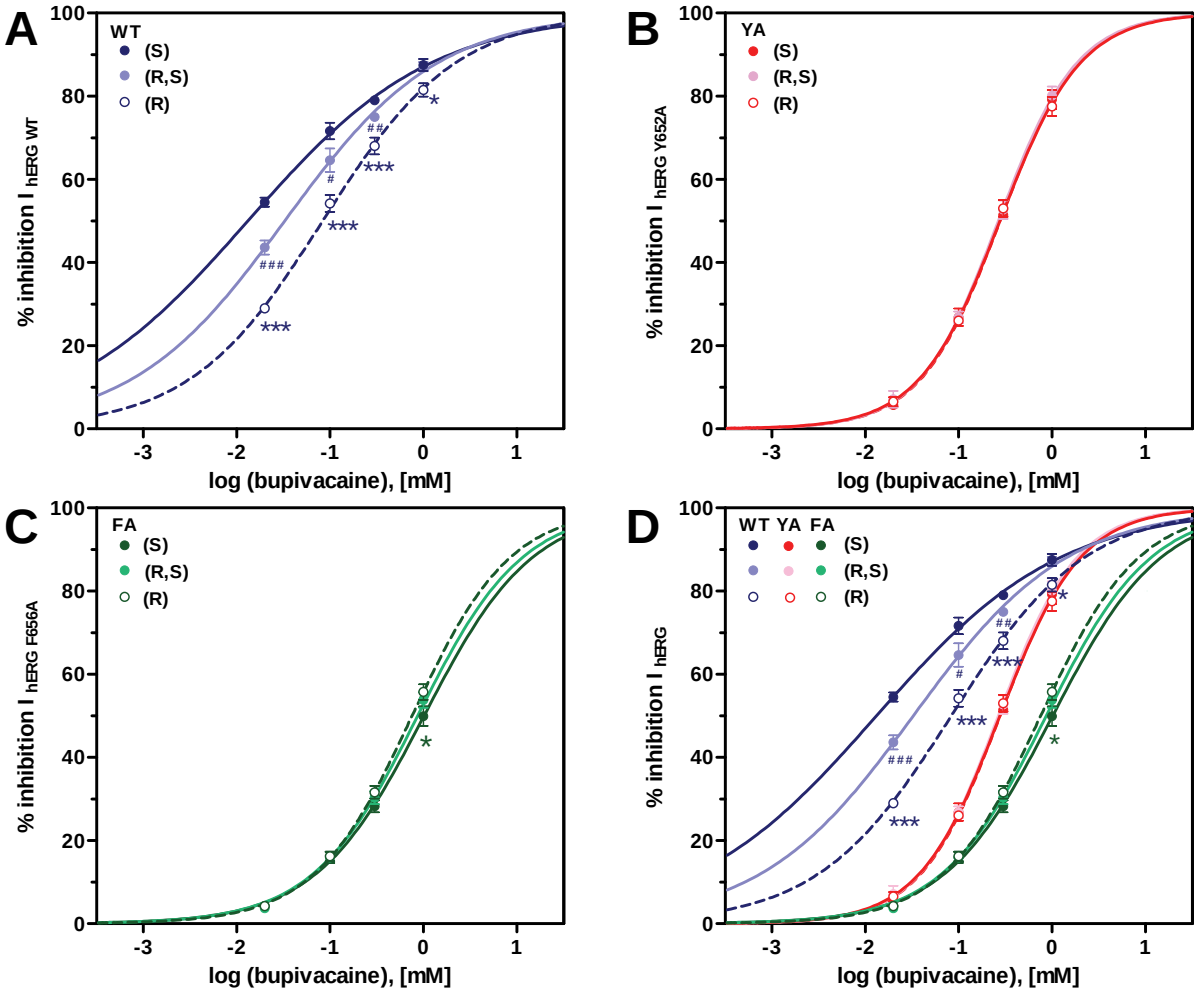

Fig. 2: Dose-response curves of inhibition of hERG current by bupivacaine forms.

(**A**) Current inhibition (% inhibition of I_{hERG}) and drug concentration relationship for levo-(S)-, racemic (R,S)- and dextro-(R)-bupivacaine with hERG WT, (**B**) hERG-Y652A (YA) and (**C**) hERG-F656A (FA) channels. (**D**) Overlay of bupivacaine dose-inhibition curves show marked stereoselectivity for hERG WT, absence of difference in mutant Y652A (YA) and small reversed stereoselectivity for mutant F656A (FA). Statistical differences compared with inhibition values of levo-(S)-bupivacaine are indicated ($P<0.05$, */#; $P<0.01$, ##; $P<0.001$, ***/###).

Figure 2, Sintra Grilo *et al*.

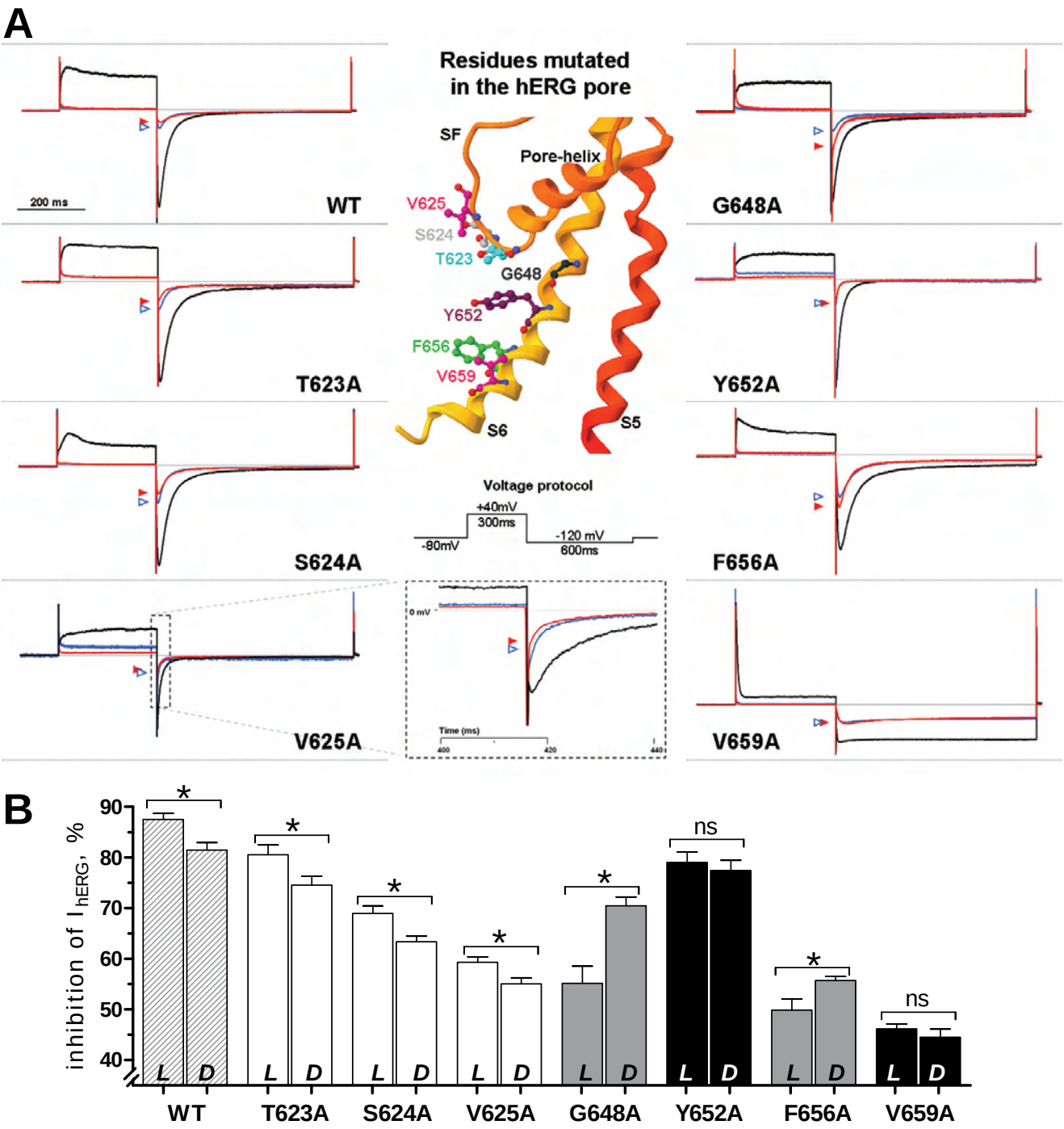

Fig. 3: Assessment of current block by perfusion of bupivacaine enantiomers at 1 mM in wild-type and mutated hERG channels.

(**A**) Representative current traces through hERG WT and mutant channels evoked with the protocol in inset. Black traces represent control current perfused with vehicle only. Dextro-(R)- and levo-(S)-bupivacaine block of current are respectively presented in blue and red traces, with peak amplitude noted by triangles with matched color. Location of the mutated residues in the S6 transmembrane helix and at the base of the SF is presented in the inset, with the color coding used in all figures. (**B**) Inhibition of I_{hERG} (in % inhibition) for WT and mutant channels under perfusion of 1 mM of levo-(S)-bupivacaine (*L*) or dextro-(R)-bupivacaine (*D*) diluted in the ES. Bar fillings (except hERG WT) agree to the following stereoselective-effect code: white, *L>D*; black, *L=D*, and gray, *L<D*. Two-sided Student's t-test was used to signify differences in current block by enantiomers ($P<0.05$,*; ns, non significant) with n= 5-10 per enantiomer and per mutant. Note that the y axis is truncated.

Figure 3, Sintra Grilo *et al*.

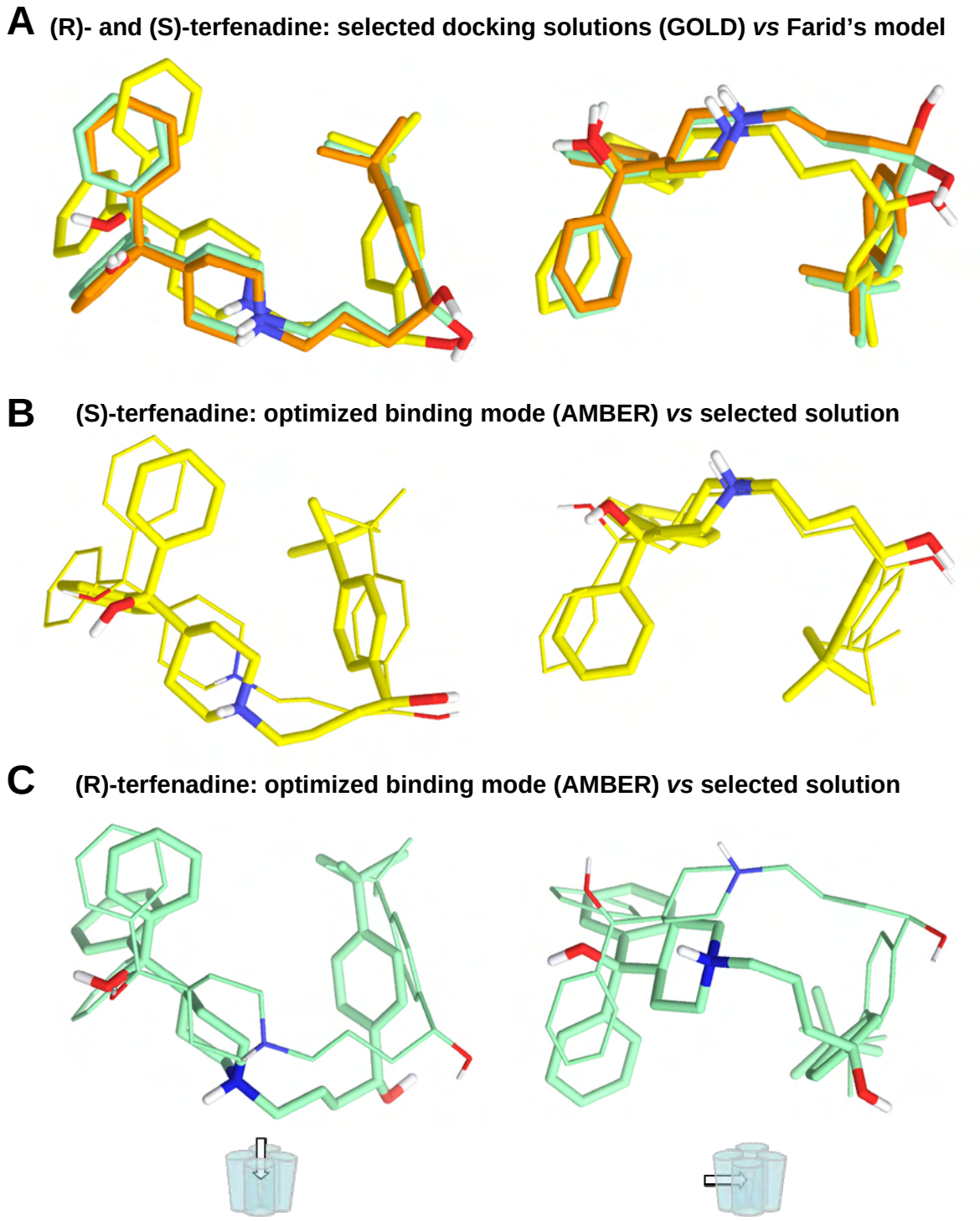

Fig. 4: Selected docking solutions (GOLD) of terfenadine enantiomers compared with binding modes after molecular mechanics optimization (AMBER) in the hERG WT channel.

(**A**) (S)-terfenadine (carbons in orange), retrieved from the model published by Farid et al., superimposes well with our final selected GOLD solutions of both (S)-terfenadine (carbons in yellow) and (R)-terfenadine (carbons in light green). (**B**) Binding modes of (S)-terfenadine before (thin stick representation) and after AMBER optimization (solid stick representation). (**C**) Binding modes of (R)-terfenadine before and after AMBER optimization (same coding). The presented binding modes are seen from two orthogonal views (arrows) as described by the scheme below. For the sake of clarity, protein atoms and non-polar hydrogens of ligands have been omitted.

Figure 4, Sintra Grilo *et al*.

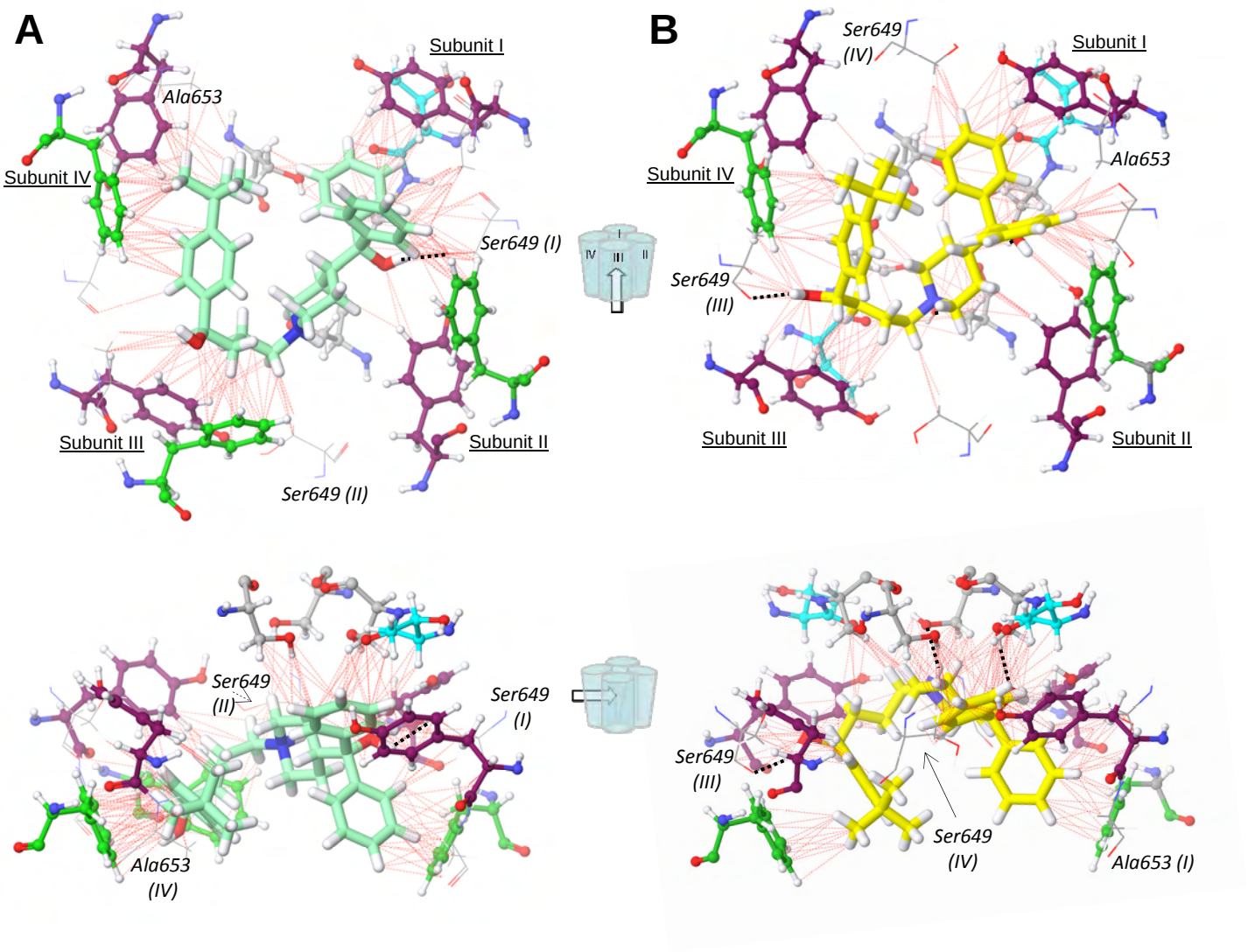

Fig. 5: Binding modes of terfenadine enantiomers optimized by molecular mechanics (AMBER) in the hERG WT channel.

(**A**) (R)-terfenadine (carbons in light green) or (**B**) (S)-terfenadine (carbons in yellow) are presented with hERG WT residues within a 5-Å shell, creating good contacts (red dashed lines) or hydrogen bonding (black dotted lines) with the ligand. Both (**A**) and (**B**) are seen from the same viewpoint (arrows), as described by the scheme. Tyr652 residues (purple) have been flexibilized during GOLD docking process. Residues investigated in this study are highlighted with ball-and-stick representation and the following color-coding: Ser624, gray; Thr623, cyan; Tyr652, purple; Phe656, green, others are in wireframe with subunit number specified between brackets when necessary. In both binding modes, the general orientation of the ligands inside the hERG WT cavity is comparable. Although (S)-terfenadine creates hydrogen bonds with channel residues, it does not interact with a supplementary Phe656 as seen for (R)-terfenadine.

Figure 5, Sintra Grilo *et al*.

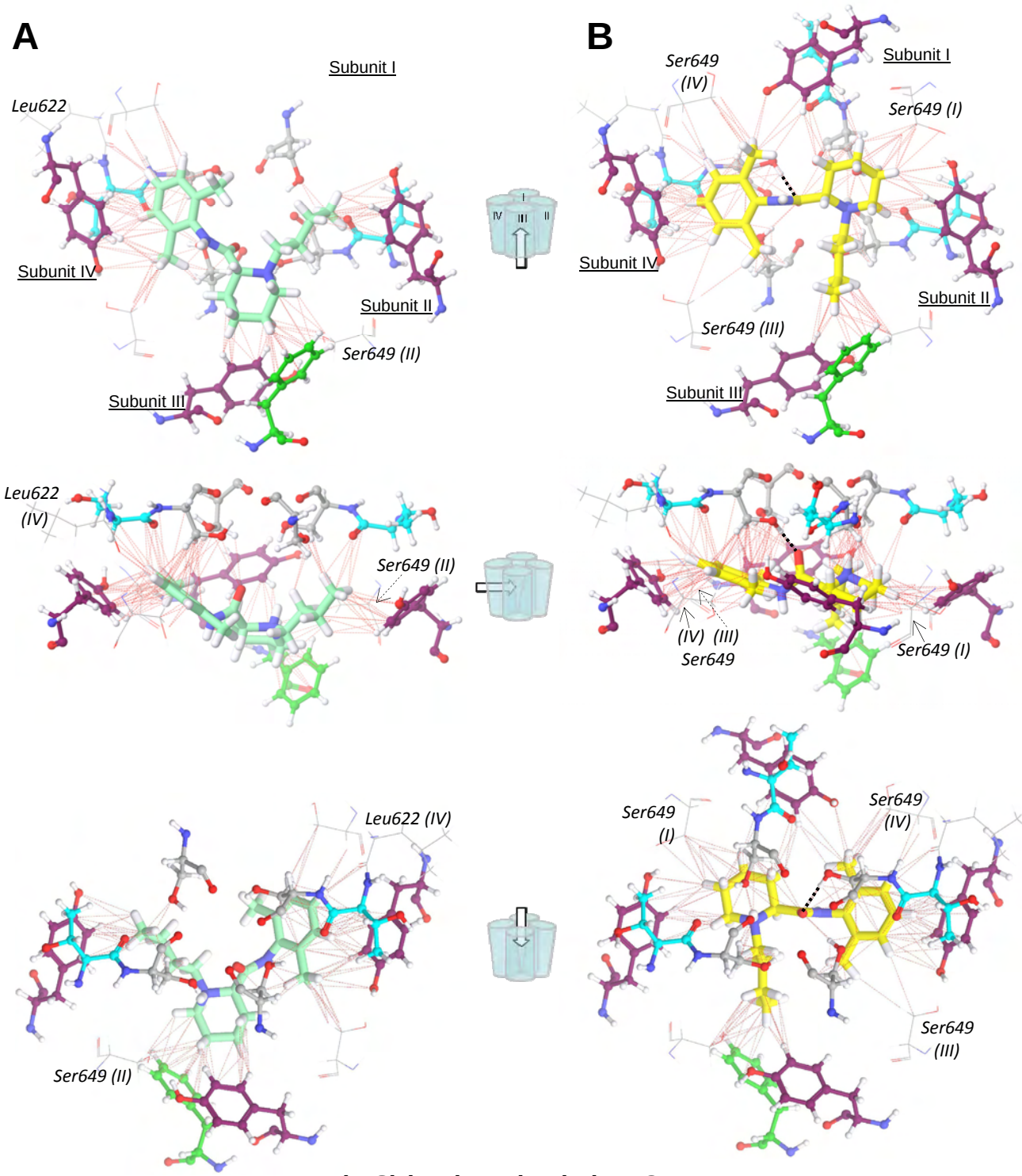

Fig. 6: Binding modes of bupivacaine enantiomers optimized by molecular mechanics in the hERG WT channel.

(**A**) Dextro-(R)-bupivacaine (carbons in light green) or (**B**) levo-(S)-bupivacaine (carbons in yellow) are presented with hERG WT residues within a 5-Å shell, creating good contacts (red dashed lines) or hydrogen bonds (black dotted lines) with the ligand. Both (**A**) and (**B**) are seen from three views as described by the scheme. Similarly to Fig. 5, residues investigated in this study are highlighted in a colored ball-and-stick representation (Ser624, gray; Thr623, cyan; Tyr652, purple; Phe656, green), others are in wireframe and labeled. Levo-(S)- and dextro-(R)-bupivacaine adopt different orientations of their butyl chain, thus keeping the amide carbonyl and protonated piperidine nitrogen facing the SF. However, only the levo-(S)-bupivacaine (closer to the SF) creates a hydrogen bond with the side-chain hydroxyl of one Ser624. In addition, the (S)-enantiomer interacts importantly with all four α-subunits (*versus* three for dextro-(R)-bupivacaine).

Figure 6, Sintra Grilo *et al*.

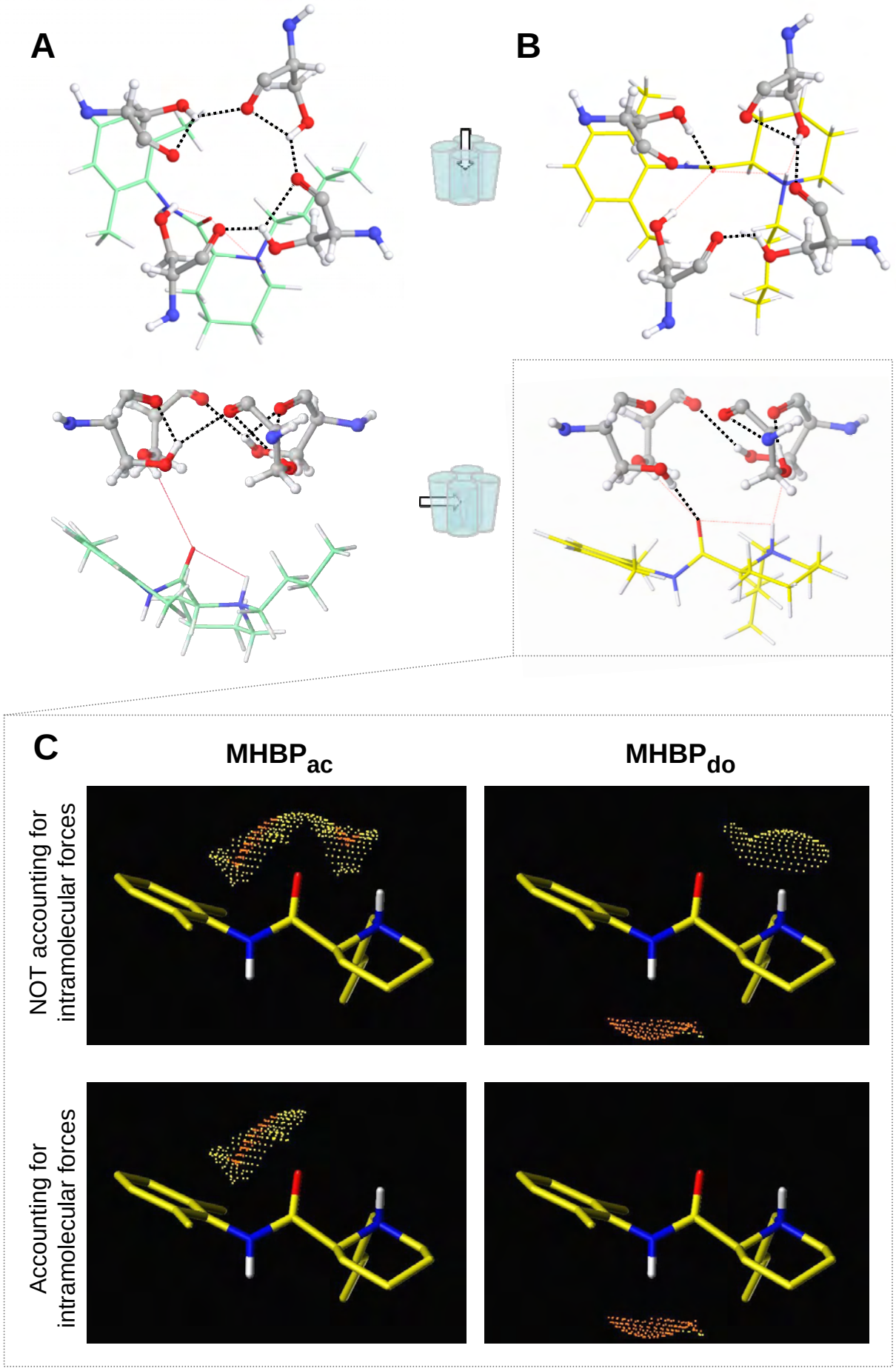

Fig. 7: Crown-shaped network of hydrogen bonds involving Ser624 residues in the WT hERG channel, and hydrogen-bonding capacity by computing the MHBPs of levo-(S)-bupivacaine.

NB: see following page for complete legend.

Figure 7, Sintra Grilo *et al*.

Fig. 7: Crown-shaped network of hydrogen bonds involving Ser624 residues in the WT hERG channel, and hydrogen-bonding capacity by computing the MHBPs of levo-(S)-bupivacaine.

(**A**) Optimized binding modes of dextro-(R)-bupivacaine (carbons in light green) and (**B**) levo-(S)-bupivacaine (carbons in yellow) observed from the viewpoint described by the central scheme (arrows). Residues Ser624 (ball-and-stick representation) from all four α-subunits present different intra- and intermolecular hydrogen-bonding networks (black dotted line) regarding (R)- and (S)-enantiomer poses. Closer location of the carbonyl of the amide in the levo-(S)-bupivacaine allows for the formation of a hydrogen bond with one Ser624 side-chain hydroxyl. Good contacts (red dashed lines) depict intra-molecular consumption of the capacity of the protonated piperidine nitrogen to create a hydrogen bond with Ser624. In (**A**), a clear crown-shaped hydrogen-bonding network is seen involving side-chain hydroxyls and backbone carbonyls of Ser624. (**C**) Representation of hydrogen-bonding capacity by computing the Molecular Hydrogen-Bonding Potentials (MHBPs) on a solvent accessible surface around the binding conformation of levo-(S)-bupivacaine. *Upper panels*: calculated acceptor ($MHBP_{ac}$) and donor ($MHBP_{do}$) potentials without taking intramolecular forces into account; *lower panels*: calculated acceptor ($MHBP_{ac}$) and donor ($MHBP_{do}$) potentials with intramolecular forces taken into account. For both donor and acceptor potentials, accounting for or neglecting the intramolecular forces explains the loss or decreased availability of both the carbonyl and the protonated amine for intermolecular interactions.

Figure 7 (continued), Sintra Grilo *et al*.

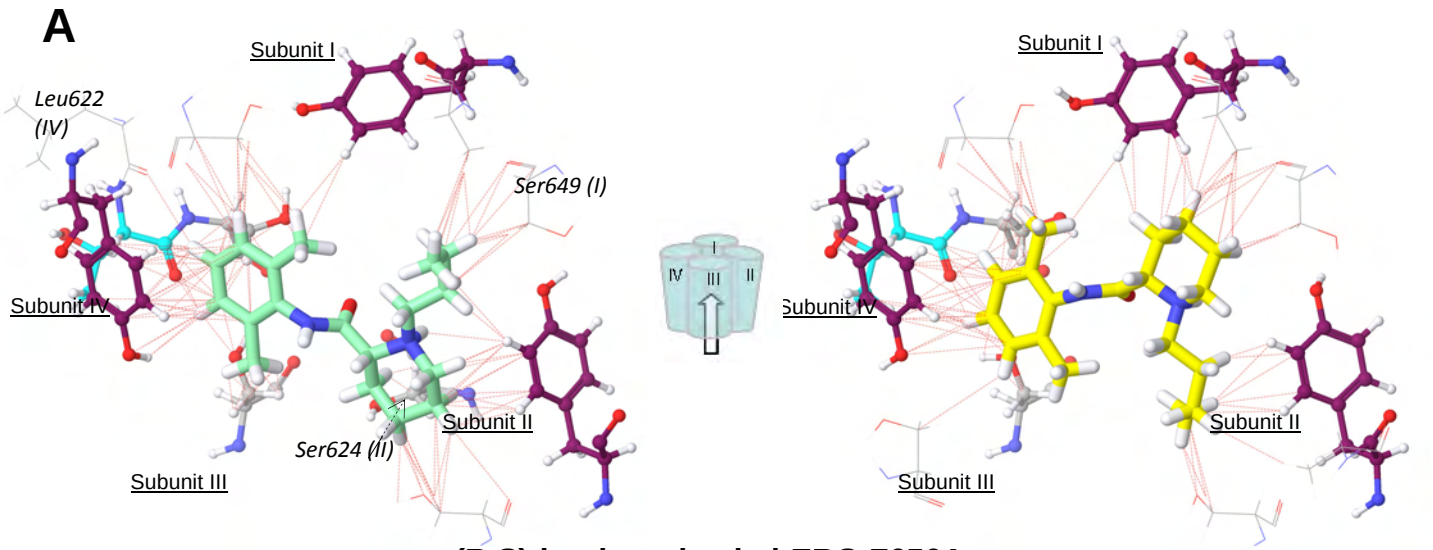

(R,S)-bupivacaine in hERG F656A

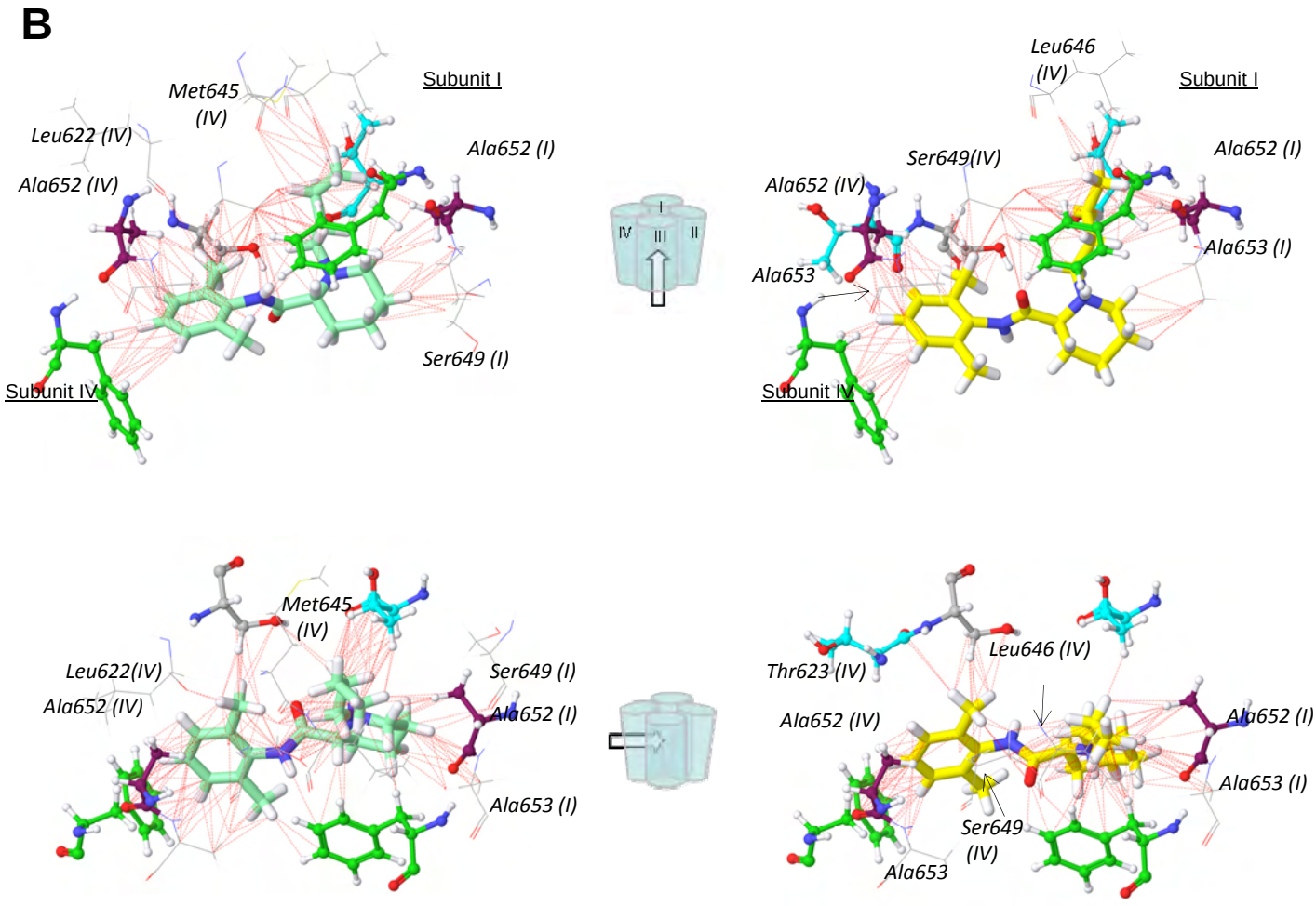

(R,S)-bupivacaine in hERG Y652A

Fig. 8: Binding modes of bupivacaine enantiomers optimized by molecular mechanics in the hERG F656A and Y652A mutant channels.

NB: see following page for complete legend.

Figure 8, Sintra Grilo *et al*.

Fig. 8: Binding modes of bupivacaine enantiomers optimized by molecular mechanics in the hERG F656A and Y652A mutant channels.

(**A**) Dextro-(R)-bupivacaine (carbons in light green) and levo-(S)-bupivacaine (carbons in yellow) inside the hERG F656A cavity, presented with good contacts (red dashed line). The poses obtained resemble the binding modes retrieved in the WT channel, except an important loss of residue participation in subunit I of hERG F656A. (**B**) Dextro-(R)- bupivacaine and levo-(S)-bupivacaine (same color-coding) inside the hERG Y652A cavity. Contrary to the results obtained with hERG WT and F656A channels, binding sites are lower and laterally shifted (contribution of two subunits only) in the Y652A cavity. In (**A**) and (**B**), viewpoints (arrows) are described by the central schemes. Residues investigated in this study are highlighted in a colored ball-and-stick representation (Ser624, gray; Thr623, cyan; Tyr652, purple; Phe656, green), while others are in wireframe and labeled.

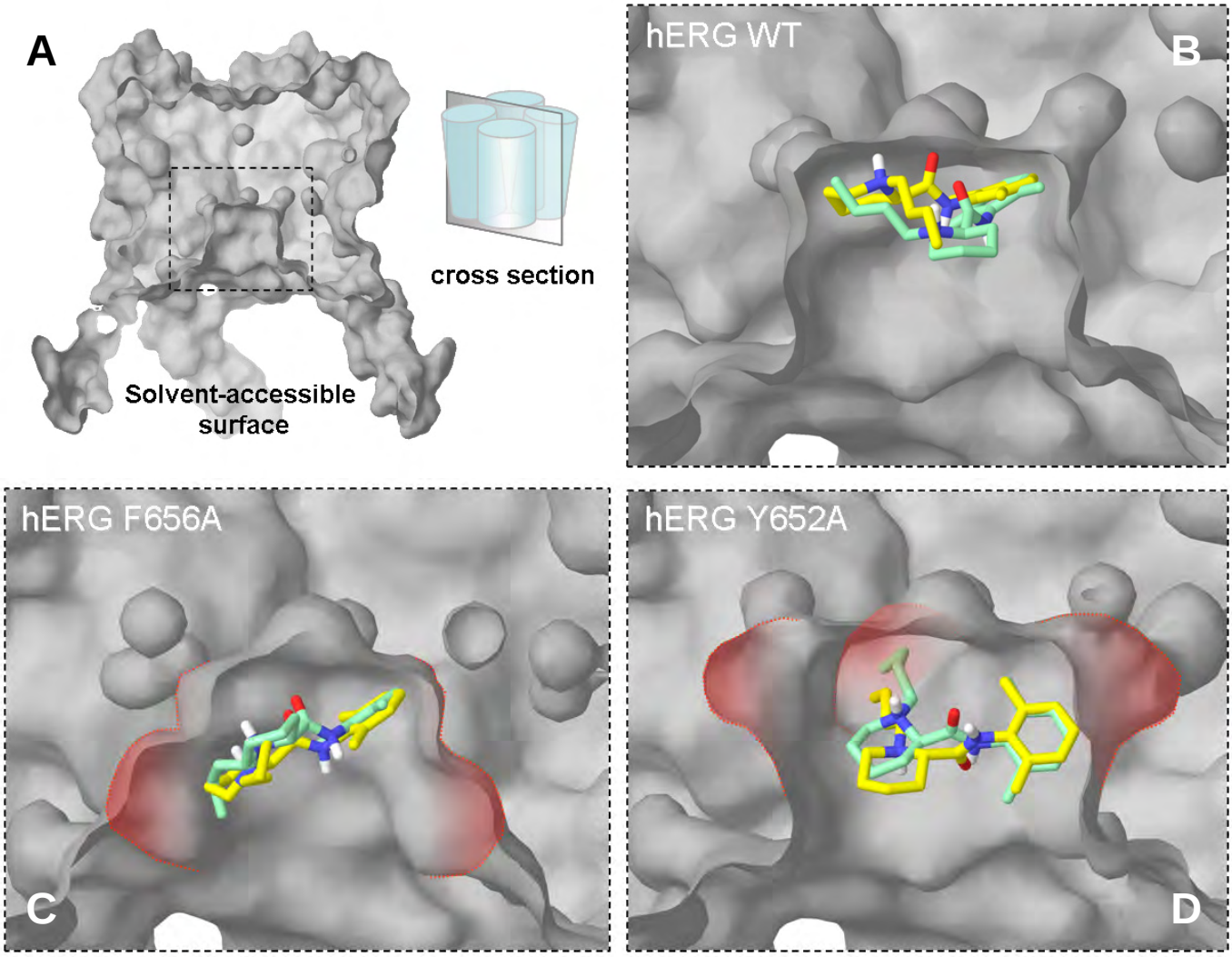

Fig. 9: Solvent accessible surface of hERG pore homology model with sagittal section through pore vestibule.
(**A**) Cross section of the hERG channel solvent accessible surface using a probe with 1.40 Å radius. (**B**) Magnification of hERG WT binding site, (**C**) of mutant hERG F656A binding site with conic shape and (**D**) of mutant hERG Y652A binding site. In (**B**) to (**D**), optimized levo-(S)-bupivacaine (carbons in yellow) and dextro-(R)-bupivacaine (carbons in light green) binding modes are presented superimposed. Mutation of residues Tyr or Phe to Ala induces opening of new cavities (red shades) in the pore vestibule that alter the binding mode of ligands compared to WT hERG channel.

Figure 9, Sintra Grilo *et al*.

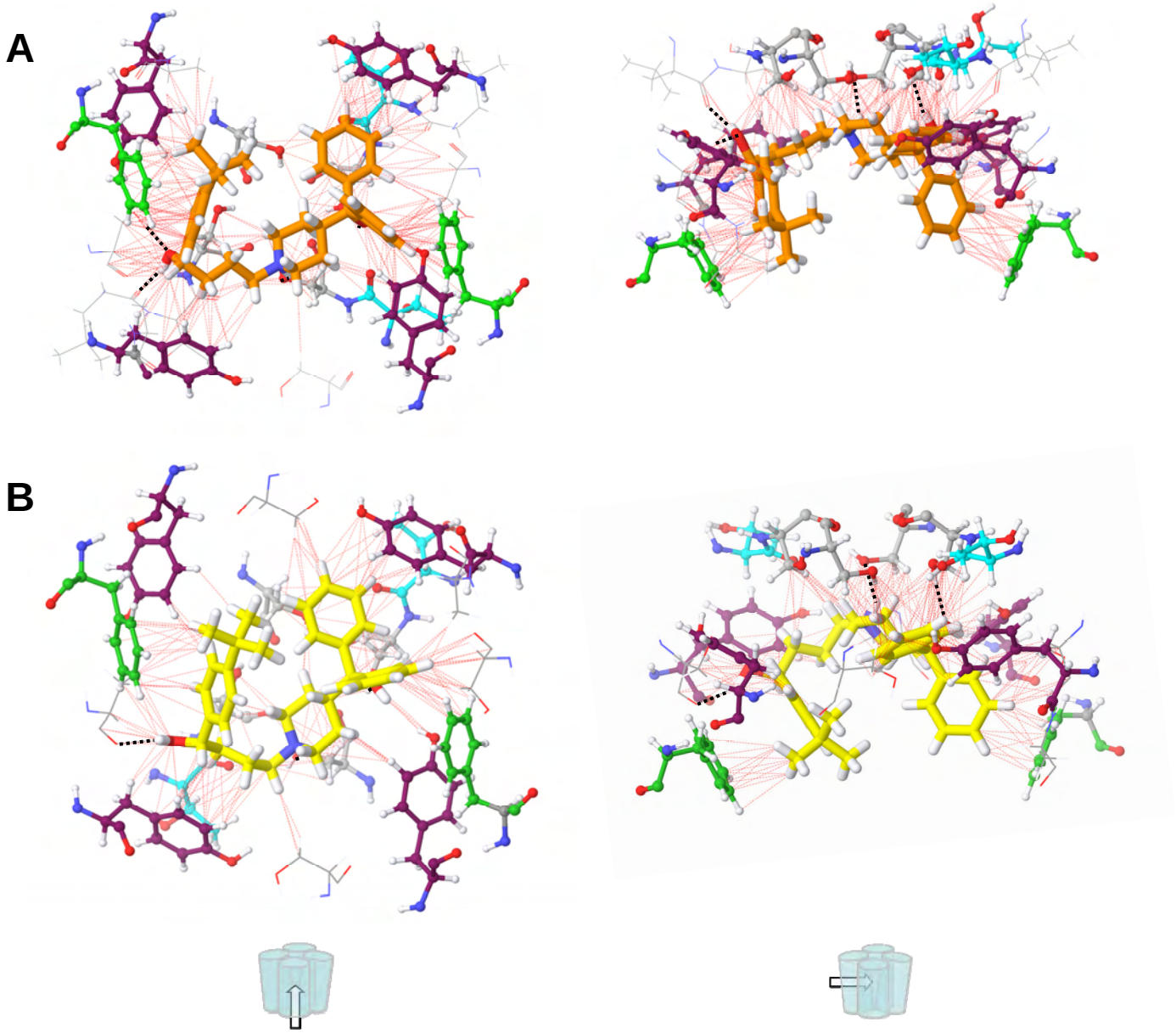

Suppl. Fig. 1: Optimized binding mode of (S)-terfenadine in hERG WT channel vs Farid's model.

(**A**) (S)-terfenadine (carbons in orange) according to the publication by Farid et al. (2006) or (**B**) (R)-terfenadine (carbons in light green) is presented with hERG WT residues, within a 5-Å shell around it, creating good contacts (red dashed lines) or hydrogen bonding (black dotted line) with the ligand. Both (**A**) and (**B**) are seen from the same viewpoint (arrows) as described by the scheme. Tyr652 residues (purple) have been flexibilized during docking process (GOLD 4.0). Residues investigated in this study are highlighted with ball-and-stick representation and following color-coding: Ser624 gray; Thr623, cyan; Tyr652, purple; Phe656, green, others are in wireframe. Except for one hydrogen bond, the major interactions between (S)-terfenadine and hERG WT residues are retrieved in our optimized binding mode compared to Farid's model.

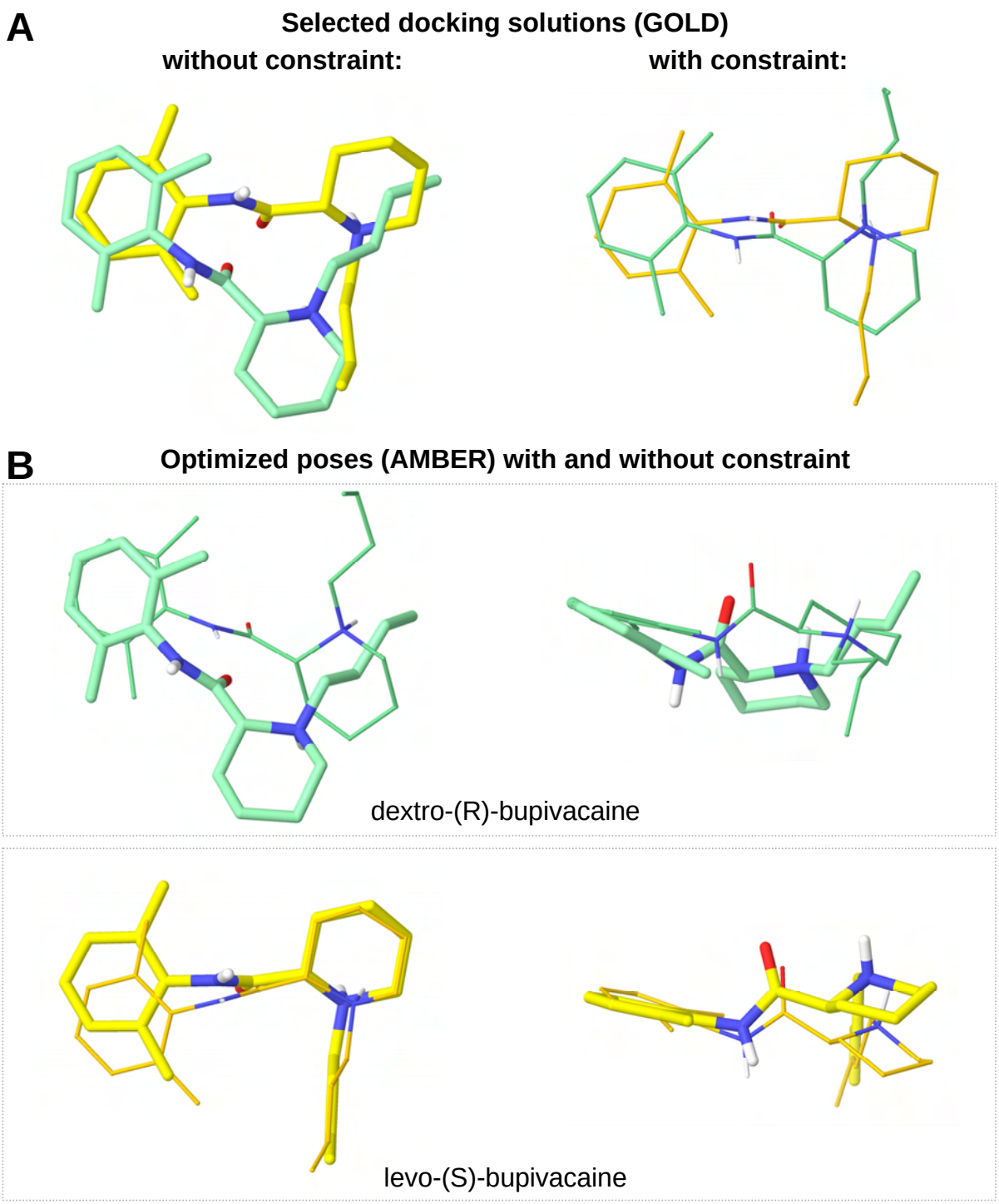

Suppl. Fig. 2: Selected docking solutions (GOLD) of bupivacaine enantiomers retrieved with or without constraint and binding modes of these poses after molecular mechanics optimization (AMBER) in the hERG WT channel.

(**A**) Selected docking solutions of dextro-(R)-bupivacaine (carbons in light green) and levo-(S)-bupivacaine (carbons in yellow) obtained either without (thick) or with (thin stick representation) hydrogen-bonding constraint. In (**A**), both superimpositions are observed from the same viewpoint. (**B**) *Upper panel*: dextro-(R)-bupivacaine poses, without (thick) or with (thin stick representation) hydrogen-bonding constraint. *Lower panel*: Similar representations regarding levo-(S)-bupivacaine poses after optimization. Each panel in (**B**) depicts bupivacaine ligands observed from two orthogonal views. Optimized poses for levo-(S)-bupivacaine show better superimposition, with and without constraint, than for dextro-(R)-bupivacaine.

IV.D. Complementary discussion

We presented here two distinct studies that, nevertheless, share a common subject: the stereoselective block of hERG channel.

As regards the effects of methadone enantiomers on hERG current (*Publication 4*), we demonstrated that (S)-methadone is more potent at blocking hERG channels than the (R)-form. Methadone is the third marketed drug (after bupivacaine and ropivacaine) proved to exert a stereoselective blocking action on I_{hERG}. Further electrophysiological experiments were carried out in our laboratory (at RT) in order to identify the stereoselective mechanism of block. For instance, a two-step protocol was used to assess voltage-dependence of block for different concentrations of (R)- and (S)-methadone. Although the results (not shown) provided no statistical differences, a tendency appeared at positive potentials (faster opening of hERG channels), for which the (S)-enantiomer blocked the current more than the (R)-form. Kinetics of the onset of block was also investigated for methadone enantiomers. During a 30-s depolarizing pulse (steady-state), perfusion of the hERG-blocker was initiated and time constants of current decrease were calculated. Here again, the rate of onset of block seemed faster for (S)- compared to (R)-methadone, although this finding was not supported by statistics (data not shown). Methadone enantiomers (20 μM at RT) were also tested separately on hERG F656A and S624A mutants: in both cases, no stereoselectivity was observed suggesting a possible role of Phe656 and Ser624 in the stereoselective recognition. Moreover, sensitivity of hERG F656A channel to (R,S)-methadone block was significantly decreased (~55% current inhibition in WT *vs* ~30% in F656A, 20μM), strengthening the idea of phenylalanine residues playing a role in the binding site. Despite these results, electrophysiological investigations of (R)- and (S)-methadone block of hERG channels ceased in favor of other running projects. Of special interest is the reproduction by another group of the stereoselective hERG blockade by methadone, thus confirming our findings. In this later publication (Lin *et al.* 2009), current block was assessed in *Xenopus* oocytes but IC_{50} values (0.10 ± 0.01 mM *vs* 0.27 ± 0.01 mM, for (S)- and (R)-form, respectively) cannot be compared to ours, as it is recognized that the

oocyte system leads to a significant underestimation of a drug's potency as a hERG-blocker. In addition, the authors did not further investigate the mechanism underlying the stereoselectivity.

It is worth mentioning that another synthetic μ-agonist – the acetylated analog of methadone – has been implicated in several cases of severe arrhythmia and TdP, thus prompting its withdrawal from the market (Deamer *et al.* 2001). Acetylation of methadone creates an additional asymmetric center and consequently four enantiomers of *acetylmethadol*, or two pairs of diastereomers named α and β (see Appendix II). Of these, the α series are more potent analgesics and less toxic than the β series. However, only the *levo-α-acetylmethadol* (LAAM), which derives from (S)-methadone, has been commercialized. This derivative was developed as a replacement for methadone owing to its extremely long half-life (effect of active metabolites) reducing the interval of drug delivery (Newman *et al.* 2002). Nevertheless, since the dextrorotary α-enantiomer (DAAM) derives from the active (R)-methadone, DAAM is expected to be more potent than LAAM (reviewed in Newcombe 2006). Indeed, LAAM has proven to be a less potent analgesic than its diastereomer, but it appeared to be the least toxic of all isomers in early animal studies (lower half maximal lethal dose). In later studies, the α-acetyl derivative of (S)-methadone was demonstrated to inhibit the hERG current ($IC_{50\ LAAM}$[9]: ~2 μM), but information about DAAM (related to (R)-methadone) or remaining enantiomers is lacking (Katchman *et al.* 2002). A study of I_{hERG} block evaluating all four enantiomers of acetylmethadol could certainly bring constructive information about mechanisms or determinants of stereoselectivity towards the K^+ channel.

As regards the clinical study of MMT patients presented in *Publication 4*, individuals identified with *CYP2B6* *6/*6 genotype showed anticipated higher plasma concentrations of (R,S)- and (S)-methadone, but also higher frequencies of prolonged and borderline QTc intervals. Since the proportion of CYP2B6 SMs in the Caucasian and African populations is non-negligible (~6%), carriers of such

[9] The chemical structure of LAAM depicted in Fig. 1 of Katchman *et al*. (2002) is wrong. Nevertheless, we assume that the drug used in the experiments was correct.

polymorphism are at potentially higher risk of severe cardiac arrhythmias and sudden death under (R,S)-methadone treatment. Knowing that the (S)-enantiomer is likely to be more cardiotoxic and that (R)-methadone is widely accepted as the "active enantiomer" for the desired effects, we suggested to reconsider the safety of the commercialized racemate towards pure (R)-methadone. Indeed, as mentioned in the discussion of *Publication 4*, such a "chiral switch" would decreased by 2-fold plasma concentrations of methadone thereby producing a safer cardiac profile, while not affecting the activity on the μ opioid receptors. Prescription of (R)-methadone would also greatly diminish the clinical concern of CYP2B6 slow metabolizer status for cardiotoxic effects. Moreover, no major effects are expected on the other beneficial activities of methadone, *i.e.* on the N-methyl-D-aspartate receptor, or serotonin and norepinephrin reuptake, since in all cases (R)- is more potent than (S)-enantiomer.

Recently, the group of Eap and colleagues investigated in a small cohort (39 MMT patients) the effect of substitution of a dose of racemate by half-dose of (R)-methadone (14 days), and they demonstrated that it significantly reduced QTc interval values. Opioid adverse effects and withdrawal symptoms were either absent or of low intensity and remained unchanged during the study, which confirmed that the half-dose of (R)-methadone was therapeutically equivalent to the racemic mixture (Ansermot *et al.* 2010). These encouraging results, in agreement our *in vitro* and *in vivo* pharmacogenetic data, should be confirmed by larger and prospective studies that assess the decrease of mortality. As a preventive measure, (R)-methadone (currently available in Germany only) should be preferred to (R,S)-methadone for all patients (treated for pain or under MMT) in order to reduce the risk of cardiac toxic effects and sudden death. As a matter of fact, early studies in the 1960's already pointed out a disadvantageous side-effect profile of racemic methadone compared to the (R)-form, but they did not receive the deserved impact (reviewed in Gaertner *et al.* 2008). Since our publication revealing the stereoselective cardiotoxicity of methadone came out, increasing number of health professionals claimed for a better assessment of risks and pure (R)-methadone

prescription (Lin *et al.* 2009; Gaertner *et al.* 2008; Wilcock & Beattie 2009; Ansermot *et al.* 2010).

Chiral switching is the term used for development and/or commercialization of single enantiomers in place of a previous racemic mixture. Reasons for marketing a pure isomer might appear purely economical – as substitution by the single enantiomer may be a good way to extend patent franchise – or because a different indication or safety profile is found, such as proposed for (R)-methadone. The potential advantages of chiral switching include an improved selectivity and decrease of side effects, a reduced propensity of drug-drug interactions or an improved onset of duration of effect (Tucker 2000). A case study of chiral switching is levo-(S)-bupivacaine. In 1979, seven cases of sudden cardiovascular collapse, occasionally lethal, were reported following presumed inadvertent intravenous injection of racemic *bupivacaine* and *etidocaine* (both local anesthetics). Re-evaluation of the systemic safety of amide anesthetics was initiated, and it ended with the conclusion that (S)-isomers were significantly less cardiotoxic than the racemic mixture of anesthetics (reviewed in Tucker 2000).

With regard to the *Publication 5*, the local anesthetic bupivacaine was, and is still to our best knowledge, the molecule presenting enantiomers with the highest stereoselective effect towards the repolarizing hERG K^+ channel (~7-fold *vs* ~2.5-fold for methadone enantiomers, at RT and similar experimental conditions). This was essential for our computational strategy since we intended to perform docking studies. Moreover, Siebrands and Friederich (2007) carried out a complete mutagenesis study on residues involved in inhibition of hERG channel by bupivacaine racemate. Their work revealed to be an important prerequisite for our study in that it comforted the hERG binding site of this anesthetic was located in the pore cavity. Different groups also concluded that bupivacaine and related molecules bound to the open and, less probably, to the inactivated states of hERG channel (Gonzalez *et al.* 2002; Siebrands & Friederich 2007), which gave confidence to the open state homology model selected.

Among the amino-amide class of local anesthetics, several molecules are used in the clinic and differ simply by the length of their N-alkyl substituent (number of carbons, nC): a butyl group (4C) for bupivacaine, a propyl group (3C) for ropivacaine, or a methyl group (1C) for mepivacaine (**Figure 20**). The substituent length was already proposed to influence the potency of these local anesthetics to block $K_v1.5$ channels (Valenzuela *et al.* 1997). Similar observations were found for hERG channels, in which the inhibitory potency of local anesthetics significantly correlated with the number of carbons of the N-substituent (Gonzalez *et al.* 2002). The length of the alkyl chain also determines the lipophilicity, which was already proposed as a structural requirement for hydrophobic interactions between the drug and the channel (Siebrands *et al.* 2005). By plotting lipophilicity against inhibition of hERG current for the racemates and single enantiomers of a series of anesthetics (**Figure 20**), it suggests the longer the alkyl chain, the higher the potency and

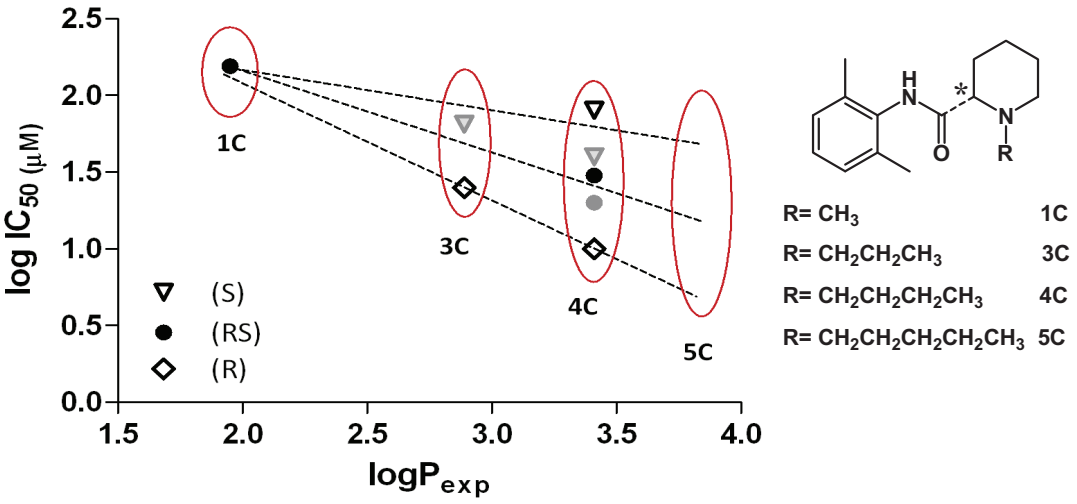

Figure 20 : Correlation between lipophilicity and potency of hERG blockade in a homolog series of local anesthetics.

Length of the N-substituent is mentioned by the number of carbons (C) and the different forms ((S), (RS) and (R)) of a molecule are assembled by a red circle: *mepivacaine* (1C), *ropivacaine* (3C), *bupivacaine* (4C) and *"pentivacaine"* (5C). Experimental logP values ($logP_{exp}$) were retrieved from the online program ADME *Boxes* (Internet Source 7). Values of IC_{50} (µM, in mammalian cells) are those from Siebrands *et al*. (2005) and ours; grey triangles are values extrapolated from percentage of inhibition. For racemic bupivacaine, both previously calculated (grey dot) and our *log IC_{50}* (black dot) are presented.

stereoselectivity of block. Obviously, this correlation is based on a too small set of data to be reliable. Nevertheless, it appears that the pentyl analog of bupivacaine, "*pentivacaine*"[10] (5C), would display higher affinity and difference between its enantiomers in the inhibition of the hERG current (**Figure 20**). This could be verified in the future by testing this drug with the presented patch-clamp–*in silico* procedure. As experimental values of inhibition were available for ropivacaine, we used the developed strategy to dock its (R)- and (S)-enantiomers in our hERG homology model. Unfortunately, convergence of docking poses was poor. This might be explained because i) ropivacaine has a lower affinity than bupivacaine for the hERG target, and thus the power of our computational tools becomes insufficient to discriminate the best pose; or because ii) ropivacaine is smaller and can therefore accommodate more easily and with different binding modes in the hERG cavity. These unproductive results using a shorter alkyl analog of bupivacaine support the idea that, conversely, a longer chain as N-substituent would yield more contrasted effects between the (R)- and (S)-enantiomer of the local anesthetics and would therefore allow to challenge and improve our model.

We are aware that the principal limitation of the work presented in *Publication 5* is the lack of the electrophysiological proof of the non-stereoselective effect of terfenadine on I_{hERG}. The main technical issue regarding chiral and all the most pharmaceutical compounds is that the commercial availability of pure enantiomers is often limited. Personal requests have to be made to the companies that produce the drug or it requires particular orders for separating the racemate, which may be quite expensive and need long time of delivery. Nevertheless, one publication, due to Pinney *et al*. (1995), assessed the action of terfenadine enantiomers on QT interval. By perfusing isolated guinea pig hearts with equal concentration of racemic mixture, pure (R)- and (S)-terfenadine, the authors demonstrated that both QT interval and APD_{90} were increased to the same extent with all forms, which supports the equivalent effect of terfenadine enantiomers.

As regards the block of hERG mutant channels, some residues demonstrated to be important in drug recognition after binding mode analysis. The residues Ser649 and,

[10] Non official name since the molecule is not marketed as a drug.

to a lesser extent, Ala653 and Leu622 revealed to be important for drug recognition. Generation of hERG channels mutated in these positions should be done to complete the picture of stereoselective effects of bupivacaine on I_{hERG}. Combination of two mutations on a subunit could also bring important insights. Imai *et al*. (2009) employed an interesting apporach that deserves attention. They developed *tandem dimers mutants* of hERG – *i.e.* two α-subunits concatenated, one WT and one mutated – that can be used for electrophysiological measurements. Using a synergic approach of patch-clamp technique and homology model (based on the MthK crystal), they generated docking poses for different well known hERG blockers, including *terfenadine*. Their binding modes for terfenadine were, however, quite dissimilar to those retrieved by Farid *et al*. (2006). In addition, Imai and coworkers concluded that Ser624 was not involved in the antihistaminic recognition, which is not consistent with the conclusions of Kamiya *et al*. (2008) or Farid *et al*. (2006). Future development of concatenated hERG channels bearing the desired combination of mutations in the four α-subunits may become a valuable tool to better assess stereoselective effects of drugs.

With regard to electrophysiological studies, it is worth mentioning that we could go further in the understanding of the mechanism of inhibition. Indeed, a single residue mutation in the hERG subunit does not only affect steric and physico-chemical properties of the K^+ channel cavity, but also affects gating and kinetics. Therefore, it cannot be ruled out that differences in channel gating may have influenced differently the local anesthetic affinity of the enantiomers. The G648A mutant, which presents marked and reversed stereoselectivity of block by bupivacaine, would be a good candidate for this type of investigation.

One major limitation of our procedure is that docking of drugs occurs in an almost static and open protein, while inhibition of I_{hERG} is assessed in a dynamic process. When currents are recorded at -120 mV, the channels have previously opened, inactivated, and are recovering from inactivation while deactivating. The physical effects of the conformation state to the binding (rearrangement of side chains in the cavity) cannot be evaluated. Masetti *et al.* (2007) presented an interesting study combining molecular dynamics (MD) and docking studies. They first generated both

closed and open state models of hERG that were subsequently submitted to MD simulations (ns time-scale) in explicit membrane environment. Then, using hERG conformations coming from MD simulations and also MD snapshots, they performed docking experiments, using GOLD, of the potent hERG blocker *astemizole.* The closed models appeared not suited for the binding astemizole, since the cavity lumen was too crowded. The authors identified reasonable binding modes only when using snapshots from MD simulations of open hERG. Moreover, they concluded that in their crude open homology model, the channel cavity was not in a proper rotamer configuration, in particular Tyr652 (Masetti *et al.* 2007). These authors assumed that exploiting MD snapshots in docking studies allowed to capture some *induced-fit effects* related to the side chain conformation of aromatic residues (Masetti *et al.* 2007). Remarkably, their findings (open state model and conformation of Tyr652) are in good agreement with the homology model of Farid *et al.* (2007), and the option that we chose, *i.e.* to flexibilize all four Tyr652 resides.

The quality of different homology models published was assessed in a recent publication (Stary *et al.* 2010), which reminded that the accuracy of the models depends critically on the sequence identity between the template and the target. The overall sequence identity of hERG compared to potential templates is low (17,6% for KcsA and 28,6% for KvAP). As regards the innermost helix (S6), sequence identities raise up to >30% and unambiguous alignment is possible owing to the presence of conserved glycines and the signature sequence of the SF (Stary *et al.* 2010). Differences in alignment of segment S5 have been generally neglected. As the S5 helices are in close contact with the S6 segments, they are likely to influence the drug binding site. The model of Farid *et al.* (2006) scored low in almost all of the quality assessments performed, although the authors of the study (Stary *et al.* 2010) mention that this model “performed quite well in docking analysis”. According to the same authors, the docking results of Farid’s model are influenced by the adjustment of glycine residues in S5 and S6 helices. This information about probable unoptimized alignment of S5 sequence in the homology model employed should be taken into account for future refinements of our model.

Importantly in our experimental recordings, the direction of ion flow inverts between the pre-pulse test (+40mV) and the repolarization step (-120 mV) due to the change in driving force. If we reconsider the "plug" theory expressed in the discussion part of *Publication 5*, we can envisage that a potent inverted flux of K^+ ions may remove blocking molecules from the binding site while the channels are open. If it is so, the process has to be fast and stabilize rapidly, as no "run-up" of peak tail current is seen between the runs. Moreover, this would allow to explain the results of Siebrands and Friederich (2007). Indeed, these authors showed that tail currents measured at -120 mV were less sensitive to inhibition by bupivacaine than those elicited at -40 mV (~5-fold difference in IC_{50} of racemic bupivacaine, in *Xenopus* oocytes). This hypothesis would deserve further investigation.

The purpose of the presented study was not, in any case, to debate the cardiac safety of the levorotatory form compared with the racemic bupivacaine. As mentioned earlier, bupivacaine is not a high-affinity blocker of hERG (IC_{50} in the μM range), and such a 7-fold difference between enantiomers has seemingly no clinical relevance. The case of methadone is different, since the difference in hERG blockade is accompanied by additional stereoselective PK and PD that emphasizes the effect of (S)-methadone. The global evaluation of the stereoselective effect of a chiral drug is mandatory, and should include the current knowledge about pharmacogenetic variations. The cavity of the hERG channel has proven to be large and promiscuous, and there might be no therapeutic compound able to exert an "all or nothing" blocking effect. Nevertheless, we are convinced that chiral molecules exist yielding a marked stereoselective effect on hERG and that these molecules could be highly informative with respect to drug binding. Jamieson *et al.* (2006) reviewed the case of *macrocyclic 3-aminopyrrolidinone* farnesyltransferase inhibitors and structural modifications to design out hERG affinity. Within this macrocyclic series, hERG binding proved to be highly sensitive to chiral modifications, as one (R,R)-compound presented high affinity towards hERG (IC_{50} from binding assays = 0.15 μM), whereas its (S,R)-diastereomer did less (IC_{50} = 9.1 μM). In addition, both presented similar potencies in the block of the pharmacological target (Bell *et al.* 2002). We believe that stereoselective computational studies, like the one performed in *Publication 5*,

help understanding the molecular requirements of block as a complementary tool to the “gold standard” electrophysiology. Moreover, we are confident that assessing small stereoselective differences of binding and block of hERG channel is an elegant way to challenge and in the end to refine current homology models.

Part V:
Conclusion and perspectives

V. Conclusion and perspectives

Since the discovery of the *human ether-à-gogo related gene* about 15 years ago, this potassium channel has become notorious because of its implications in long QT syndrome. It turned out to be a prominent issue for the pharmaceutical industry and regulators, as well as a tricky problem to solve in public health.

The promiscuous pore cavity of the hERG channel allows for accommodation of many diverse and therapeutically unrelated drugs. The resulting block of K^+ current and delayed repolarization in the cardiomyocyte are referred to as *drug-induced long QT syndrome*. There is undeniably a link between hERG channel block and the occurrence of severe *Torsades de Pointes* arrhythmias. Nevertheless, even if all drugs incriminated in QTc interval prolongation and lethal arrhythmias proved to inhibit the hERG current, the opposite is not always true. hERG channel blockade remains a surrogate marker of delayed repolarization and cardiotoxicity. For economical and time-sparing reasons, the hERG liability of a compound should be assessed as early as possible during drug development. Pharmaceutical industries put initially their hopes in *in silico* virtual screenings. These tools are currently not powerful enough to discriminate among hERG blockers of medium affinity, which may still be developed as drugs. Since inhibition of hERG remains an indirect marker of the clinical risk, it is important to keep in mind that a compound that blocks hERG might be safe in practice. *Verapamil* or *citalopram* – two "blockbuster" drugs of invaluable clinical interest – would not have been developed if the hERG assays were in place at the time. Indeed, these drugs reduce the rapid component of the repolarizing currents at therapeutic concentrations, though without affecting QT interval or TdP clinically. These exceptions may be attributed, at least in part, to drug effects on other cardiac channels, such as type-L calcium channels, that mitigate or mask hERG block. Improvement of computational assessment of hERG blockade should be pursued, yet keeping in mind to use it as an alarm instead of a rejection tool, which otherwise would paralyze the drug-development process by supporting further attrition of pharmaceutical compounds that reach clinical stages. *In silico* tools can play a role later in the development process, as medicinal chemists may optimize the lead

compound and decrease its hERG affinity by discrete modifications according to docking simulations or QSAR studies. Although the patch-clamp technique is still considered as the "gold standard" assay, preclinical tests performed in more physiological models (see Appendix III) appear better suited for evaluation of the complex torsadogenic risk of a compound. The accuracy of these preclinical assays will be confirmed in the future.

Health authorities and professionals also live with the ghost of hERG and its correlated cardiac events. The number of drugs associated with prolongation of the QT interval – directly or not, attested or suspected – is significant. The decision taken by a physician, or a regulatory agency, to recommend the use of a drug is predicated on the assumption that the benefits of the therapy prevail over the risks. Benefits are usually well defined, but the risk assessment is not so straightforward. *Torsades de Pointes* arrhythmias were initially considered as *idiosyncratic* adverse effects of drugs or, in other words, reactions that do not occur in most people and are not explained by the known mechanisms of action. In 1998, Roden reviewed the current knowledge about TdP prediction in a paper entitled "*taking the 'idio' out of 'idiosyncratic'*" (Roden 1998). Indeed, the scientific community focusing on the long QT syndrome brought a better picture of the complex underlying mechanisms. In the beginning, significant effort has been put in understanding the *congenital* form of LQTS. With approaches similar to those presented in *Part III* of this manuscript, hundreds of variants of hERG have been identified, which produce QT interval prolongation or a latent effect that increases susceptibility of delayed repolarization by particular medicines. In the clinical practice, this knowledge translates into increased attention given to the patient's or family cardiac history. In suspected cases, ECG and possibly genetic screening should be performed to confirm the risk and to preclude future cardiac events. Investigating the *drug-induced* LQTS has evidently been crucial. Online resources can help non-cardiologists to recognize the drugs associated with a known risk (*www.QTdrugs.org*). Of special interest is the recent attention given to pharmacogenetics, which underlies the genetic interindividual differences in the PK and PD of a drug. In *Part IV* of this manuscript, we showed that population at higher risk can be associated with particular genetic

variants. Moreover, stereoselective block of the hERG channel – previously neglected – was demonstrated clinically relevant for *methadone*, whereas *bupivacaine* enantiomers allowed for development of a rational *in silico* model of hERG channel block. As regards the *acquired* form of LQTS, advances made in the field have to be recognized. Female gender and hypokalaemia have long been identified as additional risk factors of TdP, as well as other cardiovascular diseases and particular health conditions reviewed in this manuscript. Nevertheless, most information about regulation of the hERG channel function, in normal and pathophysiological conditions, is lacking for the moment. We presented in *Part II* a possible means of regulation of hERG channel density at the cell surface, though direct extrapolation to LQTS is not yet possible.

Although *Torsades de Pointes* with deadly outcomes are rare, each human loss remains a tragic event. The tragedy is even worse when medicine presumed to improve the patient's condition revealed to be the trigger. Researchers and medical community are not slowing down in their attempts for understanding the *acquired*, *congenital* and *drug-induced* form of long QT syndrome in order to avoid its harmful consequences. As the hERG channel appears to bear heavy responsibility, particularly in the drug-induced and type-2 congenital forms, this amazing ion channel will certainly stand in prominent position as regards future investigations.

Postscript

One may question why this potassium channel has always been so teasing. First, it was christened *ether-à-gogo* according to a fly shaking legs like a go-go-dancer. hERG kinetics are inexplicably different from its relatives of the *eag*-family. Its pore cavity is extraordinary promiscuous to drugs, including illegal *cocaine* and *methadone*! Finally, it is keen on *Torsades de Pointes*, a ballet choreography that takes place on the ECG. Its latest trait of humor? Trafficking-defective hERG mutants can be rescued by molecules…that block the hERG channel!

Appendices

Appendix I : Compounds known to block the hERG channel

Note that IC_{50} values for inhibition of I_{hERG} (mammalian cells or *Xenopus* oocytes) or I_{Kr} (animal cardiomyocytes) are expressed between brackets (in μM) and were retrieved from the database created by R. R. Fenichel (*www.fenichel.net/pages/Professional/subpages/QT/Tables/pbydrug.htm*).

Antibiotics	
Erythromycin (55-390) 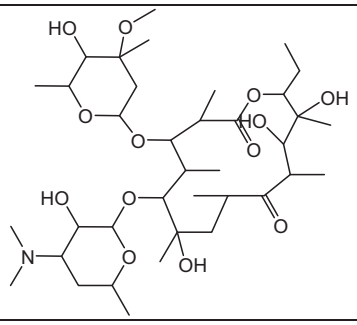	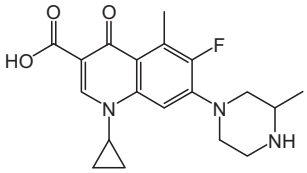 **Grepafloxacin** (27-50) Withdrawn in 1999
Antispasmodics	
Terodiline (0.004-0.700) Withdrawn in 1991 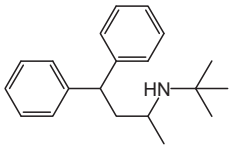	
Antihypertensive agents	
Mibefradil (Ca^{2+} channel blocker) (0.40-1.43) Withdrawn in 1998 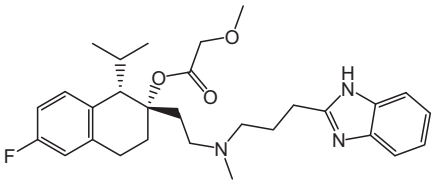	
Antidepressive agents	
Amitriptyline (3-10) 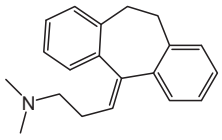	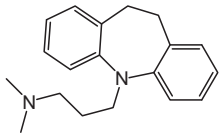 **Imipramine** (3.4)
Antipsychotics	
Sertindole (0.005-0.014) Withdrawn in 1998 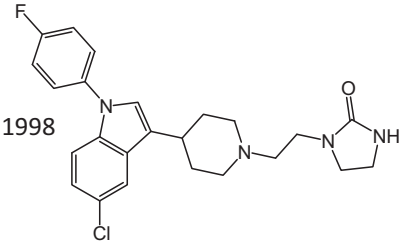	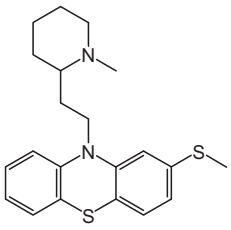 **Thioridazine** (0.04-1.25) Withdrawn in 2005

Antiarrhythmics

Sotalol (class II, III)

(100)

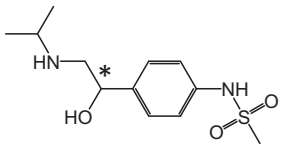

E-4031 (class III)

(0.008-1.4)

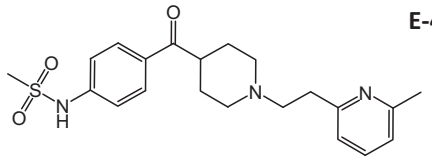

Ibutilide (class III)

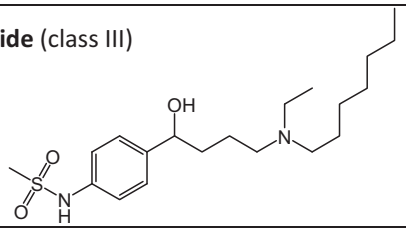

Dofetilide (class III)

0.001-0.125

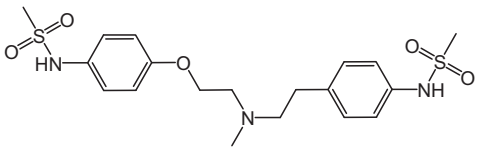

MK-499 (class III)

(0.12-0.40)

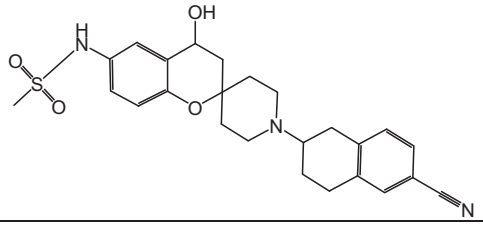

Antineoplastics

Tamoxifen (Selective Estrogen Receptor Modulator)

(~1)

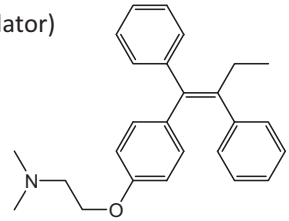

Gastro-intestinal prokinetics

Cisapride

(0.007-0.044)

Withdrawn in 2000

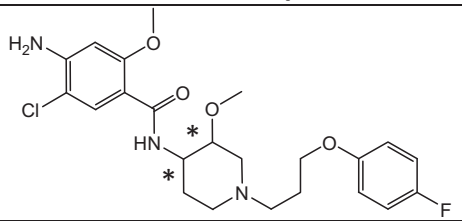

Antifungal agents

Ketoconazole

(2.5-50)

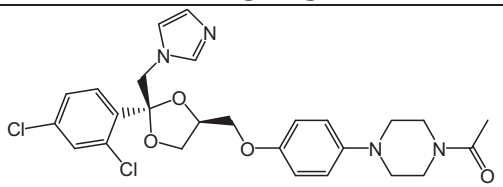

Antihistaminics (H1)

Astemizole

(0.001-0.330)

Withdrawn in 1999

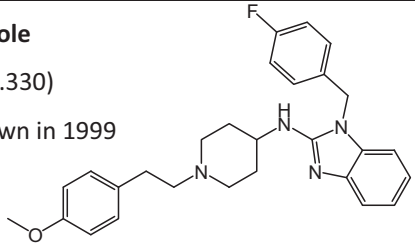

Terfenadine

(0.05-0.50)

Withdrawn in 1998

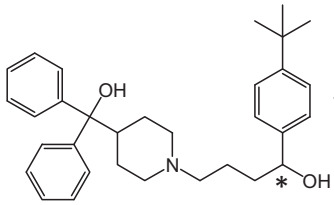

*****: chiral center

Appendix II : Chiral compounds known to block the hERG channel

Methadone

(S)-methadone

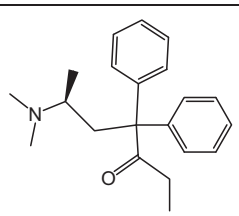

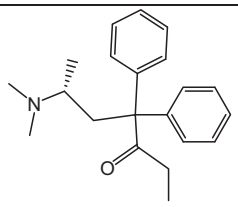

(R)-methadone

Acetylmethadol

levo-α-acetylmethadol

LAAM (3S,6S)

Only enantiomer available on the market.

Withdrawn in 1999

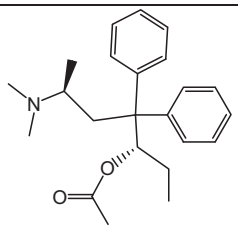

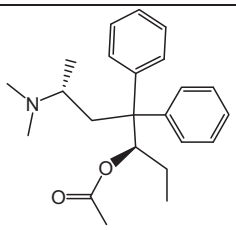

dextro-α-acetylmethadol

(3R,6R) DAAM

α diastereomers

levo-β-acetylmethadol

(3S,6R)

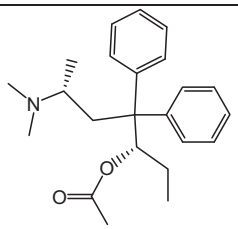

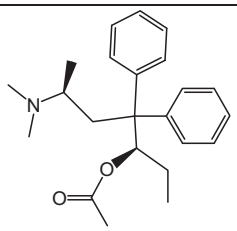

dextro-β-acetylmethadol

(3R,6S)

β diastereomers

Terfenadine

(S)-terfenadine

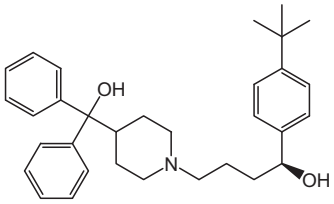

Withdrawn in 1998

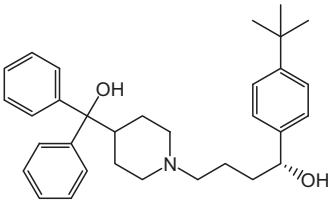

(R)-terfenadine

Withdrawn in 1998

Bupivacaine

levo-(S)-bupivacaine

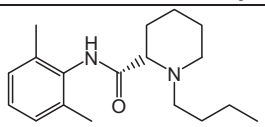

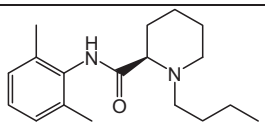

dextro-(R)-bupivacaine

Appendix III : Overview of preclinical "QT models" and parameters evaluated

	Model	Type of preparation (most common)	Parameters measured or emphasized									
			Channel or current block	Repolariz.	EADs	Triangul.	Reverse use-dep.	Instab./ Variab.	Dispers.	ECG-QT or alike	QT morphol.	TdP or alike
in silico	**Ligand- or target-based**	SAR-QSAR, decision trees, classifications, docking.	X									
in vitro	**Radiolabeled drug binding assay**	HEK293-hERG membranes (usually [^{3}H]dofetilide)	X									
	Rb^+ efflux assay	HEK293-hERG loaded with Rb^+. (Drug incubation is followed by depolariz. Rb^+ efflux is determined by flame atomic absorption of cell lysates)	X									
	hERG-Lite®	HEK293-hERG WT and class-2 mutant. (Based on pharmacological rescue of blocking drugs)	X									
in vitro ex vivo	**hERG patch-clamp "gold standard"**	channels overexpressed (in mammalian cells, X. oocytes) or in isolated cardiomyocytes	X									
ex vivo	**APD, Repolarization**	Tissue: Purkinje fibers, papillary muscl. (dog, sheep, cat, rabbit)		APD	X	X	X			X		
	Wedge	Tissue slice from left ventr. (dog, sheep, cat, rabbit, guinea pig		APD	X				X	X		X
	Langendorff	Isolated heart (rabbit, guinea pig)		MAPD	X	X	X	X	X	X		X
in vivo	**QT measurements**	Animals (dog, pig, monkey, guinea pig)								X	X	X
	Chronic AV-block	Animals (dog)		MAPD	X			X	X	X		X

Appendix III : (continued)

***List of abbreviations used in the table**:*

Repolariz. : Duration of Repolarization

EADs : Early After Depolarizations

Triangul. : Triangulation of Action Potential (shape of AP)

Reverse use-dep. : reverse use-dependence of drug

Instab. / Variab. : Instability, beat-to-beat variability of repolarization (MAPD)

Dispers. : MAPD or APD Dispersion (difference between endo- and epicardial)

QT Morphol. : QT morphology (Tpeak-Tend)

APD: Action Potential Duration

MAPD: Monophasic Action Potential Duration

Appendix IV :

PERSPECTIVES

Male and female equality: still far from goal

Liliana Sintra Grilo[1,2]
and Hugues Abriel[1,3]
[1] *Department of Pharmacology and Toxicology, University of Lausanne, Switzerland*
[2] *Pharmacochemistry, School of Pharmaceutical Sciences, University of Lausanne, University of Geneva, Switzerland*
[3] *Service of Cardiology, CHUV, Lausanne, Switzerland*

Email: hugues.abriel@unil.ch

It is well established that the cardiac electrophysiological properties of males and females are not equal. In particular, the ventricular repolarization of the female heart is characterized by a longer rate-corrected QT interval (QTc) of the electrocardiogram (ECG, see Fig. 1). This may be the reason why females are more prone to develop polymorphic ventricular tachyarrhythmias, called Torsades de Pointes (TdP), that occur when the ventricular repolarization is further delayed by intrinsic or external factors (Fig. 1) (Abi-Gerges *et al.* 2004). TdP may lead to syncope or to sudden cardiac death.

The concept of *repolarization reserve* was proposed a few years ago by Dr Roden to help predict one's risk of developing TdP (Roden, 1998). It has been suggested that, in a normal heart, rapid and orderly repolarization occurs thanks to the coordinated activation of different voltage-gated potassium channels. Several factors may reduce this repolarization reserve and make it more likely to precipitate TdP in at-risk patients. Hypokalaemia and cardiac diseases, e.g. congenital long QT syndrome (LQTS), are known to decrease the repolarization reserve, as well as treatment with drugs blocking potassium channels. It is important to note that women present an initially reduced repolarization reserve (Roden, 1998).

The potassium channel hERG (human *ether-à-go-go-related gene* channel) is under the spotlight since the discovery that many drugs may block it, and, as a consequence, the I_{Kr} current it generates. I_{Kr} is the rapidly activating delayed rectifier potassium current which plays a primary role for ventricular repolarization in humans and thus action potential duration (APD) and QTc (Fig. 1). This adverse effect of drugs, also referred as *drug-induced* LQTS (di-LQTS), should be considered as an iatrogenic channelopathy (Abriel *et al.* 2004), and, again in this case, males and females are not equal. Incidence of TdP under prescription of hERG-blocking drugs is about 60% more common in females than males (Abi-Gerges *et al.* 2004).

In an observational study (Rautaharju *et al.* 1992) investigating the sex differences of the QT interval, a 20-ms QTc shortening was observed after puberty in males, whereas female values remained unchanged throughout growth and reproductive years. Since this difference is absent before puberty, sex hormones were naturally hypothesized to play a role. The question of whether QTc is influenced by the menstrual cycle or in postmenopausal women under hormone therapy is controversial. A few studies reported no difference (Burke *et al.* 1997; Larsen *et al.* 1998), whereas others observed slight, but significant, QTc prolongation consistent with hERG inhibition by oestrogen (Rodriguez *et al.* 2001; Kadish *et al.* 2004). Moreover, removal of the ovaries in female rabbits shortened the QT interval, while hormone replacement using 17β-oestradiol (E2) lengthened it (Drici *et al.* 1996).

In this issue of *The Journal of Physiology*, Kurokawa *et al.* (2008) postulate that E2 may

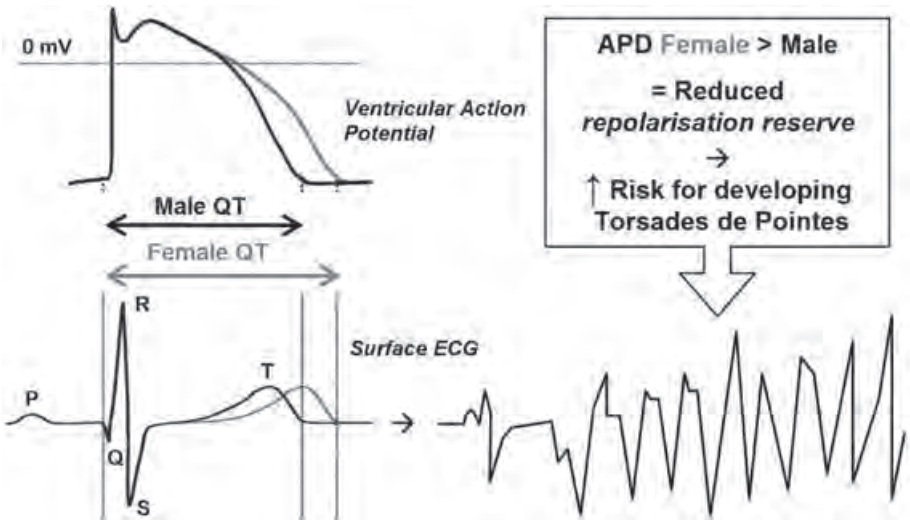

Figure 1. Scheme illustrating the ventricular action potential and surface electrocardiogram (ECG)
The QT interval – time between start of the QRS complex and end of T wave – reflects, in part, the action potential duration (APD). Females have a longer APD and QT interval than males. The *repolarization reserve* of females is smaller; hence, they are at higher risk for Torsades de Pointes when exposed to factors such as drugs blocking the hERG channel delaying further the repolarization.

DOI: 10.1113/jphysiol.2008.156398

also acutely modulate the hERG-mediated current via a non-genomic pathway. In this comprehensive study, the authors first showed a bi-phasic effect of E2 on the QT interval from Langendorff-perfused guinea pig hearts. Using high physiological concentrations of E2 (1 nM), QTc intervals were significantly prolonged, whereas at non-physiological concentrations (100 nM), it was shortened. The 1 nM effect was due to I_{Kr} inhibition, since patch-clamp recordings of cardiomyocytes showed that E2 reduced only I_{Kr}, but not I_{Ks} nor $I_{Ca,L}$. Higher E2 concentrations affected all tested currents, resulting in APD shortening. Since an oestrogen-receptor inhibitor did not antagonize the E2 effect, a direct, receptor-independent, inhibition of the cardiac I_{Kr} current was proposed.

In a second part, the authors studied the hERG channel expressed in HEK293 cells. They recorded the whole-cell biophysical properties of the suppression of the hERG current upon E2 superfusion. Maximum current was not decreased by E2, but the voltage-dependence of activation was shifted towards depolarized potentials ($\Delta V_{1/2}$: +3–4 mV), suggesting that E2 does not act as a pore blocker, but rather as a gating modifier.

The authors further investigated some of the molecular features of this interaction. Based on the main structural differences between dihydrotestosterone (DHT) and E2 (Fig. 5*A* in Kurokawa *et al.* 2008), they studied the role of the aromatic residues lining the pore of hERG. Tyr652 and Phe656 are known to be crucial for many drug–hERG interactions, and Phe specially for aromatic–aromatic ones (Stansfeld *et al.* 2007). Kurokawa *et al.* observed that only the Phe656 mutation abolished the E2-dependent modulation of hERG. Phe656 is also involved in the binding site of E4031, a potent hERG blocker. Surprisingly, E2 did not attenuate the E4031 block of hERG, as may have been expected if the two molecules would compete for the same site. Proposed explanations point at allosteric modifications of the blocker-binding site. Furthermore, ECG recordings were consistent with the patch-clamp findings, since QTc was also increased in guinea pig hearts when treated with both E4031 and E2, but not when DHT was added to E4031.

The study by Kurokawa *et al.* provides new insights into the possible causes making women more prone to develop di-LQTS. Whereas genomic effects of sex hormones have been previously shown to underlie this difference (Drici *et al.* 1996), this work convincingly describes effects of E2 that are independent of the oestrogen receptor. This new information will have to be taken into account when evaluating the risk of drug-induced TdP in females during the menstrual cycle. Future integration of these risks might one day lead to gender equality, at least in this field.

References

Abi-Gerges N, Philp K, Pollard C, Wakefield I, Hammond TG & Valentin JP (2004). *Fundam Clin Pharmacol* **18**, 139–151.

Abriel H, Schlapfer J, Keller DI, Gavillet B, Buclin T, Biollaz J, Stoller R & Kappenberger L (2004). *Swiss Med Wkly* **134**, 685–694.

Burke JH, Ehlert FA, Kruse JT, Parker MA, Goldberger JJ & Kadish AH (1997). *Am J Cardiol* **79**, 178–181.

Drici MD, Burklow TR, Haridasse V, Glazer RI & Woosley RL (1996). *Circulation* **94**, 1471–1474.

Kadish AH, Greenland P, Limacher MC, Frishman WH, Daugherty SA & Schwartz JB (2004). *Ann Noninvasive Electrocardiol* **9**, 366–374.

Kurokawa J, Tamagawa M, Harada N, Honda S-i, Bai C-X, Nakaya H & Furukawa T (2008). *J Physiol* **586**, 2961–2973.

Larsen JA, Tung RH, Sadananda R, Goldberger JJ, Horvath G, Parker MA & Kadish AH (1998). *Am J Cardiol* **82**, 993–995.

Rautaharju PM, Zhou SH, Wong S, Calhoun HP, Berenson GS, Prineas R & Davignon A (1992). *Can J Cardiol* **8**, 690–695.

Roden DM (1998). *Pacing Clin Electrophysiol* **21**, 1029–1034.

Rodriguez I, Kilborn MJ, Liu XK, Pezzullo JC & Woosley RL (2001). *JAMA* **285**, 1322–1326.

Stansfeld PJ, Gedeck P, Gosling M, Cox B, Mitcheson JS & Sutcliffe MJ (2007). *Proteins* **68**, 568–580.

doi:10.2533/chimia.2010.165 Chimia 64 (2010) 165–169

Appendix V : Stereoselective Block of hERG Channel by Bupivacaine Scrutinized at Molecular Level

Liliana Sintra Grilo[§ab], Pierre-Alain Carrupt[a], and Antoine Daina*[a]

[§]SCS–DSM Nutritional Products Award Winner (Poster Presentation)

Abstract: In the heart, the hERG voltage-gated potassium channel mediates the I_{Kr} current, which is crucial for the duration of cardiac action potential. Undesired block of the channel may prolong the QT interval with increased risk of malignant ventricular arrhythmia called *torsades de pointes*. Although the molecular determinants of hERG block are intensively studied, stereoselectivity has been poorly investigated. Levo-(*S*)-bupivacaine was the first drug reported to have higher affinity for hERG than its enantiomer. This study aims at understanding the principles underlying the stereoselectivity of bupivacaine block with the help of molecular modeling. Putative binding modes of levo-(*S*)- and dextro-(*R*)-bupivacaine inside an open form model of hERG channel were predicted by docking simulations, allowing a clear depiction of ligand-protein interactions. Estimated binding energies for both enantiomers to wild-type channel are in line with previously published electrophysiology measurements. These results may be considered as a confirmation at the molecular level of bupivacaine stereoselective binding towards hERG. Moreover this information lays the foundations for a structural guideline to filter out potentially cardiotoxic drug candidates *in silico*.

Keywords: Bupivacaine · Cardiotoxicity · Docking · hERG-block · Stereoselectivity

Introduction

The hERG (human *ether a go-go* related gene) channel is a voltage-gated potassium channel that plays a crucial role in the repolarization phase of the cardiomyocyte action potential.[1] *KCNH2* gene encodes the α-subunit that assembles into a homotetramer to form a functional channel conducting specifically K^+ ions (Fig. 1A, left). The pore-forming domain of hERG is constituted of the transmembrane helix S5, the *pore helix* and *selectivity filter*, and the S6 transmembrane domain (Fig. 1A, right). Many loss-of-function mutations in *KCNH2* gene can prolong the QT interval on the ECG and trigger potentially lethal arrhythmia known as *torsades de pointes*, which may cause sudden death.[2] Such genetic disorders are referred to as congenital Long QT Syndrome (cLQTS).[3]

Numerous structurally diverse drugs, among others antifungal ketoconazole,[4] antipsychotic chlorpromazine,[5] or prokinetic cisaprid,[6] have the ability to unintentionally block the hERG channel leading to the so-called drug-induced *Long QT Syndrome* (diLQTS).[7] Although molecular determinants of hERG block have been intensively studied, stereoselectivity has been scarcely investigated.[8–11] Levo-(*S*)-bupivacaine (Fig. 1B, left), a broadly used anesthetic, was the first drug reported to be more potent than its enantiomer (~2-fold) to block hERG channels.[9–11] We also focused our interest on another chiral drug, (*R*,*S*)-terfenadine (Fig. 1B, right). Terfenadine is a well-known high-affinity blocker of hERG,[12,13] that shares similar chemical moieties with bupivacaine. Both structures encompass a piperidine ring N-substituted by an alkyl chain. Moreover one of the terfenadine aromatic ring presents similar distance from the basic nitrogen compared to the *o,o*-dimethylphenyl of the bupivacaine. Terfenadine was employed as an anti-histaminic drug until its adverse effects on hERG[14] and QT prolongation[15] led to its withdrawal from the market. In notable contrast with bupivacaine, stereoselective block of the

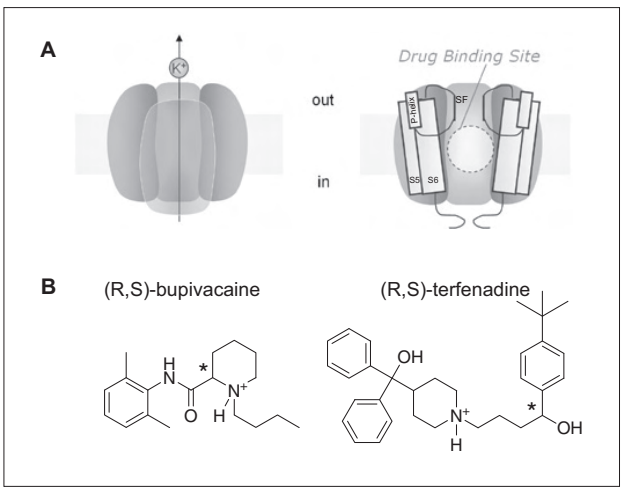

Fig. 1. (A) Cartoon depicting the tetrameric structure of hERG channel, with pore-constituting unit formed by S5 and S6 transmembrane domains, the pore-helix (P-helix) and the selectivity filter (SF). (B) Chemical structures, protonated as at pH 7.4, of (*R*,*S*)-bupivacaine and (*R*,*S*)-terfenadine with chiral center marked with an asterisk.

*Correspondence: Dr. A. Daina[a]
Tel.: + 41 22 379 33 65
Fax: + 41 22 379 33 60
E-mail: antoine.daina@unige.ch
[a]School of Pharmaceutical Sciences
University of Geneva,
University of Lausanne
30, Quai Ernest-Ansermet
CH-1211 Geneva 4
[b]Department of Clinical Research
University of Bern
Murtenstrasse 35
CH-3010 Bern

hERG channel has never been reported for terfenadine.

In the present study, the stereoselective block of the hERG channel by bupivacaine enantiomers was thoroughly investigated by a fine-tuned modeling methodology in order to rationalize the stereoselective binding at the molecular level.

Methods

Selection and Preparation of the hERG Target Structure

Different publicly available homology models of the hERG channel were considered and meticulously evaluated as potential targets for the present structure-based studies. One of the published models provided by Farid *et al*.,[16] based on the bacterial KvAP crystal (pdb entry:1orq), was finally selected for two main reasons: i) the open conformation of the channel appears accessible for the binding of ligands and ii) it was built with the ligand (*S*)-terfenadine already present inside using the so-called *induced-fit docking* protocol which involves successive steps of Glide docking and Prime protein modeling.[17] Moreover, Farid and colleagues performed Glide 3.0 docking (Schrödinger, LLC, Portland, OR) towards this structure for a set of known blockers with well-characterized effects on hERG. Interestingly their simulations predicted comparable binding modes for terfenadine, cisapride, sertindole, ibutilide and clofilium, adding confidence to the docking solutions obtained. For our needs, all hydrogens were added to the protein residues of the model by the procedure embedded in the BIOPOLYMER module of Sybyl 8.0 (Tripos Associates, Inc., St-Louis, MO), (*S*)-terfenadine was removed and the remaining hERG structure was used as target for docking without further refinement or optimization.

Preparation of Terfenadine and Bupivacaine Ligand Structures

Both enantiomers of terfenadine, *i.e.* 1-(4-*tert*-butylphenyl)-4-[4-[hydroxyl-di(phenyl)methyl]piperidin-1-yl]butan-1-ol, and both enantiomers of bupivacaine, *i.e.* 1-butyl-N-(2,6-dimethylphenyl)piperidine-2-carboxamide (Fig. 1B) were modeled with a protonated piperidine nitrogen, Gasteiger and Marsili partial atomic charges and a formal charge of +1 within the Sybyl 8.0 environment.[18] A first energy minimization was performed in the Tripos force field, but the flexibility of the piperidine rings stressed the need for further conformational search. The cationic species were submitted to a Monte Carlo (MC) conformational analysis according to the semi-empirical AM1 molecular orbital theory as implemented in Spartan '06 (Wavefunction Inc, Irvine, CA). The selected conformations were then optimized at HF/3-21G level of theory using Spartan '06 and, for every compound, the lowest energy conformer was used as ligand input for docking towards hERG.

Docking

Automated molecular docking was carried out using the GOLD program version 4.0 (Gold Suite, CCDC Software Ltd., Cambridge, UK). The binding site was defined following the definition of Stansfeld *et al*.,[19] namely as all protein atoms within 20 Å from the natural K^+ ion S_{cav}. This ion is not present in the structure, but coordinates were retrieved from backbone overlay of the selectivity filter of KcsA crystallized subunit including K^+ ions (pdb entry: 1k4c) and our target structure. Coordinates of potassium ion K3005 correspond to S_{cav}. Three independent docking simulations, each asking for 20 solutions per ligand, were run in parallel, according to the GOLD genetic algorithm default parameters. Ligands were considered as flexible and protein as rigid, except all hydroxyl and amine moieties. Moreover, the Tyr652 side-chain – crucial for binding as well as very keen to adapt its orientation – was considered as fully flexible according to the rotamer library available in GOLD 4.0. In order to limit the complexity of solution analyses due to the rotational symmetry of the tetramer, a slight constraint favoring hydrogen-bonding with Ser624 of one specific subunit was applied, in accordance with Farid's observations.

The 60 docking solutions per ligand were evaluated by the GoldScore function with default parameters. Further criteria were employed to select one or a few more docking poses to be submitted to post-docking treatment: i) the population of clusters of solutions based on rmsd on heavy atoms ii) careful visual inspection focused on intermolecular interactions involving *a priori* important pharmacophoric features such as, in particular, the protonated nitrogen atom and the aromatic rings.

Molecular Mechanics Post-docking Optimization and Binding Affinity Prediction

The best solutions according to the above-mentioned criteria and their corresponding protein structures were then submitted to molecular mechanics treatment within the AMBER 10 environment.[20] This implies the traditional all-atom AMBER force field for the protein atoms, the GAFF force field and semi-empirical AM1-BCC charges for the ligand atoms, together with implicit solvation model terms. This procedure, adapted from Graves *et al*.[21] consists of three main steps where, in our case, only the ligand is allowed to move inside the hERG channel kept rigid: i) a 100 steps minimization with a conjugate gradient method; ii) a Langevin molecular dynamic of 3000 steps at constant temperature of 300K; iii) a second minimization identical to i). The procedure, beside geometry optimization and thus refined binding mode prediction, leads to an approximation of the affinity of the ligand for the hERG channel by estimating the free energy of binding (ΔG), according to Eqn. (1):

$$\Delta G = E_{binding} = E_{complex} - (E_{protein} + E_{ligand}) \quad (1)$$

where $E_{complex}$, $E_{protein}$, E_{ligand} are the solvated internal energy of the complex, the protein and the ligand, respectively, as computed by the force fields enriched by implicit solvation terms according to the GB/SA model developed by Onufriev *et al*.[22] and the LCPO algorithm term to account for the surface area.[23]

Analysis of Binding Mode and Interactions

Geometries and intermolecular interactions within the optimized virtual complexes were finally analyzed visually and with the help of Maestro 8.5 measurement tools (Schrödinger, LLC, Portland, OR), where good contacts are defined with a cutoff ratio of 1.3 Å. Final solutions for all enantiomers were superimposed in the same coordinate system for comparison of binding modes and location of similar pharmacophoric features.

Results

Binding Modes of (R)- and (S)-Terfenadine

The redocking of (*S*)-terfenadine in the homology model, followed by force field optimization of the ligand inside the binding site, was used to calibrate the setup of the entire simulation. Parameters leading to the best overlap of selected (*S*)-terfenadine solutions and the native pose adopted in Farid's model were retained and described above. Our (*S*)-terfenadine predicted binding mode and the ligand as found in the published homology model are presented in Fig. 2A and 2C, respectively. As terfenadine was never reported as a stereoselective blocker of hERG, we performed the docking of the (*R*)-terfenadine with the same modeling protocol. Interestingly, the (*R*)-terfenadine binding mode (Fig. 2B) is very similar to that of the (*S*)-enantiomer. Location of the chiral center allows only minor conformational and positional changes for the (*R*)- and (*S*)-enantiomers, resulting globally in the flip of the hydroxyl group. For (*S*)-terfenadine, this group acts as a hydrogen donor for the oxygen of Ser649 hy-

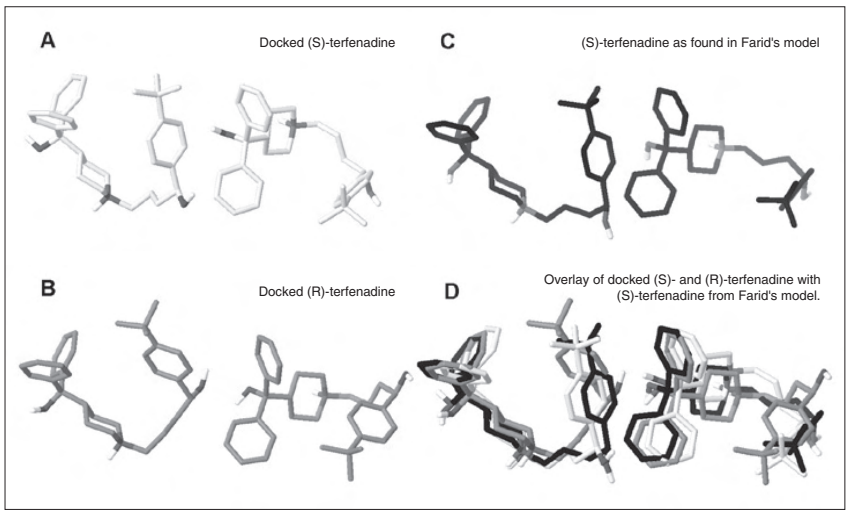

Fig. 2. Binding modes from two orthogonal views of enantiomers (*S*)-terfenadine (carbons in light grey; Panel A) and (*R*)-terfenadine (carbons in medium grey; Panel B) as predicted by our docking methodology compared with (S)-terfenadine from Farid's homology model[16] (carbon on black; Panel C). Panel D shows superimposed binding modes for terfenadine enantiomers with an excellent overlap of all poses (same color-coding). All protein atoms and non-polar hydrogens of terfenadine are omitted for clarity.

Table 1. Calculated Gibbs free energy of binding (ΔG, kcal/mol) within the AMBER 10 environment including implicit solvation and surface terms for the different ligands and estimated binding energy difference ($\Delta G_{(R)\text{-form}} - \Delta G_{(S)\text{-form}} = \Delta(\Delta G)$, kcal/mol).

Ligand	(ΔG), kcal/mol	Δ(ΔG), kcal/mol
(*R*)-terfenadine	–26.73	–0.70 (*R*)=(*S*)
(*S*)-terfenadine	–26.03	
dextro-(*R*)-bupivacaine	–17.14	3.71 (*R*)>(*S*)
levo-(*S*)-bupivacaine	–20.85	

droxyl side-chain to form a H-bond. In the case of (*R*)-terfenadine, orientation of the hydroxyl group does not allow H-bond interaction. The *tert*-butylphenyl end undergoes a 90° rotation, yet keeping its general location in the hERG binding site, thus still involved in aromatic–aromatic interactions with residue phenylalanine in position 656. As expected by the constraint, for both enantiomers Ser624 is involved in electrostatic interaction with basic nitrogen. An equivalent serine on another α-subunit is involved in hydrogen bond interaction with the hydroxyl group at the benzylic position of (*R*)- and (*S*)-terfenadine. The remarkable common binding mode predicted for both enantiomers (Fig. 2D) lets us assume there is no stereoselectivity for the binding of terfenadine within the pore of the channel.

Estimated free energies of binding (ΔG, Table 1) were calculated during optimization of ligands inside the binding site of hERG in AMBER environment using an implicit solvent model (GB/SA). For terfenadine enantiomers, (*R*)- and (*S*)-forms present similar free energies of binding, with a difference ($\Delta(\Delta G) = \Delta G_{(R)\text{-form}} - \Delta G_{(S)\text{-form}}$) lesser than 1 kcal/mol and regarded as negligible. These results also claim for the same binding affinity of terfenadine enantiomers for hERG open-channel.

Binding Modes of Dextro-(R)- and Levo-(S)-bupivacaine

After validation of the modeling strategy with terfenadine, the same methodology was followed for dextro-(*R*)- and levo-(*S*)-bupivacaine docking toward the binding site of hERG channel. Final optimized binding modes of bupivacaine were analyzed considering only residues of the pore with atoms at 5 Å distance from the ligands. The main striking difference in the binding modes of the enantiomers is the opposing orientation of the butyl chain. It is worth mentioning that the basic nitrogen of the piperidine ring as well as the carbonyl group of the amide are pointing towards the top of the hERG cavity and occupy the same position in the binding site. Good contacts between the ligand and the protein (dashed lines, Fig. 3) were elicited by Maestro measurement tools, which highlighted residues, such as Leu622, Thr623, Ser624, Ser649, Tyr652, Ala653 and Phe656, involved in the drug recognition. Among these, Tyr652 and Ser624 are the residues that display the highest number of good contacts and involve simultaneously three to four subunits of the channel (Fig. 3). Both bupivacaine enantiomers reveal electrostatic interactions between the carbonyl of the amide and Ser624 of multiple α-subunits. In the final optimized binding mode, levo-(*S*)-bupivacaine calls for the contribution of the tyrosine residues in position 652 of all α-subunits. Conversely, dextro-(*R*)-bupivacaine interacts with only three tyrosine residues. Moreover the *o,o*-dimethylphenyl group creates, for both enantiomers, numerous good contacts with Tyr652 of α-subunit I (Fig. 3), thus keeping the aromatic moiety of the ligand in a same favorable area. The number of α-subunits involved in interactions with the ligand is also different regarding Phe656, which is the second aromatic residue protruding in the inner cavity. Benzyl side-chains of two α-subunits (III and IV, Fig. 3A) are involved in good contacts with levo-(*S*)-bupivacaine, whereas for dextro-(*R*)-bupivacaine only one α-subunit (III, Fig. 3B) slightly contributes to interactions with the ligand. The difference in the molecular recognition with additional contribution of two aromatic residues could be a clue to explain the higher affinity of block described experimentally for levo-(*S*)-bupivacaine.[9–11] Moreover and in contrast to the terfenadine estimations, free energy of binding calculations predict the levo-(*S*)-bupivacaine–hERG complex to be more stable than the dextro-(*R*)-bupivacaine–hERG complex by nearly 4 kcal/mol. These results reveal a stereoselective behavior in the binding of bupivacaine within the K^+ channel, with levo-(*S*)-form showing higher affinity than the dextro-(*R*)-bupivacaine.

Discussion

Here we present a molecular investigation of hERG stereoselective block by bupivacaine enantiomers. The computational strategy was first validated by redocking (*S*)-terfenadine enantiomer toward the described homology model. The difficulty of this particular docking case laid in the symmetrical nature of the ligands together with

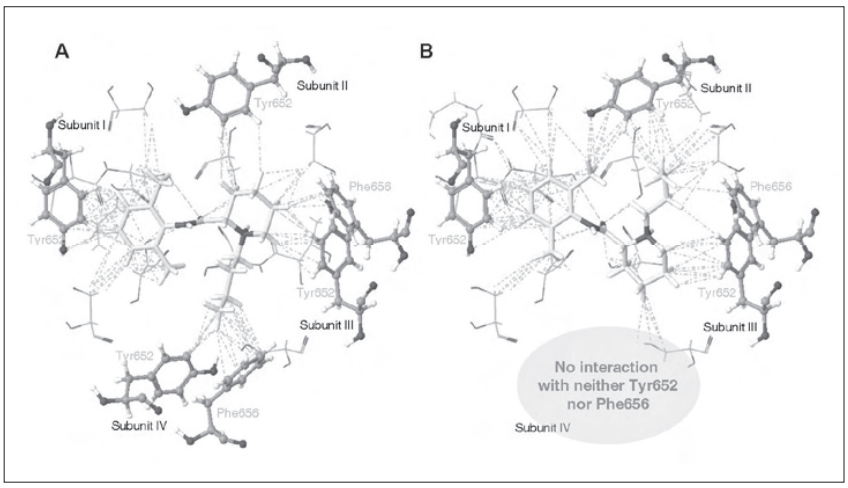

Fig. 3. (A) Dextro-(*R*)-bupivacaine and (B) levo-(*S*)-bupivacaine (in stick representation with carbons in light grey), and hERG residues (carbons in dark grey) creating good contacts (dashed lines) with the ligand within a 5 Å shell around it (Maestro 8.5). Both (A) and (B) are seen from the same viewpoint, *i.e.* from the inner side of the channel cavity. Tyr652 residues have been flexibilized during docking process (GOLD 4.0). Known important residues (Tyr652 and Phe656) are highlighted with ball-and-stick representation, others are in wireframe.

the tetrameric structure of hERG channel, which introduces a rotational symmetry. The multiplication of identical binding modes resulting from the symmetry of the channel was overcome by adding a slight constraint favoring hydrogen-bond formation with one Ser624 residue. The predicted binding mode of the (*S*)-terfenadine is very similar to the one published by Farid *et al*., though obtained by a totally different approach.[16] In their previous work, (*S*)-terfenadine blocker was shown to be in close contact with four Tyr652 and two Phe656 residues, and the nature of π–π interactions with the aromatic groups of the ligand was explicitly specified. For both (*R*)- or (*S*)-terfenadine, two of the four tyrosine side-chains display T-shaped (edge-to-face) π–π interactions with phenyl groups of the ligands.[16] Regarding phenylalanine residues, they reported two T-shaped interactions for (*R*)-terfenadine, whereas the (*S*)-enantiomer made one T-shaped and one parallel displaced stacking.[16] The binding mode of (*R*)-terfenadine was not published by Farid and colleagues, but our final binding solution offers an explanation to this difference. As mentioned before, one of the few changes observed in the docking solutions for the anti-histaminic enantiomers is the orientation of the *tert*-butylphenyl group. Undergoing a 90° rotation switches the aromatic interaction from T-shaped to parallel displaced mode. These kind of aromatic interactions are known to be isoenergetic and, as such, equally stabilizing for molecular recognition.[24] However, the parallel displaced interaction between one aromatic ring of the docked (*S*)-terfenadine and the side-chain of Phe656 appears to be far from optimal in terms of distance and parallelism. This loss of stabilization is counterbalanced by the additional hydrogen-bond between the tertiary alcohol and Ser649 side-chain predicted to be only displayed by (*S*)-terfenadine and not (*R*)-terfenadine. With the exception of these two points, both enantiomers present very similar binding modes suggesting overall similar interactions with the channel. Calculations of free energy of binding provided supplementary evidence for equal affinity of terfenadine enantiomers to hERG binding site, which is in agreement with the absence of any reported stereoselective block.

In contrast, bupivacaine was the first molecule established to block more potently the hERG channel with its levo-(*S*)-form than its racemate.[9–11] Levo-(*S*)-bupivacaine was commercialized because it was demonstrated to be safer for local anesthesia than the racemic mixture.[25] The purpose of this work was not to reconsider the extensive use of this enantiomer in anesthesiology, but to investigate the molecular determinants of hERG stereoselective block. Whereas terfenadine enantiomers presented similar binding modes, final docking solutions of bupivacaine (*R*)- and (*S*)-forms differed. Importantly, the opposing orientation of the butyl rest allows levo-(*S*)-bupivacaine to interact with two additional aromatic side-chains, Tyr652 and Phe656 of the fourth α-subunit, already known to be important for hERG block by local anesthetics.[10] This observed difference in the molecular recognition could explain the higher blocking capability of levo-(*S*)-bupivacaine displayed at electrophysiologcal level, if one assumes that binding of the molecules inside the pore prevents normal K^+ ion movement and so blocks the hERG current. The stereo-dependant binding mode is corroborated by the estimation of a more favorable free energy of binding for the levo-(*S*)-form. Moreover, Tyr652 and Phe656 aromatic residues have already been mentioned by Farid *et al.* for their influential π–π interactions with terfenadine.[16] For both enantiomers of bupivacaine, Tyr652 of the α-subunit I (Fig. 3) might be involved in parallel displaced π–π interactions with the *o,o*-dimethyphenyl ring however, the distance and angle between the two aromatic plans are not the most favorable for stabilization.

The propensity of numerous structurally diverse drugs to block the hERG channel is, at least in part, due to its unusually large cavity. In contrast to other voltage-gated K^+ channels, hERG lacks a PxP-kink motif in the S6 helices that would restrict the inner cavity size.[26] It is noteworthy that most of Farid's docked ligands as well as our bupivacaine solutions are located in the same region of the large area explored by the engine. Predicted binding modes are positioned just beneath the selectivity filter at the very top of the vestibule. Superimposition of the terfenadine and bupivacaine binding modes highlights some pharmacophoric features previously described:[27–29] aromatic rings (*o,o*-dimethylphenyl group of bupivacaine and one phenyl ring of terfenadine) as well as the basic piperidine nitrogen show remarkable overlap and appear fundamental for hERG channel to recognize these blockers.

The location of the binding site observed in the present case is due to the presence of another key structural determinant of hERG: the aromatic residues Tyr652 and Phe656 that protrude in the pore and that were identified as important partners for interaction with our ligands. Such residues are common to hERG and the related *ether à go-go* (EAG) channels, but again not to other voltage-gated channels.[30] Mutation of one of these residues into alanine has first been reported to dramatically affect block of hERG by MK-499, a methanesulfonanilide antiarrhythmic drug,[31] and has been observed later for many compounds,[31–34] including terfenadine and local anesthetics.[10] The crucial role of these aromatic amino acids has long been attributed to formation of π-stacking interactions with aromatic rings and π-cation interactions with the basic group of the ligand. Farid[16] and Zachariae[35] assign the importance of these amino acids to their concentric arrangement in the cavity allowing multiple π-stacking and/or hydrophobic interactions with various combinations of Tyr652 and Phe656

side-chains. The same observations about aromatic interactions were made for bupivacaine enantiomers. In Farid's proposed model, it is suggested that polar groups, including the highly prevalent basic nitrogen, tend to localize in a hydrophilic volume associated with Ser624.[16] Importance of this residue for binding was confirmed by Kamiya *et al.*,[36] when mutation of serine to alanine in position 624 significantly decreased terfenadine block of hERG. Surprisingly, no evident hydrogen bond was retrieved in our final optimized pose between the basic nitrogen and oxygen of Ser624 as seen for terfenadine, even though this docking solution would be favored by the constraint. The explanation lays in the geometry of bupivacaine. The predicted bioactive conformation is very close to an energy minimum and displays an intramolecular interaction between the protonated piperidine nitrogen and one electronic lone pair on the carbonyl oxygen of the amide. The H-bond donor capacity is consumed by this internal non-bonded force. However, careful inspection of the reformed complexes revealed probable electrostatic interactions between the carbonyl group and residues Ser624. The second lone pair, not involved in the intramolecular interaction, is still able to contribute significantly to intermolecular recognition inside the hydrophilic volume defined by Farid and coworkers.

Conclusion and Perspectives

This target-based study involving multiple symmetries is aimed at understanding the principles underlying the stereoselectivity of hERG block by bupivacaine. To achieve this goal, we validated our computational strategy by redocking (*S*)-terfenadine ligand in a carefully selected published homology model. We were able to reproduce, using a workflow of different modeling techniques, the binding pose obtained by Farid *et al.* Previous conclusions about the absence of stereospecific block of hERG by terfenadine were confirmed by predicting similar binding modes for both enantiomers and no significant difference in the free energy of binding. Interestingly, docking and molecular mechanics post-docking processing of bupivacaine enantiomers corroborated the stereoselective behavior towards the hERG channel. In the latter case, predicted binding modes and estimated free energies of binding indicated higher affinity of levo-(*S*)-bupivacaine for the K^+ channel binding site. Moreover, our study emphasized the role of aromatic amino acids Tyr652 and Phe656 lining the channel cavity in their π–π interactions with the ligand as well as the electrostatic interactions in the hydrophilic volume at the intracellular base of the selectivity filter associated with Ser624.

The complex case of enantiomeric block reproduced at a molecular level gives confidence to the strategy applied. Nevertheless, a more detailed understanding of the structural basis of binding would be gained by docking structurally-related molecules or simulations toward mutated hERG structures for the sake of comparison with experimental results. Furthermore, the validity domain of this model may appear to be narrowed to the structure of bupivacaine, terfenadine and possibly to chemicals sharing a similar pharmacophore. Since the hERG channel is known to recognize an extremely large variety of compounds, it is imperative to challenge our predictions with known blockers showing significant structural variations.

In this perspective, we believe this work lays robust foundations for a structure-based design approach to overcome or even anticipate serious cardiotoxic issues faced by many medicinal chemistry projects.

Received: January 5, 2010

[1] M. C. Sanguinetti, C. G. Jiang, M. E. Curran, M. T. Keating, *Cell* **1995**, *81*, 299.
[2] M. C. Sanguinetti, M. Tristani-Firouzi, *Nature* **2006**, *440*, 463.
[3] W. Shimizu, *Cardiovasc. Res.* **2005**, *67*, 347.
[4] R. Dumaine, M. L. Roy, A. M. Brown, *J. Pharmacol. Exp. Ther.* **1998**, *286*, 727.
[5] D. Thomas, K. Wu, S. Kathöfer, H. A. Katus, W. Schoels, J. Kiehn, C. A. Karle, *Brit. J. Pharmacol.* **2003**, *139*, 567.
[6] S. Mohammad, Z. Zhou, Q. Gong, C. T. January, *Am. J. Physiol.* **1997**, *273*, H2534.
[7] D. M. Roden, *N. Engl. J. Med.* **2004**, *350*, 1013.
[8] C. B. Eap, S. Crettol, J. S. Rougier, J. Schläpfer, L. Sintra Grilo, J. J. Déglon, J. Besson, M. Croquette-Krokar, P. A. Carrupt, H. Abriel, *Clin. Pharmacol. Ther.* **2007**, *81*, 719.
[9] T. Gonzalez, C. Arias, R. Caballero, I. Moreno, E. Delpon, J. Tamargo, C. Valenzuela, *Brit. J. Pharmacol.* **2002**, *137*, 1269.
[10] C. C. Siebrands, N. Schmitt, P. Friederich, *Anesthesiology* **2005**, *103*, 102.
[11] P. Friederich, A. Solth, S. Schillemeit, D. Isbrandt, *Brit. J. Anaesth.* **2004**, *92*, 93.
[12] D. Rampe, M. L. Roy, A. Dennis, A. M. Brown, *FEBS Lett.* **1997**, *417*, 28.
[13] W. J. Crumb, *J. Pharmacol. Exp. Ther.* **2000**, *292*, 261.
[14] M. Roy, R. Dumaine, A. M. Brown, *Circulation* **1996**, *94*, 817.
[15] S. P. Pinney, B. S. Koller, M. R. Franz, R. L. Woosley, *J. Cardiovasc. Pharmacol.* **1995**, *25*, 30.
[16] R. Farid, T. Day, R. A. Friesner, R. A. Pearlstein, *Bioorg. Med. Chem.* **2006**, *14*, 3160.
[17] W. Sherman, T. Day, M. P. Jacobson, R. A. Friesner, R. Farid, *J. Med. Chem.* **2006**, *49*, 534.
[18] J. Gasteiger, M. Marsili, *Tetrahedron* **1980**, *36*, 3219.
[19] P. J. Stansfeld, P. Gedeck, M. Gosling, B. Cox, J. S. Mitcheson, M. J. Sutcliffe, *Proteins: Struct. Funct. Bioinf.* **2007**, *68*, 568.
[20] AMBER 10, D. A. Case, T. A. Darden, T. E. Cheatham, C. L. Simmerling, J. Wang, R. E. Duke, R. Luo, M. Crowley, R. C. Walker, W. Zhang, M. Merz, B. Wang, S. Hayik, G. Roitberg, G. Seabra, I. Kolossváry, K. F. Wong, F. Paesani, J. Vanicek, X. Wu, S. R. Brozell, T. Steinbrecher, H. Gohlke, L. Yang, C. Tan, J. Mongan, V. Hornak, G. Cui, D. H. Mathews, M. G. Seetin, C. Sagui, V. Babin, P. A. Kollman, University of California, San Francisco, **2008**.
[21] A. P. Graves, D. M. Shivakumar, S. E. Boyce, M. P. Jacobson, D. A. Case, B. K. Shoichet, *J. Mol. Biol.* **2008**, *377*, 914.
[22] A. Onufriev, D. Bashford, D. A. Case, *Proteins: Struct. Funct. Bioinf.* **2004**, *55*, 383.
[23] J. Weiser, P. S. Shenkin, W. C. Still, *J. Comput. Chem.* **1999**, *20*, 217.
[24] P. Hobza, H. L. Selzle, E. W. Schlag, *J. Phys. Chem.* **1996**, *100*, 18790.
[25] H. Bardsley, R. Gristwood, H. Baker, N. Watson, W. Nimmo, *Br. J. Clin. Pharmacol.* **1998**, *46*, 245.
[26] J. S. Mitcheson, *Br. J. Pharmacol.* **2003**, *139*, 883.
[27] J. Morgan T.K., M. E. Sullivan, in 'Prog.Med. Chem.', Eds. G. P. Ellis, D. K. Luscomb, Elsevier Science Publishers, Amsterdam, **1992**, pp. 65–108.
[28] R. A. Pearlstein, R. J. Vaz, J. Kang, X. L. Chen, M. Preobrazhenskaya, A. E. Shchekotikhin, A. M. Korolev, L. N. Lysenkova, O. V. Miroshnikova, J. Hendrix, D. Rampe, *Bioorg. Med. Chem. Lett.* **2003**, *13*, 1829.
[29] A. Cavalli, E. Poluzzi, F. De Ponti, M. Recanatini, *J. Med. Chem.* **2002**, *45*, 3844.
[30] M. C. Sanguinetti, J. S. Mitcheson, *Trends Pharmacol. Sci.* **2005**, *26*, 119.
[31] J. S. Mitcheson, J. Chen, M. Lin, C. Culberson, M. C. Sanguinetti, *Proc. Natl. Acad. Sci. USA* **2000**, *97*, 12329.
[32] E. Ficker, W. Jarolimek, J. Kiehn, A. Baumann, A. M. Brown, *Circ. Res.* **1998**, *82*, 386.
[33] D. Fernandez, A. Ghanta, G. W. Kauffman, M. C. Sanguinetti, *J. Biol. Chem.* **2004**, *279*, 10120.
[34] J. A. Sanchez-Chapula, R. A. Navarro-Polanco, C. Culberson, J. Chen, M. C. Sanguinetti, *J. Biol. Chem.* **2002**, *26*, 23587.
[35] U. Zachariae, F. Giordanetto, A. G. Leach, *J. Med. Chem.* **2009**, *52*, 4266.
[36] K. Kamiya, R. Niwa, M. Morishima, H. Honjo, M. C. Sanguinetti, *J. Pharmacol. Sci.* **2008**, *108*, 301.

References

References

Internet sources:

1) www.rush.edu/rumc/page-1098987354128.html, accessed on March 2010.

2) www.ncbi.nlm.nih.gov/bookshelf/br.fcgi?book=cardio&part=A1016, accessed on March 2010.

3) www.rush.edu/rumc/images/ei_0018.jpg, accessed on March 2010.

4) www.nottingham.ac.uk/nursing/practice/resources/cardiology/function, accessed on March 2010.

5) www.nobelprize.org/educational_games/medicine/ecg/ecg-readmore.html, accessed on March 2010.

6) http://content.onlinejacc.org/cgi/content-nw/full/36/1/1/FIG3, accessed on March 2010.

7) ADME boxes, version 3.5.(2008) www.pharma-algorithms.com/webboxes, accessed on April 2010

Bibliographic sources:

Abbott,G.W., Sesti,F., Splawski,I., Buck,M.E., Lehmann,M.H., Timothy,K.W., Keating,M.T., & Goldstein,S.A. (1999) MiRP1 forms IKr potassium channels with HERG and is associated with cardiac arrhythmia. *Cell,* **97**, 175-187.

Abernethy,D.R., Wesche,D.L., Barbey,J.T., Ohrt,C., Mohanty,S., Pezzullo,J.C., & Schuster,B.G. (2001) Stereoselective halofantrine disposition and effect: concentration-related QTc prolongation. *Br. J. Clin. Pharmacol.,* **51**, 231-237.

Abi-Gerges,N., Philp,K., Pollard,C., Wakefield,I., Hammond,T.G., & Valentin,J.P. (2004) Sex differences in ventricular repolarization: from cardiac electrophysiology to Torsades de Pointes. *Fundam. Clin. Pharmacol.,* **18**, 139-151.

Abriel,H., Loffing,J., Rebhun,J.F., Pratt,J.H., Schild,L., Horisberger,J.D., Rotin,D., & Staub,O. (1999) Defective regulation of the epithelial Na+ channel by Nedd4 in Liddle's syndrome. *J. Clin. Invest,* **103**, 667-673.

Abriel,H. & Staub,O. (2005) Ubiquitylation of ion channels. *Physiology,* **20**, 398-407.

Ackerman,M.J. (2004) Cardiac channelopathies: it's in the genes. *Nature Medicine,* **10**, 463-464.

Al-Owais,M., Bracey,K., & Wray,D. (2009) Role of intracellular domains in the function of the herg potassium channel. *Eur. Biophys. J.*.

Anantharam,A. & Abbott,G.W. (2005) Does hERG coassemble with a beta subunit? Evidence for roles of MinK and MiRP1. *Novartis. Found. Symp.,* **266**, 100-112.

Anderson,C.L., Delisle,B.P., Anson,B.D., Kilby,J.A., Will,M.L., Tester,D.J., Gong,Q., Zhou,Z., Ackerman,M.J., & January,C.T. (2006) Most LQT2 mutations reduce Kv11.1 (hERG) current by a class 2 (trafficking-deficient) mechanism. *Circulation,* **113**, 365-373.

Ansermot,N., Albayrak,O., Schlapfer,J., Crettol,S., Croquette-Krokar,M., Bourquin,M., Deglon,J.J., Faouzi,M., Scherbaum,N., & Eap,C.B. (2010) Substitution of (R,S)-methadone by (R)-methadone: Impact on QTc interval. *Arch. Intern. Med.,* **170**, 529-536.

Anson,B.D., Ackerman,M.J., Tester,D.J., Will,M.L., Delisle,B.P., Anderson,C.L., & January,C.T. (2004) Molecular and functional characterization of common polymorphisms in HERG (KCNH2) potassium channels. *Am. J. Physiol Heart Circ. Physiol,* **286**, H2434-H2441.

Antzelevitch,C., Nesterenko,V.V., & Yan,G.X. (1995) Role of M cells in acquired long QT syndrome, U waves, and torsade de pointes. *J. Electrocardiol.,* **28 Suppl**, 131-138.

Aronov,A.M. (2006) Common pharmacophores for uncharged human ether-a-go-go-related gene (hERG) blockers. *J. Med. Chem.,* **49**, 6917-6921.

Aronov,A.M. & Goldman,B.B. (2004) A model for identifying HERG K^+ channel blockers. *Bioorg. Med. Chem.,* **12**, 2307-2315.

Balijepalli,R.C. & Kamp,T.J. (2008) Caveolae, ion channels and cardiac arrhythmias. *Prog. Biophys. Molec. Biol.,* **98**, 149-160.

Balijepalli,S.Y., Anderson,C.L., Lin,E.C., & January,C.T. (2010) Rescue of Mutated Cardiac Ion Channels in Inherited Arrhythmia Syndromes. *J. Cardiovasc. Pharmacol.*.

Bauer,C.K. & Schwarz,J.R. (2001) Physiology of EAG K+ channels. *J. Membr. Biol.,* **182**, 1-15.

Bazett,H.C. (1918) An analysis of the time relationship of electrocardiograms. *Heart,* **7**, 353-370.

Behr,E.R. & Mahida,S. (2009) Takotsubo cardiomyopathy and the long-QT syndrome: an insult to repolarization reserve. *Europace.,* **11**, 697-700.

Bell,I.M., Gallicchio,S.N., Abrams,M., Beese,L.S., Beshore,D.C., Bhimnathwala,H., Bogusky,M.J., Buser,C.A., Culberson,J.C., Davide,J., Ellis-Hutchings,M., Fernandes,C., Gibbs,J.B., Graham,S.L., Hamilton,K.A., Hartman,G.D., Heimbrook,D.C., Homnick,C.F., Huber,H.E., Huff,J.R., Kassahun,K., Koblan,K.S., Kohl,N.E., Lobell,R.B., Lynch,J.J., Jr., Robinson,R., Rodrigues,A.D., Taylor,J.S., Walsh,E.S., Williams,T.M., & Zartman,C.B. (2002) 3-Aminopyrrolidinone farnesyltransferase inhibitors: design of macrocyclic compounds with improved pharmacokinetics and excellent cell potency. *J. Med. Chem.,* **45**, 2388-2409.

Ben-Saadon,R., Zaaroor,D., Ziv,T., & Ciechanover,A. (2006) The polycomb protein Ring1B generates self atypical mixed ubiquitin chains required for its in vitro histone H2A ligase activity. *Mol. Cell,* **24**, 701-711.

Bendahhou,S., Marionneau,C., Haurogne,K., Larroque,M.M., Derand,R., Szuts,V., Escande,D., Demolombe,S., & Barhanin,J. (2005) In vitro molecular interactions and distribution of KCNE family with KCNQ1 in the human heart. *Cardiovasc. Res.,* **67**, 529-538.

Benhorin,J., Taub,R., Goldmit,M., Kerem,B., Kass,R.S., Windman,I., & Medina,A. (2000) Effects of flecainide in patients with new SCN5A mutation: mutation-specific therapy for long-QT syndrome? *Circulation,* **101**, 1698-1706.

Benson,M.D., Li,Q.J., Kieckhafer,K., Dudek,D., Whorton,M.R., Sunahara,R.K., Iniguez-Lluhi,J.A., & Martens,J.R. (2007) SUMO modification regulates inactivation of the voltage-gated potassium channel Kv1.5. *Proc. Natl. Acad. Sci. U. S. A.,* **104**, 1805-1810.

Berube,J., Caouette,D., & Daleau,P. (2001) Hydrogen peroxide modifies the kinetics of HERG channel expressed in a mammalian cell line. *J. Pharmacol. Exp. Ther.,* **297**, 96-102.

Berube,J., Chahine,M., & Daleau,P. (1999) Modulation of HERG potassium channel properties by external pH. *Pflügers Arch. Eur. J. Physiol.,* **438**, 419-422.

Bianchi,L., Wible,B., Arcangeli,A., Taglialatela,M., Morra,F., Castaldo,P., Crociani,O., Rosati,B., Faravelli,L., Olivotto,M., & Wanke,E. (1998) herg encodes a K+ current highly conserved in tumors of different histogenesis: a selective advantage for cancer cells? *Cancer Res.,* **58**, 815-822.

Boehmer,C., Laufer,J., Jeyaraj,S., Klaus,F., Lindner,R., Lang,F., & Palmada,M. (2008) Modulation of the voltage-gated potassium channel Kv1.5 by the SGK1 protein kinase involves inhibition of channel ubiquitination. *Cell Physiol Biochem.,* **22**, 591-600.

Bristow,M.R., Minobe,W., Rasmussen,R., Hershberger,R.E., & Hoffman,B.B. (1988) Alpha-1 adrenergic receptors in the nonfailing and failing human heart. *J. Pharmacol. Exp. Ther.,* **247**, 1039-1045.

Bruce,M.C., Kanelis,V., Fouladkou,F., Debonneville,A., Staub,O., & Rotin,D. (2008) Regulation of Nedd4-2 self-ubiquitination and stability by a PY motif located within its HECT-domain. *Biochem. J.,* **415**, 155-163.

Busse,D., Templin,S., Mikus,G., Schwab,M., Hofmann,U., Eichelbaum,M., & Kivisto,K.T. (2006) Cardiovascular effects of (R)- and (S)-verapamil and racemic verapamil in humans: a placebo-controlled study. *Eur. J. Clin. Pharmacol.,* **62**, 613-619.

Bylebyl,J. (1979) *William Harvey and his age*, Johns Hopkins University Press, Baltimore.

Camm,A.J., Malik,M., & Yap,Y.G. (2004) Introduction, in *Aquired Long QT Syndrome*, Blackwell Futura.

Caner,H., Groner,E., Levy,L., & Agranat,I. (2004) Trends in the development of chiral drugs. *Drug Discov. Today,* **9**, 105-110.

Cao,X.R., Lill,N.L., Boase,N., Shi,P.P., Croucher,D.R., Shan,H., Qu,J., Sweezer,E.M., Place,T., Kirby,P.A., Daly,R.J., Kumar,S., & Yang,B. (2008) Nedd4 controls animal growth by regulating IGF-1 signaling. *Sci. Signal.,* **1**, ra5.

Cavalli,A., Poluzzi,E., De Ponti,F., & Recanatini,M. (2002) Toward a pharmacophore for drugs inducing the long QT syndrome: insights from a CoMFA study of HERG K^+ channel blockers. *J. Med. Chem.,* **45**, 3844-3853.

Chapman,H., Ramström,C., Korhonen,L., Laine,M., Wann,K.T., Lindholm,D., Pasternack,M., & Törnquist,K. (2005) Downregulation of the HERG (KCNH2) K^+ channel by ceramide: evidence for ubiquitin-mediated lysosomal degradation. *J. Cell Sci.,* **118**, 5325-5334.

Chen,J., Sroubek,J., Krishnan,Y., Li,Y., Bian,J.S., & McDonald,T.V. (2009) PKA phosphorylation of Herg protein regulates the rate of channel synthesis. *Am J Physiol Heart Circ Physiol,* 01252.

Chen,L., Marquardt,M.L., Tester,D.J., Sampson,K.J., Ackerman,M.J., & Kass,R.S. (2007) Mutation of an A-kinase-anchoring protein causes long-QT syndrome. *Proc. Natl. Acad. Sci. U. S. A,* **104**, 20990-20995.

Chen,S.Z., Jiang,M., & Zhen,Y.S. (2005) [Correlation of HERG K+ channel protein expression to chemosensitivity of tumor cells to doxorubicin and its modulation by erythromycin]. *Ai. Zheng.,* **24**, 924-929.

Chikamori,T., Takata,J., Seo,H., Matsumura,Y., Kitaoka,H., Sugimoto,K., & Doi,Y. (1996) Diagnostic significance of an exercise-induced prominent U wave in acute myocardial infarction. *Am. J. Cardiol.,* **78**, 1277-1281.

Committee for Proprietary Medicinal Products (1997) *The assessment of the potential for QT interval prolongation by non-cardiovascular medicinal products*, Committee for Proprietary Medicinal Products, London.

Crettol,S., Deglon,J.J., Besson,J., Croquette-Krokar,M., Hammig,R., Gothuey,I., Monnat,M., & Eap,C.B. (2006) ABCB1 and cytochrome P450 genotypes and phenotypes: influence on methadone plasma levels and response to treatment. *Clin. Pharmacol. Ther.,* **80**, 668-681.

Crettol,S., Deglon,J.J., Besson,J., Croquette-Krokkar,M., Gothuey,I., Hammig,R., Monnat,M., Huttemann,H., Baumann,P., & Eap,C.B. (2005) Methadone enantiomer plasma levels, CYP2B6, CYP2C19, and CYP2C9 genotypes, and response to treatment. *Clin. Pharmacol. Ther.,* **78**, 593-604.

Crotti,L., Lundquist,A.L., Insolia,R., Pedrazzini,M., Ferrandi,C., De Ferrari,G.M., Vicentini,A., Yang,P., Roden,D.M., George,A.L., Jr., & Schwartz,P.J. (2005) KCNH2-K897T is a genetic modifier of latent congenital long-QT syndrome. *Circulation,* **112**, 1251-1258.

Cui,J., Melman,Y., Palma,E., Fishman,G.I., & McDonald,T.V. (2000) Cyclic AMP regulates the HERG K+ channel by dual pathways. *Curr. Biol.,* **10**, 671-674.

Curran,M.E., Splawski,I., Timothy,K.W., Vincent,G.M., Green,E.D., & Keating,M.T. (1995) A molecular basis for cardiac arrhythmia: HERG mutations cause long QT syndrome. *Cell,* **80**, 795-803.

De Ponti,F., Poluzzi,E., Montanaro,N., & Ferguson,J. (2000) QTc and psychotropic drugs. *Lancet,* **356**, 75-76.

Deamer,R.L., Wilson,D.R., Clark,D.S., & Prichard,J.G. (2001) Torsades de pointes associated with high dose levomethadyl acetate (ORLAAM). *J. Addict. Dis.,* **20**, 7-14.

Dessertenne,F. (1966) La tachycardie ventriculaire a deux foyers opposes variables. *Arch. Mal Coeur Vaiss.,* **59**, 263-272.

Doddareddy,M.R., Klaasse,E.C., Ijzerman,A.P., & Bender,A. (2010) Prospective Validation of a Comprehensive In silico hERG Model and its Applications to Commercial Compound and Drug Databases. *ChemMedChem.*.

Doyle,D.A., Cabral,J.M., Pfuetzner,R.A., Kuo,A., Gulbis,J.M., Cohen,S.L., Chait,B.T., & MacKinnon,R. (1998) The structure of the potassium channel: molecular basis of K^+ conduction and selectivity. *Science,* **280**, 69-77.

Drici,M.D., Burklow,T.R., Haridasse,V., Glazer,R.I., & Woosley,R.L. (1996) Sex hormones prolong the QT interval and downregulate potassium channel expression in the rabbit heart. *Circulation,* **94**, 1471-1474.

Duncan,R.S., Ridley,J.M., Dempsey,C.E., Leishman,D.J., Leaney,J.L., Hancox,J.C., & Witchel,H.J. (2006) Erythromycin block of the HERG K^+ channel: accessibility to F656 and Y652. *Biochem. Biophys. Res. Commun.,* **341**, 500-506.

Eap,C.B., Buclin,T., & Baumann,P. (2002) Interindividual variability of the clinical pharmacokinetics of methadone: implications for the treatment of opioid dependence. *Clin. Pharmacokinet.,* **41**, 1153-1193.

Ehret,G.B., Voide,C., Gex-Fabry,M., Chabert,J., Shah,D., Broers,B., Piguet,V., Musset,T., Gaspoz,J.M., Perrier,A., Dayer,P., & Desmeules,J.A. (2006) Drug-induced long QT syndrome in injection drug users receiving methadone: high frequency in hospitalized patients and risk factors. *Arch. Intern. Med.,* **166**, 1280-1287.

Ehrlich,J.R., Pourrier,M., Weerapura,M., Ethier,N., Marmabachi,A.M., Hebert,T.E., & Nattel,S. (2004) KvLQT1 modulates the distribution and biophysical properties of HERG. A novel alpha-subunit interaction between delayed rectifier currents. *J. Biol. Chem.,* **279**, 1233-1241.

Ekberg,J., Schuetz,F., Boase,N.A., Conroy,S.-J., Manning,J., Kumar,S., Poronnik,P., & Adams,D.J. (2007) Regulation of the voltage-gated K^+ channels KCNQ2/3 and KCNQ3/5 by ubiquitination. Novel role for nedd4-2. *J. Biol. Chem.,* **282**, 12135-12142.

Ekins,S., Crumb,W.J., Sarazan,R.D., Wikel,J.H., & Wrighton,S.A. (2002) Three-dimensional quantitative structure-activity relationship for inhibition of human ether-a-go-go-related gene potassium channel. *J. Pharmacol. Exp. Ther.,* **301**, 427-434.

Embark,H.M., Bohmer,C., Vallon,V., Luft,F., & Lang,F. (2003) Regulation of KCNE1-dependent K(+) current by the serum and glucocorticoid-inducible kinase (SGK) isoforms. *Pflugers Arch.,* **445**, 601-606.

Emmi,A., Wenzel,H.J., Schwartzkroin,P.A., Taglialatela,M., Castaldo,P., Bianchi,L., Nerbonne,J., Robertson,G.A., & Janigro,D. (2000) Do glia have heart? Expression and functional role for ether-a-go-go currents in hippocampal astrocytes. *J. Neurosci.,* **20**, 3915-3925.

Es-Salah-Lamoureux,Z., Fougere,R., Xiong,P.Y., Robertson,G.A., & Fedida,D. (2010) Fluorescence-tracking of activation gating in human ERG channels reveals rapid S4 movement and slow pore opening. *PLoS. One.,* **5**, e10876.

Escande,D., Mestre,M., Cavero,I., Brugada,J., & Kirchhof,C. (1992) RP 58866 and its active enantiomer RP 62719 (terikalant): blockers of the inward rectifier K+ current acting as pure class III antiarrhythmic agents. *J. Cardiovasc. Pharmacol.,* **20 Suppl 2**, S106-S113.

Etheridge,S.P., Compton,S.J., Tristani-Firouzi,M., & Mason,J.W. (2003) A new oral therapy for long QT syndrome: long-term oral potassium improves repolarization in patients with HERG mutations. *J. Am. Coll. Cardiol.,* **42**, 1777-1782.

Fakitsas,P., Adam,G., Daidie,D., van Bemmelen,M.X., Fouladkou,F., Patrignani,A., Wagner,U., Warth,R., Camargo,S.M., Staub,O., & Verrey,F. (2007) Early aldosterone-induced gene product regulates the epithelial sodium channel by deubiquitylation. *J. Am. Soc. Nephrol.,* **18**, 1084-1092.

Farid,R., Day,T., Friesner,R.A., & Pearlstein,R.A. (2006) New insights about HERG blockade obtained from protein modeling, potential energy mapping, and docking studies. *Bioorg. Med. Chem.,* **14**, 3160-3173.

Ficker,E., Dennis,A.T., Obejero-Paz,C.A., Castaldo,P., Taglialatela,M., & Brown,A.M. (2000) Retention in the endoplasmic reticulum as a mechanism of dominant-negative current suppression in human long QT syndrome. *J. Mol. Cell Cardiol.,* **32**, 2327-2337.

Ficker,E., Dennis,A.T., Wang,L., & Brown,A.M. (2003) Role of the cytosolic chaperones Hsp70 and Hsp90 in maturation of the cardiac potassium channel hERG. *Circ. Res.,* **92**, e87-100.

Ficker,E., Jarolimek,W., Kiehn,J., Baumann,A., & Brown,A.M. (1998) Molecular determinants of dofetilide block of HERG K+ channels. *Circ. Res.,* **82**, 386-395.

Ficker,E., Obejero-Paz,C.A., Zhao,S., & Brown,A.M. (2002) The binding site for channel blockers that rescue misprocessed human long QT syndrome type 2 ether-a-gogo-related gene (HERG) mutations. *J. Biol. Chem.,* **277**, 4989-4998.

Fodstad,H., Bendahhou,S., Rougier,J.S., Laitinen-Forsblom,P.J., Barhanin,J., Abriel,H., Schild,L., Kontula,K., & Swan,H. (2006) Molecular characterization of two founder mutations causing long QT syndrome and identification of compound heterozygous patients. *Ann. Med.,* **38**, 294-304.

Fotia,A.B., Ekberg,J., Adams,D.J., Cook,D.I., Poronnik,P., & Kumar,S. (2004) Regulation of neuronal voltage-gated sodium channels by the ubiquitin-protein ligases Nedd4 and Nedd4-2. *J. Biol. Chem.,* **279**, 28930-28935.

Fraser-Reid,B., Wu,Z., Andrews,C.W., Skowronsky,E., & Bowen,J.P. (1991) Torsional effects in glycoside reactivity: saccharide couplings mediated by acetal protecting groups. *J. Am. Chem. Soc.,* **113**, 1434-1435.

Furley,D. & Wilkie,J. (1984) *Galen on respiration and the arteries*, Princeton University Press.

Gaertner,J., Voltz,R., & Ostgathe,C. (2008) Methadone: a closer look at the controversy. *J. Pain Symptom. Manage.,* **36**, e4-e7.

Gamper,N., Fillon,S., Feng,Y., Friedrich,B., Lang,P.A., Henke,G., Huber,S.M., Kobayashi,T., Cohen,P., & Lang,F. (2002) K+ channel activation by all three isoforms of serum- and glucocorticoid-dependent protein kinase SGK. *Pflugers Arch.,* **445**, 60-66.

Ganapathi,S.B., Fox,T.E., Kester,M., & Elmslie,K.S. (2010) Ceramide modulates HERG potassium channel gating by translocation into lipid rafts. *Am. J. Physiol Cell Physiol*.

Gang,H. & Zhang,S. (2006) Na^+ permeation and block of hERG potassium channels. *J. Gen. Physiol.,* **128**, 55-71.

Gentile,S., Martin,N., Scappini,E., Williams,J., Erxleben,C., & Armstrong,D.L. (2008) The human ERG1 channel polymorphism, K897T, creates a phosphorylation site that inhibits channel activity. *Proc. Natl. Acad. Sci. U. S. A,* **105**, 14704-14708.

Girish,M.P., Gupta,M.D., Mukhopadhyay,S., Yusuf,J., Sunil Roy,T.N., & Trehan,V. (2005) U wave: an important noninvasive electrocardiographic diagnostic marker. *Indian Pacing Electrophysiol. J.,* **5**, 63-65.

Gong,Q., Anderson,C.L., January,C.T., & Zhou,Z. (2002) Role of glycosylation in cell surface expression and stability of HERG potassium channels. *Am J Physiol Heart Circ Physiol,* **283**, H77-H84.

Gong,Q., Keeney,D.R., Molinari,M., & Zhou,Z. (2005) Degradation of trafficking-defective long QT syndrome type II mutant channels by the ubiquitin-proteasome pathway. *J. Biol. Chem.,* **280**, 19419-19425.

Gong,Q., Zhang,L., Vincent,G.M., Horne,B.D., & Zhou,Z. (2007) Nonsense mutations in hERG cause a decrease in mutant mRNA transcripts by nonsense-mediated mRNA decay in human long-QT syndrome. *Circulation,* **116**, 17-24.

Gonzalez,T., Arias,C., Caballero,R., Moreno,I., Delpon,E., Tamargo,J., & Valenzuela,C. (2002) Effects of levobupivacaine, ropivacaine and bupivacaine on HERG channels: stereoselective bupivacaine block. *Brit. J. Pharmacol.,* **137**, 1269-1279.

Grunnet,M., Behr,E.R., Calloe,K., Hofman-Bang,J., Till,J., Christiansen,M., McKenna,W.J., Olesen,S.P., & Schmitt,N. (2005) Functional assessment of compound mutations in the KCNQ1 and KCNH2 genes associated with long QT syndrome. *Heart Rhythm,* **2**, 1238-1249.

Grunnet,M., Hansen,R.S., & Olesen,S.P. (2008) hERG1 channel activators: a new anti-arrhythmic principle. *Prog. Biophys. Mol. Biol.,* **98**, 347-362.

Guasti,L., Crociani,O., Redaelli,E., Pillozzi,S., Polvani,S., Masselli,M., Mello,T., Galli,A., Amedei,A., Wymore,R.S., Wanke,E., & Arcangeli,A. (2008) Identification of a posttranslational mechanism for the regulation of hERG1 K+ channel expression and hERG1 current density in tumor cells. *Mol. Cell Biol.,* **28**, 5043-5060.

Guo,J., Massaeli,H., Xu,J.M., Jia,Z.C., Wigle,J.T., Mesaeli,N., & Zhang,S.T. (2009) Extracellular K+ concentration controls cell surface density of I-Kr in rabbit hearts and of the HERG channel in human cell lines. *J. Clin. Invest.,* **119**, 2745-2757.

Gussak,I., Brugada,P., Brugada,J., Wright,R.S., Kopecky,S.L., Chaitman,B.R., & Bjerregaard,P. (2000) Idiopathic short QT interval: a new clinical syndrome? *Cardiology,* **94**, 99-102.

Gustina,A.S. & Trudeau,M.C. (2009) A recombinant N-terminal domain fully restores deactivation gating in N-truncated and long QT syndrome mutant hERG potassium channels. *Proc. Natl. Acad. Sci. U. S. A,* **106**, 13082-13087.

Gutstein,D.E., Liu,F.Y., Meyers,M.B., Choo,A., & Fishman,G.I. (2003) The organization of adherens junctions and desmosomes at the cardiac intercalated disc is independent of gap junctions. *J. Cell Sci.,* **116**, 875-885.

Hardman,R.M., Stansfeld,P.J., Dalibalta,S., Sutcliffe,M.J., & Mitcheson,J.S. (2007) Activation gating of hERG potassium channels - S6 glycines are not required as gating hinges. *J. Biol. Chem.,* **282**, 31972-31981.

Hartigan-Go,K., Bateman,D.N., Daly,A.K., & Thomas,S.H.L. (1996) Stereoselective cardiotoxic effects of terodiline. *Clin. Pharmacol. Ther.,* 89-98.

He,Y., Hryciw,D.H., Carroll,M.L., Myers,S.A., Whitbread,A.K., Kumar,S., Poronnik,P., & Hooper,J.D. (2008) The ubiquitin-protein ligase Nedd4-2 differentially interacts with and regulates members of the Tweety family of chloride ion channels. *J. Biol. Chem.,* **283**, 24000-24010.

Heath,B.M. & Terrar,D.A. (2000) Protein kinase C enhances the rapidly activating delayed rectifier potassium current, IKr, through a reduction in C-type inactivation in guinea-pig ventricular myocytes. *J. Physiol,* **522 Pt 3**, 391-402.

Henke,G., Maier,G., Wallisch,S., Boehmer,C., & Lang,F. (2004) Regulation of the voltage gated k^+ channel Kv1.3 by the ubiquitin ligase Nedd4-2 and the serum and glucocorticoid inducible kinase SGK1. *J. Cellul. Physiol.,* **199**, 194-199.

Hershko,A., Ciechanover,A., Heller,H., Haas,A.L., & Rose,I.A. (1980) Proposed role of ATP in protein breakdown: conjugation of protein with multiple chains of the polypeptide of ATP-dependent proteolysis. *Proc. Natl. Acad. Sci. U. S. A,* **77**, 1783-1786.

Hershko,A., Heller,H., Elias,S., & Ciechanover,A. (1983) Components of ubiquitin-protein ligase system. Resolution, affinity purification, and role in protein breakdown. *J. Biol. Chem.,* **258**, 8206-8214.

Hewitt,M., Cronin,M.T., Madden,J.C., Rowe,P.H., Johnson,C., Obi,A., & Enoch,S.J. (2007) Consensus QSAR models: do the benefits outweigh the complexity? *J. Chem. Inf. Model.,* **47**, 1460-1468.

Hicke,L., Schubert,H.L., & Hill,C.P. (2005) Ubiquitin-binding domains. *Nat. Rev. Mol. Cell Biol.,* **6**, 610-621.

Hirose,K., Yamaguchi,H., Oshima,Y., Choraku,M., Hirono,A., Takamori,N., & Tamura,K. (2008) Severe respiratory failure and torsades de pointes induced by disopyramide in a patient with myasthenia gravis. *Intern. Med.,* **47**, 1703-1708.

Hondeghem,L.M. & Snyders,D.J. (1990) Class III antiarrhythmic agents have a lot of potential but a long way to go. Reduced effectiveness and dangers of reverse use dependence. *Circulation,* **81**, 686-690.

Hryciw,D.H., Ekberg,J., Lee,A., Lensink,I.L., Kumar,S., Guggino,W.B., Cook,D.I., Pollock,C.A., & Poronnik,P. (2004) Nedd4-2 functionally interacts with ClC-5: involvement in constitutive albumin endocytosis in proximal tubule cells. *J. Biol. Chem.,* **279**, 54996-55007.

Ikeda,F. & Dikic,I. (2008) Atypical ubiquitin chains: new molecular signals. 'Protein Modifications: Beyond the Usual Suspects' review series. *EMBO Rep.,* **9**, 536-542.

Ilsley,J.L., Sudol,M., & Winder,S.J. (2002) The WW domain: linking cell signalling to the membrane cytoskeleton. *Cell Signal.,* **14**, 183-189.

Imai,Y.N., Ryu,S., & Oiki,S. (2009) Docking model of drug binding to the human ether-a-go-go potassium channel guided by tandem dimer mutant patch-clamp data: a synergic approach. *J. Med. Chem.,* **52**, 1630-1638.

Ingelman-Sundberg,M. (2001) Pharmacogenetics: an opportunity for a safer and more efficient pharmacotherapy. *J. Intern. Med.,* **250**, 186-200.

Ito,K., Sugihara,H., Kinoshita,N., Azuma,A., & Matsubara,H. (2005) Assessment of Takotsubo cardiomyopathy (transient left ventricular apical ballooning) using 99mTc-tetrofosmin, 123I-BMIPP, 123I-MIBG and 99mTc-PYP myocardial SPECT. *Ann. Nucl. Med.,* **19**, 435-445.

Jamieson,C., Moir,E.M., Rankovic,Z., & Wishart,G. (2006) Medicinal chemistry of hERG optimizations: highlights and hang-ups. *J. Med. Chem.,* **49**, 5029-5046.

Jenke,M., Sanchez,A., Monje,F., Stuhmer,W., Weseloh,R.M., & Pardo,L.A. (2003) C-terminal domains implicated in the functional surface expression of potassium channels. *EMBO J.,* **22**, 395-403.

Jentsch,T.J., Hubner,C.A., & Fuhrmann,J.C. (2004) Ion channels: Function unravelled by dysfunction. *Nature Cell Biol.,* **6**, 1039-1047.

Jervell,A. & Lange-Nielsen,F. (1957) Congenital deaf-mutism, functional heart disease with prolongation of the Q-T interval and sudden death. *Am. Heart J.,* **54**, 59-68.

Jespersen,T., Membrez,M., Nicolas,C.S., Pitard,B., Staub,O., Olesen,S.-P., Baro,I., & Abriel,H. (2007) The KCNQ1 potassium channel is down-regulated by ubiquitylating enzymes of the Nedd4/Nedd4-like family. *Cardiovascul. Res.,* **74**, 64-74.

Jiang,Y., Ruta,V., Chen,J., Lee,A., & MacKinnon,R. (2003) The principle of gating charge movement in a voltage-dependent K+ channel. *Nature,* **423**, 42-48.

Jones,S.E., Ogura,T., Shuba,L.M., & McDonald,T.F. (1998) Inhibition of the rapid component of the delayed-rectifier K+ current by therapeutic concentrations of the antispasmodic agent terodiline. *Br. J. Pharmacol.,* **125**, 1138-1143.

Jurkiewicz,N.K., Wang,J., Fermini,B., Sanguinetti,M.C., & Salata,J.J. (1996) Mechanism of action potential prolongation by RP 58866 and its active enantiomer, terikalant. Block of the rapidly activating delayed rectifier K^+ current, I_{Kr}. *Circulation.,* **94**, 2938-2946.

Kagan,A. & McDonald,T.V. (2005) Dynamic control of hERG/I(Kr) by PKA-mediated interactions with 14-3-3. *Novartis. Found. Symp.,* **266**, 75-89.

Kamiya,K., Niwa,R., Morishima,M., Honjo,H., & Sanguinetti,M.C. (2008) Molecular determinants of hERG channel block by terfenadine and cisapride. *J. Pharmacol. Sci.,* **108**, 301-307.

Kamynina,E., Debonneville,C., Bens,M., Vandewalle,A., & Staub,O. (2001a) A novel mouse Nedd4 protein suppresses the activity of the epithelial Na+ channel. *FASEB J.,* **15**, 204-214.

Kamynina,E., Tauxe,C., & Staub,O. (2001b) Distinct characteristics of two human Nedd4 proteins with respect to epithelial Na(+) channel regulation. *Am. J. Physiol Renal Physiol,* **281**, F469-F477.

Kanai,Y., Tateyama,S., Nakamura,T., Kasaba,T., & Takasaki,M. (1999) Effects of levobupivacaine, bupivacaine, and ropivacaine on tail-flick response and motor function in rats following epidural or intrathecal administration. *Reg Anesth. Pain Med.,* **24**, 444-452.

Kanelis,V., Rotin,D., & Forman-Kay,J.D. (2001) Solution structure of a Nedd4 WW domain-ENaC peptide complex. *Nat. Struct Biol.,* **8**, 407-412.

Karle,C.A., Zitron,E., Zhang,W., Kathofer,S., Schoels,W., & Kiehn,J. (2002) Rapid component I(Kr) of the guinea-pig cardiac delayed rectifier K(+) current is inhibited by beta(1)-adrenoreceptor activation, via cAMP/protein kinase A-dependent pathways. *Cardiovasc. Res.,* **53**, 355-362.

Katchman,A.N., McGroary,K.A., Kilborn,M.J., Kornick,C.A., Manfredi,P.L., Woosley,R.L., & Ebert,S.N. (2002) Influence of opioid agonists on cardiac human ether-a-go-go-related gene K(+) currents. *J. Pharmacol. Exp. Ther.,* **303**, 688-694.

Khan,I.A. (2002a) Clinical and therapeutic aspects of congenital and acquired long QT syndrome. *Am. J. Med.,* **112**, 58-66.

Khan,I.A. (2002b) Long QT syndrome: diagnosis and management. *Am. Heart J.,* **143**, 7-14.

Khan,I.A. & Gowda,R.M. (2004) Novel therapeutics for treatment of long-QT syndrome and torsade de pointes. *Int. J. Cardiol.,* **95**, 1-6.

Kim,H.T., Kim,K.P., Lledias,F., Kisselev,A.F., Scaglione,K.M., Skowyra,D., Gygi,S.P., & Goldberg,A.L. (2007) Certain pairs of ubiquitin-conjugating enzymes (E2s) and ubiquitin-protein ligases (E3s) synthesize nondegradable forked ubiquitin chains containing all possible isopeptide linkages. *J. Biol. Chem.,* **282**, 17375-17386.

Kimura,Y., Takayanagi,K., Sakai,Y., Satoh,T., Fujito,T., Inoue,T., Hayashi,T., Morooka,S., & Takabatake,Y. (1994) Torsades de pointes in paced patients with sick sinus syndrome after disopyramide administration. *Jpn. Heart J.,* **35**, 153-161.

Kirchhof,P., Franz,M.R., Bardai,A., & Wilde,A.M. (2009) Giant T-U waves precede torsades de pointes in long QT syndrome. A systematic electrocardiographic analysis in patients with acquired and congenital QT prolongation. *J. Am. Coll. Cardiol.,* **54**, 143-149.

Komander,D. (2009) The emerging complexity of protein ubiquitination. *Biochem. Soc. Trans.,* **37**, 937-953.

Komander,D., Clague,M.J., & Urbe,S. (2009) Breaking the chains: structure and function of the deubiquitinases. *Nat. Rev. Mol. Cell Biol.,* **10**, 550-563.

Kupershmidt,S., Snyders,D.J., Raes,A., & Roden,D.M. (1998) A K+ channel splice variant common in human heart lacks a C-terminal domain required for expression of rapidly activating delayed rectifier current. *J. Biol. Chem.,* **273**, 27231-27235.

Kupershmidt,S., Yang,T., Chanthaphaychith,S., Wang,Z.Q., Towbin,J.A., & Roden,D.M. (2002) Defective human ether-a-go-go-related gene trafficking linked to an endoplasmic reticulum retention signal in the C terminus. *J. Biol. Chem.,* **277**, 27442-27448.

Kurokawa,J., Tamagawa,M., Harada,N., Honda,S., Bai,C.X., Nakaya,H., & Furukawa,T. (2008) Acute effects of oestrogen on the guinea pig and human I-Kr channels and drug-induced prolongation of cardiac repolarization. *J. Physiol.,* **586**, 2961-2973.

Larsen,A.P., Olesen,S.P., Grunnet,M., & Jespersen,T. (2008) Characterization of hERG1a and hERG1b potassium channels-a possible role for hERG1b in the I (Kr) current. *Pflugers Arch.,* **456**, 1137-1148.

Larsen,A.P., Olesen,S.P., Grunnet,M., & Poelzing,S. (2010) Pharmacological Activation of I Impairs Conduction in Guinea Pig Hearts. *J. Cardiovasc. Electrophysiol.*.

Lee-Son,S., Wang,G.K., Concus,A., Crill,E., & Strichartz,G. (1992) Stereoselective inhibition of neuronal sodium channels by local anesthetics. Evidence for two sites of action? *Anesthesiology,* **77**, 324-335.

Lin,C.R., Somberg,T., Molnar,J., & Somberg,J. (2009) The effects of chiral isolates of methadone on the cardiac potassium channel IKr. *Cardiology,* **113**, 59-65.

Lin,J., Lin,S., Choy,P.C., Shen,X., Deng,C., Kuang,S., Wu,J., & Xu,W. (2008) The regulation of the cardiac potassium channel (HERG) by caveolin-1. *Biochem. Cell Biol.,* **86**, 405-415.

Linna,E.H., Perkiomaki,J.S., Karsikas,M., Seppanen,T., Savolainen,M., Kesaniemi,Y.A., Makikallio,T., & Huikuri,H.V. (2006) Functional significance of KCNH2 (HERG) K897T polymorphism for cardiac repolarization assessed by analysis of T-wave morphology. *Ann. Noninvasive. Electrocardiol.,* **11**, 57-62.

Long,S.B., Campbell,E.B., & MacKinnon,R. (2005) Voltage sensor of kv1.2: Structural basis of electromechanical coupling. *Science,* **309**, 903-908.

Lu,Y., Mahaut-Smith,M.P., Varghese,A., Huang,C.L.H., Kemp,P.R., & Vandenberg,J.I. (2001) Effects of premature stimulation on HERG K+ channels. *J. Physiol.,* **537**, 843-851.

Ludwig,J., Owen,D., & Pongs,O. (1997) Carboxy-terminal domain mediates assembly of the voltage-gated rat ether-a-go-go potassium channel. *EMBO J.,* **16**, 6337-6345.

Maier,G., Palmada,M., Rajamanickam,J., Shumilina,E., Böhmer,C., & Lang,F. (2006) Upregulation of HERG channels by the serum and glucocorticoid inducible kinase isoform SGK3. *Cell. Physiol. Biochem.,* **18**, 177-186.

Marban,E. (2002) Cardiac channelopathies. *Nature,* **415**, 213-218.

Marieb,E.N. (1998) The Cardiovascular System: the Heart, in *Human Anatomy and Physiology*, p. 656-690. Pearson Benjamin Cummings.

Martin,R.L., Su,Z., Limberis,J.T., Palmatier,J.D., Cowart,M.D., Cox,B.F., & Gintant,G.A. (2006) In vitro preclinical cardiac assessment of tolterodine and terodiline: multiple factors predict the clinical experience. *J. Cardiovasc. Pharmacol.,* **48**, 199-206.

Masetti,M., Cavalli,A., & Recanatini,M. (2007) Modeling the hERG potassium channel in a phospholipid bilayer: molecular dynamics and drug docking studies. *J. Comput. Chem.*.

Massaeli,H., Guo,J., Xu,J., & Zhang,S. (2010) Extracellular K+ is a prerequisite for the function and plasma membrane dtability of HERG channels. *Circ. Res.,* CIRCRESAHA.

Mbai,M., Rajamani,S., & January,C.T. (2002) The anti-malarial drug halofantrine and its metabolite N-desbutylhalofantrine block HERG potassium channels. *Cardiovasc. Res.,* **55**, 799-805.

McDonald,T.V., Yu,Z., Ming,Z., Palma,E., Meyers,M.B., Wang,K.W., Goldstein,S.A., & Fishman,G.I. (1997) A minK-HERG complex regulates the cardiac potassium current I(Kr). *Nature,* **388**, 289-292.

Medeiros-Domingo,A., Iturralde-Torres,P., & Ackerman,M.J. (2007) Clinical and genetic characteristics of long QT syndrome. *Rev. Esp. Cardiol.,* **60**, 739-752.

Meijler,F.L. & Janse,M.J. (1988) Morphology and electrophysiology of the mammalian atrioventricular node. *Physiol Rev.,* **68**, 608-647.

Michalets,E.L. & Williams,C.R. (2000) Drug interactions with cisapride: clinical implications. *Clin. Pharmacokinet.,* **39**, 49-75.

Milnes,J.T., Crociani,O., Arcangeli,A., Hancox,J.C., & Witchel,H.J. (2003a) Blockade of HERG potassium currents by fluvoxamine: incomplete attenuation by S6 mutations at F656 or Y652. *Brit. J. Pharmacol.,* **139**, 887-898.

Milnes,J.T., Dempsey,C.E., Ridley,J.M., Crociani,O., Arcangeli,A., Hancox,J.C., & Witchel,H.J. (2003b) Preferential closed channel blockade of HERG potassium currents by chemically synthesised BeKm-1 scorpion toxin. *FEBS Lett.,* **547**, 20-26.

Mitcheson,J.S., Chen,J., Lin,M., Culberson,C., & Sanguinetti,M.C. (2000a) A structural basis for drug-induced long QT syndrome. *Proc. Natl. Acad. Sci. USA,* **97**, 12329-12333.

Mitcheson,J.S., Chen,J., & Sanguinetti,M.C. (2000b) Trapping of a methanesulfonanilide by closure of the HERG potassium channel activation gate. *J. Gen. Physiol.,* **115**, 229-239.

Morais Cabral,J.S., Lee,A., Cohen,S.L., Chait,B.T., Li,M., & MacKinnon,R. (1998) Crystal structure and functional analysis of the HERG potassium channel N terminus: A eukaryotic PAS domain. *Cell,* **95**, 649-655.

Morgan,T.K., Jr. & Sullivan,M.E. (1992) An overview of class III electrophysiological agents: a new generation of antiarrhythmic therapy. *Prog. Med. Chem.,* **29**, 65-108.

Moss,A.J., Zareba,W., Kaufman,E.S., Gartman,E., Peterson,D.R., Benhorin,J., Towbin,J.A., Keating,M.T., Priori,S.G., Schwartz,P.J., Vincent,G.M., Robinson,J.L., Andrews,M.L., Feng,C., Hall,W.J., Medina,A., Zhang,L., & Wang,Z. (2002) Increased risk of arrhythmic events in long-QT syndrome with mutations in the pore region of the human ether-a-go-go-related gene potassium channel. *Circulation,* **105**, 794-799.

Nademanee,K. (2009) Genotype-phenotype relationship in the long QT syndrome: brimming with knowledge but thirsting for a therapeutic solution. *J. Am. Coll. Cardiol.,* **54**, 2063-2064.

Nakajima,T., Furukawa,T., Hirano,Y., Tanaka,T., Sakurada,H., Takahashi,T., Nagai,R., Itoh,T., Katayama,Y., Nakamura,Y., & Hiraoka,M. (1999) Voltage-shift of the current activation in HERG S4 mutation (R534C) in LQT2. *Cardiovasc. Res.,* **44**, 283-293.

Nakajima,T., Furukawa,T., Tanaka,T., Katayama,Y., Nagai,R., Nakamura,Y., & Hiraoka,M. (1998) Novel mechanism of HERG current suppression in LQT2: shift in voltage dependence of HERG inactivation. *Circ. Res.,* **83**, 415-422.

Nef,H.M., Mollmann,H., Akashi,Y.J., & Hamm,C.W. (2010) Mechanisms of stress (Takotsubo) cardiomyopathy. *Nat. Rev. Cardiol.*.

Newcombe, D. A. L (2006) An examination of the pharmacodynamics and pharmacokinetics of Levo-alpha-actelymethadol (LAAM), compared to methadone, in opioid maintenance patients. *PhD Thesis.* University of Adelaide

Newman,J.L., Vann,R.E., May,E.L., & Beardsley,P.M. (2002) Heroin discriminative stimulus effects of methadone, LAAM and other isomers of acetylmethadol in rats. *Psychopharmacology (Berl),* **164**, 108-114.

Numaguchi,H., Johnson,J.P., Jr., Petersen,C.I., & Balser,J.R. (2000) A sensitive mechanism for cation modulation of potassium current. *Nat. Neurosci.,* **3**, 429-430.

O'Brien,S.E. & de Groot,M.J. (2005) Greater than the sum of its parts: combining models for useful ADMET prediction. *J. Med. Chem.,* **48**, 1287-1291.

Opthof,T. (1988) The mammalian sinoatrial node. *Cardiovasc. Drugs Ther.,* **1**, 573-597.

Österberg,F. & Aqvist,J. (2005) Exploring blocker binding to a homology model of the open hERG K^+ channel using docking and molecular dynamics methods. *FEBS Lett.,* **579**, 2939-2944.

Paavonen,K.J., Chapman,H., Laitinen,P.J., Fodstad,H., Piippo,K., Swan,H., Toivonen,L., Viitasalo,M., Kontula,K., & Pasternack,M. (2003) Functional characterization of the common amino acid 897 polymorphism of the cardiac potassium channel KCNH2 (HERG). *Cardiovasc. Res.,* **59**, 603-611.

Pardo-Lopez,L., Garcia-Valdes,J., Gurrola,G.B., Robertson,G.A., & Possani,L.D. (2002) Mapping the receptor site for ergtoxin, a specific blocker of ERG channels. *FEBS Lett.,* **510**, 45-49.

Patel,C. & Antzelevitch,C. (2008) Cellular basis for arrhythmogenesis in an experimental model of the SQT1 form of the short QT syndrome. *Heart Rhythm,* **5**, 585-590.

Paul,A.A., Witchel,H.J., & Hancox,J.C. (2001) Inhibition of HERG potassium channel current by the class 1a antiarrhythmic agent disopyramide. *Biochem. Biophys. Res. Commun.,* **280**, 1243-1250.

Paulussen,A., Raes,A., Matthijs,G., Snyders,D.J., Cohen,N., & Aerssens,J. (2002) A novel mutation (T65P) in the PAS domain of the human potassium channel HERG results in the long QT syndrome by trafficking deficiency. *J. Biol. Chem.,* **277**, 48610-48616.

Paulussen,A.D., Gilissen,R.A., Armstrong,M., Doevendans,P.A., Verhasselt,P., Smeets,H.J., Schulze-Bahr,E., Haverkamp,W., Breithardt,G., Cohen,N., & Aerssens,J. (2004) Genetic variations of KCNQ1, KCNH2, SCN5A, KCNE1, and KCNE2 in drug-induced long QT syndrome patients. *J. Mol. Med.,* **82**, 182-188.

Pearlstein,R.A., Vaz,R.J., Kang,J., Chen,X.L., Preobrazhenskaya,M., Shchekotikhin,A.E., Korolev,A.M., Lysenkova,L.N., Miroshnikova,O.V., Hendrix,J., & Rampe,D. (2003) Characterization of HERG potassium channel inhibition using CoMSiA 3D QSAR and homology modeling approaches. *Bioorg. Med. Chem. Lett.,* **13**, 1829-1835.

Perez Riera,A.R., Ferreira,C., Filho,C.F., Ferreira,M., Meneghini,A., Uchida,A.H., Schapachnik,E., Dubner,S., & Zhang,L. (2008) The enigmatic sixth wave of the electrocardiogram: the U wave. *Cardiol. J.,* **15**, 408-421.

Perrin,M.J., Subbiah,R.N., Vandenberg,J.I., & Hill,A.P. (2008) Human ether-a-go-go related gene (hERG) K+ channels: function and dysfunction. *Prog. Biophys. Mol. Biol.,* **98**, 137-148.

Persaud,A., Alberts,P., Amsen,E.M., Xiong,X., Wasmuth,J., Saadon,Z., Fladd,C., Parkinson,J., & Rotin,D. (2009) Comparison of substrate specificity of the ubiquitin ligases Nedd4 and Nedd4-2 using proteome arrays. *Mol. Syst. Biol.,* **5**, 333.

Petrecca,K., Atanasiu,R., Akhavan,A., & Shrier,A. (1999) N-linked glycosylation sites determine HERG channel surface membrane expression. *J. Physiol,* **515 (Pt 1)**, 41-48.

Pham,T.V. & Rosen,M.R. (2002) Sex, hormones, and repolarization. *Cardiovascul. Res.,* **53**, 740-751.

Pinney,S.P., Koller,B.S., Franz,M.R., & Woosley,R.L. (1995) Terfenadine increases the Qt interval in isolated guinea-pig heart. *J. Cardiovasc. Pharmacol.,* **25**, 30-34.

Piper,D.R., Sanguinetti,M.C., & Tristani-Firouzi,M. (2005) Voltage sensor movement in the hERG K+ channel. *Novartis. Found. Symp.,* **266**, 46-52.

Piper,D.R., Varghese,A., Sanguinetti,M.C., & Tristani-Firouzi,M. (2003) Gating currents associated with intramembrane charge displacement in HERG potassium channels. *Proc. Natl. Acad. Sci. U. S. A,* **100**, 10534-10539.

Plant,P.J., Yeger,H., Staub,O., Howard,P., & Rotin,D. (1997) The C2 domain of the ubiquitin protein ligase Nedd4 mediates Ca2+-dependent plasma membrane localization. *J. Biol. Chem.,* **272**, 32329-32336.

Pond,A.L., Scheve,B.K., Benedict,A.T., Petrecca,K., Van Wagoner,D.R., Shrier,A., & Nerbonne,J.M. (2000) Expression of distinct ERG proteins in rat, mouse, and human heart. Relation to functional I(Kr) channels. *J. Biol. Chem.,* **275**, 5997-6006.

Popp,B.D., Hutchinson,D.S., Evans,B.A., & Summers,R.J. (2004) Stereoselectivity for interactions of agonists and antagonists at mouse, rat and human beta3-adrenoceptors. *Eur. J. Pharmacol.,* **484**, 323-331.

Potet,F., Bouyssou,T., Escande,D., & Baro,I. (2001) Gastrointestinal prokinetic drugs have different affinity for the human cardiac human ether-a-gogo K(+) channel. *J. Pharmacol. Exp. Ther.,* **299**, 1007-1012.

Priori,S.G., Napolitano,C., & Schwartz,P.J. (1999) Low penetrance in the long-QT syndrome : clinical impact. *Circulation,* **99**, 529-533.

Priori,S.G., Schwartz,P.J., Napolitano,C., Bianchi,L., Dennis,A., De,F.M., Brown,A.M., & Casari,G. (1998) A recessive variant of the Romano-Ward long-QT syndrome? *Circulation,* **97**, 2420-2425.

Priori,S.G., Schwartz,P.J., Napolitano,C., Bloise,R., Ronchetti,E., Grillo,M., Vicentini,A., Spazzolini,C., Nastoli,J., Bottelli,G., Folli,R., & Cappelletti,D. (2003) Risk stratification in the long-QT syndrome. *N. Engl. J. Med.,* **348**, 1866-1874.

Rajamani,S., Anderson,C.L., Anson,B.D., & January,C.T. (2002) Pharmacological rescue of human K(+) channel long-QT2 mutations: human ether-a-go-go-related gene rescue without block. *Circulation,* **105**, 2830-2835.

Rajamani,S., Eckhardt,L.L., Valdivia,C.R., Klemens,C.A., Gillman,B.M., Anderson,C.L., Holzem,K.M., Delisle,B.P., Anson,B.D., Makielski,J.C., & January,C.T. (2006) Drug-induced long QT syndrome: hERG K+ channel block and disruption of protein trafficking by fluoxetine and norfluoxetine. *Br. J. Pharmacol.,* **149**, 481-489.

Ravens,U. & Cerbai,E. (2008) Role of potassium currents in cardiac arrhythmias. *Europace,* **10**, 1133-1137.

Recanatini,M., Cavalli,A., & Masetti,M. (2005) In silico modelling – pharmacophores and hERG channel models. Novartis Found.Symp. 266, 171-181.

Redfern,W.S., Carlsson,L., Davis,A.S., Lynch,W.G., MacKenzie,I., Palethorpe,S., Strang,I., Siegl,P.K.S., Sullivan,A.T., Wallis,R., Camm,A.J., & Hammond,T.G. (2003) Relationships between preclinical cardiac electrophysiology, clinical QT interval prolongation and torsade de pointes for a broad range of drugs: evidence for a provisional safety margin in drug development. *Cardiovascul. Res.,* **58**, 32-45.

Ritsema van Eck,H.J., Kors,J.A., & van,H.G. (2005) The U wave in the electrocardiogram: a solution for a 100-year-old riddle. *Cardiovasc. Res.,* **67**, 256-262.

Rivera-Ruiz,M., Cajavilca,C., & Varon,J. (2008) Einthoven's string galvanometer: the first electrocardiograph. *Tex. Heart Inst. J.,* **35**, 174-178.

Robenek,H., Weissen-Plenz,G., & Severs,N.J. (2008) Freeze-fracture replica immunolabelling reveals caveolin-1 in the human cardiomyocyte plasma membrane. *J. Cell Mol. Med.,* **12**, 2519-2521.

Roden,D.M. (1998) Taking the "idio" out of "idiosyncratic": Predicting torsades de pointes. *Pace-Pacing and Clinical Electrophysiology,* **21**, 1029-1034.

Roden,D.M. (2004) Drug-induced prolongation of the QT interval. *N. Engl. J. Med.,* **350**, 1013-1022.

Roden,D.M. (2006) Long QT syndrome: reduced repolarization reserve and the genetic link. *J. Intern. Med.,* **259**, 59-69.

Roden,D.M., Balser,J.R., George,A.L., Jr., & Anderson,M.E. (2002) Cardiac ion channels. *Annu. Rev. Physiol,* **64**, 431-475.

Roden,D.M. & Viswanathan,P.C. (2005) Genetics of acquired long QT syndrome. *J. Clin. Invest.,* **115**, 2025-2032.

Roepke,T.K. & Abbott,G.W. (2006) Pharmacogenetics and cardiac ion channels. *Vasc. Pharmacol.,* **44**, 90-106.

Romano,C., Gemme,G., & Pongiglione,R. (1963) Rare Cardiac Arrhythmias of the Pediatric Age. *Minerva Pediatr.,* **15**, 1155-1164.

Rosati,B., Marchetti,P., Crociani,O., Lecchi,M., Lupi,R., Arcangeli,A., Olivotto,M., & Wanke,E. (2000) Glucose- and arginine-induced insulin secretion by human pancreatic beta-cells: the role of HERG K(+) channels in firing and release. *FASEB J.,* **14**, 2601-2610.

Rossenbacker,T., Mubagwa,K., Jongbloed,R.J., Vereecke,J., Devriendt,K., Gewillig,M., Carmeliet,E., Collen,D., Heidbuchel,H., & Carmeliet,P. (2005) Novel Mutation in the Per-Arnt-Sim Domain of KCNH2 Causes a Malignant Form of Long-QT Syndrome. *Circulation,* **111**, 961-968.

Roth,J. (2002) Protein N-glycosylation along the secretory pathway: Relationship to organelle topography and function, protein quality control, and cell interactions. *Chemical Reviews,* **102**, 285-303.

Roti,E.C., Myers,C.D., Ayers,R.A., Boatman,D.E., Delfosse,S.A., Chan,E.K., Ackerman,M.J., January,C.T., & Robertson,G.A. (2002) Interaction with GM130 during HERG ion channel trafficking. Disruption by type 2 congenital long QT syndrome mutations. Human Ether-a-go-go-Related Gene. *J. Biol. Chem.,* **277**, 47779-47785.

Rougier,J.S., Albesa,M., & Abriel,H. (2010) Ubiquitylation and SUMOylation of Cardiac Ion Channels. *J. Cardiovasc. Pharmacol.*.

Rougier,J.S., van Bemmelen,M.X., Bruce,M.C., Jespersen,T., Gavillet,B., Apothéloz,F., Cordonier,S., Staub,O., Rotin,D., & Abriel,H. (2005) Molecular determinants of voltage-gated sodium channel regulation by the Nedd4/Nedd4-like proteins. *Am. J. Physiol. Cell. Physiol.,* **288**, 692-701.

Saenen,J.B., Labro,A.J., Raes,A., & Snyders,D.J. (2006) Modulation of HERG gating by a charge cluster in the N-terminal proximal domain. *Biophys. J.,* **91**, 4381-4391.

Samuelov-Kinori,L., Kinori,M., Kogan,Y., Swartzon,M., Shalev,H., Guy,D., Ferenidou,F., Mashav,N., Sadeh,B., Atzmony,L., Kliuk-Ben-Basat,O., Steinvil,A., & Justo,D. (2009) Takotsubo cardiomyopathy and QT interval prolongation: who are the patients at risk for torsades de pointes? *J. Electrocardiol.,* **42**, 353-357.

Sanguinetti,M.C., Jiang,C.G., Curran,M.E., & Keating,M.T. (1995) A mechanistic link between an inherited and an acquired cardiac-arrhythmia - Herg encodes the I-Kr potassium channel. *Cell,* **81**, 299-307.

Sanguinetti,M.C., Jurkiewicz,N.K., Scott,A., & Siegl,P.K. (1991) Isoproterenol antagonizes prolongation of refractory period by the class III antiarrhythmic agent E-4031 in guinea pig myocytes. Mechanism of action. *Circ. Res.,* **68**, 77-84.

Sanguinetti,M.C. & Tristani-Firouzi,M. (2006) hERG potassium channels and cardiac arrhythmia. *Nature,* **440**, 463-469.

Sansom,M.S.P. & Weinstein,H. (2000) Hinges, swivels and switches: the role of prolines in signalling via transmembrane alpha-helices. *Trends in Pharmacological Sciences,* **21**, 445-451.

Schild,L., Lu,Y., Gautschi,I., Schneeberger,E., Lifton,R.P., & Rossier,B.C. (1996) Identification of a PY motif in the epithelial Na channel subunits as a target sequence for mutations causing channel activation found in Liddle syndrome. *EMBO J.,* **15**, 2381-2387.

Schimpf,R., Veltmann,C., Wolpert,C., & Borggrefe,M. (2009) Channelopathies: Brugada syndrome, long QT syndrome, short QT syndrome, and CPVT. *Herz,* **34**, 281-288.

Schonherr,R. & Heinemann,S.H. (1996) Molecular determinants for activation and inactivation of HERG, a human inward rectifier potassium channel. *J. Physiol,* **493 (Pt 3)**, 635-642.

Schwartz,P.J., Priori,S.G., Locati,E.H., Napolitano,C., Cantu,F., Towbin,J.A., Keating,M.T., Hammoude,H., Brown,A.M., & Chen,L.S. (1995) Long QT syndrome patients with mutations of the SCN5A and HERG genes have differential responses to Na+ channel blockade and to increases in heart rate. Implications for gene-specific therapy. *Circulation,* **92**, 3381-3386.

Sesti,F., Abbott,G.W., Wei,J., Murray,K.T., Saksena,S., Schwartz,P.J., Priori,S.G., Roden,D.M., George,A.L., Jr., & Goldstein,S.A. (2000) A common polymorphism associated with antibiotic-induced cardiac arrhythmia. *Proc. Natl. Acad. Sci. U. S. A,* **97**, 10613-10618.

Severs,N.J. (2000) The cardiac muscle cell. *Bioessays,* **22**, 188-199.

Shearwin-Whyatt,L., Dalton,H.E., Foot,N., & Kumar,S. (2006) Regulation of functional diversity within the Nedd4 family by accessory and adaptor proteins. *BioEssays,* **28**, 617-628.

Shi,P.P., Cao,X.R., Sweezer,E.M., Kinney,T.S., Williams,N.R., Husted,R.F., Nair,R., Weiss,R.M., Williamson,R.A., Sigmund,C.D., Snyder,P.M., Staub,O., Stokes,J.B., & Yang,B. (2008) Salt-sensitive hypertension and cardiac hypertrophy in mice deficient in the ubiquitin ligase Nedd4-2. *Am. J. Physiol Renal Physiol,* **295**, F462-F470.

Shimizu,W. (2005) The long QT syndrome: therapeutic implications of a genetic diagnosis. *Cardiovascul. Res.,* **67**, 347-356.

Shimizu,W., Moss,A.J., Wilde,A.A., Towbin,J.A., Ackerman,M.J., January,C.T., Tester,D.J., Zareba,W., Robinson,J.L., Qi,M., Vincent,G.M., Kaufman,E.S., Hofman,N., Noda,T., Kamakura,S., Miyamoto,Y., Shah,S., Amin,V., Goldenberg,I., Andrews,M.L., & McNitt,S. (2009) Genotype-phenotype aspects of type 2 long QT syndrome. *J. Am. Coll. Cardiol.,* **54**, 2052-2062.

Shoeb,F., Malykhina,A.P., & Akbarali,H.I. (2003) Cloning and functional characterization of the smooth muscle ether-a-go-go-related gene K+ channel. Potential role of a conserved amino acid substitution in the S4 region. *J. Biol. Chem.,* **278**, 2503-2514.

Siebrands,C.C. & Friederich,P. (2007) Structural requirements of human ether-a-go-go-related gene channels for block by bupivacaine. *Anesthesiology,* **106**, 523-531.

Siebrands,C.C., Schmitt,N., & Friederich,P. (2005) Local anesthetic interaction with human ether-a-go-go-related gene (HERG) channels. *Anesthesiology,* **103**, 102-112.

Smith,P.L., Baukrowitz,T., & Yellen,G. (1996) The inward rectification mechanism of the HERG cardiac potassium channel. *Nature,* **379**, 833-836.

Smith,P.L. & Yellen,G. (2002) Fast and slow voltage sensor movements in HERG potassium channels. *J. Gen. Physiol,* **119**, 275-293.

Snyder,P.M. (2009) Down-regulating destruction: phosphorylation regulates the E3 ubiquitin ligase Nedd4-2. *Sci. Signal.,* **2**, e41.

Snyder,P.M., Olson,D.R., & Thomas,B.C. (2002) Serum and glucocorticoid-regulated kinase modulates Nedd4-2-mediated inhibition of the epithelial Na+ channel. *J. Biol. Chem.,* **277**, 5-8.

Solc,D. (2007) The heart and heart conducting system in the kingdom of animals: A comparative approach to its evolution. *Exp. Clin. Cardiol.,* **12**, 113-118.

Spector,P.S., Curran,M.E., Keating,M.T., & Sanguinetti,M.C. (1996a) Class III antiarrhythmic drugs block HERG, a human cardiac delayed rectifier K+ channel. Open-channel block by methanesulfonanilides. *Circ. Res.,* **78**, 499-503.

Spector,P.S., Curran,M.E., Zou,A., Keating,M.T., & Sanguinetti,M.C. (1996b) Fast inactivation causes rectification of the IKr channel. *J. Gen. Physiol,* **107**, 611-619.

Splawski,I., Timothy,K.W., Tateyama,M., Clancy,C.E., Malhotra,A., Beggs,A.H., Cappuccio,F.P., Sagnella,G.A., Kass,R.S., & Keating,M.T. (2002) Variant of SCN5A sodium channel implicated in risk of cardiac arrhythmia. *Science,* **297**, 1333-1336.

Stansfeld,P.J., Gedeck,P., Gosling,M., Cox,B., Mitcheson,J.S., & Sutcliffe,M.J. (2007) Drug block of the hERG potassium channel: insight from modeling. *Proteins: Struct. Funct. Bioinf.,* **68**, 568-580.

Stary,A., Wacker,S.J., Boukharta,L., Zachariae,U., Karimi-Nejad,Y., Aqvist,J., Vriend,G., & de Groot,B.L. (2010) Toward a consensus model of the hERG potassium channel. *Chem. Med. Chem.,* **00**, 1-14.

Staub,O., Dho,S., Henry,P., Correa,J., Ishikawa,T., McGlade,J., & Rotin,D. (1996) WW domains of Nedd4 bind to the proline-rich PY motifs in the epithelial Na+ channel deleted in Liddle's syndrome. *EMBO J.,* **15**, 2371-2380.

Sticherling,C., Schaer,B.A., Ammann,P., Maeder,M., & Osswald,S. (2005) Methadone-induced torsade de pointes tachycardias. *Swiss Med Wkly,* **135**, 282-285.

Su,Z., Limberis,J., Martin,R.L., Xu,R., Kolbe,K., Heinemann,S.H., Hoshi,T., Cox,B.F., & Gintant,G.A. (2007) Functional consequences of methionine oxidation of hERG potassium channels. *Biochem. Pharmacol.,* **74**, 702-711.

Subbiah,R.N., Kondo,M., Campbell,T.J., Kondo,M., Campbell,T.J., & Vandenberg,J.I. (2005) Tryptophan scanning mutagenesis of the HERG K^+ channel: the S4 domain is loosely packed and likely to be lipid exposed. *J. Physiol.,* **569**, 367-379.

Sun,Z., Milos,P.M., Thompson,J.F., Lloyd,D.B., Mank-Seymour,A., Richmond,J., Cordes,J.S., & Zhou,J. (2004) Role of a KCNH2 polymorphism (R1047 L) in dofetilide-induced Torsades de Pointes. *J. Mol. Cell Cardiol.,* **37**, 1031-1039.

Swynghedauw,B. & Chevalier,B. (1995) Biological characteristics of the myocardium during the regression of cardiac hypertrophy due to mechanical overload. *J. Heart Valve Dis.,* **4 Suppl 2**, S154-S159.

Taglialatela,M., Castaldo,P., Iossa,S., Pannaccione,A., Fresi,A., Ficker,E., & Annunziato,L. (1997) Regulation of the human ether-a-gogo related gene (HERG) K+ channels by reactive oxygen species. *Proc. Natl. Acad. Sci. U. S. A.,* **94**, 11698-11703.

Takemasa,H., Nagatomo,T., Abe,H., Kawakami,K., Igarashi,T., Tsurugi,T., Kabashima,N., Tamura,M., Okazaki,M., Delisle,B.P., January,C.T., & Otsuji,Y. (2008) Coexistence of hERG current block and disruption of protein trafficking in ketoconazole-induced long QT syndrome. *Br. J. Pharmacol.,* **153**, 439-447.

Terai,T., Furukawa,T., Katayama,Y., & Hiraoka,M. (2000) Effects of external acidosis on HERG current expressed in Xenopus oocytes. *J. Mol. Cell Cardiol.,* **32**, 11-21.

Thai,K.M. & Ecker,G.F. (2007) Predictive models for HERG channel blockers: ligand-based and structure-based approaches. *Curr. Med. Chem.,* **14**, 3003-3026.

Thomas,A.R., Chan,L.N., Bauman,J.L., & Olopade,C.O. (1998) Prolongation of the QT interval related to cisapride-diltiazem interaction. *Pharmacotherapy,* **18**, 381-385.

Thomas,D., Karle,C.A., & Kiehn,J. (2004) Modulation of HERG potassium channel function by drug action. *Annals of Medicine,* **36**, 41-46.

Thomas,D., Zhang,W., Wu,K., Wimmer,A.B., Gut,B., Wendt-Nordahl,G., Kathofer,S., Kreye,V.A., Katus,H.A., Schoels,W., Kiehn,J., & Karle,C.A. (2003) Regulation of HERG potassium channel activation by protein kinase C independent of direct phosphorylation of the channel protein. *Cardiovasc. Res.,* **59**, 14-26.

Tierney,M.G., Uhthoff,T.L., Kravcik,S., & Wielgosz,A.T. (1997) Potential cisapride-erythromycin interaction. *Can. J. Clin. Pharmacol.,* **4**, 82-84.

Triggle,D.J. (1996) Ion channels as pharmacologic receptors: the chirality of drug interactions. *Chirality,* **8**, 35-38.

Trudeau,M.C., Warmke,J.W., Ganetzky,B., & Robertson,G.A. (1995) Herg, a human inward rectifier in the voltage-gated potassium channel family. *Science,* **269**, 92-95.

Tsuji,Y., Opthof,T., Yasui,K., Inden,Y., Takemura,H., Niwa,N., Lu,Z., Lee,J.K., Honjo,H., Kamiya,K., & Kodama,I. (2002) Ionic mechanisms of acquired QT prolongation and torsades de pointes in rabbits with chronic complete atrioventricular block. *Circulation,* **106**, 2012-2018.

Tucker,G.T. (2000) Chiral switches. *The Lancet,* **355**, 1085-1087.

Ueda,K., Valdivia,C., Medeiros-Domingo,A., Tester,D.J., Vatta,M., Farrugia,G., Ackerman,M.J., & Makielski,J.C. (2008) Syntrophin mutation associated with long QT syndrome through activation of the nNOS-SCN5A macromolecular complex. *Proc. Natl. Acad. Sci. U. S. A,* **105**, 9355-9360.

Valenzuela,C., Delpon,E., Franqueza,L., Gay,P., Snyders,D.J., & Tamargo,J. (1997) Effects of ropivacaine on a potassium channel (hKv1.5) cloned from human ventricle. *Anesthesiology,* **86**, 718-728.

Valenzuela,C., Delpon,E., Tamkun,M.M., Tamargo,J., & Snyders,D.J. (1995a) Stereoselective block of a human cardiac potassium channel (Kv1.5) by bupivacaine enantiomers. *Biophys. J.,* **69**, 418-427.

Valenzuela,C., Snyders,D.J., Bennett,P.B., Tamargo,J., & Hondeghem,L.M. (1995b) Stereoselective block of cardiac sodium channels by bupivacaine in guinea pig ventricular myocytes. *Circulation,* **92**, 3014-3024.

Valiyaveetil,F.I., Sekedat,M., MacKinnon,R., & Muir,T.W. (2004) Glycine as a D-amino acid surrogate in the K(+)-selectivity filter. *Proc. Natl. Acad. Sci. U. S. A,* **101**, 17045-17049.

Valko,K., Du,C.M., Bevan,C., Reynolds,D.P., & Abraham,M.H. (2001) Rapid method for the estimation of octanol/water partition coefficient (log P_{oct}) from gradient RP-HPLC retention and a hydrogen bond acidity term ($\Sigma\alpha_2^H$). *Curr. Med. Chem.,* **8**, 1137-1146.

van Bemmelen,M.X., Rougier,J.S., Gavillet,B., Apotheloz,F., Daidie,D., Tateyama,M., Rivolta,I., Thomas,M.A., Kass,R.S., Staub,O., & Abriel,H. (2004) Cardiac voltage-gated sodium channel nav1.5 is regulated by Nedd4-2 mediated ubiquitination. *Circ. Res.,* **95**, 284-291.

Vandenberg,J.I., Torres,A.M., Campbell,T.J., & Kuchel,P.W. (2004) The HERG K^+ channel: progress in understanding the molecular basis of its unusual gating kinetics. *Eur. Biophys. J.,* **33**, 89-97.

Vanhoutte,F., Vereecke,J., Carmeliet,E., & Verbeke,N. (1991) Effects of the enantiomers of disopyramide and its major metabolite on the electrophysiological characteristics of the guinea-pig papillary muscle. *Naunyn-Schmiedberg's Arch. Pharmacol.,* **344**, 662-673.

Vereecke,J. & Carmeliet,E. (2000) The effect of external pH on the delayed rectifying K+ current in cardiac ventricular myocytes. *Pflugers Arch.,* **439**, 739-751.

Waldegger,S., Niemeyer,G., Mörike,K., Wagner,C.A., Suessbrich,H., Busch,A.E., Lang,F., & Eichelbaum,M. (1999) Effect of verapamil enantiomers and metabolites on cardiac K^+ channels expressed in xenopus oocytes. *Cell. Physiol. Biochem.,* **9**, 81-89.

Walker,B.D., Valenzuela,S.M., Singleton,C.B., Tie,H., Bursill,J.A., Wyse,K.R., Qiu,M.R., Breit,S.N., & Campbell,T.J. (1999) Inhibition of HERG channels stably expressed in a mammalian cell line by the antianginal agent perhexiline maleate. *Br. J. Pharmacol.,* **127**, 243-251.

Walker,V.E., Atanasiu,R., Lam,H., & Shrier,A. (2007) Co-chaperone FKBP38 promotes HERG trafficking. *J. Biol. Chem.,* **282**, 23509-23516.

Walker,V.E., Wong,M.J.H., Atanasiu,R., Hantouche,C., Young,J.C., & Shrier,A. (2009) Hsp40 chaperones promote degradation of the hERG potassium channel. *J. Biol. Chem.*.

Wang,J., Myers,C.D., & Robertson,G.A. (2000) Dynamic control of deactivation gating by a soluble amino-terminal domain in HERG K(+) channels. *J. Gen. Physiol,* **115**, 749-758.

Wang,J., Trudeau,M.C., Zappia,A.M., & Robertson,G.A. (1998) Regulation of deactivation by an amino terminal domain in human ether-a-go-go-related gene potassium channels. *J. Gen. Physiol,* **112**, 637-647.

Wang,L., Dennis,A.T., Trieu,P., Charron,F., Ethier,N., Hebert,T.E., Wan,X., & Ficker,E. (2009) Intracellular potassium stabilizes human ether-a-go-go-related gene channels for export from endoplasmic reticulum. *Mol. Pharmacol.,* **75**, 927-937.

Wang,Q., Curran,M.E., Splawski,I., Burn,T.C., Millholland,J.M., VanRaay,T.J., Shen,J., Timothy,K.W., Vincent,G.M., de,J.T., Schwartz,P.J., Toubin,J.A., Moss,A.J., Atkinson,D.L., Landes,G.M., Connors,T.D., & Keating,M.T. (1996) Positional cloning of a novel potassium channel gene: KVLQT1 mutations cause cardiac arrhythmias. *Nat. Genet.,* **12**, 17-23.

Wang,Q., Shen,J., Splawski,I., Atkinson,D., Li,Z., Robinson,J.L., Moss,A.J., Towbin,J.A., & Keating,M.T. (1995) SCN5A mutations associated with an inherited cardiac arrhythmia, long QT syndrome. *Cell,* **80**, 805-811.

Ward,O.C. (1964) A New Familial Cardiac Syndrome in Children. *J. Ir. Med. Assoc.,* **54**, 103-106.

Warmke,J.W. & Ganetzky,B. (1994) A family of potassium channel genes related to eag in drosophila and mammals. *Proc. Natl. Acad. Sci. U. S. A,* **91**, 3438-3442.

Weissman,A.M. (2001) Themes and variations on ubiquitylation. *Nat. Rev. Mol. Cell Biol.,* **2**, 169-178.

Wesche,D.L., Schuster,B.G., Wang,W.-X., & Woosley,R.L. (2000) Mechanism of cardiotoxicity of halofantrine. *Clin. Pharmacol. Ther.,* 521-529.

Westenskow,P., Splawski,I., Timothy,K.W., Keating,M.T., & Sanguinetti,M.C. (2004) Compound mutations: a common cause of severe long-QT syndrome. *Circulation,* **109**, 1834-1841.

Wible,B.A., Hawryluk,P., Ficker,E., Kuryshev,Y.A., Kirsch,G., & Brown,A.M. (2005) HERG-Lite®: a novel comprehensive high-throughput screen for drug-induced hERG risk. *J. Pharmacol. Toxicol. Methods,* **52**, 136-145.

Wilcock,A. & Beattie,J.M. (2009) Prolonged QT interval and methadone: implications for palliative care. *Curr. Opin. Support. Palliat. Care,* **3**, 252-257.

Wilkinson,K.D. (2009) DUBs at a glance. *J. Cell Sci.,* **122**, 2325-2329.

Xiao,J., Luo,X., Lin,H., Zhang,Y., Lu,Y., Wang,N., Zhang,Y., Yang,B., & Wang,Z. (2007) MicroRNA miR-133 represses HERG K+ channel expression contributing to QT prolongation in diabetic hearts. *J. Biol. Chem.,* **282**, 12363-12367.

Yang,B. & Kumar,S. (2010) Nedd4 and Nedd4-2: closely related ubiquitin-protein ligases with distinct physiological functions. *Cell Death. Differ.,* **17**, 68-77.

Yang,I.C.H., Scherz,M.W., Bahinski,A., Bennett,P.B., & Murray,K.T. (2000) Stereoselective interactions of the enantiomers of chromanol 293B with human voltage-gated potassium channels[1]. *J. Pharmacol. Exp. Ther.,* **294**, 955-962.

Yang,T., Snyders,D.J., & Roden,D.M. (1997) Rapid inactivation determines the rectification and [K+]o dependence of the rapid component of the delayed rectifier K+ current in cardiac cells. *Circ. Res.,* **80**, 782-789.

Zeng,H., Lozinskaya,I.M., Lin,Z., Willette,R.N., Brooks,D.P., & Xu,X. (2006) Mallotoxin is a novel human ether-a-go-go-related gene (hERG) potassium channel activator. *J. Pharmacol. Exp. Ther.,* **319**, 957-962.

Zhang,S., Zhou,Z., Gong,Q., Makielski,J.C., & January,C.T. (1999) Mechanism of block and identification of the verapamil binding domain to HERG potassium channels. *Circ. Res.,* **84**, 989-998.

Zhang,Y., Xiao,J., Wang,H., Luo,X., Wang,J., Villeneuve,L.R., Zhang,H., Bai,Y., Yang,B., & Wang,Z. (2006) Restoring depressed HERG K+ channel function as a mechanism for insulin treatment of abnormal QT prolongation and associated arrhythmias in diabetic rabbits. *Am. J. Physiol Heart Circ. Physiol,* **291**, H1446-H1455.

Zhou,Z., Gong,Q., Epstein,M.L., & January,C.T. (1998a) HERG channel dysfunction in human long QT syndrome. Intracellular transport and functional defects. *J. Biol. Chem.,* **273**, 21061-21066.

Zhou,Z., Gong,Q., Ye,B., Fan,Z., Makielski,J.C., Robertson,G.A., & January,C.T. (1998b) Properties of HERG channels stably expressed in HEK 293 cells studied at physiological temperature. *Biophys. J.,* **74**, 230-241.

Zhou,Z.F., Gong,Q.M., & January,C.T. (1999) Correction of defective protein trafficking of a mutant HERG potassium channel in human long QT syndrome - Pharmacological and temperature effects. *J. Biol. Chem.,* **274**, 31123-31126.